

HORIZON-CL5-2022-D3-01-11

Demonstration of innovative forms of storage and their successful operation and integration into innovative energy system and grid architectures



AGISTIN

Advanced Grid Interfaces for
innovative Storage INtegration

D6.3 Technical-Economic Sizing, Operation and Control Tools for Irrigation System Modernisation into Energy Storage Systems

Document properties

FUNDING PROGRAM	HORIZON EUROPE
GRANT AGREEMENT NUMBER	101096197
PROJECT	AGISTIN
DELIVERABLE ID	D6.3
TITLE	Technical-economic sizing, operation and control tools for irrigation system modernisation into energy storage systems
DISTRIBUTION LEVEL	PU
DUE DATE	30-06-2025
DATE SUBMITTED	30-06-2025
VERSION	V1.0
WORK PACKAGE	WP6
LEAD PARTICIPANT	UPC
TOTAL NUMBER OF PAGES	151



AGISTIN

Advanced Grid Interfaces for innovative STorage INtegration

All intellectual property rights are owned by the AGISTIN consortium members and are protected by the applicable laws. Except where otherwise specified, all document contents are: “© AGISTIN project - All rights reserved”. Reproduction is not authorized without prior written agreement. The commercial use of any information contained in this document may require a license from the owner of that information. All AGISTIN consortium members are also committed to publish accurate and up-to-date information and take the greatest care to do so. However, the AGISTIN consortium members cannot accept liability for any inaccuracies or omissions, nor do they accept liability for any direct, indirect, special, consequential, or other losses or damages of any kind arising out of the use of this information. Views and opinion stated in this report reflects the opinion of the authors and not the opinion of the European Commission. The European Union is not liable for any use that may be made of the information contained in this document.

Version history

VERSION	DATE	COMMENT
V0.1	06-06-2025	FIRST DRAFT
V1.0	30-06-2025	FINAL VERSION FOR SUBMISSION





Contents

1	Introduction	12
1.1	The AGISTIN Project	12
1.2	Work package 6 and Objective of the Deliverable	12
1.3	Structure of the Deliverable	13
2	Irrigation communities	14
2.1	Current situation	14
2.2	Potential available energy estimation	15
2.3	Comunitat de Regants Segrià-Sud	16
2.4	Other communities	18
2.5	CEDER-CIEMAT	22
3	Optimisation and redesign for active role of irrigation systems as energy storage in the electrical grid	23
3.1	Introduction	23
3.1.1	State of the art	24
3.1.2	Objective	25
3.2	Approach	26
3.2.1	Other approaches / tested approaches	26
3.3	Optimisation tool	27
3.3.1	Device models	27
3.3.2	Objective function	39
3.3.3	Solving the problem	39
3.3.4	Scalability	40
3.4	Study cases	44
3.4.1	Academic case	45
3.4.2	Comunitat de Regants Les Planes i Aixalelles	47
3.4.3	Comunitat de Regants Segrià-Sud	53
3.4.4	CEDER-CIEMAT	71
3.5	Conclusions	75
3.5.1	Future work	76
4	Energy storage sizing to prevent water hammer on PV pumping systems	77
4.1	Introduction	78
4.1.1	Water hammer in PV pumping	79
4.1.2	Contributions	80
4.2	Problem description	80
4.3	Methodology (Off-grid)	82
4.4	Study case	85
4.4.1	Clouds	86
4.4.2	Results	87
4.4.3	Feasibility and impact assessment	88



- 4.4.4 Sensitivity analysis 90
- 4.5 Methodology (Grid connected) 93
 - 4.5.1 PV disconnects, pump does not stop 94
 - 4.5.2 PV disconnects, pump can stop 97
 - 4.5.3 PV does not disconnect 100
- 4.6 Aqueous ECR battery 103
 - 4.6.1 Results 103
 - 4.6.2 Results (Grid connected) 103
- 4.7 Conclusion 104
 - 4.7.1 Future work 105
- 5 Potential grid services 106
 - 5.1 Legislative context 106
 - 5.2 Applications in power system operation 107
 - 5.2.1 Long term storage 107
 - 5.2.2 Short term storage 108
 - 5.2.3 Comparison and requirements of long and short term storage 109
 - 5.2.4 Services with revenue in Spain 110
- 6 Real-time operation & control for innovative irrigation canal-based energy storage systems 113
 - 6.1 Introduction 113
 - 6.2 Problem definition 116
 - 6.3 Methodology 117
 - 6.3.1 Development of OFO-based controller for pump-based irrigation plants 119
 - 6.4 Performance assessment 121
 - 6.4.1 Study case 121
 - 6.4.2 Preliminary results 122
 - 6.5 Conclusions 123
 - 6.5.1 Future work 124
- 7 Fundamental AGI topologies and control strategies 125
 - 7.1 Introduction 125
 - 7.2 Comparing AC and DC microgrid approaches 127
 - 7.3 Control architectures for the converter connected to the primary grid 128
 - 7.3.1 Dual-Port control 129
 - 7.4 Discussion on possible AGI configurations 130
 - 7.5 Models to study the connection to the primary grid 131
 - 7.5.1 Steady-state Model 132
 - 7.5.2 Linear Model 133
 - 7.6 Initial Results 135
 - 7.6.1 Power flow solution 136
 - 7.6.2 Small-Signal analysis 137
 - 7.6.3 PV step change 137
 - 7.6.4 Grid angle step change 139
 - 7.7 Future work 140
- Bibliography 141

List of Figures

2.1	Evolution of the irrigated and dry crops extension in Spain between 2004 and 2023	15
2.2	Declared agricultural land in Catalonia, classified into irrigated and dry (year 2023)	15
2.3	Location of the reservoirs of the analysed irrigation communities next to the main participating rivers and tributaries. Colours correspond to different irrigation communities.	16
2.4	Facilities at the CR Segrià-Sud	18
2.5	Irrigation communities in the region considered for further analysis	19
2.6	Facilities at the CR de Les Planes i Aixalelles	20
2.7	CEDER-CIEMAT case schematic.	22
3.1	Location of the state of the art references.	24
3.2	Definition of the variables of a source	28
3.3	Reservoir definition	29
3.4	Definition of the flow direction in a pipe device	29
3.5	Characteristic curve of a pipe	30
3.6	Definition of the flow and electric power direction in a pump device	31
3.7	Operating region of a variable speed pump.	31
3.8	Operating region of linear approximation model	32
3.9	Definition of the flow and electric power direction in a new pump device	34
3.10	Definition of the flow and electric power direction in a turbine device	35
3.11	Comparison of different methods using equality, inequality, and linearized constraints. . . .	42
3.12	Study case diagram.	45
3.13	Maximum capacity, already installed and newly sized (dim.) magnitudes of the PV, battery and turbine elements.	46
3.14	Volume at the reservoirs (R0, R1) and flow of both pumps (P1, P2), irrigation at reservoir 1 (Irr) and turbine (T1).	47
3.15	Power balance of the system (defined positive if consumed by the element) and electricity cost.	47
3.16	Battery state of charge and power (defined positive if absorbed).	48
3.17	CR Les Planes i Aixalelles study case base system.	48
3.18	Average daily irrigation demand on CR Les Planes i Aixalelles (S: Summer, W: Winter). Real data from 1 year and 90% confidence interval.	48
3.19	Variations on the study case	50
3.20	Results of the base case.	51
3.21	Results of PaT case (Case 1).	51
3.22	Results of grid connected case (Case 2).	52
3.23	Results of grid connected + PaT case (Case 3).	52
3.24	CR Segrià-Sud Base case system.	53
3.25	CR Segrià-Sud water consumption for irrigation.	54
3.26	CR Segrià-Sud system division.	55
3.27	CR Segrià-Sud lower and upper divisions and assumptions.	55
3.28	Grid equivalent GHG emission factor, cost of electricity and sell price for the defined typical days.	56

3.29 CR Segrià-Sud upper results - Base case.	60
3.30 CR Segrià-Sud upper results - PaT case (Case 1).	61
3.31 CR Segrià-Sud upper results - grid connected case (Case 2).	62
3.32 CR Segrià-Sud upper results - PaT + grid connected case (Case 3).	63
3.33 CR Segrià-Sud upper results - emissions case (Case 3-em).	64
3.34 CR Segrià-Sud lower results - Base case.	67
3.35 CR Segrià-Sud lower results - grid connected case (Case 2).	68
3.36 CR Segrià-Sud lower results - PaT + grid connected case (Case 3).	69
3.37 CR Segrià-Sud lower results - emissions case (Case 3-em).	70
3.38 Spiderplots resulting from the sensitivity analysis.	71
3.39 CEDER case representation with Pyomo blocks.	72
3.40 CEDER results - Case 1 in summer.	72
3.41 CEDER results - Case 1 in winter.	73
3.42 CEDER results - Case 2 in summer.	73
3.43 CEDER results - Case 2 in winter.	74
3.44 CEDER results - Case 3 in summer.	74
3.45 CEDER results - Case 3 in winter.	74
3.46 CEDER costs results comparison.	75
4.1 Electrical scheme of a PV pumping system.	78
4.2 Sketch representation of an irradiance drop event.	79
4.3 Irradiance drop event with ESS.	81
4.4 Data key points that define a cloud.	82
4.5 Location of the irradiance sensor and study case on the CR Segrià-Sud facilities.	85
4.6 Power generation and consumption of a PV pump system in the Segrià-Sud facilities, corresponding to 25th July 2022.	86
4.7 Rank function plot of clouds' duration and shaded radiant exposure.	87
4.8 Number of pump stopping events shading a certain energy, from data and estimator	87
4.9 Costs per year for different technologies and base case.	88
4.10 Costs per year for different technologies and base case and sensitivity for interest rate i and cost of energy c_{grid}	90
4.11 Sensitivity of the costs per year for different technologies and base case for irradiance threshold G_{th}	91
4.12 Cost function and minimum value for different irradiance thresholds between 100 and 600 W/m^2	92
4.13 Sketch representation of the grid connected PV pumping system.	93
4.14 Strategy 1.	94
4.15 Costs per year for different technologies and grid connected case 1.	96
4.16 Costs per year for different technologies and grid connected case 1 and sensitivity for interest rate i , cost of energy c_{grid} and penalty t_p	96
4.17 Strategy 2.	97
4.18 Costs per year for different technologies and grid connected case 2.	99
4.19 Costs per year for different technologies and grid connected case 2 and sensitivity for interest rate i , cost of energy c_{grid} and penalty t_p	99
4.20 Considered behaviour with grid and PV connected.	100
4.21 Costs per year for different technologies and grid connected with PV.	102
4.22 Costs per year for different technologies and grid connected case 1 and sensitivity for interest rate i , cost of energy c_{grid} and penalty t_p	102
4.23 Optimal sizing $E_{(1)}$ for the Geyser Aqueous ECR energy storage system for a range of capital cost and sensitivity for cost of energy c_{grid}	104
5.1 ACER's proposal on Requirements for generation in mixed-technology sites	107

5.2	Division of frequency regulation, frequency curve example (top) and power type responsibilities (bottom)	108
6.1	Online Feedback optimisation structure based on gradient flow.	117
6.2	Relationship between offline and online optimisation tools.	120
6.3	Model of the simplest test case.	121
6.4	Testing of the plant with a good estimation of water consumption for irrigation.	122
6.5	Testing of the plant with a wrong estimation of water consumption for irrigation.	123
7.1	Maximum Power Point Tracking.	127
7.2	AC vs DC interconnections.	128
7.3	Example of a DC voltage control architecture.	129
7.4	Example of an AC grid-forming control architecture with droop control.	129
7.5	Dual-Port control architecture.	130
7.6	Schemes of the analysed AGI configurations.	130
7.7	VSC electric scheme model.	131
7.8	Controlled current source model.	131
7.9	Initial case study scheme.	136
7.10	Linear and non-linear models comparison.	137
7.11	Main converter active and reactive power.	138
7.12	Main converter dc voltage and angle.	139
7.13	Main converter active and reactive power.	139
7.14	Main converter voltage and current magnitudes.	140

List of Tables

2.1	Potential available energy storage capacity	17
2.2	CR Segrià-Sud legacy equipment	17
2.3	CR Segrià-Sud potential energy storage	17
2.4	CR Les Planes i Aixalelles legacy equipment	19
2.5	CR Les Planes i Aixalelles potential energy storage	19
2.6	CR Garrigues Sud legacy equipment	20
2.7	CR Garrigues Sud potential energy storage	21
2.8	CR Zona Oriental de la Terra Alta legacy equipment	21
2.9	CR Zona Oriental de la Terra Alta potential energy storage (*: equipment planned or under construction)	21
2.10	CEDER potential energy storage	22
3.1	Results of time and final cost value and comparison between algorithms and methods.	43
3.2	Characteristics of the case's elements (in p.u.)	45
3.3	Variables linked by arcs	45
3.4	Costs in €/p.u.	46
3.5	Characteristics of the case's elements	49
3.6	Cases summary	53
3.7	Characteristics of the CR Segria-Sud case's devices	54
3.8	Results (Upper)	57

3.9	Results (Lower)	65
3.10	Sensitivity analysis total cost average	66
3.11	Objectives values and execution time per case and season.	75
4.1	Irrigation communities with PV pumping systems in Catalunya.	78
4.2	Characteristics of the PV pumping system	85
4.3	Capital and operation costs of the analysed energy storage systems	86
4.4	Statistical description of the properties of the observed clouds.	86
4.5	Statistical description of the clouds dataset.	87
4.6	Sizing results	88
4.7	Properties of the ESS technologies	89
4.8	PS3 sensitivity analysis results for cost of energy and real interest rate	91
4.9	PS3 sensitivity analysis results for irradiance threshold	91
4.10	Grid connected base case characteristics	93
4.11	Grid connected sizing results (Strategy 1)	95
4.12	PS3 sensitivity analysis results for cost of energy, real interest rate and excess power term	96
4.13	Grid connected sizing results (Strategy 2)	99
4.14	Grid connected sizing results (without PV disconnection)	102
4.15	Maximum capital cost for $E_{(1)} \leq 0,1$ kWh for different cost of energy values	103
4.16	Maximum capital cost for different excess power term (grid connected cases)	104
5.1	Comparison and requirements.	111
6.1	Parameters of the simple test case.	121
7.1	Main converter parameters.	136
7.2	Power flow solution.	136
7.3	System's eigenvalues.	138

Acronyms

AC alternating current

ACATCOR Associació Catalana de Comunitats de Regants

ACER Agency for Cooperation of Energy Regulators

aFRR automatic frequency restoration reserve

AGI advanced grid interface

AGISTIN Advanced Grid Interfaces for innovative SStorage INtegration

CEDER Centro de Desarrollo de Energías Renovables

CIEMAT Centro de Investigaciones Energéticas Medioambientales y Tecnológicas

CR Comunitat de Regants

DC direct current

ECR electrochemical recuperator

EMS energy management system

ENTSO-E European Network of Transmission System Operators for Electricity

ESS energy storage system

FCR frequency containment reserve

FENACORE Federación Nacional de Comunidades de Regantes

Flow redox flow battery

Fw flywheel

GHG greenhouse gas

IPOPT interior point optimiser

LCOS levelised cost of storage

Lead lead acid battery

LIB lithium-ion battery

mFRR manual frequency restoration reserve

MINLP mixed integer non-linear programming

MPPT maximum power point tracking

NLP non-linear programming

PaT pump as turbine

PPMs power park modules

PSH pumped-storage hydropower

PV photovoltaic

PVPC voluntary price for the small consumer

RR replacement reserve

SD standard deviation

SOC state of charge

Uc ultracapacitor

Symbols



Battery



Grid



New pump



Pipe



Pump



Pump as turbine (reversible pump)



Reservoir



Solar photovoltaic



Source



Turbine

1 Introduction

1.1 The AGISTIN Project

The AGISTIN project represents an ambitious endeavor at the intersection of innovative energy storage, renewable technologies, demand response, and grid integration. With its focus on advanced grid-integrated technologies, AGISTIN seeks to pave the way for a more sustainable and efficient energy future.

AGISTIN, aims to demonstrate the feasibility of integrated energy systems combining a variety of technologies, such as renewable energy sources, electric vehicle chargers, and industrial loads, by means of advanced grid infrastructure and hybrid AC/DC coupling. By doing so, AGISTIN aspires to showcase how these integrated systems can deliver cost savings, improved energy efficiency, and reduced environmental impacts.

The AGISTIN project is built around three demonstrations:

1. fast charging stations of electric vehicles,
2. large pumping loads used for agricultural irrigation, and
3. green hydrogen production.

This deliverable focuses on the advanced grid interface (AGI)-integrated innovative storage applications in large irrigation systems, which is briefly outlined in the next section.

1.2 Work package 6 and Objective of the Deliverable

Work package 6 of the AGISTIN project demonstrates the AGI-integrated innovative storage applications in large irrigation systems. In this document we explore reservoir based irrigation systems and their potential role as active grid participants as energy storage systems in the form of pumped-storage hydropower (PSH). We also analyse the use of energy storage system (ESS) to mitigate the water hammer effects on photovoltaic (PV) pumping systems.

The objective of this deliverable is to define the methodologies to analyse, optimise and control irrigation systems to actively participate in the grid and integrate energy storage systems.

1.3 Structure of the Deliverable

Section 2 introduces the concepts of irrigation communities, reservoir-based irrigation systems and analyses their potential energy storage use. Section 3 describes and tests the methodology developed to analyse, size and optimise large-scale reservoir-based irrigation systems to participate in the electrical grid as energy storage systems. Section 4 describes the water hammer issues photovoltaic pumping systems may experience and develops a methodology to size energy storage systems that prevent them. Section 5 analyses the grid services that irrigation systems could provide in their role as energy storage as well as the considered energy storage systems to prevent water hammer issues. Section 6 describes the formulation on which the controller is based and then discusses the implementation of the controller in pump-based irrigation plants. Section 7 explores the fundamental AGI topologies and control strategies.

2 Irrigation communities

Irrigation communities, also known as water user associations or irrigation associations, are user associations whose function is to distribute water from a certain public concession among irrigators and other users. Their water distribution systems may take many forms depending on whether they are pressurised or open canals and whether they use water storage in the form of reservoirs or deliver straight from the main water source. The focus of this work are pump-fed reservoir-based irrigation systems. In such systems, a pumping station transfers water to a higher reservoir from the main source or an intermediate reservoir. Then, a series of canals or pipes deliver water to the users, usually by gravity.

The purpose of this chapter is to present and compile the considered irrigation communities. All data in this document have been acquired from public reports of public works from the pertinent departments from the Generalitat de Catalunya¹ and Gobierno de España².

This chapter is structured as follows:

- i Section 2.1 introduces the current situation of the irrigated land and irrigation communities in Spain.
- ii Section 2.2 analyses the irrigation systems in Catalunya and estimates the potential available energy.
- iii Section 2.3 describes the facilities of the Comunitat de Regants Segrià-Sud.
- iv Section 2.4 describes the facilities of extra irrigation communities that were considered in this project.
- v Section 2.5 describes the facilities of the CEDER-CIEMAT.

2.1 Current situation

The total number of irrigation communities in Spain surpasses 7 200, as declared by Federación Nacional de Comunidades de Regantes (FENACORE), and compresses a total of $13,07 \cdot 10^6$ ha of dry land and $3,63 \cdot 10^6$ ha of irrigated land [1], the share of which has been steadily increasing for the last 20 years (Figure 2.1).

The region of Catalunya compresses 562 769 ha of dry land and 251 769 ha of irrigated land, of which 148 389 ha of the latter are found in the province of Lleida [1]. Figure 2.2 maps the agricultural land officially declared in Catalunya in 2023 [2], depicting the interest of irrigated land in the western region along the Ebre and Segre river basins. Opposed to the rest of Spain, since 2008 there has been a loss in agricultural land in Catalunya (857 653 ha of dry land and 308 889 ha of irrigated land in 2008). This is attributed to abandonment of land and change of its use to urban land [3]. The number of irrigation communities in the region of Catalunya approaches 100, 90 of which are a part of the Associació Catalana de Comunitats de Regants (ACATCOR)³.

¹Plataforma de Serveis de Contractació Pública <https://contractaciopublica.cat/ca/inici>

²Plataforma de Contratación del Sector Público <https://contrataciondelestado.es/wps/portal/plataforma>

³ACATCOR <https://acatcor.cat/>

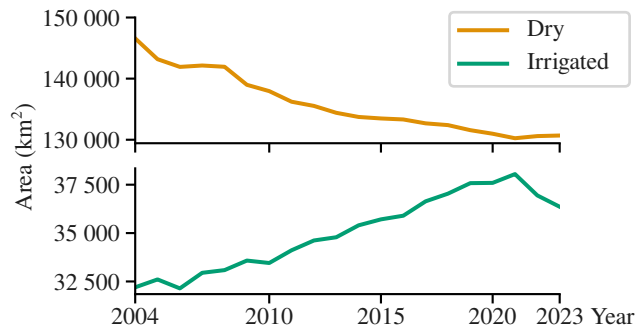


Figure 2.1 – Evolution of the irrigated and dry crops extension in Spain between 2004 and 2023 [1]

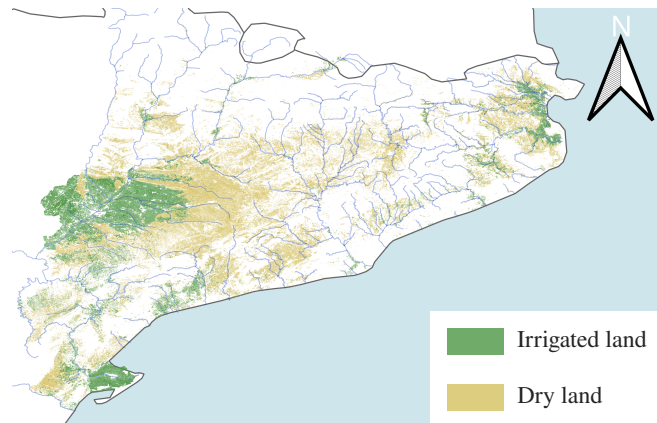


Figure 2.2 – Declared agricultural land in Catalonia, classified into irrigated and dry (year 2023) [2]

With the objective of increasing the irrigation efficiency, since the year 2002 [4] there has been in Spain a substitution of the irrigation by gravity methods to pressurised methods, fundamentally drip irrigation, increasing the share of pressurised irrigation from 41,0 % in 2000 to 80,1 % in 2023 [1]. The water consumption was reduced from 5 051,9 m³/ha·year in the year 2000 to 4 105,32 m³/ha·year in the year 2018 [5], but it also increased the energy consumption of the irrigation systems [6]. The catalan Irrigation Plan 2008-2020 (*Pla de Regadius 2008-2020*) [3] set as objectives to modernise the irrigation systems present in the region and transform the areas with agricultural potential into irrigated land. From 2008 to 2023, the share of pressurised irrigation in Catalunya increased from 44,8 % to 56,9 % [1]. An updated Irrigation Plan is scheduled for 2025. In an interview in the national television, the Minister of Agriculture, Livestock, Fisheries and Food (*Ministre d'Agricultura, Ramaderia, Pesca i Alimentació*) of the Generalitat de Catalunya Òscar Ordeig (since August 2024), declared that the new Irrigation Plan will span from 2025 to 2040 and focus on the modernisation of the irrigation systems in Catalunya, implementing new technologies of water regeneration and desalination and avoid the desertification and abandonment of agricultural land [7]. Therefore, a will exists from the government and administration to maintain and increase the irrigated land area, as well as construct new irrigation systems infrastructure.

2.2 Potential available energy estimation

We analysed the potential available energy of the Ebre and Segre river basins in Catalunya using reservoirs as energy storage. We identified and obtained data from a total of 27 irrigation communities which own feasible systems for such purpose, pinpointed in Figure 2.3. These systems take water from rivers Ebre and some of its main tributaries Cinca, Segre, Set, Matarranya, Montsant and Siurana as well as from Canal d'Aragó i Catalunya. Little and sparse data is available from irrigation systems, thus we established contact with the administration [3, 8, 9, 10, 11] and representatives from irrigation communities as well

as collected available data from public tenders [12, 13, 14, 15, 16, 17, 18, 19, 20, 21, 22, 23, 24]. Then, for each reservoir present in the systems we estimated the potential energy defined as:

$$E = \rho g \Delta H W, \quad (2.1)$$

where ρ is the density of the water assumed $1\,000\text{ kg/m}^3$, g the gravity acceleration constant near the surface of the Earth, assumed $9,81\text{ m/s}^2$, ΔH (m) the average difference of heights between a reservoir and its direct source and W (m^3) the volumetric capacity of the reservoir. The results are summarised in Table 2.1. We published the whole dataset, which is publicly available in [25].

The calculation does not consider the efficiency of the pumping systems and turbines or pump as turbine (PaT)s required to extract the energy. It does not examine either the operation of reservoirs in series, which will have an influence on the amount of energy that can be extracted on irrigation communities that have several reservoirs in series. Since not all of the required data could be gathered, some values were estimated as well as reservoirs were excluded from the analysis.

Assuming a cost of $340 \pm 60\text{ \$/kWh}$ [26] and a ratio of $1\text{ \$} = 0,86\text{ €}$ (as per June 2025), the capital investment required for an stationary energy storage system (ESS) of such characteristics would range in $643 \pm 114\text{ M€}$.

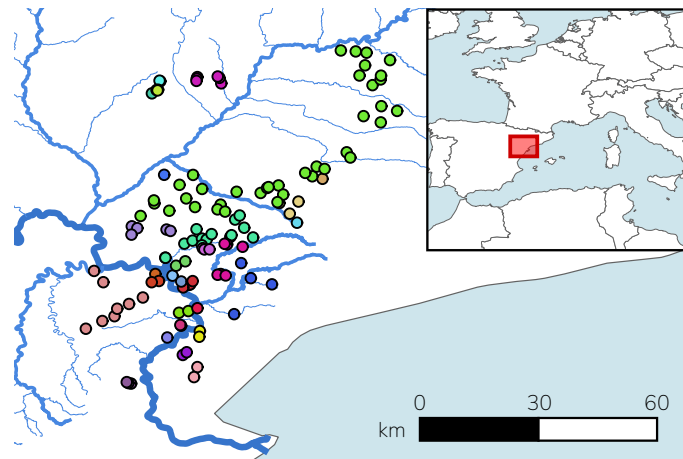


Figure 2.3 – Location of the reservoirs of the analysed irrigation communities next to the main participating rivers and tributaries. Colours correspond to different irrigation communities.

2.3 Comunitat de Regants Segrià-Sud

The Comunitat de Regants Segrià-Sud is located in the province of Lleida, at geographic coordinates N $41^\circ 21' 44''$ E $0^\circ 27' 14''$, and has influence over the municipalities of Almatret, Llardecans, Maials, Seròs and Torrebesses.

Its facilities consist of 4 pumping stations with 18,4 MW of installed power, 5 reservoirs with a total capacity of $980\,000\text{ m}^3$ and 3 solar photovoltaic (PV) plants totalling 1,3 MWp (Figure 2.4). Pumping stations PS0 and PS1 deliver water from the river Ebre to reservoir R1, from where it is distributed to reservoirs R2, R3 and R4 via pumping station PS2. Pumping station PS3 takes water from reservoir R4 to reservoir R5. Two of the PV plants are located at pumping station PS2 and the remaining one is projected to be installed at PS3 [21, 22, 27, 28, 29, 30].

Table 2.2 summarises the equipment present at the facilities of the Comunitat de Regants Segrià-Sud and Table 2.3 shows its potential energy storage as computed with (2.1).

Table 2.1 – Potential available energy storage capacity (*: volume was estimated from reservoir surface). Data from [25].

Irrigation community	Reservoirs	E [MWh]
Aigües del Montsant *	6	5,04
Albí	3	6,44
Algerri Balaguer	6	111,73
Ascó 2a zona *	2	4,76
Aubarrells	2	6,03
Bassanova	3	0,87
Benissanet	2	10,45
Garrigues Sud	15	158,30
Ginestar	2	11,46
Les Planes i Aixalelles	1	3,58
Monredons-Valls	1	18,64
Mora d'Ebre *	2	10,12
Mora la Nova *	1	3,83
Palma d'Ebre	3	47,84
Perelló	2	10,15
Pinell de Brai	1	16,48
Progrés *	1	1,60
Rasquera	2	34,13
Riu Rinet	2	7,10
Segarra Garrigues	38	1 186,21
Segrià Sud	5	255,01
Torre de l'Espanyol *	4	5,28
Torres de Segre	1	101,02
Vilosell	1	12,26
Vingalís	2	18,10
Xerta Sènia	3	23,57
Zona Oriental Terra Alta	8	183,54
TOTAL		2 223,52

Table 2.2 – CR Segrià-Sud legacy equipment. (*: equipment planned or under construction)

Pumping station	N. Pumps	Power [kW]	Flow [m ³ /h]	Solar PV [kWp]
PS0	3	3 x 950	11 520	-
PS1	3	3 x 3 200	11 520	-
PS2	9	3 x 250	3 154	-
		3 x 315	2 010	523,00
		3 x 1 250	6 570	527,50
PS3	3	3 x 160	2 778	274,68*

Table 2.3 – CR Segrià-Sud potential energy storage

Reservoir	Volume [m ³]	Average altitude [m]	Energy [MWh]
Ebre River (Ribarroja)	-	70	-
Reservoir R1	142 869	331	101,73
Reservoir R2	297 042	359	22,62
Reservoir R3	85 268	419	20,38
Reservoir R4	269 485	426	69,27
Reservoir R5	185 814	447	10,97

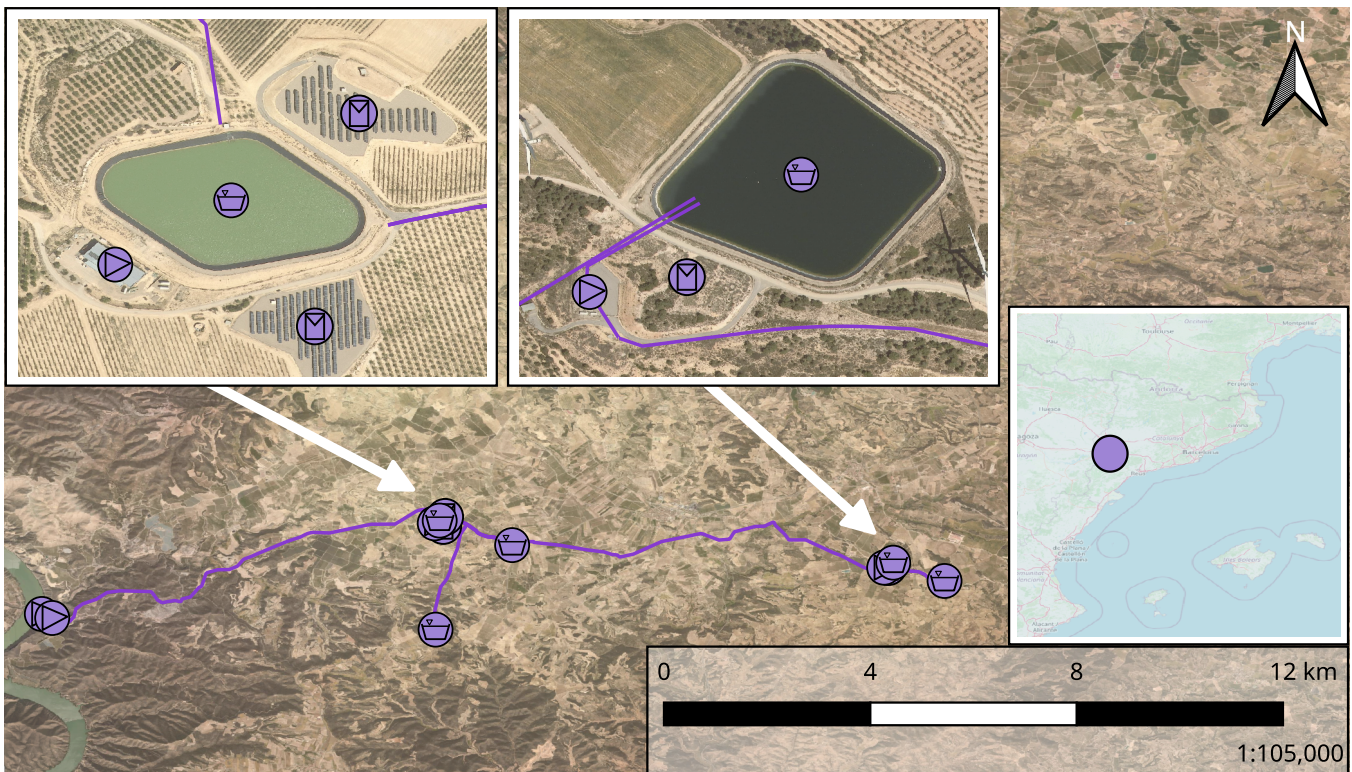


Figure 2.4 – Facilities at the CR Segrià-Sud. Ortophoto from Institut Cartogràfic i Geològic de Catalunya [31], World map from OpenStreetMap [32].

2.4 Other communities

Besides the CR Segrià-Sud being already in the project, we made a call for data to the irrigation communities involved with ACATCOR, the main Catalan association of irrigation communities. Several have answered and are depicted in Figure 2.5. Ebre and Segre, the two main rivers of the region which feed the communities reservoirs, are highlighted as well.

Comunitat de Regants de Les Planes i Aixalelles

The Comunitat de Regants de Les Planes i Aixalelles is located in the province of Tarragona, at geographic coordinates N 41° 12' 39" E 0° 34' 32", and has influence over the municipalities of Ascó, Flix and Vinebre.

Their facilities consist of a pumping station, a reservoir and a solar PV plant (Figure 2.6). The pumping station consists of 2 pumps of 110 kW powered by a three-phase motor with squirrel cage rotor. The reservoir can hold a volume of 13 000 m³ and is located at an altitude of 138 m over sea level, 101 m above the pumping station. The solar PV plant, in service since march of 2023, is built of 468 PV panels for a total of 215,28 kWp. An anti-freezing system allows the facilities to work on colder conditions, extending the irrigation season on winter time [19, 33, 34].

Table 2.4 summarises the equipment present at the facilities of the Comunitat de Regants de Les Planes i Aixalelles and Table 2.5 shows its potential energy storage as computed with (2.1).

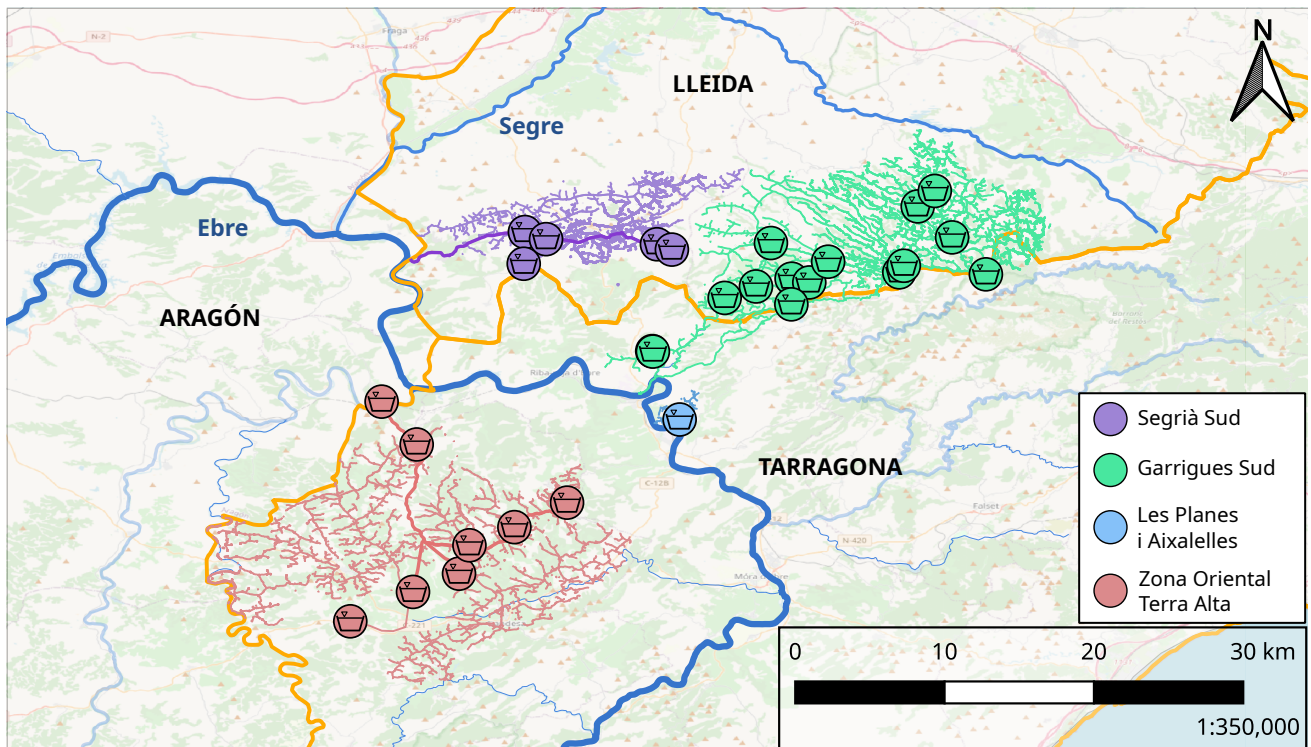


Figure 2.5 – Irrigation communities in the region considered for further analysis. World map from OpenStreetMap [32]. Data from [8].

Table 2.4 – CR Les Planes i Aixalletes legacy equipment

Pumping station	N. Pumps	Power [kW]	Flow [m ³ /h]	Solar PV [kWp]
PS1	1+1	(1+1) x 110	200	215,28

Table 2.5 – CR Les Planes i Aixalletes potential energy storage

Reservoir	Volume [m ³]	Average altitude [m]	Energy [MWh]
Ebre River (Ascó)	-	37	-
Reservoir R1	13 000	138	3,58

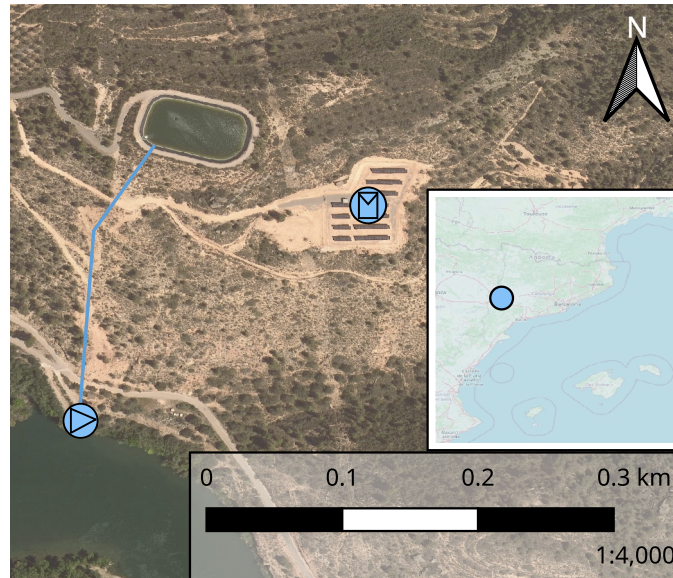


Figure 2.6 – Facilities at the CR de Les Planes i Aixalelles. Ortophoto from Institut Cartogràfic i Geològic de Catalunya [31], World map from OpenStreetMap [32].

Comunitat de Regants del Garrigues Sud

The Comunitat de Regants del Garrigues Sud is located in the province of Lleida, at geographic coordinates N 41° 22' 16" E 0° 39' 42", and has influence over the county of Les Garrigues.

Their facilities consist of 8 pumping stations, 15 reservoirs and 2 solar PV plants [18, 35, 36].

Table 2.6 summarises the equipment present at the facilities of the Comunitat de Regants del Garrigues Sud and Table 2.7 shows its potential energy storage as computed with (2.1).

Table 2.6 – CR Garrigues Sud legacy equipment

Pumping station	N. Pumps	Power [kW]	Flow [m ³ /h]	Solar PV [kWp]
PS1	3+1	(3+1) × 450	1 537	601,88
PS2	3+1	(3+1) × 315	1 353	462,24
PS3	1+1	(1+1) × 400	800	-
PS4	1+1	(1+1) × 75	118	-
PS5	3+1	(3+1) × 355	1 080	-
PS6	2+1	(2+1) × 110	608	-
PS1-IV	3+1	7 500	6 109	-
PS2-IV	3+1	8 400	6 109	-

Comunitat de Regants de la Zona Oriental de la Terra Alta

The Comunitat de Regants de la Zona Oriental de la Terra Alta is located in the province of Tarragona, at geographic coordinates N 41° 7' 5" E 0° 22' 23", and has influence over the county of Terra Alta.

Their facilities consist of 4 pumping stations and 7 reservoirs [24].

Table 2.8 summarises the equipment present at the facilities of the Comunitat de Regants de la Zona Oriental de la Terra Alta and Table 2.9 shows its potential energy storage as computed with (2.1).

Table 2.7 – CR Garrigues Sud potential energy storage

Reservoir	Volume [m ³]	Average altitude [m]	Energy [MWh]
Ebre River (Flix)	-	40,4	-
Reservoir R0	3 600	203	1,60
Reservoir R1	14 688	198	0,25
Reservoir R2	74 870	323	25,50
Reservoir R3	280	418	0,07
Reservoir R4	40	470	0,02
Reservoir R5	54 000	518	28,77
Reservoir R6	54 000	580	9,05
Break	4 668	217	2,26
Break BT-0	1 000	328	0,78
Reservoir E1	92 000	619	16,49
Reservoir E2	35 500	545	18,60
Reservoir E3	82 900	662	18,52
Reservoir E4	91 000	685	5,88
Reservoir E5	65 800	637	12,08
Reservoir E6	56 600	781	18,43

Table 2.8 – CR Zona Oriental de la Terra Alta legacy equipment (*: equipment planned or under construction)

Pumping station	N. Pumps	Power [kW]	Flow [m ³ /h]	Solar PV [kWp]
PS0	3+1	(3+1) × 680	9 000	-
PS1	3+1	(3+1) × 8 351	9 000	-
PS2	12	(1+1) × 600	608	-
		(2+1) × 794	1 109	-
		(2+1) × 914	2 268	-
		(3+1) × 914	4 266	-
PS3	2+1	(2+1) × 150	252	-
PS4*	2+1	(2+1) × 178	1 620	-

Table 2.9 – CR Zona Oriental de la Terra Alta potential energy storage (*: equipment planned or under construction)

Reservoir	Volume [m ³]	Average altitude [m]	Energy [MWh]
Ribarroja reservoir	-	69	-
Tank	3 600	88	0,19
Reservoir R1	50 000	359	36,86
Reservoir R2.1	150 000	445	35,15
Reservoir R2.2	270 000	457	72,47
Reservoir R2.3	33 000	465	9,53
Reservoir R2.4	41 000	521	18,10
Reservoir R3	30 800	551	2,56
Reservoir R4*	70 000	503	8,68

2.5 CEDER-CIEMAT

Centro de Desarrollo de Energías Renovables (CEDER)-Centro de Investigaciones Energéticas Medioambientales y Tecnológicas (CIEMAT) is located in the province of Soria at geographic coordinates N 41°36'22" E 2°27'37" is a center dedicated to the investigation in renewable energies and storage systems.

Since the center is not dedicated to the supplying of water to fields and the facilities are fully dedicated to research finalities, the 3 reservoirs are relatively smaller than in irrigation communities. Table 2.10 shows the characteristics of these reservoirs.

Table 2.10 – CEDER potential energy storage

Reservoir	Volume [m ³]	Average altitude [m]	Energy [MWh]
Reservoir R0	2 000	1 019	-
Reservoir R1	1 500	1 086	0,27
Reservoir R2	500	1 096	0,09

The pumping station is composed of 4 pumps of 7,5 kW each connected to reservoir 1 and 2. The pumps are connected to a common bus with the grid and a 16 kW PV plant. Furthermore, a turbine of 40 kW is installed in the same pumping station. Note that the pumping station can pump to the reservoir 1 or 2 but only can turbine from the reservoir 1, and reservoir 1 and 2 are connected through a pipe with a valve. A 90 kW flow battery with 400 kWh capacity is also present in the system. The system is represented in Figure 2.7.

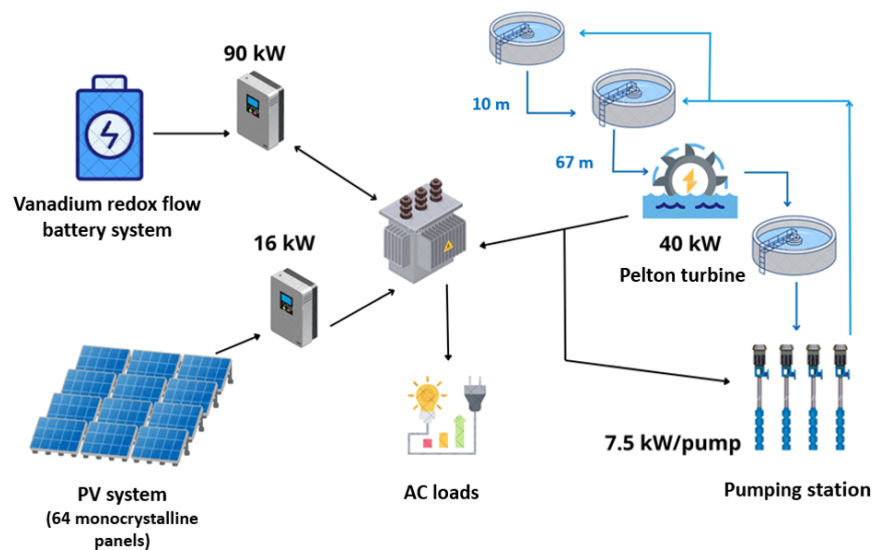


Figure 2.7 – CEDER-CIEMAT case schematic. Figure provided by CEDER-CIEMAT.

3 Optimisation and redesign for active role of irrigation systems as energy storage in the electrical grid

Currently, irrigation systems are viewed by the bulk power grid as energy demand points. Hence, the only form of interaction that occurs between these systems is limited to the unidirectional power flow from the grid to the pumping stations of the irrigation system. The demand profile of the pumping stations is correlated with the times when energy has a lower price (off-peak periods). However, the water stored in reservoirs at different heights can be regarded as a form of energy storage. In order to release the full potential of irrigation systems as grid-service providers, a redesign of the system components is required to increase its operational capacity.

Therefore, within the framework of this project, we analyse the potential capacity of reservoir-based irrigation systems to adopt an active role in the electrical grid providing services such as energy storage.

This chapter is structured as follows:

- i Section 3.1 introduces the topic and reviews the state of the art solutions.
- ii Section 3.2 introduces our approach.
- iii Section 3.3 describes the methodology and optimisation tool we developed to address the topic.
- iv Section 3.4 analyses several study cases applying the developed methodology.
- v Section 3.5 concludes the study and provides additional future research settled on the obtained results.

3.1 Introduction

Irrigation communities' water distribution systems may take many forms depending on whether they are pressurised or open canals and whether they use water storage in the form of reservoirs or deliver straight from the main water source. On this work, we focus on pump-fed reservoir-based irrigation systems. In such systems, a pumping station transfers water from the main source or an intermediate reservoir to a higher reservoir. From there, a series of canals or pipes deliver water to the users, usually by gravity.

The energy requirements for the pumping stations of these systems are significant, ranging from hundreds of MWh to GWh. These requirements can account for more than 70 % of their operating costs. In the Languedoc-Roussillon Regional Hydraulic Network (France) 95 % of the annual 80 GWh stem from pumping stations [37]. However, energy demand is characterised by a seasonal nature, with the system remaining close to inactive during winter months, when irrigation demand drops.

In several cases, irrigation communities decide to install solar photovoltaic (PV) pumping systems. On-site PV generation reduces energy consumption from the electrical grid or replaces diesel pumping systems.

Despite their potential, the role of irrigation systems as active players in the electricity grid has hardly been investigated or considered. As energy storage and demand response become increasingly relevant for grid stability [38], the unique characteristics of irrigation systems pose them as valuable providers of grid services.

To provide grid services, it is essential to maintain enough water in reservoirs, enabling the flexibility to shift energy consumption or even supply power back to the grid. Achieving this will require precise long-term planning and, if necessary, the replacement of specific assets of pumping stations.

3.1.1 State of the art

Previous works have addressed the matter of improving energy efficiency and reducing energy demand of irrigation systems. As noticed by [37], this can be achieved by optimising their design and operation and applying correcting measures, as well as using the existing infrastructure for energy production either from solar or hydraulic sources. Many different proposals can be found in the literature to exploit the potential that hydropower irrigation systems can provide. We classified these references according to whether they address reservoir-based energy storage, take advantage of the water flow running through open canals, or extract power from excess pressure on irrigation hydrants (Figure 3.1). Notice that several of them are located in Europe, which may suggest a localised raise of the interest on the topic but could also emerge from geographic research bias on funding, publication and recommendation [39] as well as our own bias.

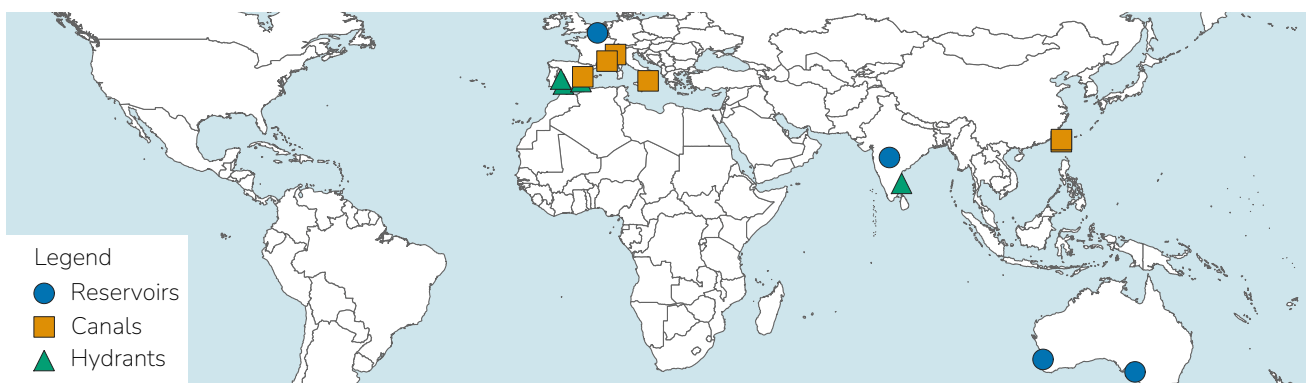


Figure 3.1 – Location of the state of the art references.

Reservoir-based energy storage

On the Vidarbha region (India), [40] estimated the capacity of 19 projects involving micro-hydro power generation on irrigation dams, with results ranging from 150 kW to 2 200 kW. On Froyennes (Belgium), [41] selected and tested a 30 kW pump running in reverse, or pump as turbine (PaT), with a variable frequency driver for a micro pumped-storage hydropower (PSH) facility. The facility consisted of two 650 m³ storm-water basins, a total of 110,2 kWp of PV peak power, four 2,4 kWp wind turbines and a centralised controller which integrated everything with a micro energy grid. On Perth (Australia), [42] developed and tested a two layer energy management system (EMS) for farmhouses to manage a PV-PSH facility and the scheduling of the irrigation system. The methodology comprised the utilisation of neural network models for the prediction of weather and demand, in combination with a genetic algorithm for cost minimisation. The EMS was verified on a system consisting on a 3,0 kW pump and a 0,768 kW

turbine. Same authors modelled on [43] a PSH system which was validated on an experimental setup. On the Mount Lofty Ranges (Australia), [44] developed a combined 3,0 kW PaT with PV for household demand storing water in irrigation reservoirs. They compared the performance of the analysed system to a commercial battery energy storage system and estimated the former levelised cost of storage (LCOS) to be 30 % lower than the latter. On Catalonia (Spain), we preliminarily analysed a simple irrigation system consisting of a single 13 000 m³ reservoir with a grid connected 110 kW pump and a 215,3 kWp PV pumping system and noticed it was feasible to run the system for energy storage in winter [45].

Flow on canals

On Chia-Nan (Taiwan), [46] elaborated a preliminary location analysis for turbine placement on irrigation canals and installed a 1,5 kW water wheel in a canal on Yunlin (Taiwan) [47]. On the Piedmont (Italy), [48] analysed the combined use of irrigation and hydroelectric production and estimated between 3,5 MW and 9,0 MW of extra combined hydraulic power could be obtained through the introduction of small hydropower plants in irrigation systems. As reported by [49], on the Canal de Provence (France) an agreement between the public company responsible for the water management and the main irrigators union made it possible to invest in a hydropower plant which uses the flow of the canal to generate 5 GWh annually. On Calabria (Italy), [50] developed a methodology and evaluated the placement of micro hydropower plants on irrigation systems' pipelines, calculating from 100 kW to 300 kW of feasible installed power on the analysed case study and noticing investment returns heavily depend on national subsidies for renewable energy. On Valencia (Spain), [51] analysed the deployment of Archimedes screw turbines to extract from 1 to 5 annual GWh from the canal.

Excess pressure on hydrants

On Andalusia (Spain), [52] validated, on a model, a methodology for PaT selection to extract the potential of excess pressure points and in [53] estimated a potential of 21,05 GWh per year on Sevilla and Córdoba (Spain) using the same power extraction method. On Vellore (India), [54] developed a pico hydropower generation system with a 0,74 kW induction motor to extract power directly from an irrigation hydrant to generate 150 W. On Córdoba (Spain), [55] analysed the environmental and economic impact of a 0,66 kWp PV with a 4 kW PaT system to recover energy from excess pressure and compared it to that of a 6 kVA diesel generator. The study concluded that the impacts are considerably lower for the novel system, even to that of a lone PV plant, but the corresponding battery highly contributes on the minerals and metals aspect of the environmental impact. On Alicante (Spain), [56] proposed an optimisation methodology and developed software to size and choose the best location of micro hydropower systems for irrigation systems, considering different configurations with floating PV, ground PV, PaT, battery energy storage and grid connection.

3.1.2 Objective

To our best knowledge, there is no open source software that can accurately analyse and optimise irrigation systems for active participation on the grid, considering not only the energy flow but also the bounds and feasible operating points of the hydraulics equipment. The main novel contribution of this work is the development of a multi-physics open source optimisation tool based in Python and utilising the Pyomo libraries [57, 58]. The tool facilitates the efficient and clear formulation of optimisation problems, by linking pre-defined models. The tool then invokes a numerical solver algorithm to compute a solution to the problem. The intricacies of the solver are not addressed in this document ¹. We presented an initial

¹Readers interested in the subject are referred to [59].

version of the optimisation methodology in [60], which was yet on an early stage of development. In this work, we have addressed the main scalability issues which allowed us to evaluate the performance of the tool through a real case study of an irrigation system located in the region of Catalonia, north-eastern Spain, and owned by the *Comunitat de Regants Segrià-Sud*. We have fixed errors and developed some features we considered necessary as well. Also, we analysed and estimated the potential energy storage capacity of the irrigation communities within the same region.

3.2 Approach

The proposed optimisation methodology is written in Python and built using the Pyomo library [57]. Pyomo is an open source Python-based software package for the formulation and analysis of optimisation models. In particular, we exploit its characteristic of structured modelling by means of blocks [58], which allows us to program the problem in an object-oriented environment.

The analysed case stems from an optimal pump scheduling and water-power flow problem which is NP-hard and requires convex and non-convex non-linear constraints and binary decision variables [61]. Therefore, the type of optimisation problem considered in this tool is contained in a mixed integer non-linear programming (MINLP) formulation expressed as follows:

$$\begin{aligned}
 & \underset{\mathbf{x}, \mathbf{b}}{\text{minimise}} && f(\mathbf{x}, t), \\
 & \text{subject to} && \mathbf{h}(\mathbf{x}, \mathbf{b}, t) = \mathbf{0}, \\
 & && \mathbf{g}(\mathbf{x}, \mathbf{b}, t) \leq \mathbf{0}, \\
 & && \mathbf{x} \in \mathcal{X}, \\
 & && \mathbf{b} \in \mathcal{B}, \\
 & && \forall t \in \{t_0, \dots, t_f\},
 \end{aligned} \tag{3.1}$$

where \mathbf{x} , \mathbf{b} represent the continuous and binary decision variables, which belong to the feasible regions \mathcal{X} and \mathcal{B} , respectively. The scalar variable t is an independent term that expresses the time defined in a time frame between the initial time t_0 and the final time t_f considered for the optimisation problem. $f(\cdot)$ is a scalar objective function. Finally, $\mathbf{h}(\cdot)$ and $\mathbf{g}(\cdot)$ are both sets of non-linear functions that define the constraints of the problem.

After testing several proposals, compiled in Section 3.2.1, the final decision was an object-oriented methodology through the use of the *Python* library *Pyomo* [57, 58, 62]. We identified an object-oriented approach as the most logical approach to solve the problem.

3.2.1 Other approaches / tested approaches

Before adopting the *Pyomo* object-oriented approach the following concepts were considered:

- Numerical resolution in Matlab [63]: After acknowledging how hydraulic machinery and devices operate, all the resulting equations and constraints were tested as a feasibility problem on Matlab interior point optimiser (IPOPT). Although it is fast to write code for simple and small problems, maintenance becomes an issue, especially for bigger problems.
- Scipy [64]: Both linear and non-linear examples were tested in the *Scipy Python* library, however it was finally discarded due to scalability issues and hard maintenance.



- Pyomo [57]: Within the research group is common to utilise the *Pyomo Python* library for optimisation problems. The first attempt was hard-coding the constraints, however using Sets supported multiple instances of predefined models. The later was however not satisfactory when connecting those models between them, since it required multiple matrices of binary values to define each mathematical relation. To bypass this annoyance we developed an automatic constraints' code writer based on *Python* classes.

3.3 Optimisation tool

The optimisation tool has a dual purpose of sizing and optimal scheduling. The former is to provide a sizing of new elements or a redesign of those already installed in the irrigation system. The latter is to arrange an optimal strategy of the system's operation, based on the current and newly sized elements characteristics and forecasting of the weather conditions, irrigation use and energy costs.

We conceptualised the methodology in an object-oriented structure using the Pyomo Network capabilities of the Pyomo Python library. Pyomo offers a modelling structure called *Block*. A block is defined as a container for organising a set of variables, parameters and constraints conceptually associated with a single entity, i.e. a sub-model. To generate the whole system, blocks may then be assembled with their corresponding parameters and connected between them using *Arcs*, which define relations between their variables.

In our application, the sub-model of a particular physical device encapsulated in a block contains the equations that define its steady-state operating characteristic. These equations can be algebraic or differential, although the latter are transformed into difference equations with a given sampling interval using a backward Euler formulation. Since the steady-state characteristic is defined for the whole system, rather than imposed by a single entity, we use arcs to share the value between the connected variables. Consider a set \mathcal{D} of $N_{\mathcal{D}}$ devices. Assume that any device has at least one time-dependant variable $x_{d_k}(t) \forall k \in \mathcal{D}$. Two types of relation can be established in such set using Pyomo Network's arcs:

- *Equality*: linked variables will be equated to each other,

$$x_{d_j}(t) = x_{d_i}(t) \quad \forall (i, j) \in \mathcal{D}. \quad (3.2)$$

- *Extensive*: linked variables will be balanced, i.e., the magnitude of the central device, for instance $j \in \mathcal{D}$, will be equal to the sum of the magnitudes of the devices connected to it,

$$x_{d_j}(t) = \sum_{i \in \mathcal{D}-j} x_{d_i}(t). \quad (3.3)$$

Within the scope of this tool, arcs connect hydraulic or electrical variables. For example a block of a pump would contain variables for *head* and *flow*, which would be connected with equality and extensive relations respectively.

The set of inequality constraints and part of the set of equality constraints of the problem are defined by the equations determining the individual behaviour of each element, which are contained in the declared blocks. The rest of the equality constraints are defined by arcs connecting blocks. The feasibility domain is then defined once all the blocks and arcs that constitute the system are declared.

3.3.1 Device models

The application considers the following electrical and hydraulic devices which are present or relevant in irrigation systems.

Source of water flow

Delivers a defined flow of water $Q(t)$. Consider it as the hydraulic equivalent of a current source or as a pump with a constant flow-head characteristic. Sources are used as known water consumption, such as irrigation demands or weather conditions in the form of evaporation and rainfall. Inlet and outlet flows of the i -th source, $Q_{in,i} \in \mathbb{R}$ and $Q_{out,i} \in \mathbb{R}$ (m^3/s), are defined positive if exiting the device and both connect with (3.3). The flow delivered by the i -th source is defined as $Q_i(t)$ (m^3/s), then:

$$Q_{out,i}(t) = Q_i(t) \quad (3.4)$$

$$Q_{in,i}(t) = -Q_i(t) \quad (3.5)$$

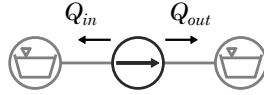


Figure 3.2 – Definition of the variables of a source. In favour of visual exemplification the source connects to two reservoirs, depicted in lighter tone.

Source of water flow summary

Variables:

- Flow (in):
 $Q_{in,i} \in \mathbb{R}$. Connection: (3.3)
- Flow (out):
 $Q_{out,i} \in \mathbb{R}$. Connection: (3.3)

Constraints:

- Inlet flow (3.5):
 $Q_{in,i}(t) = -Q_i(t)$
- Outlet flow (3.4):
 $Q_{out,i}(t) = Q_i(t)$

Reservoir

Conceived as water storage to provide water to users. The variables that define the i -th reservoir are flow $Q_i \in \mathbb{R}$ (m^3/s), defined positive if entering the reservoir, volume $W_i \in [W_i, \overline{W}_i]$ (m^3) and height $z_i \in [z_i, \overline{z}_i]$ (m). Flow connects with (3.3) and height connects with (3.2). Volume boundaries at final time may be defined independently to impose a certain condition such as a cycle $W_i(t = t_f) \in [W_{f,i}, \overline{W}_{f,i}]$. An initial volume is set with $W_{i,0}$ (m^3). Volume variation constraint is discretised using the backward Euler method (3.6). Water height is simplified as a linear interpolation function of the volume (3.7).

$$\begin{cases} W_i(t) = W_i(t - \Delta t) + \Delta t Q_i(t) & \text{if } t > t_0 \\ W_i(t) = W_{i,0} + \Delta t Q_i(t) & \text{otherwise} \end{cases} \quad (3.6)$$

$$z_i(t) = \frac{W_i(t) - W_i}{\overline{W}_i - W_i} (\overline{z}_i - z_i) + z_i \quad (3.7)$$

Reservoir summary

Variables:

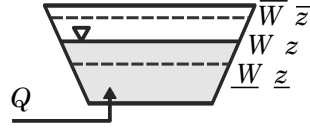


Figure 3.3 – Reservoir definition

- Flow (positive if *in*):
 $\mathbf{Q}_i \in \mathbb{R}$. Connection: (3.3)
- Volume:
 $\mathbf{W}_i \in [\underline{W}_i, \overline{W}_i]$
- Height:
 $\mathbf{z}_i \in [\underline{z}_i, \overline{z}_i]$. Connection: (3.2)

Constraints:

- Volume variation (3.6):

$$\begin{cases} W_i(t) = W_i(t - \Delta t) + \Delta t Q_i(t) & \text{if } t > t_0 \\ W_i(t) = W_{0,i} + \Delta t Q_i(t) & \text{otherwise} \end{cases}$$
- Height variation (3.7):

$$z_i(t) = \frac{W_i(t) - \underline{W}_i}{\overline{W}_i - \underline{W}_i} (\overline{z}_i - \underline{z}_i) + \underline{z}_i$$

Pipe

Connects hydraulic devices and transports water between reservoirs. The variables that define the *i*-th pipe are total flow $\mathbf{Q}_i \in [-\overline{Q}_i, \overline{Q}_i]$ (m³/s), defined positive from lower to higher ground (Figure 3.4), positive flow $\mathbf{Q}_{p,i} \in [0, \overline{Q}_i]$ (m³/s), negative flow $\mathbf{Q}_{n,i} \in [0, \overline{Q}_i]$ (m³/s), dynamic head $\mathbf{H}_i \geq 0$ (m), lower end height $\mathbf{z}_{low,i} \geq 0$ (m) and higher end height $\mathbf{z}_{high,i} \geq 0$ (m). Flow connects with (3.3) while head and heights connect with (3.2). The dynamic head of the system considers a quadratic expression in terms of flow, which may be positive or negative depending on its direction (3.8) (Figure 3.5), where K_i is the linear pressure loss coefficient of the hydraulic circuit. To model this sign function behaviour we defined positive and negative flow as variables constrained by (3.9) and (3.10). Additionally, if the difference of heights between reservoirs is considerably larger than their depth, the term $z_{high,i}(t) - z_{low,i}(t)$ can be assumed constant in (3.8).

$$H_i(t) = z_{high,i}(t) - z_{low,i}(t) + K_i \left[(Q_{p,i}(t))^2 - (Q_{n,i}(t))^2 \right] \quad (3.8)$$

$$Q_i(t) = Q_{p,i}(t) - Q_{n,i}(t) \quad (3.9)$$

$$0 = Q_{p,i}(t) Q_{n,i}(t) \quad (3.10)$$

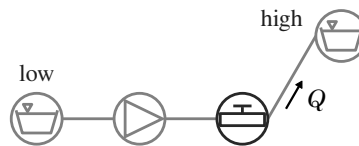


Figure 3.4 – Definition of the flow direction in a pipe device

Pipe summary

Variables:

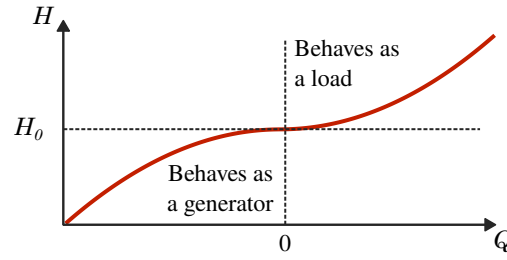


Figure 3.5 – Characteristic curve of a pipe

- Flow (positive from *low* to *high*):
 $\mathbf{Q}_i \in [-\bar{Q}_i, \bar{Q}_i]$. Connection: (3.3)
- Positive flow (from *low* to *high*):
 $\mathbf{Q}_{p,i} \in [0, \bar{Q}_i]$
- Negative flow (from *high* to *low*):
 $\mathbf{Q}_{n,i} \in [0, \bar{Q}_i]$
- Pressure difference:
 $\mathbf{H}_i \geq 0$. Connection: (3.2)
- Height (lower end):
 $\mathbf{z}_{low,i} \geq 0$. Connection: (3.2)
- Height (higher end):
 $\mathbf{z}_{high,i} \geq 0$. Connection: (3.2)

Constraints:

- Pressure (3.8):

$$H_i(t) = H_{0,i}(t) + K_i \left[(Q_{p,i}(t))^2 - (Q_{n,i}(t))^2 \right]$$
- Total flow (3.9):

$$Q_i(t) = Q_{p,i}(t) - Q_{n,i}(t)$$
- Flow coherence (3.10):

$$0 = Q_{p,i}(t) Q_{n,i}(t)$$

Pump

Converts electrical power into hydraulic power using an electric motor. We consider the association of a motor and a pump as a single device. The variables that define the i -th pump are inlet and outlet flows $\mathbf{Q}_{in,i} \in [-\bar{Q}_i, 0]$ and $\mathbf{Q}_{out,i} \in [0, \bar{Q}_i]$ (m^3/s), defined positive if exiting the pump, dynamic head $\mathbf{H}_i \in [0, A_i]$ (m), hydraulic power $\mathbf{p}_{h,i} \in [0, \bar{p}_{h,i}]$ (W), electric power $\mathbf{p}_{e,i} \in [0, \bar{p}_{e,i}]$ (W), defined positive if consumed (Figure 3.6), and a binary variable to determine whether the pump is ON or OFF $\beta_{ON,i} \in \{0, 1\}$. Flows and electric power connect with (3.3) while head connects with (3.2). Pumps are characterised by its head-flow curve, determined by coefficients A_i and B_i , and efficiency η_i , which we assumed constant in the operating range. Since we consider variable speed pumps, we can use the inequality (3.11) proposed by [65] which reduces the hardness of the optimisation problem. In such constraint \bar{n}_i (rpm) is the maximum allowed rotational speed and $n_{N,i}$ (rpm) the nominal rotational speed. Constraints (3.12) and (3.13) define the operating range of the pump and determine its state. The hydraulic power is defined as

(3.14) and the required electrical power as (3.15). Dynamic head of a pump should be connected to that of a pipe, then an operating point or region is defined for both as depicted in Figure 3.7.

$$H_i(t) \leq \left(\frac{\bar{n}_i}{n_{N,i}} \right)^2 A_i - B_i (Q_{out,i}(t))^2 \quad (3.11)$$

$$Q_{in,i}(t) = -Q_{out,i}(t) \quad (3.12)$$

$$\beta_{ON,i}(t) \underline{Q}_i \leq Q_i(t) \leq \beta_{ON,i}(t) \bar{Q}_i \quad (3.13)$$

$$p_{h,i}(t) = \rho g Q_i(t) H_i(t) \quad (3.14)$$

$$p_{e,i}(t) \eta_i = p_{h,i}(t) \quad (3.15)$$

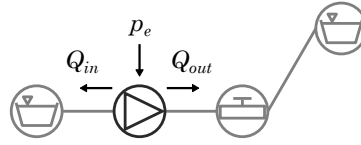


Figure 3.6 – Definition of the flow and electric power direction in a pump device

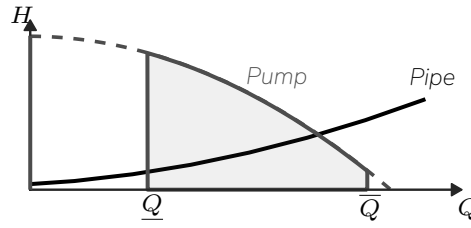


Figure 3.7 – Operating region of a variable speed pump.

Pump summary

Variables:

- Flow (inlet):
 $\mathbf{Q}_{in,i} \in [-\bar{Q}_i, 0]$. Connection: (3.3)
- Flow (outlet):
 $\mathbf{Q}_{out,i} \in [0, \bar{Q}_i]$. Connection: (3.3)
- Head:
 $\mathbf{H}_i \in [0, A_i]$. Connection: (3.2)
- Hydraulic power:
 $\mathbf{P}_{h,i} \in [0, \bar{P}_{h,i}]$
- Electric power:
 $\mathbf{P}_{e,i} \in [0, \bar{P}_{e,i}]$. Connection: (3.3)
- Pump ON:
 $\beta_{ON,i} \in \{0, 1\}$

Constraints:

- Pressure (3.11):
 $H_i(t) \leq A_i - B_i (Q_{out,i}(t))^2$
- Flow coherence (3.12):
 $Q_{in,i}(t) = -Q_{out,i}(t)$

- Hydraulic power (3.14):
 $p_{h,i}(t) = \rho g Q_i(t) H_i(t)$
- Electrical power (3.15):
 $p_{e,i}(t) \eta_i = p_{h,i}(t)$
- Flow limits (3.13):
 $\beta_{ON,i}(t) \underline{Q}_i \leq Q_i(t) \leq \beta_{ON,i}(t) \bar{Q}_i$

Pump (linear approximation)

Quadratic expressions can increase the computational cost of the problem, as seen in the H - Q characteristic curve in the pump model. Therefore, relaxing this expression is an interesting approach.

Previously, the relaxation of the same expression was achieved by substituting the equality constraint with an inequality constraint in the H - Q expression, allowing the elimination of the variable representing the pump speed, as suggested in [65]. Thanks to this improvement, it is now possible to construct a pump model where the quadratic expression is replaced with a linear approximation while maintaining the inequality constraint.

For a better approximation of the original curve, the method divides the space between \underline{Q}_i and \bar{Q}_i into $N_{L,i}$ intervals, fixing these points on the original curve. Then, a constraint is formulated for each line using an inequality, ensuring that the operating area lies below the approximation and, therefore, below the original curve—without requiring any binary variables.

Figure 3.8 illustrates an example of this approximation using three equidistant intervals, along with the operating area for the optimisation problem.

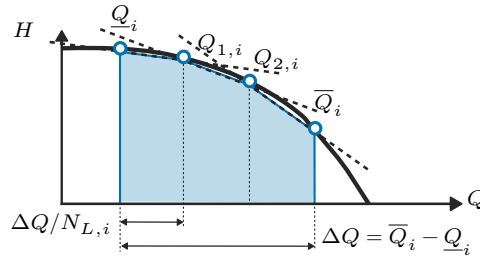


Figure 3.8 – Operating region of linear approximation model

The constraints are built by using the following expressions:

$$H_{l,i}(t) \leq \frac{H_{l+1,i} - H_{l,i}}{Q_{l+1,i} - Q_{l,i}} (Q_{out,i}(t) - Q_{l,i}) + H_{l,i} \quad l = 1, \dots, N_L \quad (3.16)$$

$$Q_{l,i} = \underline{Q}_i + l \frac{\bar{Q}_i - \underline{Q}_i}{N_{L,i}} \quad l = 1, \dots, N_L \quad (3.17)$$

$$H_{l,i} = \left(\frac{\bar{n}_i}{n_{N,i}} \right)^2 A_i - B_i (Q_{l,i}(t))^2 \quad l = 1, \dots, N_L \quad (3.18)$$

Constraint (3.16) represents the line that approximates the curve, while (3.17) is used to calculate the key points that minimize the error. Finally, (3.18) projects the key flow points onto the original nominal curve of the pump.

With the modification the variables and parameters are:

Linear Pump summary

Variables:

- Flow (inlet):
 $\mathbf{Q}_{in,i} \in [-\bar{Q}_i, 0]$. Connection: (3.3)
- Flow (outlet):
 $\mathbf{Q}_{out,i} \in [0, \bar{Q}_i]$. Connection: (3.3)
- Head:
 $\mathbf{H}_i \in [0, A_i]$. Connection: (3.2)
- Hydraulic power:
 $\mathbf{P}_{h,i} \in [0, \bar{p}_{h,i}]$
- Electric power:
 $\mathbf{P}_{e,i} \in [0, \bar{p}_{e,i}]$. Connection: (3.3)
- Pump ON:
 $\beta_{ON,i} \in \{0, 1\}$

Constraints:

- Pressure (3.16):
$$H_{l,i}(t) \leq \frac{H_{l+1,i} - H_{l,i}}{Q_{l+1,i} - Q_{l,i}} (Q_{out,i}(t) - Q_{l,i}) + H_{l,i} \quad l = 1, \dots, N_L$$
- Flow key points (3.17):
$$Q_{l,i} = \underline{Q}_i + l \frac{\bar{Q}_i - \underline{Q}_i}{N_{L,i}} \quad l = 1, \dots, N_L$$
- Flow points projection (3.18):
$$H_{l,i} = \left(\frac{\bar{n}_i}{n_{N,i}} \right)^2 A_i - B_i (Q_{l,i}(t))^2 \quad l = 1, \dots, N_L$$
- Flow coherence (3.12):
$$Q_{in,i}(t) = -Q_{out,i}(t)$$
- Hydraulic power (3.14):
$$p_{h,i}(t) = \rho g Q_i(t) H_i(t)$$
- Electrical power (3.15):
$$p_{e,i}(t) \eta_i = p_{h,i}(t)$$
- Flow limits (3.13):
$$\beta_{ON,i}(t) \underline{Q}_i \leq Q_i(t) \leq \beta_{ON,i}(t) \bar{Q}_i$$

Pump (sizing)

Sizes and sets up a new pump. Since new turbo-machinery are designed ad hoc, we consider their rated electrical power as the decision variable $p_{dim,i}$ (W). The variables that define the i -th new pump are inlet and outlet flows $\mathbf{Q}_{in,i} \in [-\bar{Q}_i, 0]$ and $\mathbf{Q}_{out,i} \in [0, \bar{Q}_i]$ (m^3/s), defined positive if exiting the pump, dynamic head $\mathbf{H}_i \geq 0$ (m), hydraulic power $\mathbf{P}_{h,i} \in [0, \bar{p}_{h,i}]$ (W) and electric power $\mathbf{P}_{e,i} \in [0, \bar{p}_{e,i}]$ (W). Flows and electric power connect with (3.3) while head connects with (3.2). We assume no further information on

the pump is available, then it is characterised just by its forecasted average efficiency η_i and formulated with (3.12), (3.14), (3.15) and (3.19).

$$p_{dim,i} \geq p_{e,i}(t) \quad (3.19)$$

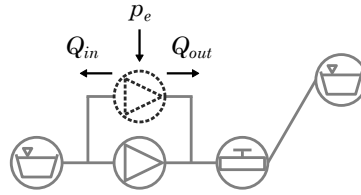


Figure 3.9 – Definition of the flow and electric power direction in a new pump device

Pump (sizing) summary

Variables:

- Sized power:
 $p_{dim,i} \in [0, \bar{p}_{dim,i}]$
- Flow (inlet):
 $\mathbf{Q}_{in,i} \in [-\bar{Q}_i, 0]$. Connection: (3.3)
- Flow (outlet):
 $\mathbf{Q}_{out,i} \in [0, \bar{Q}_i]$. Connection: (3.3)
- Head:
 $\mathbf{H}_i \geq 0$. Connection: (3.2)
- Hydraulic power:
 $\mathbf{p}_{h,i} \in [0, \bar{p}_{h,i}]$
- Electric power:
 $\mathbf{p}_{e,i} \in [0, \bar{p}_{e,i}]$. Connection: (3.3)

Constraints:

- Sizing (3.19):
 $p_{dim,i} \geq p_{e,i}(t)$
- Flow coherence (3.12):
 $Q_{in,i}(t) = -Q_{out,i}(t)$
- Hydraulic power (3.14):
 $p_{h,i}(t) = \rho g Q_i(t) H_i(t)$
- Electrical power (3.15):
 $p_{e,i}(t) \eta_i = p_{h,i}(t)$

Turbine (sizing)

Converts hydraulic power into rotational mechanical power and then to electric power through the use of mechanically coupled generators. Since no turbines are currently present in the system, we modelled them following a sizing approach as well. The variables that define the i -th new turbine are inlet and outlet flows $\mathbf{Q}_{in,i} \in [-\bar{Q}_i, 0]$ and $\mathbf{Q}_{out,i} \in [0, \bar{Q}_i]$ (m^3/s), defined positive if exiting the turbine, dynamic head $\mathbf{H}_i \geq 0$ (m), hydraulic power $\mathbf{p}_{h,i} \in [-\bar{p}_{h,i}, 0]$ (W) and electric power $\mathbf{p}_{e,i} \in [-\bar{p}_{e,i}, 0]$ (W), defined positive if consumed. Flows and electric power connect with (3.3) while head connects with (3.2). We assume no further information on the turbine is available, then it is characterised just by its forecasted

average efficiency η_i and formulated with (3.12), (3.14), (3.20) and (3.21). The turbine is considered to be operated with adjustable speed, which allows for a greater range of operation and is specially convenient to extract power from irrigation reservoirs [66].

$$p_{e,i}(t) = p_{h,i}(t)\eta_i \quad (3.20)$$

$$p_{dim,i} \geq -p_{e,i}(t) \quad (3.21)$$

Constraint (3.14) involves a product of two variables. To reduce the complexity of the problem we propose the following approximation:

$$p_{h,i}(t) = \rho g Q_{in,i}(t) \hat{H}_i, \quad (3.22)$$

where \hat{H} (m) is the estimation of the dynamic head and can be determined, for instance, as

$$\hat{H}_i = \Delta z_i - \left(\frac{\bar{p}_{h,i}}{\rho g \Delta z_i} \right)^2, \quad (3.23)$$

with Δz_i (m) the difference of heights between the reservoirs the turbine operates with.

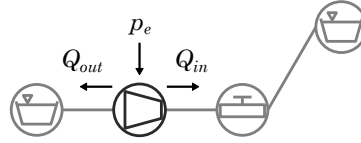


Figure 3.10 – Definition of the flow and electric power direction in a turbine device

Turbine summary

Variables:

- Sized power:
 $p_{dim,i} \in [0, \bar{p}_{dim,i}]$
- Flow (inlet):
 $Q_{in,i} \in [-\bar{Q}_i, 0]$. Connection: (3.3)
- Flow (outlet):
 $Q_{out,i} \in [0, \bar{Q}_i]$. Connection: (3.3)
- Head:
 $H_i \geq 0$. Connection: (3.2)
- Hydraulic power:
 $P_{h,i} \in [-\bar{p}_{h,i}, 0]$
- Electric power:
 $P_{e,i} \in [-\bar{p}_{e,i}, 0]$. Connection: (3.3)

Constraints:

- Sizing (3.21):
 $p_{dim,i} \geq -p_{e,i}(t)$
- Flow coherence (3.12):
 $Q_{in,i}(t) = -Q_{out,i}(t)$
- Hydraulic power (3.14):
 $p_{h,i}(t) = \rho g Q_{in,i}(t) H_i(t)$
- Electrical power (3.20):
 $p_{e,i}(t) = p_{h,i}(t) \eta_i$



Pump as turbine (PaT)

Pumps as turbines is a controversial topic on hydraulics and hydropower. Extracting power with the application of a pump instead of a turbine is an easily implementable and economical solution for small hydropower purposes [67]. Defining their characteristics is still a complex and complicated problem and requires data that is usually not available. However, other authors' work analysing and reviewing pumps working as turbines proved useful to us when defining their behaviour in the optimisation model. In [68] the authors reviewed PaT performance prediction and stability literature and [41] implemented a 30 kW PaT with a variable frequency driver on their storm-water basin based micro energy grid. From this works we extracted that single stage centrifugal PaTs are the most recommended, pump geometry is a fundamental parameter to predict the performance of it working as a turbine, the performance of PaTs may range from 50 to 80 %, and that operating the PaT with a variable frequency driver increases its operating range and may rise its efficiency to closely match that of working in pump mode. The optimisation tool does not consider an explicit device for a PaT, but its implementation can be achieved by defining a pump and a turbine properly connected in parallel, as exemplified in [45].

Energy balance node

All equipment that consumes or delivers electrical power, p_e (W), are connected to energy balance nodes which aggregate and distribute the power among the connected devices. For a set of electrical devices \mathcal{X} connected to the same energy balance node, the balance imposed is

$$\sum_{x \in \mathcal{X}} p_{e,x}(t) = 0. \quad (3.24)$$

Energy balance node summary

Variables:

- None

Constraints:

- Power balance (3.24):

$$\sum_{x \in \mathcal{X}} p_{e,x}(t) = 0$$

Electrical grid

Delivers or accepts electrical power from connected devices. We modelled the grid as an ideal voltage source limited by the maximum power of the connection, which may be either a physical or a legal constraint. The variables that define the i -th grid are the total power $\mathbf{p}_i \in [-\bar{p}_i, \bar{p}_i]$ (W) and the powers flowing from and to the grid $\mathbf{p}_{\text{from},i} \in [0, \bar{p}_i]$ $\mathbf{p}_{\text{to},i} \in [0, \bar{p}_i]$ (W), defined positive if consumed. Total electric power connects with (3.3). A grid device is governed by its own power balance (3.25) and, additionally, a boundary may be set on a specific timestamp t_c to represent a contractual restriction (3.26).

$$p_i(t) = p_{\text{from},i}(t) - p_{\text{to},i}(t) \quad (3.25)$$

$$p_i(t_c) \leq \bar{p}_{i,t_c} \quad (3.26)$$

Electrical grid summary

Variables:

- Power (total):
 $\mathbf{p}_i \in [-\bar{p}_i, \bar{p}_i]$. Connection: (3.3)
- Power (from):
 $\mathbf{p}_{\text{from},i} \in [0, \bar{p}_i]$
- Power (to):
 $\mathbf{p}_{\text{to},i} \in [0, \bar{p}_i]$

Constraints:

- Power balance (3.25):
 $p_i(t) = p_{\text{from},i}(t) - p_{\text{to},i}(t)$

Solar PV

Converts irradiance into electrical power. The amount of power it can generate depends on the size of the plant $p_{\text{inst},i}$ (W), the efficiency of the converter η_i and the weather conditions, i.e. the irradiance level $G_i(t)$ (W/m²). We consider the size of the plant may be increased. The variables that define the i -th PV plant are the generated power $\mathbf{p}_i \in [-\bar{p}_i, 0]$ (W), defined positive if consumed, and the new sized power $p_{\text{dim},i} \in [0, \bar{p}_i - p_{\text{inst},i}]$ (W). Generated electric power connects with (3.3). The generated power is defined with (3.27) where the meteorological forecast m_{forecast} values are expressed in per unit as (3.28).

$$p_i(t) \geq -(p_{\text{inst},i} + p_{\text{dim},i}) m_{\text{forecast}}(t) \eta_i \quad (3.27)$$

$$m_{\text{forecast}}(t) = \frac{G_i(t)}{1000} \quad (3.28)$$

Solar PV summary

Variables:

- Power:
 $\mathbf{p}_i \in [-\bar{p}_i, 0]$. Connection: (3.3)
- New sized power:
 $p_{\text{dim},i} \in [0, \bar{p}_i - p_{\text{inst},i}]$

Constraints:

- Power balance (3.27):
 $p_i(t) \geq p_{\text{from},i}(t) - p_{\text{to},i}(t)$

Battery (sizing)

Stores energy from an electrical source. Our optimisation problem considers the sizing of new batteries. The variables that define the i -th battery are the total power transfer $\mathbf{p}_i \in [-\bar{p}_i, \bar{p}_i]$ (W), defined positive if consumed, the charge and discharge power $\mathbf{p}_{\text{ch},i} \in [0, \bar{p}_i]$ $\mathbf{p}_{\text{dc},i} \in [0, \bar{p}_i]$ (W), the stored energy $\mathbf{E}_i \in [0, \bar{E}_i \overline{SOC}_i]$ (Wh) and the sized power $p_{\text{dim},i} \in [0, \bar{p}_i]$ (W) and capacity $E_{\text{dim},i} \in [0, \bar{E}_i]$ (Wh). Electric power connects with (3.3). The sized power limits the charge, discharge and total power (3.29), (3.30), (3.31) and the sized capacity limits the energy stored through the state of charge bounds $SOC_i \in [\underline{SOC}_i, \overline{SOC}_i]$ (3.32), (3.33). Energy stored variation constraint is discretised using the backward Euler method considering the charge and discharge efficiencies $\eta_{\text{ch},i}$ $\eta_{\text{dc},i}$ (3.34).

$$p_i(t) = p_{ch,i}(t) - p_{dc,i}(t) \quad (3.29)$$

$$p_{ch,i}(t) \leq p_{dim,i} \quad (3.30)$$

$$p_{dc,i}(t) \leq p_{dim,i} \quad (3.31)$$

$$E_i(t) \leq E_{dim,i} \overline{SOC}_i \quad (3.32)$$

$$E_i(t) \geq E_{dim,i} \underline{SOC}_i \quad (3.33)$$

$$\begin{cases} E_i(t) = E_i(t - \Delta t) + \Delta t(p_{ch,i}(t) \eta_{ch,i} - p_{dc,i}(t) \eta_{dc,i}) & \text{if } t > t_0 \\ E_i(t) = E_i(t = t_f) + \Delta t(p_{ch,i}(t) \eta_{ch,i} - p_{dc,i}(t) \eta_{dc,i}) & \text{otherwise} \end{cases} \quad (3.34)$$

Battery summary

Variables:

- Power:
 $\mathbf{p}_i \in [-\bar{p}_i, \bar{p}_i]$. Connection: (3.3)
- Charging power:
 $\mathbf{p}_{ch,i} \in [0, \bar{p}_i]$
- Discharging power:
 $\mathbf{p}_{dc,i} \in [0, \bar{p}_i]$
- Energy stored:
 $\mathbf{E}_i \in [0, \bar{E}_i \overline{SOC}_i]$
- New sized power:
 $p_{dim,i} \in [0, \bar{p}_i]$
- New sized capacity:
 $E_{dim,i} \in [0, \bar{E}_i]$

Constraints:

- Power balance (3.29):
 $p_i(t) \geq p_{ch,i}(t) - p_{dc,i}(t)$
- Charging power limit (3.30):
 $p_{ch,i}(t) \leq p_{dim,i}$
- Discharging power limit (3.31):
 $p_{dc,i}(t) \leq p_{dim,i}$
- Maximum charge (3.32):
 $E_i(t) \leq E_{dim,i} \overline{SOC}_i$
- Minimum charge (3.33):
 $E_i(t) \geq E_{dim,i} \underline{SOC}_i$
- Stored energy (3.34):
 $\begin{cases} E_i(t) = E_i(t - \Delta t) + \Delta t(p_{ch,i}(t) \eta_{ch,i} - p_{dc,i}(t) \eta_{dc,i}) & \text{if } t > t_0 \\ E_i(t) = E_i(t = t_f) + \Delta t(p_{ch,i}(t) \eta_{ch,i} - p_{dc,i}(t) \eta_{dc,i}) & \text{otherwise} \end{cases}$

3.3.2 Objective function

We are interested in two main objectives of this optimisation problem: an optimal average daily planing strategy to minimize the operational cost while providing storage services to the grid and satisfying the irrigation demand; and an optimal sizing of new elements (e.g batteries, pumps, turbines) or redesign of the already installed elements (e.g PV plants), to minimize the sum of the operating costs C_{op} (€) and capital costs C_{cap} (€) (3.35). Operating costs may consider the energy exchanges with the grid and other maintenance costs while capital costs account for the additional installed capacity of the new elements.

$$f(\cdot) = C_{op} + C_{cap} \quad (3.35)$$

The objective function is further detailed in the particular study cases along Section 3.4.

We also defined an objective function from the perspective of the administration or a grid operator with the purpose of reducing the overall greenhouse gas (GHG) emissions of the grid. Instead of defining operation costs in monetary value we applied the emission factor of the grid to the energy exchanges with the grid. This objective function assumes an average behaviour of the grid and does not distinguish the technologies participating in the daily market. Further details are given in the particular study case in Section 3.4.3.

3.3.3 Solving the problem

To solve the optimisation problem a suitable optimisation algorithm is required. We have achieved successful results with the following free open source software:

- Couenne: branch and bound algorithm <https://github.com/coin-or/Couenne>.
- Bonmin: Bonmin (Basic Open-source Nonlinear Mixed INteger programming) is an open-source solver for MINLP problems <https://github.com/coin-or/Bonmin>. It incorporates different algorithms to solve the models: Branch and bound (B-BB) is the simplest and default algorithm, based on solving a continuous non-linear program at each node of the search tree and branching on variables [69]. Outer approximation decomposition (B-OA), introduced first in [70] and [71], is implemented using *lpopt* to solve the non-linear programming (NLP) problems and *Cbc* to solve the mixed-integer linear programming (MILP) problems. The Quesada and Grossman branch and cut (B-QG) algorithm, presented in [72], consists of an algorithm to solve convex MINLP problems based on LP and NLP sub-problems, by avoiding the sequential solution of NLP sub-problems and MILP master problems, that is required in the standard implementation of the generalized Benders decomposition (GBD) and B-OA algorithms, achieving up to an 84 % reduction of the number of nodes that need to be examined. The hybrid outer approximation based in branch-and-cut (B-Hyb) solves more NLPs to reduce the size of the tree, by reducing the algorithm to the classical NLP B-BB and the B-OA algorithm [70]. The outer-approximation based branch-and-cut with specific configuration (B-ECP) algorithm is based on the B-QG algorithm but implementing a linearization-based algorithm [73]. Finally, the iterated feasibility pump algorithm (B-iPF) combines between solving NLP and MILP problems [70].
- Interior Point Optimizer (IPOPT): interior point algorithm to find local solutions to non-linear optimisation problems <https://github.com/coin-or/Ipopt>. It is a non-linear programming (NLP) solver so it is only suitable when no binary variables are present among the problem.

3.3.4 Scalability

This section details the performance and scalability issues the methodology is and has been subject to, as well as some approaches we attempted to reduce their effect:

- Binary and non-linear problem: the introduction of non-linearities and binary variables from hydraulics' behaviour makes the analysis a MINLP problem. Non-linearities arise from the quadratic characteristic curves of pipes and pumps (3.8) (3.11) and hydraulic power computation (3.14), which is implicitly cubic. We required binary variables to model whether a pump is active (3.13). The linearised pump approach (3.16) and the approximation of the turbines' dynamic head (3.22) address non-linearities regarding pumps and turbines. However, further work is required to reduce the remaining definitions.
- Dynamics: We approached time dependency and dynamics of the reservoir and battery devices (3.6) (3.34) following an Euler discretisation methodology, such that the formulation preserves simplicity.
- Time period: Even relatively small irrigation systems require considerable computational power and robust algorithms to be optimised for time periods considering 24 or 48 hours. Such a methodology does not have (yet) the capability to solve big systems for 8 760 hours to consider a full year. We have addressed this issue in the study cases by analysing two reference days, then extracting conclusions for the full year.
- Large systems: systems with a large number of non-linear devices such as pumps, pipes or turbines, are demanding or even intractable for the solver's algorithm. Although this issue has been dampened by linearising some hydraulic constraints, it is still a very present issue.
- Initialisation: the ability to find global optimum or even find a solution is highly dependent on the initialisation values of the variables. This is specially relevant on large systems. Fixing the values of variables with prior knowledge does also help to reach global minimum solutions.

Relaxation results

In this section we show the results from testing three modelling strategies for the pump device: considering an *equality* quadratic characteristic curve constraint, *inequality* characteristic curve constraint (3.11) and *linearizing* the characteristic curve expression (3.16). Furthermore, we explore several Bonmin solver algorithms for the different optimisation problems: Quesada and Grossman (B-QG), Branch and Bound (B-BB), Extended Cutting Plane (B-ECP) and Outer Approximation (B-OA); which were the algorithms that performed the best in the analysed problems.

Section 3.3.1 compresses all of the definitions and relaxations, however below follows a quick summary to introduce the results:

The head expression of a variable speed pump is given by a quadratic constraint, both in terms of flow and rotational speed. For the i -th pump, at time t :

$$H_i(t) = (n_i(t))^2 A_i - B_i (Q_{out,i}(t))^2 .$$

In [61] is proposed to transform the previous expression into an inequality. This modification sets the working area of the pump and allows for the removal of the rotational speed variable $n_i(t)$:

$$H_i(t) \leq \bar{n}_i^2 A_i - B_i (Q_{out,i}(t))^2 .$$

The previous relaxation supports a linear approximation. This can be achieved by generating a piecewise function of N_L linear functions that approximate the curve inside the working limit of the pump $[Q_i, \bar{Q}_i]$. This approach does not only reduce the complexity of the dynamic head expression but of the hydraulic power as well.

To reduce the impact of the approximation in the solution and ensure that the model returns inside the actual dynamic head curve we took a conservative approach by setting the linear approximation below it. A linear constraint is built per each segment that approximates the curve, each consisting in an inequality to avoid using binary variables as in a regular piecewise function:

$$H_{l,i}(t) \leq \frac{H_{l+1,i} - H_{l,i}}{Q_{l+1,i} - Q_{l,i}} (Q_{out,i}(t) - Q_{l,i}) + H_{l,i} \quad l = 1, \dots, N_L.$$

Therefore, by incorporating the approximation we replace a quadratic constraint for N_L linear constraints and 2 extra variables per step time of optimisation.

$$Q_{l,i} = \underline{Q}_i + l \frac{\bar{Q}_i - \underline{Q}_i}{N_{L,i}} \quad l = 1, \dots, N_L$$

$$H_{l,i} = \bar{n}_i^2 A_i - B_i (Q_{l,i})^2 \quad l = 1, \dots, N_L$$

Therefore, by applying this we do not use a quadratic expression but we add N_L constraints and 2 extra variables per time step to the problem.

We tested 5 different systems with 6 different algorithms: Case C0 is explained in detail in Section 3.4.1 and the remaining 4 in Section 3.4.2. Case C0 considers 5 time steps and consists on a two reservoir system with two pumps, one turbine, a PV system connected to the grid and the sizing of a possible battery. The original execution time was 16.75 seconds. Cases C1, C2, C3 and C4 consist in two 24 hour typical averaged days (for a total of 48 time steps), one for summer and one for winter, over a system with two reservoirs, a grid connected pump and a PV pump which is not connected to the grid. Case C2 considers a pump as a turbine, in case C3 the PV plant is connected to the grid as well and case C4 optimises the operation of the system with both the PV plant connected to the grid and a pump running as a turbine. The source of the data used to analyse this system is a real case scenario near the Ebre river in the region of Catalunya (Spain). The original execution times were 9 minutes, 12 minutes, 65 minutes and 7 minutes respectively.

We measured the performance of the computations in terms of execution time T_e (s) and final cost value G (€). The relaxation techniques must deliver lower execution times and not distance the solution from the real global optimum, which could derive from the relaxations defining a different problem. The study cases were solved using an *Intel i5-8265U CPU @ 1.60 GHz* laptop with 8 GB of RAM. We ran each case for a total of 10 experiences. However, in large execution time cases only 2 experiences were solved, which is the case of B-BB cases C2 and C3 with *equality* constraint, B-BB case C2 with *3 interval linear* constraint and B-BB case C1 with *4 interval linear* constraint.

The box plots displayed in Figures 3.11a, 3.11b and 3.11c compare the execution times for each analysed technique and algorithm. B-OA is not presented since it resulted similar to B-QG. A star symbol (★) marks those cases that did not converge to a solution for a given method and algorithm. Figure 3.11a compares the equality (*Eq*) method with inequality (*Ine*), Figure 3.11b compares the equality with linearized approximation with 3 intervals (*Lin3*) and lastly Figure 3.11c compares equality and linearized with 4 intervals (*Lin4*).

Table 3.1 summarises the results of B-BB, B-QG, B-OA and B-ECP for each method and case. Base values are highlighted with underline, while the other values express in percentage the relative difference to the base value.

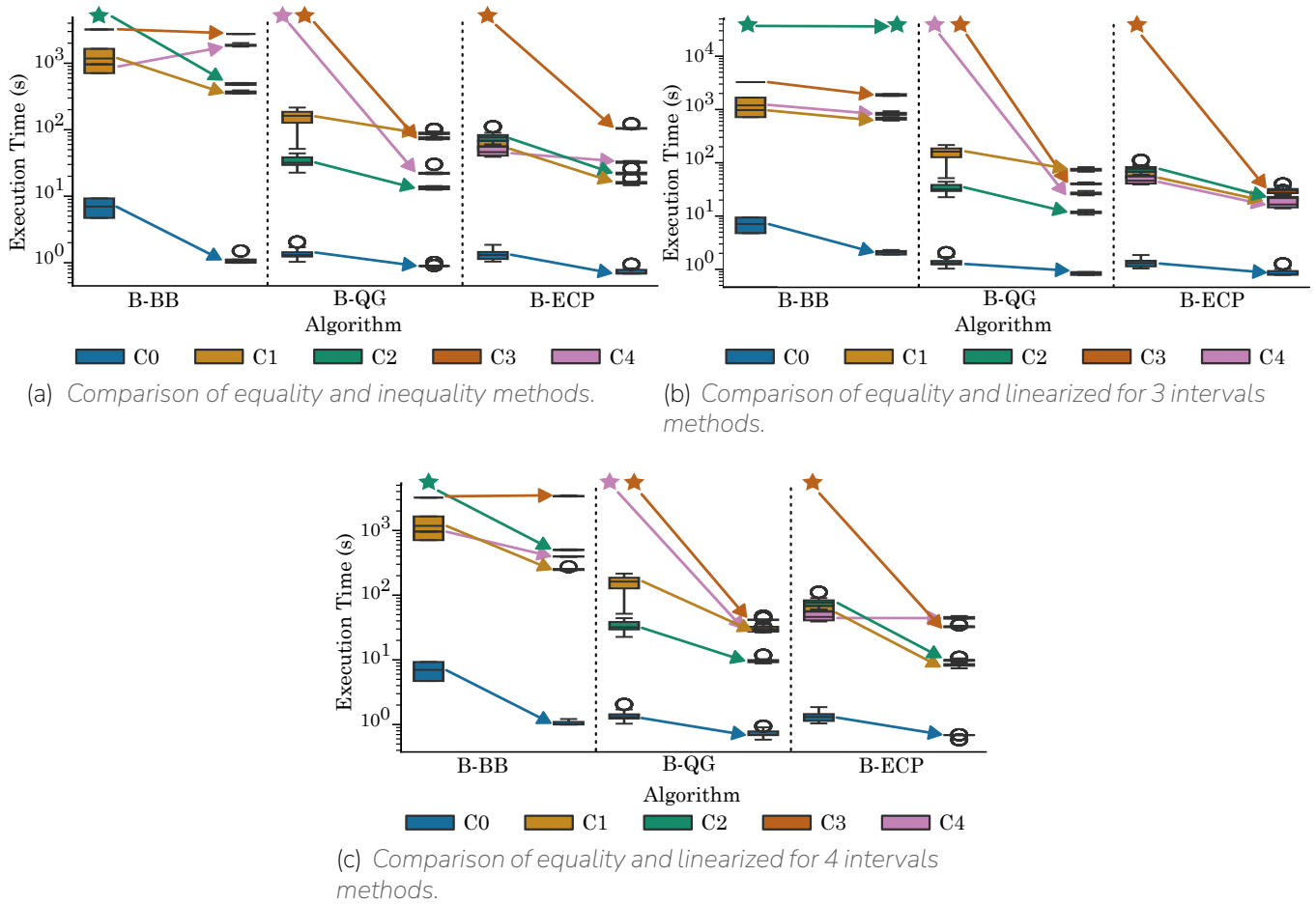


Figure 3.11 – Comparison of different methods using equality, inequality, and linearized constraints.

Table 3.1 – Results of time and final cost value and comparison between algorithms and methods.

		B-BB				B-OA				B-QG				B-ECP			
		Eq	lne	Lin3	Lin4	Eq	lne	Lin3	Lin4	Eq	lne	Lin3	Lin4	Eq	lne	Lin3	Lin4
C0	T_e [s, %]	<u>7.0</u>	-84.0	-70.3	-84.8	<u>1.8</u>	-21.2	-52.8	-47.6	<u>1.4</u>	-35.0	-39.8	-47.2	<u>1.3</u>	-44.6	-33.1	-49.1
	G [€, %]	<u>-2005</u>	0	0	0	<u>-2005</u>	0	0	0	<u>-2005</u>	0	0	0	<u>-2005</u>	0	0	0
C1	T_e [s, %]	<u>1179</u>	-69.0	-43.1	-78.6	<u>91.2</u>	-1.0	-34.0	-14.8	<u>152.6</u>	-41.4	-51.1	-79.8	<u>59.9</u>	-73.3	-53.8	-86.2
	G [€, %]	<u>32.0</u>	-22.0	-8.1	-14.5	<u>25.4</u>	-1.9	2.0	-1.0	<u>25.4</u>	-1.9	2.4	-1.0	<u>20.7</u>	-1.9	0	-1.0
C2	T_e [s, %]	*	<u>486</u>	*	3.2	<u>38.8</u>	-12.6	-40.8	-51.4	<u>32.9</u>	-59.5	-64.3	-70.6	<u>78.1</u>	-71.5	-71.7	-87.3
	G [€, %]	*	<u>12.9</u>	*	15.9	<u>12.6</u>	-8.4	5.1	2.5	<u>12.8</u>	-0.2	5.8	3.2	<u>20.1</u>	-31.3	-34.0	-34.3
C3	T_e [s, %]	<u>3218</u>	-14.5	-41.9	5.6	*	*	<u>109</u>	-23.0	*	<u>76.4</u>	-46.9	-44.8	*	<u>106</u>	-71.3	-69.1
	G [€, %]	<u>-29.7</u>	0	-1.0	0	*	*	<u>-29.7</u>	0	*	<u>-29.7</u>	0	0	*	<u>-29.7</u>	0	0
C4	T_e [s, %]	<u>961.8</u>	94.6	-13.2	-58.9	*	<u>596</u>	-93.3	-84.8	*	<u>22.9</u>	15.7	24.1	<u>48.1</u>	-32.3	-59.4	-7.2
	G [€, %]	<u>-27.4</u>	-17.7	-0.1	-28.9	*	<u>-30.6</u>	0.2	0.2	*	<u>-30.6</u>	0	0	<u>-30.6</u>	-1.0	-0.1	0

 *: Solution did not converge. Underline: base value (T_e in s and G in €)

The results show an improvement in the convergence and execution time from the original problem to the relaxed problem. In some cases the relaxation achieved a reduction of time execution up to an 86 %. Furthermore, we conclude that by applying the proposed relaxation methods, different solvers are capable of converging to a solution, while with the original problem this was not possible, for instance case C3 for almost every Bonmin algorithm and case C2 for B-BB.

The approximation of the pump constraint by using a set of linear segments clearly improve the execution time when using B-OA or B-QG algorithms, since neither of the algorithms apply any kind of linearization. For the B-ECP algorithm the difference between the inequality method and linear approximation is not clear, possibly since the B-ECP algorithm already implements a linearization process.

Regarding the use of different number of linearisation intervals in the segmentation of the pump head constraint, there are no substantial improvements in terms of execution time neither dissimilarities in the final goal value.

Furthermore, we observe that problems with the equality constraint have a high execution time dispersion compared to the same model solved with the alternative methods.

Regarding to the comparison between the different Bonmin algorithms is noted that B-ECP overpowers the other algorithms in almost all cases. However, B-QG combined with linearised methods results in many cases into execution times similar or even better to B-ECP.

The B-BB algorithm returns the highest execution times compared to the other Bonmin algorithms, and show results similar to [60] and [45], where Couenne was used.

Regarding the final cost value the majority of results show no significant discrepancies. However, in some cases the relaxed problem achieve an improved solution with up to 34 % reduction of the minimal value, feasible as well for the original problem. When using the relaxation techniques, it is noted that the B-ECP algorithm in some cases found a better minimal point as solution compared to others solvers or algorithms.

3.4 Study cases

This section presents the study cases we analysed with the methodology described previously in this chapter. The objectives of the study cases are to demonstrate the functionalities of the methodology and to acquire knowledge about the active participation of irrigation systems on the electrical grid:

1. Academic case (Section 3.4.1): simple non-existent academic system for testing purposes.
2. Comunitat de Regants de Les Planes i Aixalelles (Section 3.4.2): real scenario of a small irrigation system with a PV pump and a grid connected pump. The objective is to compare the addition of a battery energy storage system to employing a pump as a turbine.
3. Comunitat de Regants Segrià-Sud (Section 3.4.3): real scenario of a large irrigation system with several pumping stations consisting of both PV pumps and grid connected pumps. The objective is to analyse how the dependencies and interactions of several reservoirs affects the redesign.
4. CEDER (Section 3.4.4): real scenario of small irrigation system in CEDER facilities. The objective is to evaluate the impact of the battery to be installed in site, and the potential of the storage to provide energy to local loads.

3.4.1 Academic case

This study case, which was presented in [60], consists of a pair of identical pumps, a solar PV plant, and a lithium-ion battery connected to the main grid. The hydraulic circuit includes one pipe to connect two reservoirs. The upper reservoir is used for irrigation. A turbine in parallel with the pumps is set for sizing. A schematic of this plant is shown in Figure 3.12 and its characteristics are collected in Table 3.2.

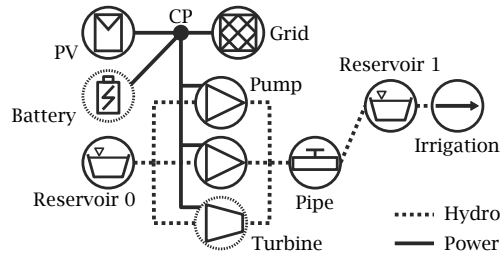


Figure 3.12 – Study case diagram.

Table 3.2 – Characteristics of the case's elements (in p.u.)

Device	Characteristics
Global	$\Delta t = 1, \rho = 1, g = 1$
Reservoir 0	$\underline{W} = 0, \overline{W} = 10, \underline{z} = 0, \overline{z} = 0,05$
Reservoir 1	$\underline{W} = 0, \overline{W} = 10, \underline{z} = 0,75, \overline{z} = 0,80$
Pipe	$K = 0,01$
Pumps	$\overline{p}_e = 1, \eta = 0,9, \underline{Q} = 0,5, \overline{Q} = 2, A = 1, B = 0,1$
Turbine	$\eta = 0,85$
PV	$p_{inst} = 1, m_f = [0, 0,1, 0,6, 1,2, 0,2], \eta = 0,98$
Battery	$\eta_{ch} = 0,9, \eta_{dch} = 0,9, \underline{SOC} = 0,2, \overline{SOC} = 1$

Each of the elements of the plant is modelled by means of a specific function that takes a block object and assigns to it the variables, parameters, and equations that define an element, as detailed above. Moreover, the initialisation of the decision variables is provided at that time.

Finally, the arcs are declared so that the connected variables are shared between blocks. The connections and variables shared for the study case are summarised in Table 3.3.

Table 3.3 – Variables linked by arcs

Block 1	Block 2	Variables	Block 1	Block 2	Variable
Res 0	Pumps	Q	Res 0	Turbine	Q
Res 0	Pipe	z_{low}	Turbine	CP	p_e
Pumps	Pipe	Q, H	Turbine	Pipe	Q, H
Pipe	Res 1	Q, z_{high}	Res 1	Irrigation	Q
PV	CP	p_e	Grid	CP	p_e
Battery	CP	p_e	Pumps	CP	p_e

Therefore, this example uses the constraints of the devices presented in Section 3.3.1 as well as both kinds of arc relations (3.2)-(3.3). In addition, two inequality constraints are added to ensure the availability of resources at the end of the simulation. In particular, the volume of water in reservoir 1 at the end of the simulation must be within a $\pm 10\%$ margin of the initial volume:

$$0,9 W_{Res1}(t_0) \leq W_{Res1}(t_f) \leq 1,1 W_{Res1}(t_0). \quad (3.36)$$

The objective function considers the operational costs and gains over a time horizon that spans from $t_0 = 0$ to $t_f = 4$ and capital expenditures to size new infrastructure as follows:

$$\begin{aligned}
 f(\cdot) = & \sum_{t=t_0}^{t_f} [p_{f,g}(t) c_{buy,g}(t) - p_{t,g}(t) c_{sell,g}(t)] \Delta t + \\
 & + p_{dim,PV} c_{p,PV} + p_{dim,turb} c_{p,turb} + \\
 & + p_{dim,bat} c_{p,bat} + e_{dim,bat} c_{e,bat},
 \end{aligned} \tag{3.37}$$

with $c_{sell,g}$ the price paid for injecting energy to the grid, $c_{buy,g}$ the market cost of electricity $c_{p,PV}$, $c_{p,turb}$, $c_{p,bat}$ and $c_{e,bat}$ the capital costs per unit power p or energy e for sizing PV, turbines and batteries respectively. Their values, displayed in Table 3.4, derive from normalising the costs provided in [74].

Table 3.4 – Costs in €/p.u.

Param	Value	Param	Value	Param	Value
$c_{buy,g}$	$\in [0,05, 0,20]$	$c_{p,turb}$	0,00143	$c_{p,PV}$	0,00126
$c_{sell,g}$	$c_{buy,g}/2$	$c_{p,bat}$	0,00171	$c_{e,bat}$	0,00856

From all of the above information, Pyomo constructs an optimisation problem composed of 289 decision variables, of which 15 binary and 274 continuous, 309 constraints, and 1 objective function. This problem was solved using the COIN-OR Couenne solver [75]. The computation took 16,75 s on a 11th Gen Intel Core i7 @ 3,40 GHz laptop with 16,0 GB of RAM.

Results

This section discusses the results obtained by solving the optimisation problem described in the previous section.

All of the magnitudes presented in this section are expressed using the per unit (p.u.) system, with the nominal flow and head of the pumps serving as bases for calculation. Volume is expressed in units of volume (u.v.), corresponding to a 1 p.u. of flow during a unit of time (u.t.).

Evaluating the objective function for the optimal sizing and operation computed returns a total value of - 1 918,06 €.

The optimal solution is to extend the solar PV plant to the entire available area $p_{dim,PV} = 1,0$ p.u., size a new turbine $p_{dim,turb} = 1,1$ p.u. and add a battery of $p_{dim,bat} = 0,8$ p.u. and $e_{dim,bat} = 2,0$ p.u. The PV, battery and turbine maximum capacity were arbitrarily limited to 2,0 p.u. Figure 3.13 portrays the final sizing along with the previously installed capacity.

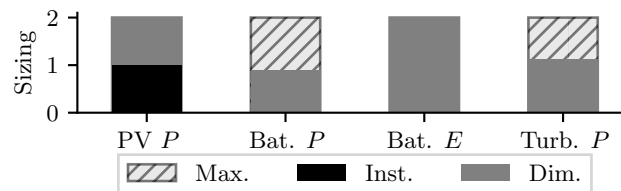


Figure 3.13 – Maximum capacity, already installed and newly sized (dim.) magnitudes of the PV, battery and turbine elements.

Considering the new equipment, the optimal operation of the system is detailed in Figure 3.14. Besides, Figure 3.15 depicts the power balance of the system along with the electricity market cost $c_{buy,g}$ at each

time frame. Figure 3.16 details the operation of the battery. Pumps run during low-cost periods and the turbine, if enough volume is available, does so when prices are high. The system also takes advantage of the PV plant during high irradiance periods to operate the pumps and charge the battery.

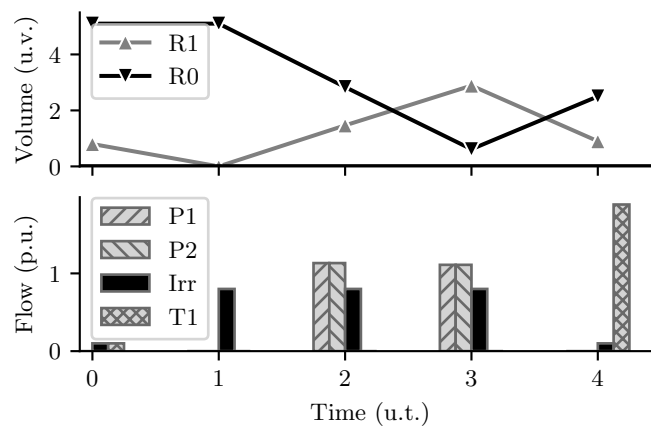


Figure 3.14 – Volume at the reservoirs (R0, R1) and flow of both pumps (P1, P2), irrigation at reservoir 1 (Irr) and turbine (T1).

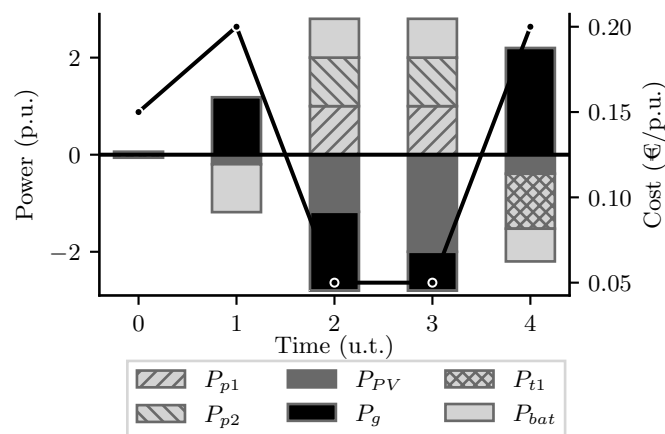


Figure 3.15 – Power balance of the system (defined positive if consumed by the element) and electricity cost.

3.4.2 Comunitat de Regants Les Planes i Aixalelles

This study case, presented in [45], is based on the facility of the Comunitat de Regants (CR) de Les Planes i Aixalelles (Section 2.4). The original irrigation system takes water from a river and raises it to a 13 000 m³ reservoir through a pumping station composed of a pair of 110 kW pumps equally characterised. The vertical distance between the river and the reservoir is about 110 m. The electrical power to supply the pumps comes from the power grid and from a 215,3 kWp PV plant which is owned by the irrigation community and is not grid connected. Figure 3.17 shows a scheme of this plant.

The pumping system is currently in operation between midnight and 8 a.m., when electricity prices are lowest. In addition, during the day, the energy produced by the PV plant is used to drive a pump if it generates enough power. In summer, water requirements are at their highest and pumps may operate up to 15 hours a day, but in winter, the need for irrigation decreases and pumps remain almost inactive (Figure 3.18).

The base case, depicted in Figure 3.17, considers both the grid connected and the PV pumps which possess the same electrical and hydraulic characteristics. A currently non-existing battery coupled to the

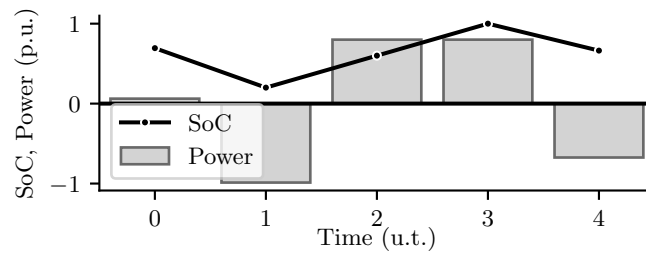


Figure 3.16 – Battery state of charge and power (defined positive if absorbed).

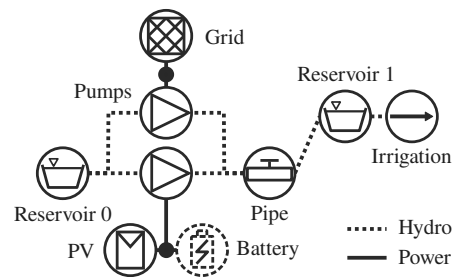


Figure 3.17 – CR Les Planes i Aixalelles study case base system.

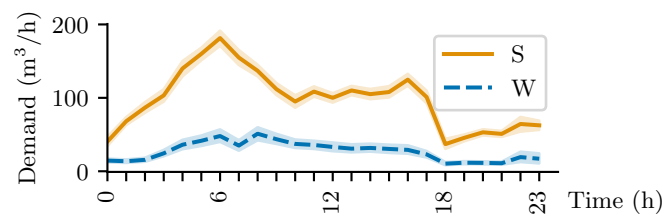


Figure 3.18 – Average daily irrigation demand on CR Les Planes i Aixalelles (S: Summer, W: Winter). Real data from 1 year and 90% confidence interval.

PV plant is set for sizing. The upper reservoir has a capacity of 13 000 m³ and is limited to a minimum volume of 9 000 m³, which corresponds to 3 days of autonomy during the irrigation season. This lower limit is arbitrary and set by the plant operator. To maintain operability, its initial and final volumes, $W_{R1}(t_0)$ and $W_{R1}(t_f)$ respectively, are set to be within a $\pm 5\%$ range (3.38). A sufficiently large reservoir models the river. Table 3.5 summarises the base case characteristics.

$$1,05 W_{R1}(t_0) \geq W_{R1}(t_f) \geq 0,95 W_{R1}(t_0) \quad (3.38)$$

Table 3.5 – Characteristics of the case's elements

Device	Characteristics
Reservoir 1	Volume $\in [9\ 000, 13\ 000]$ m ³ Height w.r.t. Reservoir 0 $\in [105, 111]$ m
Pipe	Quadratic losses coef. = 60 s ² /m ⁵
Pumps ^a	Power = 110 kW, $\eta = 0,8$, $\eta_{pat} = 0,5$ Flow $\in [0,6, 1,9]$ p.u. Nominal flow = 0,056 m ³ /s A = 120 m, B = 3 865 s ² /m ⁵
PV	Peak power = 215,3 kWp Converter efficiency = 0,98
Battery	Max. size energy/power 200 kWh/200 kW Allowed state of charge $\in [0,2, 1,0]$ p.u. Charge/discharge efficiency = 0,8

^a η efficiency and η_{pat} efficiency as a turbine

The objective function designed for this study considers the cost of buying $c_{buy,g}$ and price of selling $c_{sell,g}$ electricity to the grid, as well as the capital expenditures of sizing a new battery $c_{p,bat}$, $c_{e,bat}$.

$$f(\mathbf{x}) = \sum_{t=0}^T [p_{f,g}(t) c_{buy,g}(t) - p_{t,g}(t) c_{sell,g}(t)] \Delta t + p_{dim,bat} c_{p,bat} + e_{dim,bat} c_{e,bat}, \quad (3.39)$$

where \mathbf{x} is the decision vector composed of $p_{f,g}$ (kW), the power consumed from the grid and $p_{t,g}$ (kW) the power injected to the grid. Δt is the time step, which is equal to 1 h in the study case. Based on irrigation demand (Figure 3.18), the case study considers, in parallel, two standard days which correspond to summer and winter and also determine the irradiance on the PV plant. $p_{dim,bat}$ (W) and $e_{dim,bat}$ (Wh) are the power and energy sized for the battery. The electricity prices are based on the market from the Iberian Peninsula, and the costs of sizing the battery energy $c_{e,bat} = 0,2054$ €/(Wh day) and power $c_{p,bat} = 0,0410$ €/(W day) are based on [74] for a Li-ion battery, normalised for 1 day and considering 20 years for the project lifetime.

We considered the following modifications over the base case, which are detailed in Figure 3.19.

1. *Pump as turbine*: The pump connected to the grid can now be operated reversibly, i.e. *pump as turbine* (PaT), acting as a low efficiency Francis turbine. The other pump is kept connected to the PV and battery system. The PaT is modelled as a pump and a turbine operating in parallel, with the addition of (3.40) preventing them from operating simultaneously.

$$Q_{out,Turbine}(t) Q_{out,Pump}(t) = 0 \quad \forall t \quad (3.40)$$

2. *Grid connected*: Both pumps are connected to a common bus with the grid, PV panels and battery system.
3. *PaT + Grid connected*: Fusing both previous cases, electrical elements are connected to a common bus with the grid and one pump is allowed to run in reversible mode.

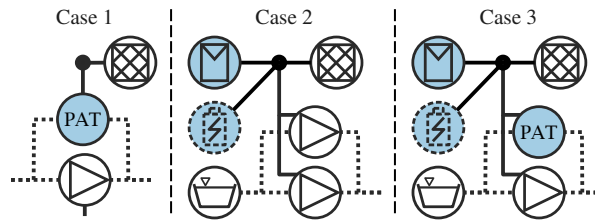


Figure 3.19 – Variations on the study case. Devices which present changes are highlighted.

Overall, in this study case, we analyse whether the reversible use of pumps allows stored energy to be harnessed. In addition, we also consider the sizing of batteries to determine the effect of the price of energy on the decision to install such equipment.

Results

The results obtained from the base case (Figure 3.17) represent an optimal performance according to what is currently known. This means using the PV pumping system at its full potential and backing it up with the grid-connected pump during low-cost periods. No battery is found required or sized for any of the cases studied due to its high capital costs. The system works at full capacity in summer and is underutilised in winter, as can be observed on Figures 3.20a and 3.20b. Figure 3.20a displays the powers consumed (>0) by the PV plant P_{PV} , PV pump $P_{p,PV}$, grid connected pump $P_{p,g}$, the available PV power \hat{P}_{PV} and the power exchanged with the grid P_g , as well as the cost and sell price of electrical energy. Figure 3.20b does the same for the flows delivered to reservoir 1 from both pumps $Q_{p,PV}$ and $Q_{p,g}$ and the irrigation demand Q_{irr} , along with the volume present at the reservoir and its bounds. This nomenclature is kept through the other cases.

1. *Pump as turbine*: Allowing the grid connected pump to operate as a turbine favors the usage of the pumping facility as a PV storage system, in which the PV pump transfers water to the highest reservoir during peak irradiance hours, then the PaT converts its potential energy into electricity to feed the grid during high sell price periods. This behaviour is illustrated in Figures 3.21a-3.21b in comparison to the underutilisation from the base case (Figures 3.20a-3.20b). Summer season presents no divergence from the base case and is therefore omitted from this discussion.
2. *Grid connected*: Connecting the whole facility to the grid allows for energy exchanges, which extract the full potential of the PV system. Pumps operation is rescheduled, as Figures 3.22a-3.22b portrays, and the available PV power fully exploited.
3. *PaT + Grid connected*: In such circumstances the optimisation must decide whether to inject the energy to the grid straight from the PV plant or store it in the form of potential energy in the reservoir and inject it during higher sell price periods. With the data fed and parameters set for the study case, the resulting operation (Figures 3.23a-3.23b) indicates that running the PaT during the highest sell price hours at winter is the optimal scheduling.

Table 3.6 summarises the operation and sizing costs per day, after simulating each case for summer and winter conditions. It also displays the computation time in seconds on a *11th Gen Intel Core i7 @ 3.40 GHz* laptop with 16,0 GB of RAM. From Table 3.6, it can be seen that the Base case is the most

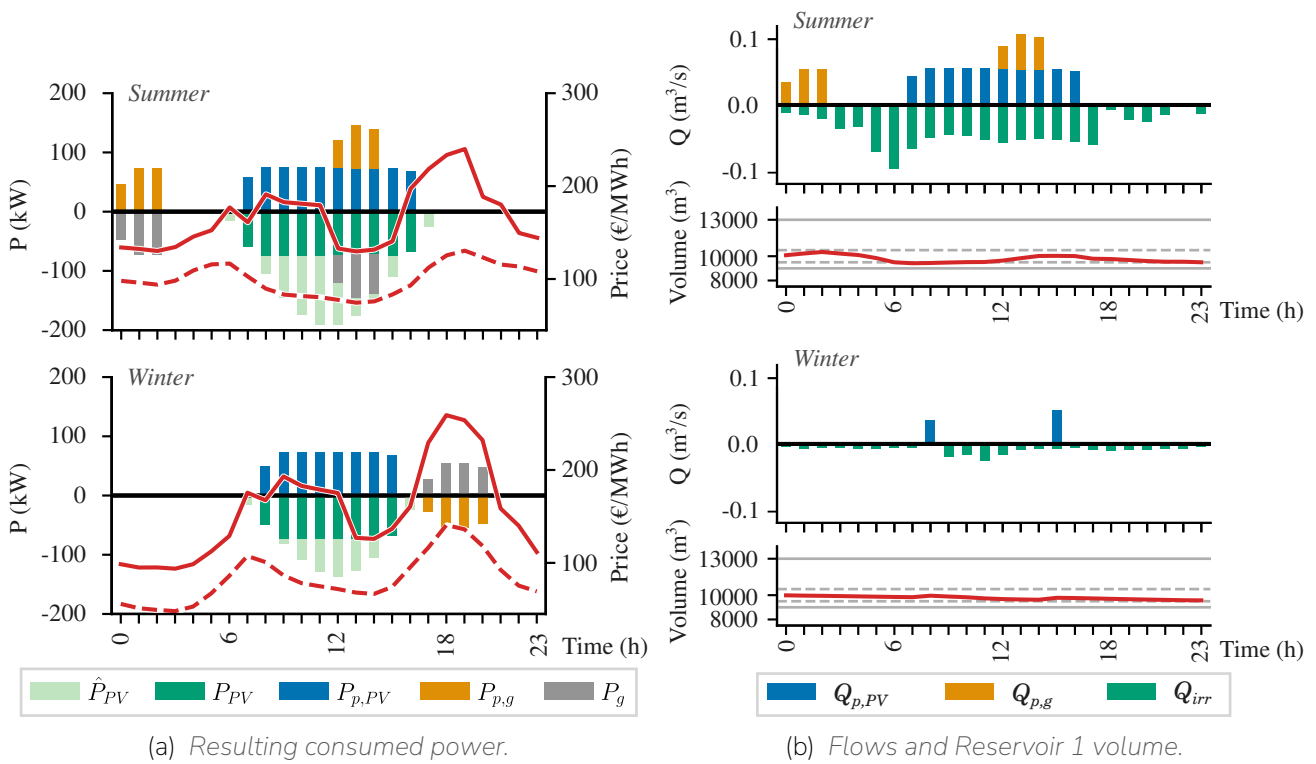


Figure 3.20 – Results of the base case.

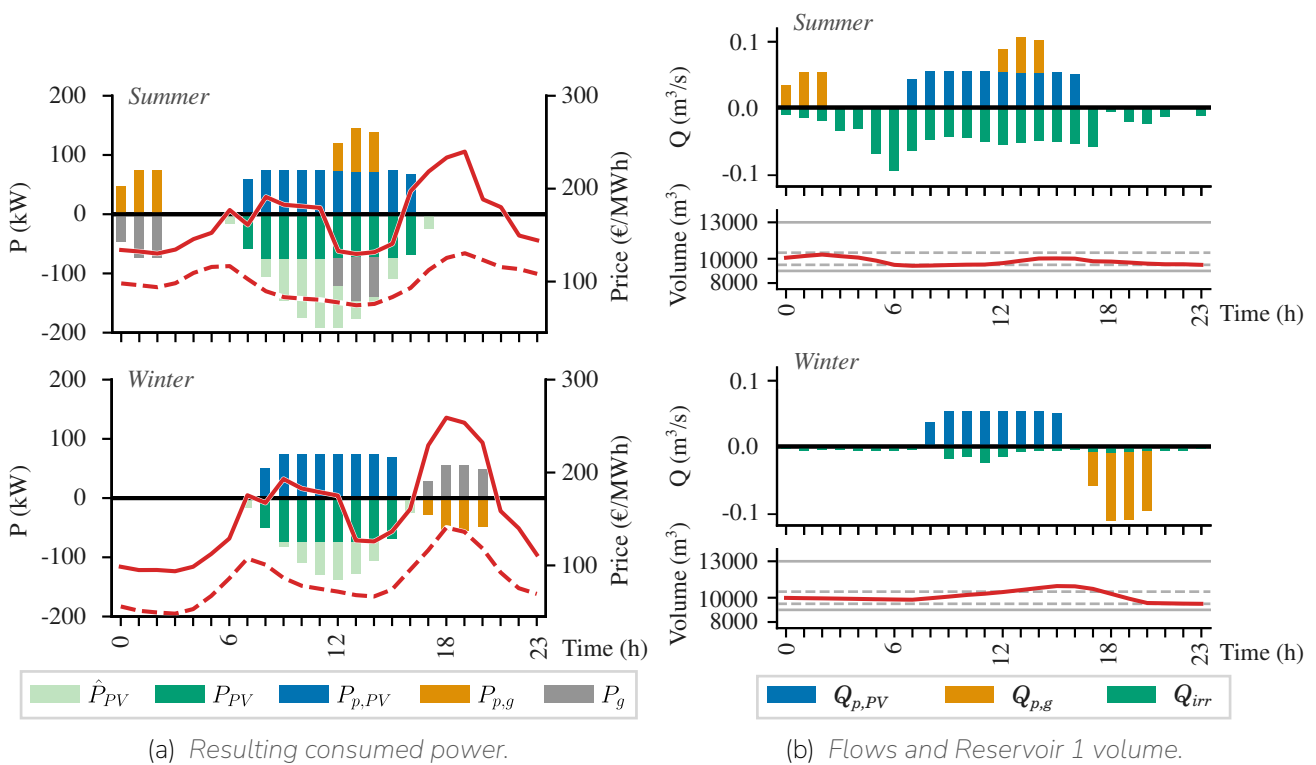


Figure 3.21 – Results of PaT case (Case 1).

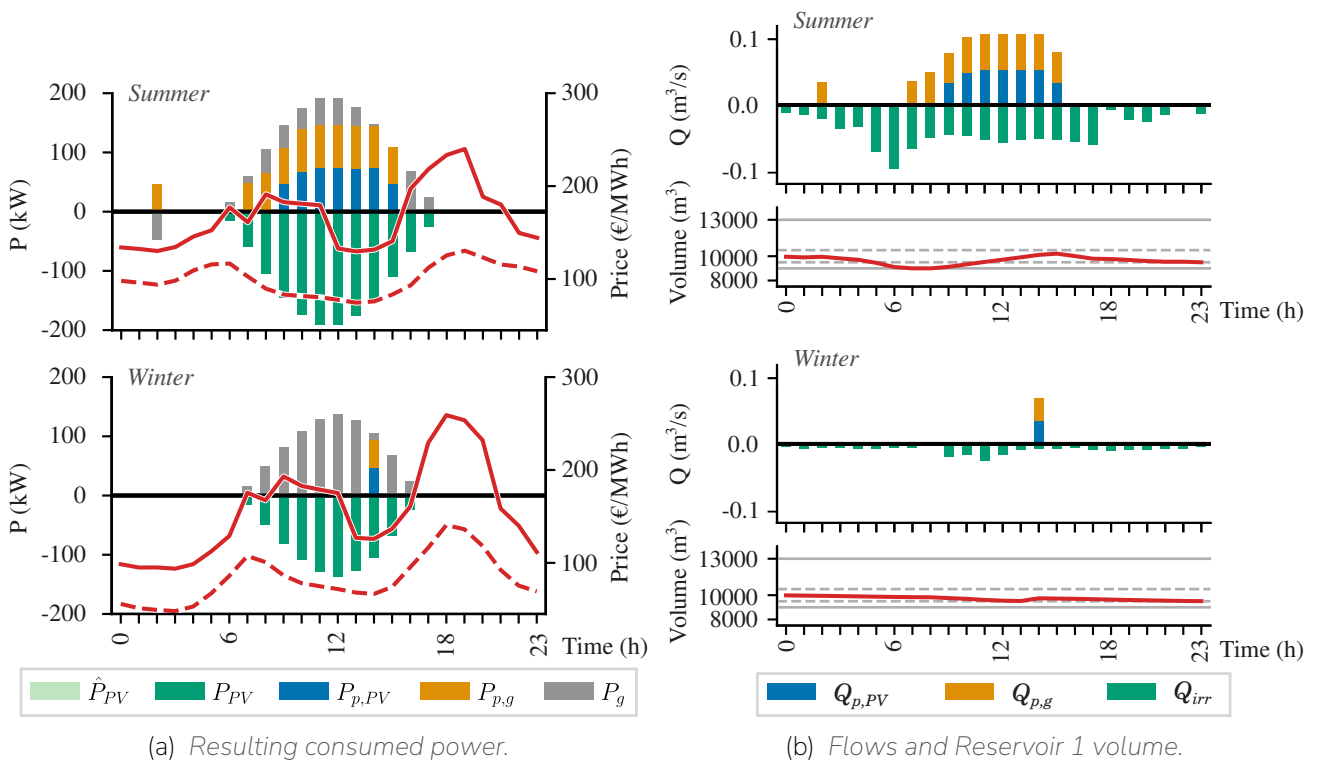


Figure 3.22 – Results of grid connected case (Case 2).

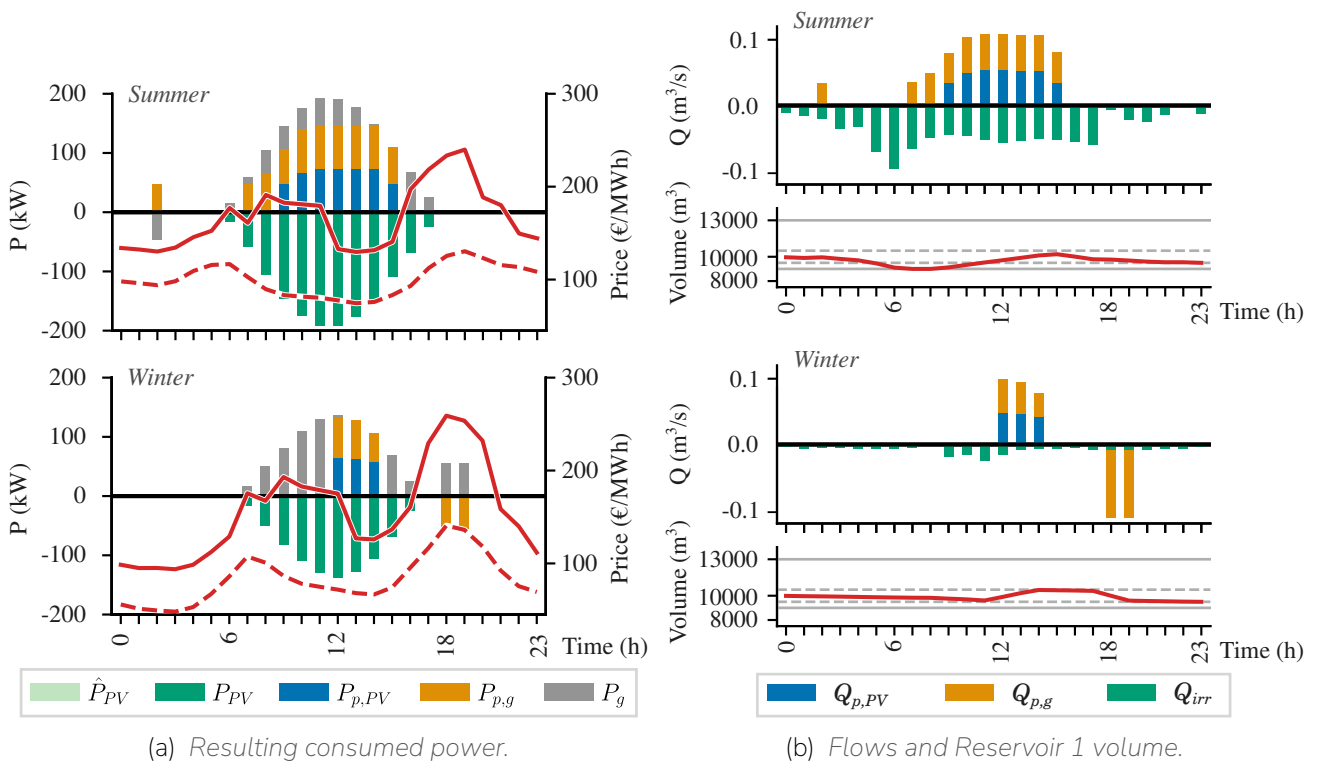


Figure 3.23 – Results of grid connected + PaT case (Case 3).

expensive solution, whereas remodelling to the Case 3 topology (grid connected PV + PaT) results the most profitable option.

Table 3.6 – Cases summary

Case	Base	Case 1	Case 2	Case 3
Cost [€/day]	12,50	7,03	-12,05	-15,30
Exec. time [s]	4	10	5	12

3.4.3 Comunitat de Regants Segrià-Sud

This study case, presented in [76], is based on the facility of the Comunitat de Regants (CR) Segrià-Sud (Section 2.4). The original irrigation system takes water from the river Ebre and raises it to a system of 5 reservoirs through 4 pumping stations composed of several kW to MW pumps. The vertical distance between the river and the highest reservoir is about 380 m. The electrical power that supplies the pumps comes from the power grid and from three PV plants with 523,00 kWp, 527,50 kWp and 274,68 kWp installed peak power. The PV plants are owned by the irrigation community and are not grid connected. Figure 3.24 shows a scheme of the CR Segrià-Sud facilities and Table 3.7 summarises the characteristics of its devices.

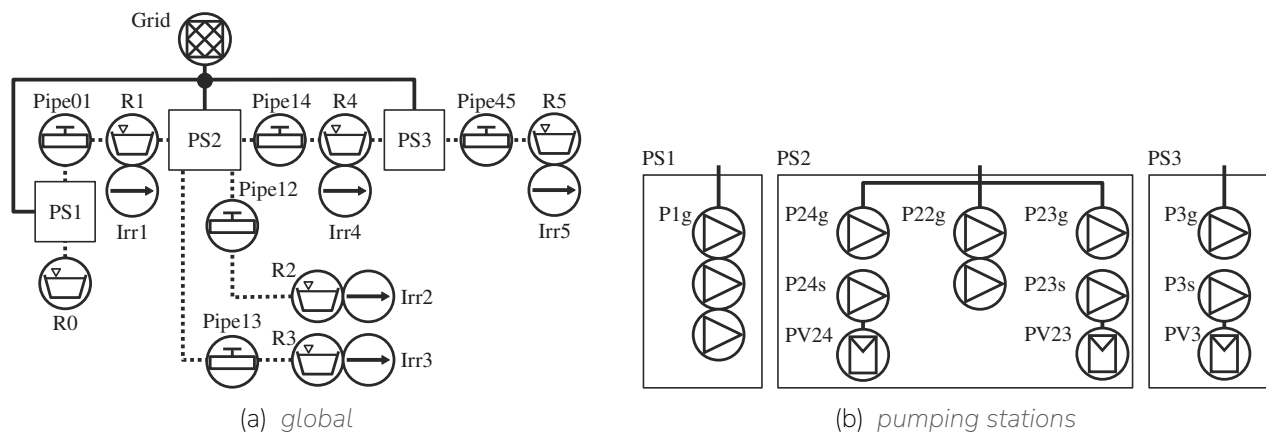


Figure 3.24 – CR Segrià-Sud Base case system.

The pumping stations currently operate between midnight and 8 a.m., when both the electrical power and energy term prices are the lowest. During the day, the energy produced by the PV plants is used to drive the PV pumps if enough solar power is available. Irrigation requirements are at their highest in summer, but in winter, the need for irrigation considerably reduces. Figure 3.25 displays the average daily irrigation demand for each reservoir stratified in winter and summer seasons, with a 95 % confidence interval².

Our scope is limited by the scalability issues the optimisation methodology presents (Section 3.3.4). To reduce the complexity of the problem we split the system in two sections *upper* and *lower*, as depicted in Figures 3.26-3.27. The subdivisions assume the following premises:

- *Lower section*: Reservoir R0 (river Ebre) has infinite capacity, modelled as a large enough value, such that it can provide and absorb as much water as required without it having an effect on its manometric height. Irrigation from reservoirs R2 and R3 are directly aggregated to R1 and their pertinent hydraulic elements are not considered. Irrigation from reservoir R5 is directly aggregated to R4 and its pertinent hydraulic elements are not considered.

²We could not effectively obtain reliable data from Reservoir 4, thus we assumed the demand to be similar to Reservoir 5 since they are located next to each other and share similar altitudes and crop areas [22]

Table 3.7 – Characteristics of the CR Segria-Sud case's devices

Device	Characteristics
Reservoirs	R0: $W \in [120, 240] 10^3 \text{ m}^3$, $z \in [129, 131] \text{ m}$ R1: $W \in [96, 143] 10^3 \text{ m}^3$, $z \in [336, 339] \text{ m}$ R2: $W \in [250, 297] 10^3 \text{ m}^3$, $z \in [355, 365] \text{ m}$ R3: $W \in [70, 86] 10^3 \text{ m}^3$, $z \in [418, 421] \text{ m}$ R4: $W \in [184, 270] 10^3 \text{ m}^3$, $z \in [427, 431] \text{ m}$ R5: $W \in [128, 186] 10^3 \text{ m}^3$, $z \in [448, 451] \text{ m}$
Pipes	Pipe01: $K = 27,90 \text{ s}^2/\text{m}^5$ Pipe12: $K = \text{N/D}$ Pipe13: $K = 6,12 \text{ s}^2/\text{m}^5$ Pipe14: $K = 27,81 \text{ s}^2/\text{m}^5$ Pipe45: $K = 6,10 \text{ s}^2/\text{m}^5$
Pumps ^a	P1 (x3): $\bar{P} = 3\,200 \text{ kW}$, $\eta = 0,922$, $\eta_{pat} = 0,7$, $Q \in [0,3, 1,1] \text{ p.u.}$, $Q_n = 1,06 \text{ m}^3/\text{s}$, $A = 300 \text{ m}$, $B = 62,208 \text{ s}^2/\text{m}^5$ P22 (x1): $\bar{P} = 315 \text{ kW}$, N/D P23 (x2): $\bar{P} = 250 \text{ kW}$, $\eta = 0,82$, $\eta_{pat} = 0,7$, $Q \in [0,3, 1,1] \text{ p.u.}$, $Q_n = 0,285 \text{ m}^3/\text{s}$, $A = 105,81 \text{ m}$, $B = 324 \text{ s}^2/\text{m}^5$ P24 (x2): $\bar{P} = 1\,250 \text{ kW}$, $\eta = 0,92$, $\eta_{pat} = 0,7$, $Q \in [0,3, 1,1] \text{ p.u.}$, $Q_n = 0,913 \text{ m}^3/\text{s}$, $A = 148 \text{ m}$, $B = 103,7 \text{ s}^2/\text{m}^5$ P3 (x2): $\bar{P} = 160 \text{ kW}$, $\eta = 0,86$, $\eta_{pat} = 0,7$, $Q \in [0,6, 1,2] \text{ p.u.}$, $Q_n = 0,469 \text{ m}^3/\text{s}$, $A = 37,8 \text{ m}$, $B = 38,9 \text{ s}^2/\text{m}^5$
PV	PV23: $P_{inst} = 523,0 \text{ kWp}$, $\eta = 0,98$ PV24: $P_{inst} = 527,5 \text{ kWp}$, $\eta = 0,98$ PV3: $P_{inst} = 274,7 \text{ kWp}$, $\eta = 0,98$

^a η efficiency and η_{pat} efficiency as a turbine

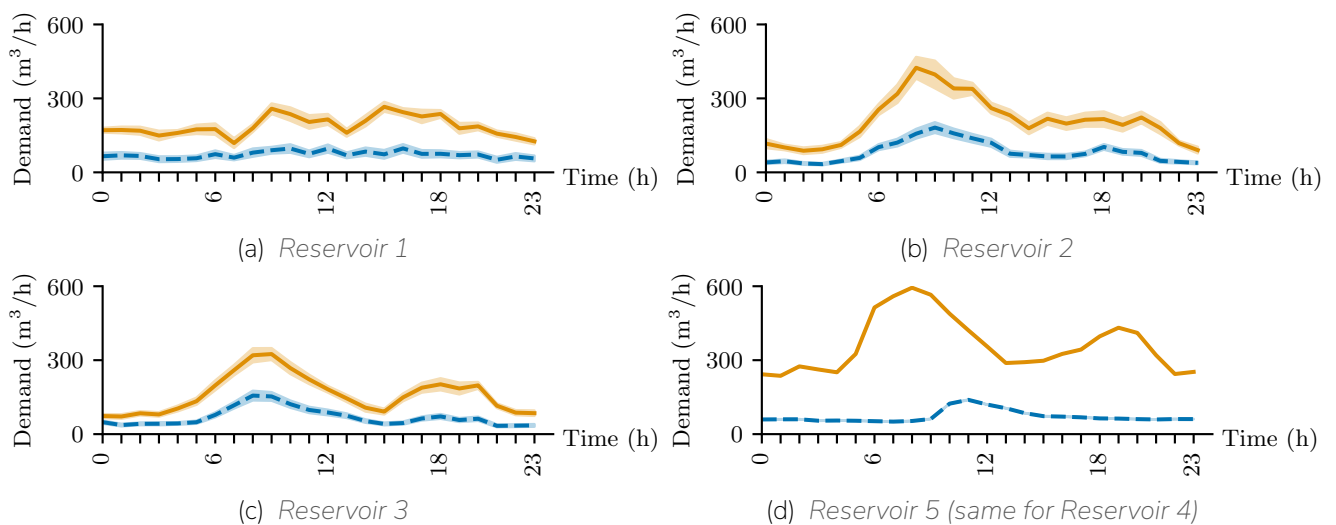


Figure 3.25 – CR Segrià-Sud water consumption for irrigation.

- *Upper* section: Reservoir R0 will provide the required amount of water to reservoir R1, hence the latter has infinite capacity, modelled as a large enough value. Reservoirs R2 and R3 and their pertinent hydraulic elements are not considered.

These assumptions entail the following constraints on the present analysis:

- It is not possible to include reservoirs R2 and R3 and their pertinent hydraulic elements.
- Reverse flow cannot be considered for Pipe01 on the *lower* section and for Pipe14 on the *upper* section.
- The total operating cost obtained by the optimisation does not correspond to the total operating cost of the facility.
- The total operating cost of the facility is not obtainable due to the removal of reservoirs R2 and R3.
- An estimate total cost of operating the R0-R1-R4-R5 circuit can be obtained by adding the *Base* case operating costs of the left-out pumping station on either section (costs from pumping station PS1 on the *upper* section and costs from pumping station PS3 on the *lower* section).

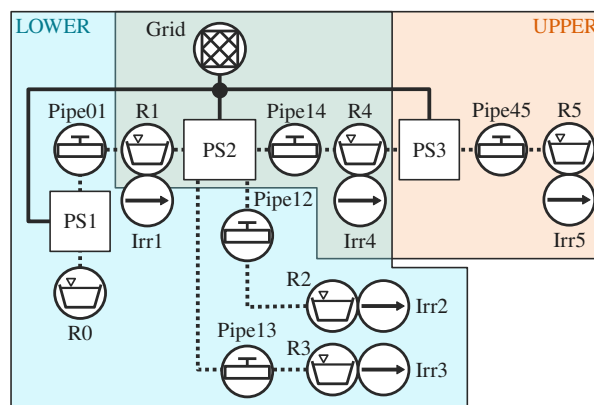


Figure 3.26 – CR Segrià-Sud system division.

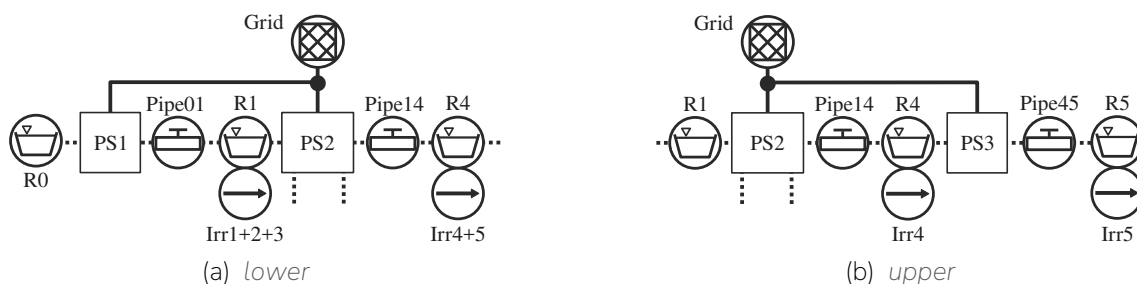


Figure 3.27 – CR Segrià-Sud lower and upper divisions and assumptions.

For each division we considered analogous modifications over the *Base* case as for the CR Les Planes i Aixalelles analysis (see Section 3.4.2):

1. *Pump as turbine*: The grid connected pump can be operated reversibly (PaT), with a lower efficiency considered $\eta_{pat} = 0,7$ based on [41]. The other pump is kept connected to the PV system. The pumps selected for such function are Pump24g in *lower* section and Pump3g in *upper* section. The PaT is modelled as stated in Section 3.3.1, with a pump and a turbine operating in parallel and the addition of (3.40) preventing them from operating simultaneously.
2. *Grid connected*: All PV systems and pumps are connected to a common bus to the grid. The system is allowed to import and export electricity from the grid applying the corresponding costs and prices.

3. *PaT + Grid connected*: Combining both previous cases, all of the electrical elements are connected to a common bus with the grid and the originally grid connected pump is allowed to run in reversible mode (Pump24g in *lower* section and Pump3g in *upper* section).

Notice that, due to imposing the condition of cycle by limiting the minimum volume value of the reservoirs at the end of the time period (see Section 3.3.1), the total volume of water that the system obtains from the river is strictly the irrigation demand on all of the cases.

The objective of this study case is to analyse the behaviour of a multi-reservoir system and the effects of running a PaT at several locations. We defined two representative days for the electrical grid costs and GHG emission factor, depicted in Figure 3.28, which consist of the average daily evolution of the months of January (winter) and August (summer) of 2024 [77]. We also analyse the sensitivity of the solution to the fluctuation of parameters of relevance which present a significant uncertainty or are likely to evolve in the future: irrigation demand, price of exporting electricity to the grid and the efficiency of running PaTs.

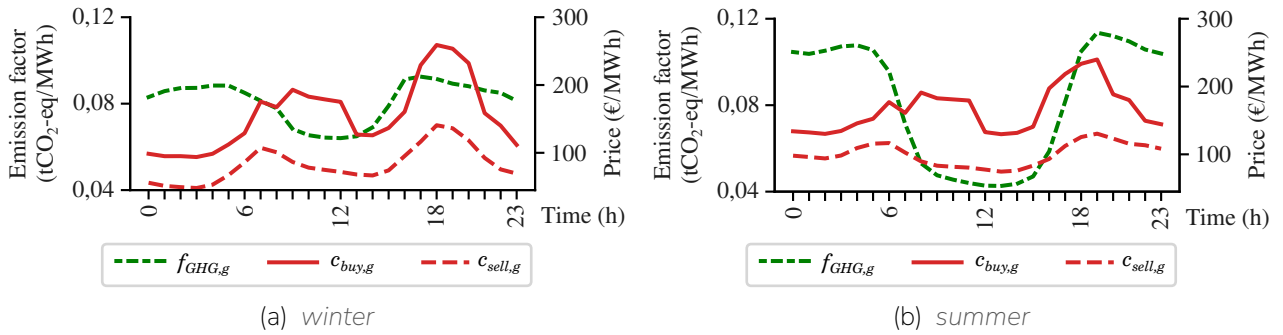


Figure 3.28 – Grid equivalent GHG emission factor, cost of electricity and sell price for the defined typical days. Data from [77].

We defined the objective function for the analysis of the CR Segrià-Sud system from the point of view of the community, which objective is to reduce the operating costs. The function considers the cost of buying $c_{buy,g}$ (€/MWh) and price of selling $c_{sell,g}$ (€/MWh) electricity to the grid and the energy imports $p_{f,g}$ (MW) and exports $p_{t,g}$ (MW):

$$f(\mathbf{x}) = \sum_{t=0}^T [p_{f,g}(t) c_{buy,g}(t) - p_{t,g}(t) c_{sell,g}(t)] \Delta t \quad (3.41)$$

We also defined an objective function from the perspective of the administration or a grid operator with the purpose of reducing the overall GHG emissions of the grid, which we applied to Case 3 and named it Case 3-em:

$$f(\mathbf{x}) = \sum_{t=0}^T [p_{f,g}(t) - p_{t,g}(t)] f_{GHG,g}(t) \Delta t \quad (3.42)$$

with $f_{GHG,g}$ (tCO₂-eq/MWh) the GHG emission factor of the grid. This objective function assumes an average behaviour of the grid and does not distinguish the technologies participating in the daily market.

Results (Upper)

This section presents the results obtained from the *upper* section of the irrigation system analysis, which are summarised on Table 3.8 and Figures 3.29-3.33. The computation time of each case, running the COIN-OR Bonmin algorithms [75] on a 11th Gen Intel Core i7 @ 3.40 GHz laptop with 16,0 GB of RAM,

Table 3.8 – Results (Upper)

Case	Base	Case 1	Case 2	Case 3	Case 3-em
Computation time [s]	5,80	23,44	34,92	14,81	39,20
Energy imported average [kWh/d]	1 233,51	1 074,86	227,30	234,78	783,74
" winter [kWh/d]	0,00	0,00	1,20	0,00	17,01
" summer [kWh/d]	2 467,02	2 179,72	453,39	469,56	1 550,46
Energy exported average [kWh/d]	-	202,17	1 067,50	1 051,99	1 376,02
" winter [kWh/d]	-	385,55	2 071,96	2 027,12	2 089,75
" summer [kWh/d]	-	18,78	63,04	76,86	662,29
Maximum imported power winter [kW]	0,00	0,00	1,20	0,00	17,01
" summer [kW]	485,11	501,71	375,46	391,64	311,12
Maximum exported power winter [kW]	-	112,00	480,50	480,50	480,50
" summer [kW]	-	18,78	57,84	57,84	219,69
GHG emissions average [kgCO ₂ -eq/d]	119,17	94,60	-52,92	-51,96	- 68,43
" winter [kgCO ₂ -eq/d]	0,00	-34,68	-144,56	-143,20	-146,15
" summer [kgCO ₂ -eq/d]	238,35	223,89	38,71	39,28	9,29
Energy expense average [€/d]	166,85	144,89	31,19	32,17	118,87
" winter [€/d]	0,00	0,00	0,15	0,00	3,11
" summer [€/d]	333,70	289,77	62,23	64,33	243,62
Energy income average [€/d]	-	26,24	87,30	88,41	119,61
" winter [€/d]	-	50,03	167,19	167,87	163,56
" summer [€/d]	-	2,45	7,40	8,95	75,65
Total cost average [€/d]	166,85	118,65	-56,10	-56,24	-0,74
" winter [€/d]	0,00	-50,03	-167,04	-167,87	-160,45
" summer [€/d]	333,70	287,32	54,83	55,34	158,67

was 5,80 s for the *Base case*, 23,44 s for *Case 1*, 34,92 s for *Case 2*, 14,81 s for *Case 3* and 39,20 s for *Case 3-em*.

Economic analysis

The total optimal cost of operating the system results the highest for the *Base case*, with an average daily cost of 166,85 €/d, followed by *Case 1 (PaT)* with 118,65 €/d. *Case 2 (Grid connected)* and *Case 3 (PaT + Grid connected)* manage to obtain benefits by exporting the electricity generated by the PV systems and the energy storage service with the PaT, with an average daily operating cost of -56,10 €/d and -56,24 €/d respectively.

In summer the system requires to import close to 2 500 kWh/d from the grid to pump the water required for irrigation. In winter the same can be achieved by the solar pump itself and requires no imports from the grid.

Regarding the employment of PaT both *Case 1* and *Case 3* use the available PV power to pump further water than required and store it in reservoir R5 to later turbine it during the highest import cost/export price periods. In winter, this energy is exported to the grid to obtain revenue in both *Case 1* and *Case 3*. Furthermore, in *Case 1*, in summer it is also used by the grid connected pump in pumping station PS2 to deliver water to reservoir R4, which implies it is more cost-effective to not import energy from the grid than the income obtained from exporting it. This strategy would be particularly convenient in an scenario where the grid operator does not allow the injection of energy to the grid, as a way of storing the extra energy from the PV systems to self-supply.

Technical analysis

The average energy exchange, computed as the difference between energy imports and exports, results positive for the *Base case* (1 233,51 kWh/d) and *Case 1* (872,69 kWh/d) and negative for *Case 2* (-840,2 kWh/d), *Case 3* (-817,21 kWh/d) and *Case 3-em* (-592,28 kWh/d). The system can provide the most energy to the grid by directly exporting the energy resulting from the PV excess.

It is relevant to analyse the maximum power exchanged with the grid to determine the required size of possible power electronics or protections participating in the system. The resulting maximum power exchanged with the grid is 485,11 kW for *Base case*, 501,71 kW for *Case 1* and 408,50 kW for *Case 2*, *Case 3* and *Case 3-em*.

The round-trip efficiency of the system as an energy storage equivalent system can be estimated from cases with PaT (*Case 1* and *Case 3*) as

$$\hat{\eta}_{ESS} = \frac{E_{ESS,out}}{E_{ESS,in}} = \frac{\sum_{turb \in \mathcal{T}} E_{e,turb}}{\sum_{pump \in \mathcal{P}} E_{e,pump} - \sum_{pump \in \mathcal{P}} E_{e,pump,irr}}, \quad (3.43)$$

where $E_{ESS,out}$ (Wh) and $E_{ESS,in}$ (Wh) are the energy *out* and *in* from the energy storage system respectively, which are defined by the electrical energy exported by the turbines $E_{e,turb}$ (Wh) within the turbines set \mathcal{T} and the difference between the electrical energy imported by the pumps $E_{e,pump}$ (Wh) and the electrical energy imported by the pumps exclusively for irrigation purposes $E_{e,pump,irr}$ (Wh). The latter is obtained by comparison from a reference case: *Base matching Case 1 (PaT)* and *Case 2 (grid connected)* matching both *Case 3* and *Case 3-em (grid connected and PaT)*. Such a procedure obtained an average $\hat{\eta}_{ESS} = 0,5061$ (SD 0,04).

Environmental analysis

From a GHG emissions point of view, considering the typical day grid's equivalent CO₂ factor evolution in summer and winter (Figure 3.28) and null for the irrigation system, results in positive emissions for the *Base case* and *Case 1*, and negative (avoided emissions) for *Case 2*, *Case 3* and *Case 3-em*. The latter, as expected, derives the best for such a purpose and utilises its energy storage capabilities to maximise the energy delivered to the grid during high emission factor hours (early morning and evening in summer). Fair compensations should however apply to the irrigation community since this operation strategy is not as economically beneficial as *Case 3* solution with an average difference of 55,50 €/d for an average

reduction of 16,47 kgCO₂-eq/d in emissions.

The daily water consumption is maintained for all the cases, as stated above, since a cycle condition is imposed in the reservoir device. In essence, the modelling of the system implicitly considers the extra daily impact on the water source and cancels it.

Results (Lower)

This section presents the results obtained from the *lower* section of the irrigation system analysis, which are summarised on Table 3.9 and Figures 3.34-3.37. The computation time of each case, running the COIN-OR Bonmin algorithms [75] on a 13th Gen Intel Core i7 @ 2.40 GHz laptop with 16.0 GB of RAM, was 12,36 s for the *Base* case, 399,11 s for *Case 2*, 1 273,53 s for *Case 3* and 15,44 s for *Case 3-em*. *Case 1* of the *lower* section could not be computed, evidencing the complexity of the optimisation problem. It should be acknowledged that this section of the irrigation system is not the target of the demonstrator. Further research will be conducted to achieve lower computational complexities.

In the PAT + Grid connected scenario, a simplification of the pipe flow equation was introduced to mitigate the computational complexity of the non-linear problem. Specifically, a constant hydraulic head was assumed for the pipes between nodes R0–R1 and R1–R4. This constant value represents an intermediate elevation between the dynamic head associated with pump operation in the corresponding segment and the maximum head at the upper operating point. This assumption was adopted due to significant elevation differences between reservoirs, which posed convergence difficulties for the non-linear solver. To enhance the robustness of the formulation, the maximum flow rate was constrained to the value corresponding to the maximum operating point of the pump, accounting for head losses based on the quadratic formulation of pipe flow. While this simplification neglects continuous variation in head losses, its impact on performance estimation was found to be limited. The maximum observed error in power calculation resulting from this approximation was 7,03 %, corresponding to an underestimation. When compared directly to the reference pump power, the deviation was bounded by a maximum of 5,03 %.

Economic analysis

The total optimal cost of operating the system results the highest for the *Base* case, with an average daily cost of 1 754,31 €/d, followed by *Case 2 (Grid connected)* with 1 659,68 €/d and *Case 3 (PaT + Grid connected)* with 1 632,21 €/d.

In summer the system requires to import up to 22 000 kWh/d from the grid to pump the water required for irrigation. In winter the same can be achieved with just 5 400 kWh/d by the solar pump itself and requiring imports from the grid to run the grid connected pumps from PS1.

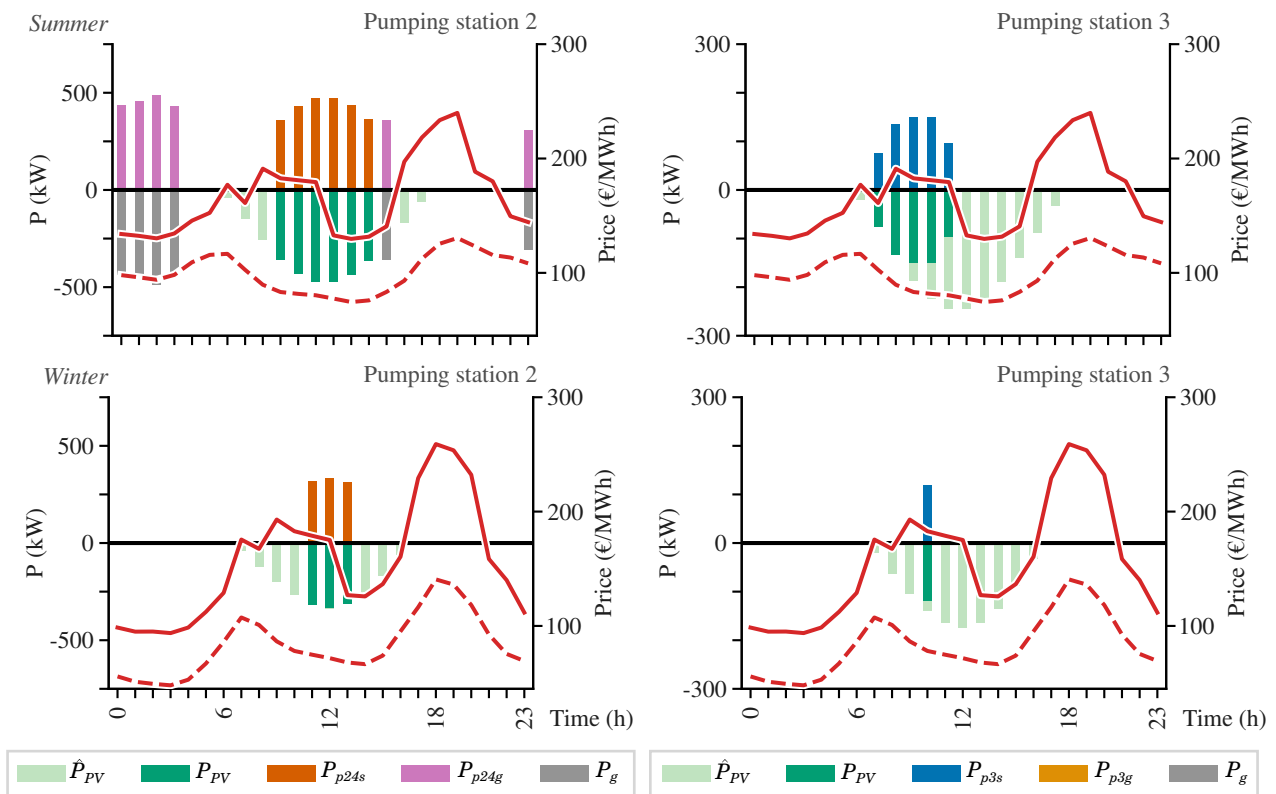
Regarding the employment of PaT *Case 3* use the available PV power to pump further water than required and store it in reservoir R4 to later turbine it during the highest import cost/export price periods. In winter, this energy is exported to the grid to obtain revenue in *Case 3*.

Technical analysis

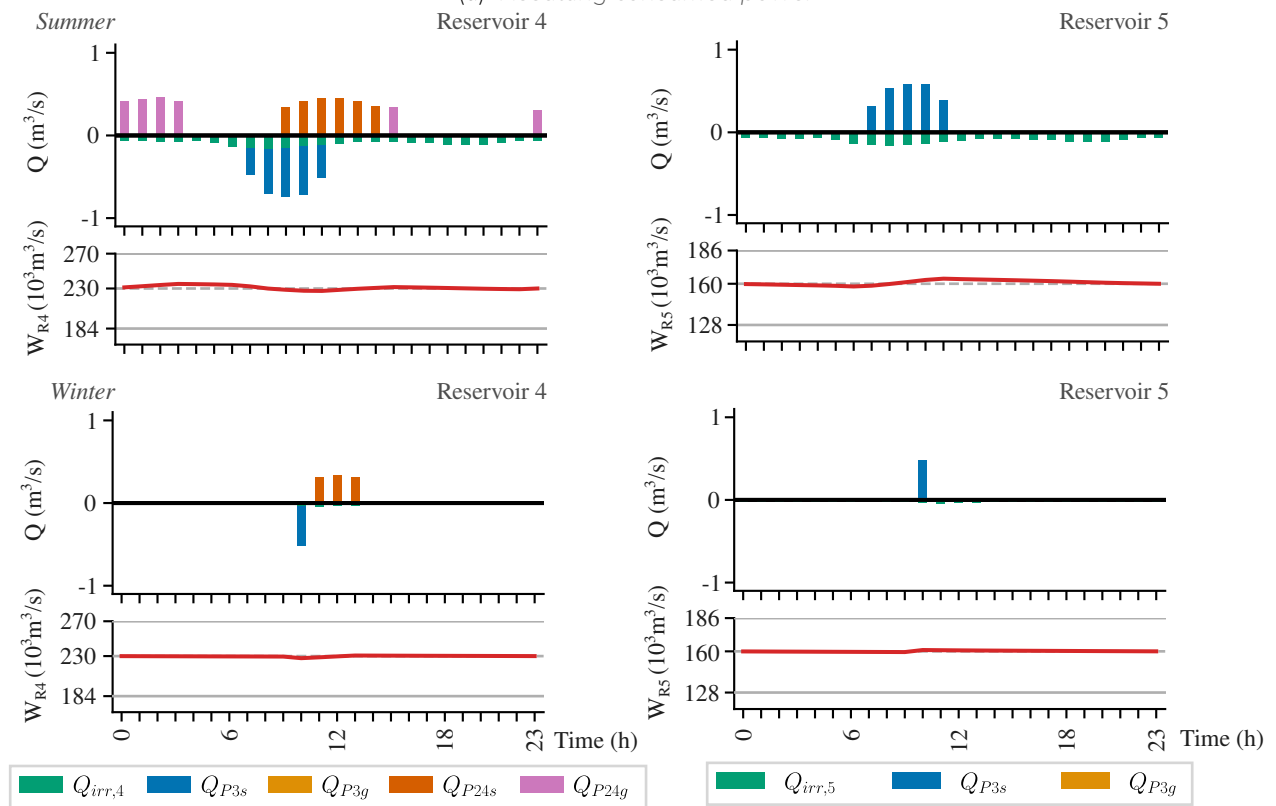
The average energy exchange, computed as the difference between energy imports and exports, results positive for the *Base* case (13 571,40 kWh/d), *Case 2* (12 509,52 kWh/d), *Case 3* (12 946,70 kWh/d) and *Case 3-em* (14 321,29 kWh/d). The system can import the least energy from the grid by directly exporting the energy resulting from the PV excess as in *Case 2*.

It is relevant to analyse the maximum power exchanged with the grid to determine the required size of possible power electronics or protections participating in the system. The resulting maximum power exchanged with the grid is 2 315,78 kW for *Base* case, 2 272,36 kW for *Case 2*, 3 853,23 kW for *Case 3* and 3 448,49 kW for *Case 3-em*.

The round-trip efficiency of the system as an energy storage equivalent system, estimated with (3.43), obtained an average $\hat{\eta}_{ESS} = 0,5075$ (SD 0,15).

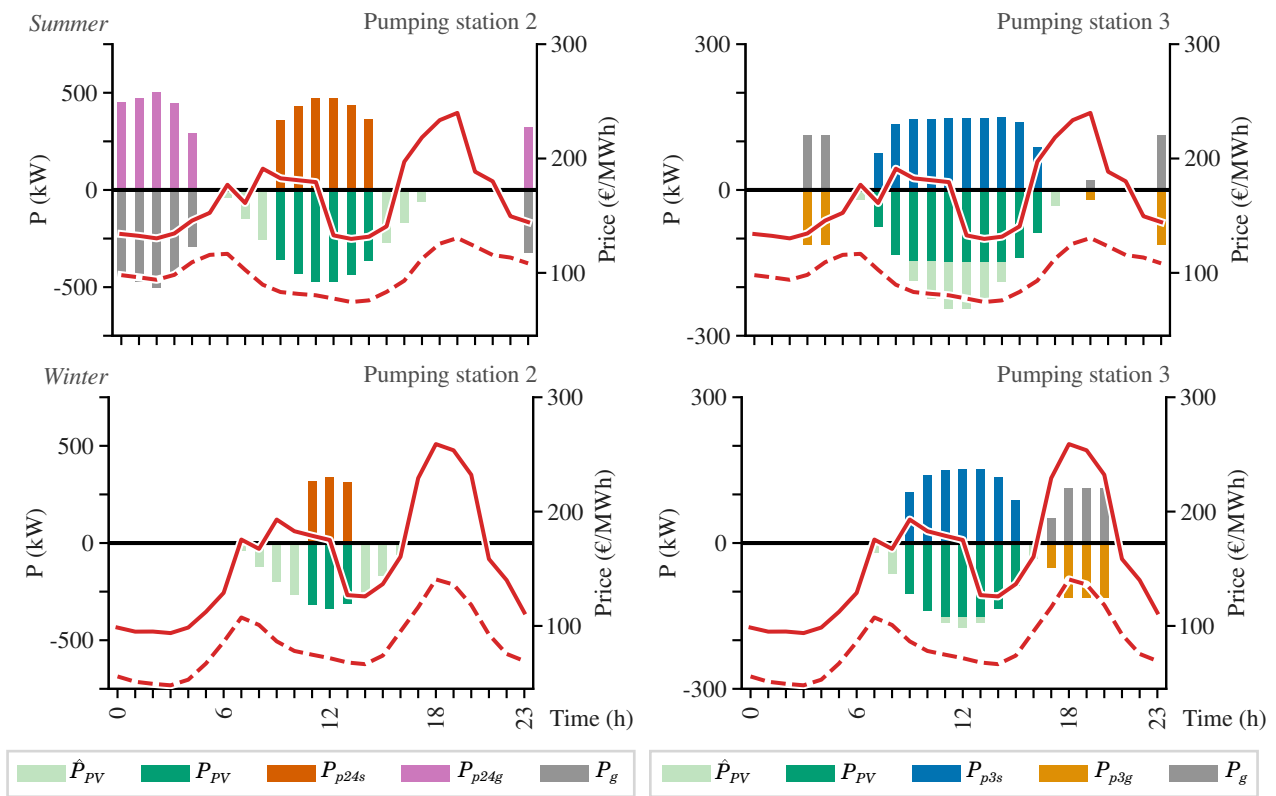


(a) Resulting consumed power

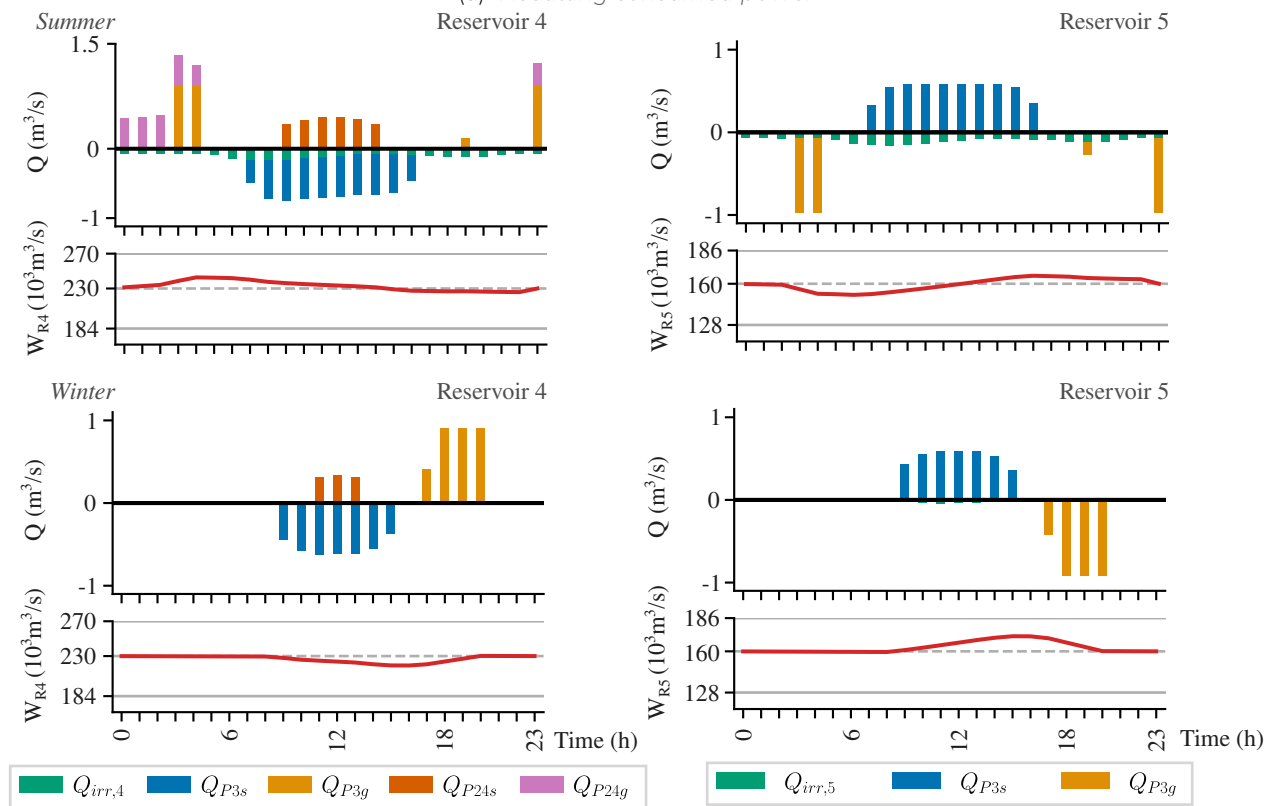


(b) Flows and volume of reservoirs R4 and R5

Figure 3.29 – CR Segrià-Sud upper results - Base case.

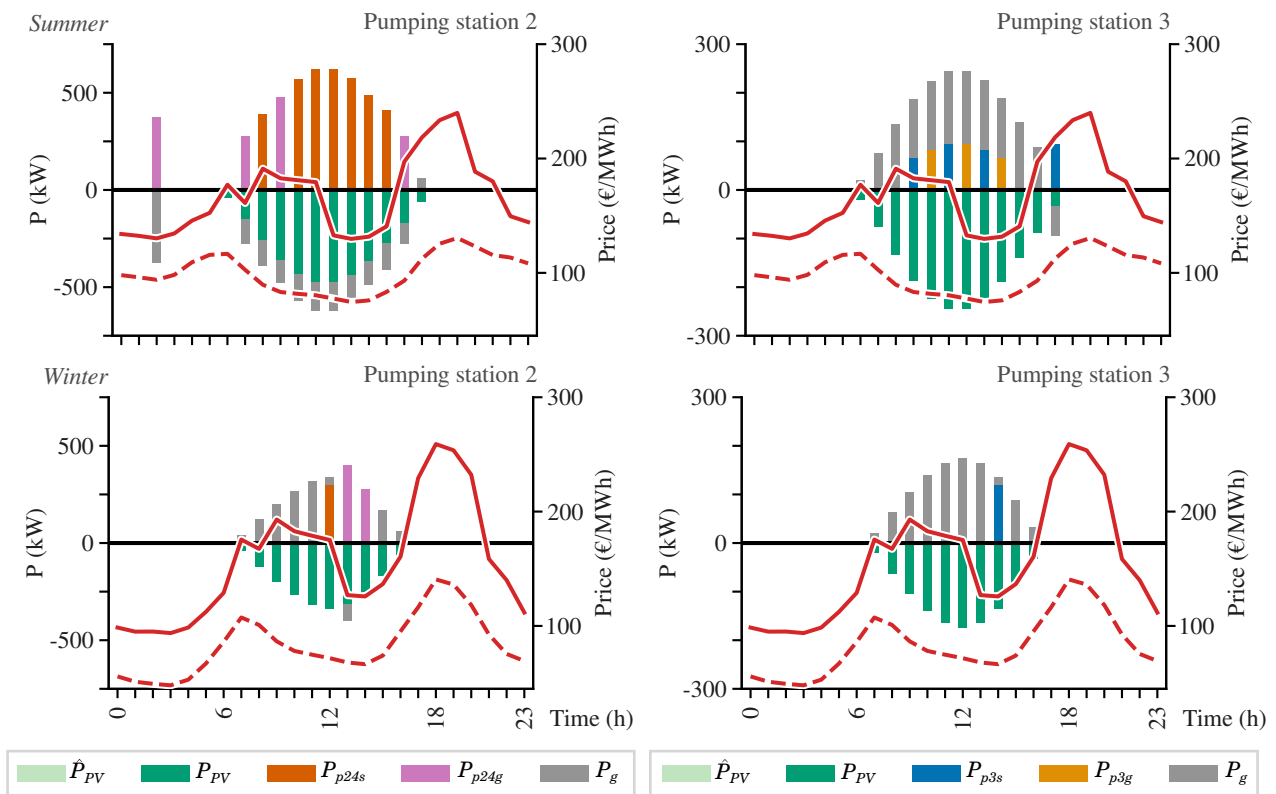


(a) Resulting consumed power

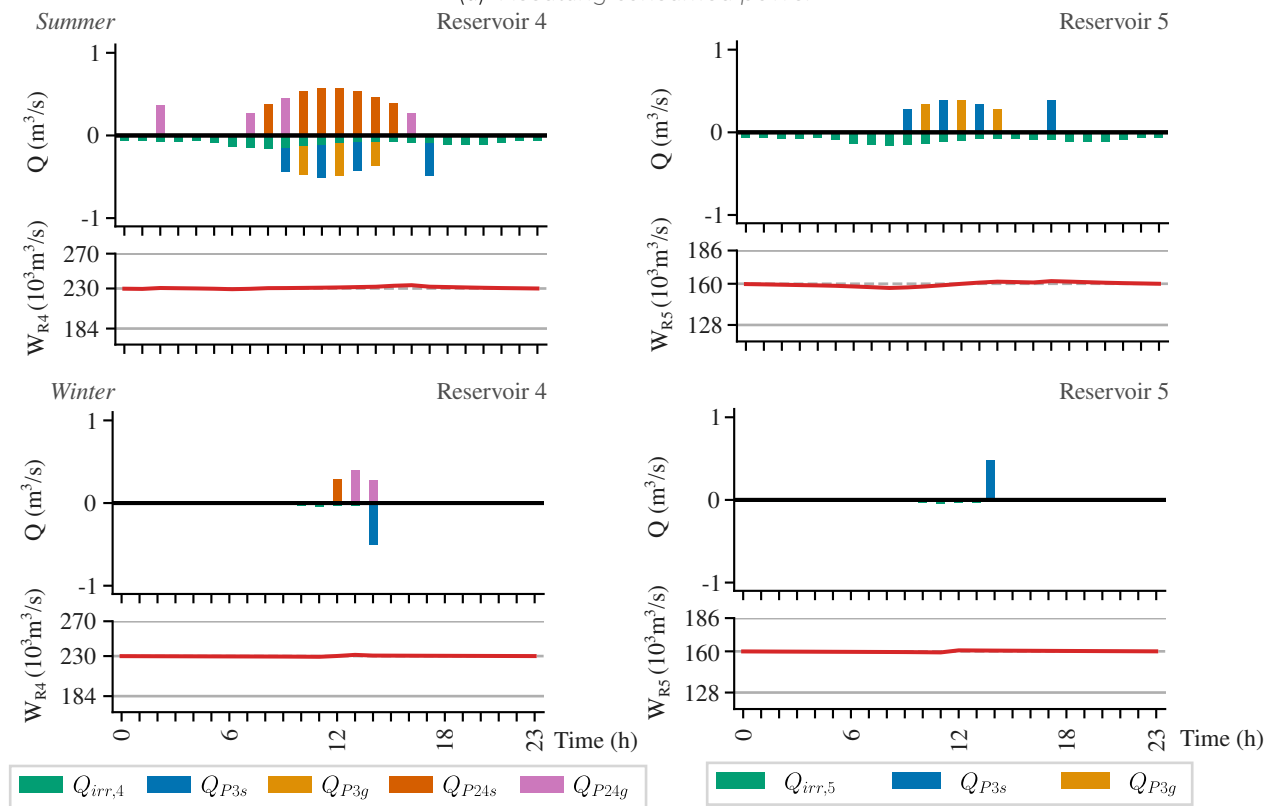


(b) Flows and volume of reservoirs R4 and R5

Figure 3.30 – CR Segrià-Sud upper results - PaT case (Case 1).

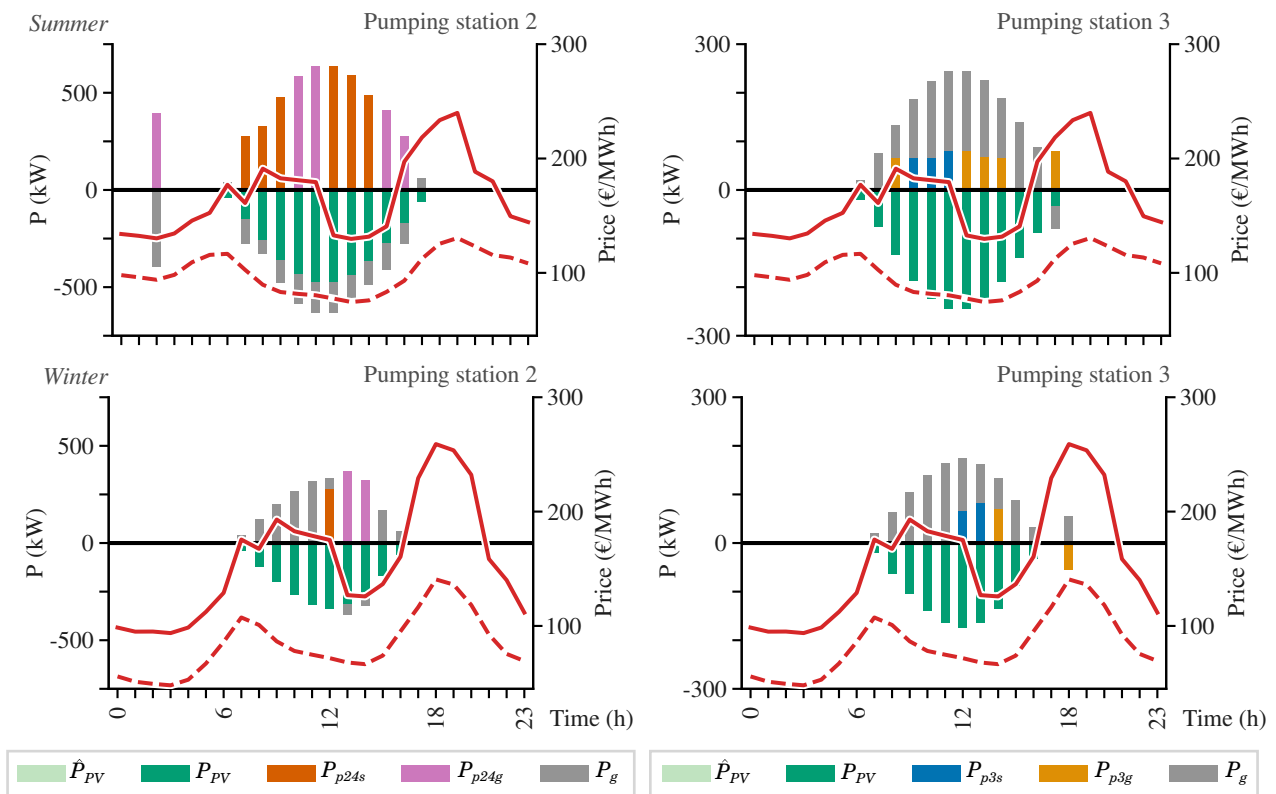


(a) Resulting consumed power

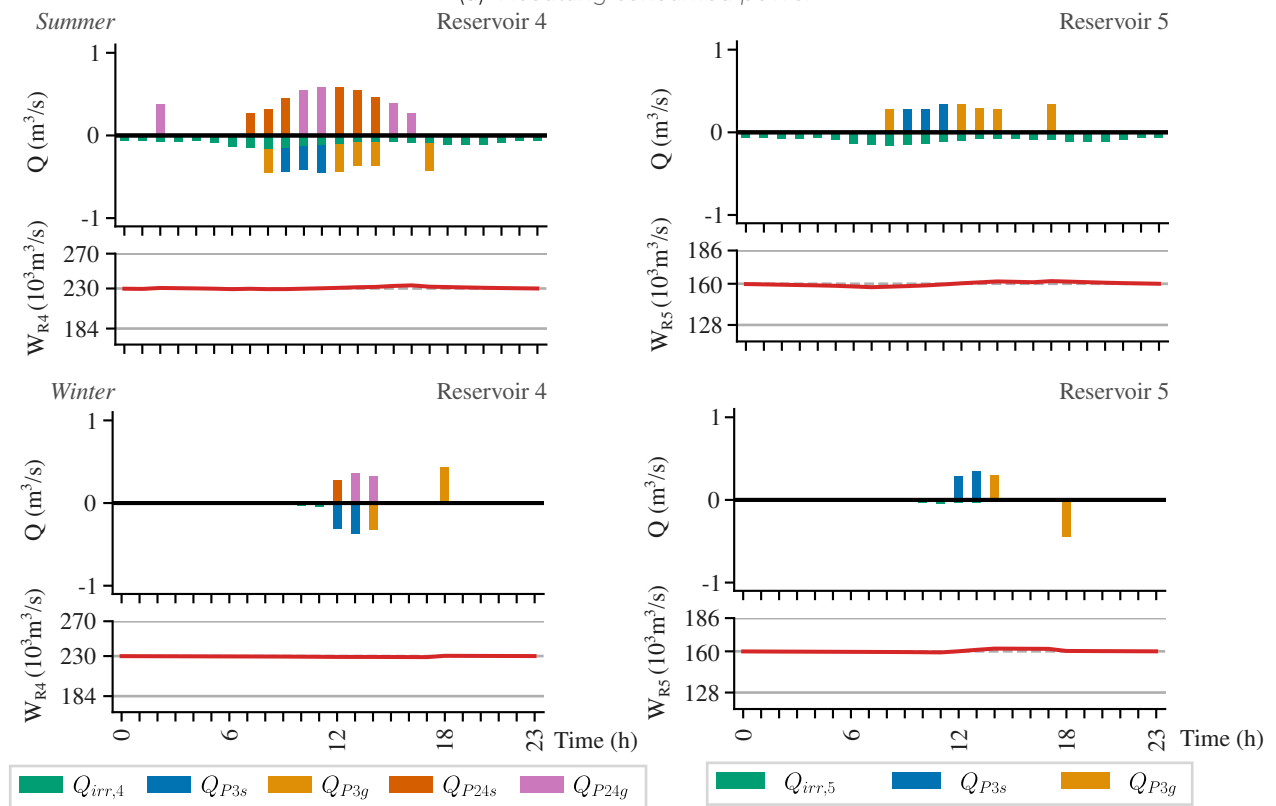


(b) Flows and volume of reservoirs R4 and R5

Figure 3.31 – CR Segrià-Sud upper results - grid connected case (Case 2).

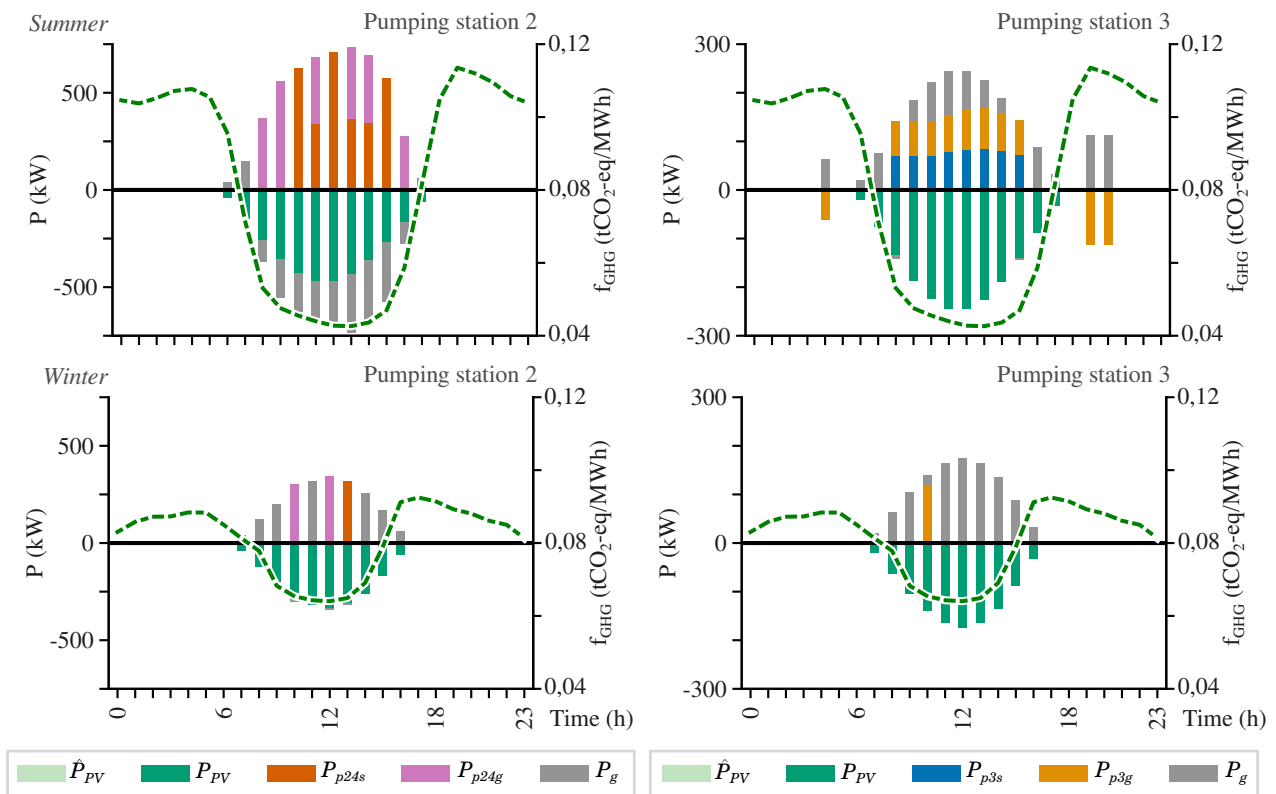


(a) Resulting consumed power

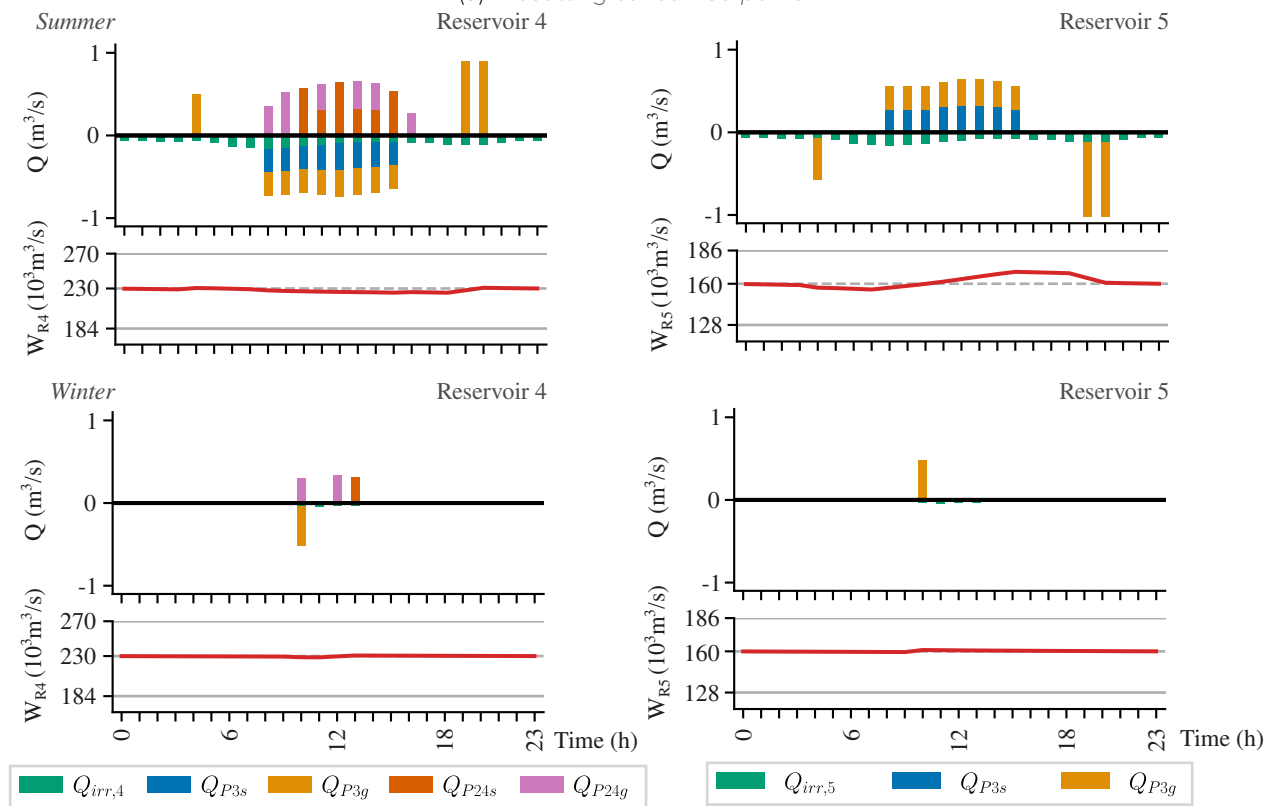


(b) Flows and volume of reservoirs R4 and R5

Figure 3.32 – CR Segrià-Sud upper results - PaT + grid connected case (Case 3).



(a) Resulting consumed power



(b) Flows and volume of reservoirs R4 and R5

Figure 3.33 – CR Segrià-Sud upper results - emissions case (Case 3-em).

Table 3.9 – Results (Lower)

Case	Base	Case 2	Case 3	Case 3-em
Computation time [s]	12,36	399,11	1 273,53	15,44
Energy imported average [kWh/d]	13 571,40	13 061,10	13 567,10	15 251,30
" winter [kWh/d]	5 371,68	5 107,54	5 695,48	4 680,16
" summer [kWh/d]	21 771,20	21 014,60	21 438,70	25 822,40
Energy exported average [kWh/d]	-	551,58	620,40	930,01
" winter [kWh/d]	-	1 000,09	971,06	390,21
" summer [kWh/d]	-	103,07	269,75	1 469,81
Maximum imported power winter [kW]	1 245,88	1 112,90	2 484,61	1 054,80
" summer [kW]	2 315,78	2 272,36	3 853,23	3 448,49
Maximum exported power winter [kW]	-	265,56	381,98	168,52
" summer [kW]	-	61,60	166,68	875,00
GHG emissions average [kgCO ₂ -eq/d]	1 153,78	1 053,35	1 049,50	652,74
" winter [kgCO ₂ -eq/d]	464,23	361,76	414,46	275,01
" summer [kgCO ₂ -eq/d]	1 843,32	1 744,94	1 684,55	1 030,47
Energy expense average [€/d]	1 754,31	1 706,36	1 698,71	2 432,11
" winter [€/d]	515,31	505,64	538,14	770,86
" summer [€/d]	2 993,32	2 907,08	2 859,28	4 093,36
Energy income average [€/d]	-	46,68	66,50	110,64
" winter [€/d]	-	81,57	105,69	34,75
" summer [€/d]	-	11,79	27,31	186,53
Total cost average [€/d]	1 754,31	1 659,68	1 632,21	2 321,47
" winter [€/d]	515,31	424,06	432,44	736,10
" summer [€/d]	2 993,32	2 895,30	2 831,97	3 906,83

Environmental analysis

From a GHG emissions point of view, considering the typical day grid's equivalent CO₂ factor evolution in summer and winter (Figure 3.28) and null for the irrigation system, results in positive emissions for all cases. Case 3-em, as expected, derives the best for such a purpose and utilises its energy storage capabilities to maximise the energy delivered to the grid during high emission factor hours (mostly evening in summer). Fair compensations should however apply to the irrigation community since this operation strategy is not as economically beneficial as Case 3 solution with an average difference of 689,26 €/d for an average reduction of 396,76 kgCO₂-eq/d in emissions.

The daily water consumption is maintained for all the cases, as stated above, since a cycle condition is imposed in the reservoir device. In essence, the modelling of the system implicitly considers the extra daily impact on the water source and cancels it.

Sensitivity analysis

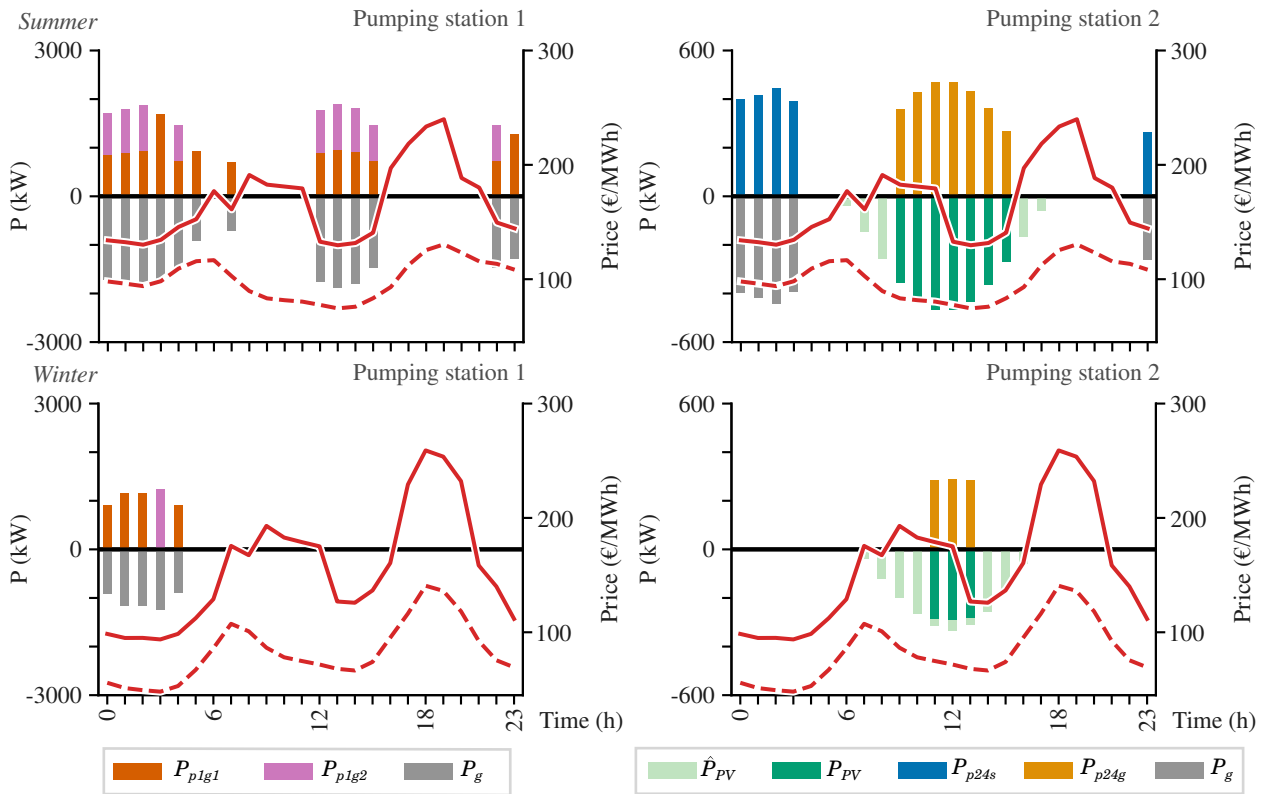
This section covers a sensitivity analysis on the most relevant parameters of the upper section of the Segrià-Sud irrigation system. The results of the sensitivity analysis are displayed in Table 3.10 and the *spiderplots* in Figure 3.38. *Spiderplots* plot a curve for each variable on a single $x - y$ plot showing the change in goal value over a relative change of the variable values from the base case. Their purpose is to display information about a certain number of variables including their limits, impact on the outcome and the amount of change required to reach a break even point [78].

We applied the following variations over the base case:

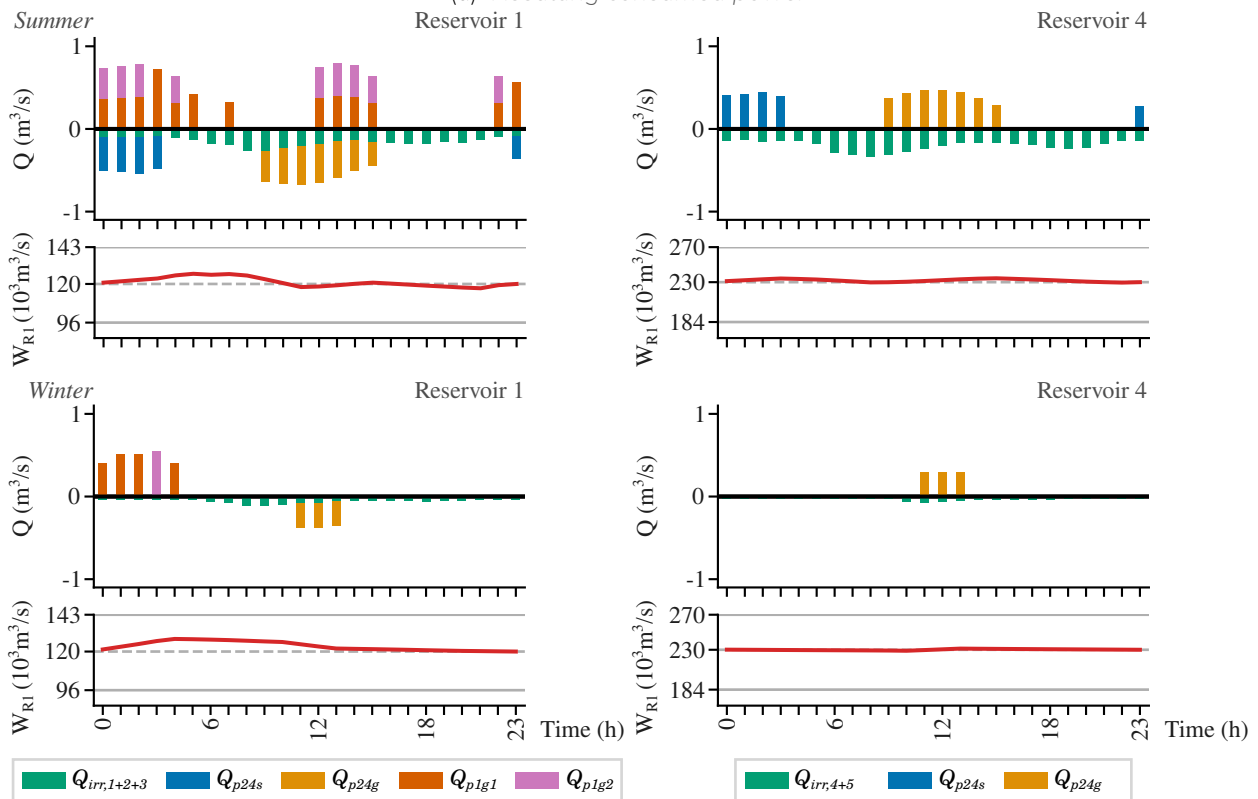
- Irrigation demand $Q_{irr} \pm 20\%$. As reviewed in Section 2.1, there is an interest from the administration to increase the share of irrigated land as well as a reduction of the water demand from these crops. We conceive two scenarios: an increase of the general irrigation demand due to a substitution of dry land to irrigated or a decrease of the general irrigation demand driven by water efficiency requirements.
- Selling price of electricity $c_{sell} \pm 20\%$ from 8:00 h to 16:00 h. The mass implementation of solar PV may drive market prices down during high intensity solar hours, as it has been noticed from self-consumption surplus prices reaching negative values in Spain [77]. We also analyse the opposite scenario where the market prices increase instead, which would decrease the incentives to drive the facilities as an energy storage system.
- Efficiency of PaT $\eta_{pat} \in (0,5, 0,8)$. As stated in Section 3.3.1, it is not a trivial task to define the characteristics and behaviour of a PaT, therefore we based the range of values of its performance in previous work and literature [41, 68].

Table 3.10 – Sensitivity analysis total cost average (€/d). ^(t) marks the cases where the system makes use of the pump as a turbine.

Case	Base	Case 1	Case 2	Case 3
base	166,85	^(t) 118,65	-56,10	^(t) -56,24
-20% Q_{irr}	95,90	^(t) 45,12	-126,13	^(t) -126,52
+20% Q_{irr}	267,63	^(t) 214,98	24,35	24,35
-20% c_{sell}	166,85	^(t) 119,00	-40,10	^(t) -41,50
+20% c_{sell}	166,85	^(t) 118,28	-71,77	-71,77
$\eta_{pat} = 0,5$	166,85	^(t) 137,22	-56,10	-56,10
$\eta_{pat} = 0,6$	166,85	^(t) 125,62	-56,10	^(t) -56,34
$\eta_{pat} = 0,8$	166,85	^(t) 112,00	-56,10	^(t) -56,63

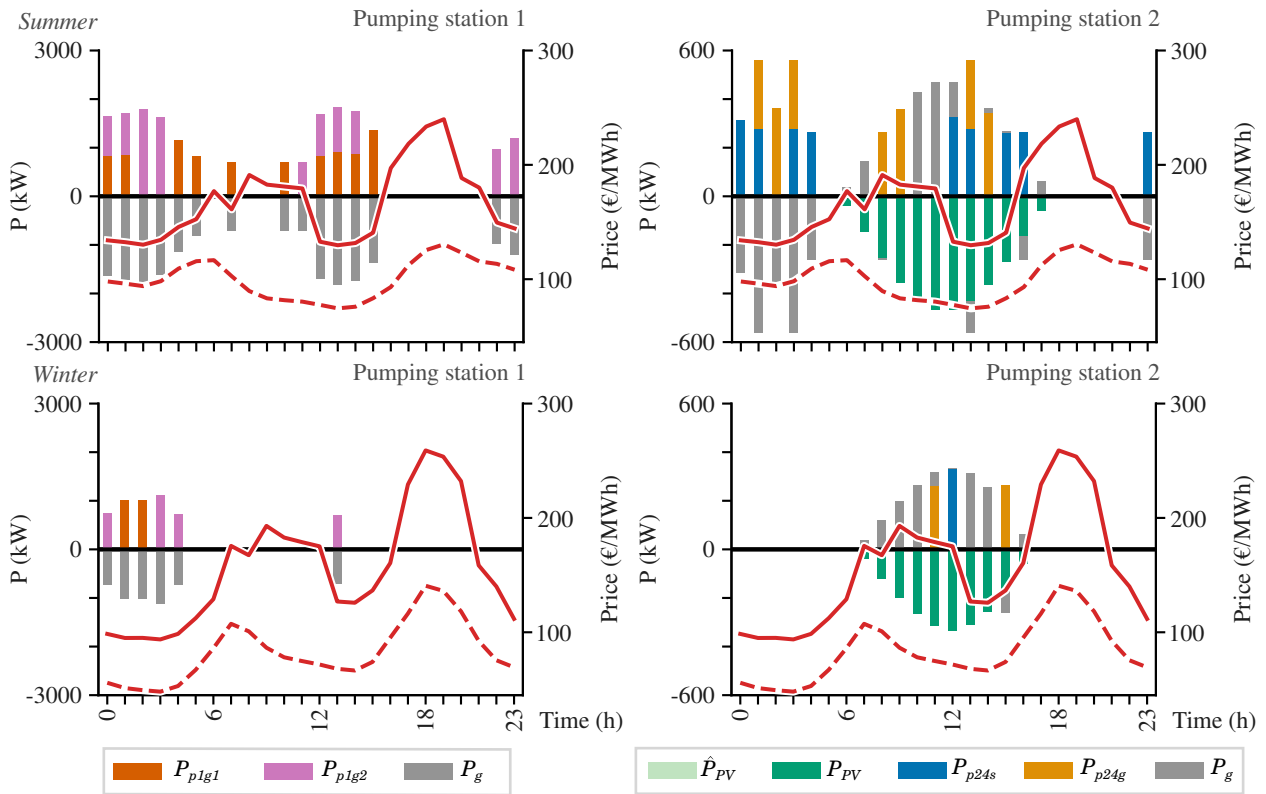


(a) Resulting consumed power

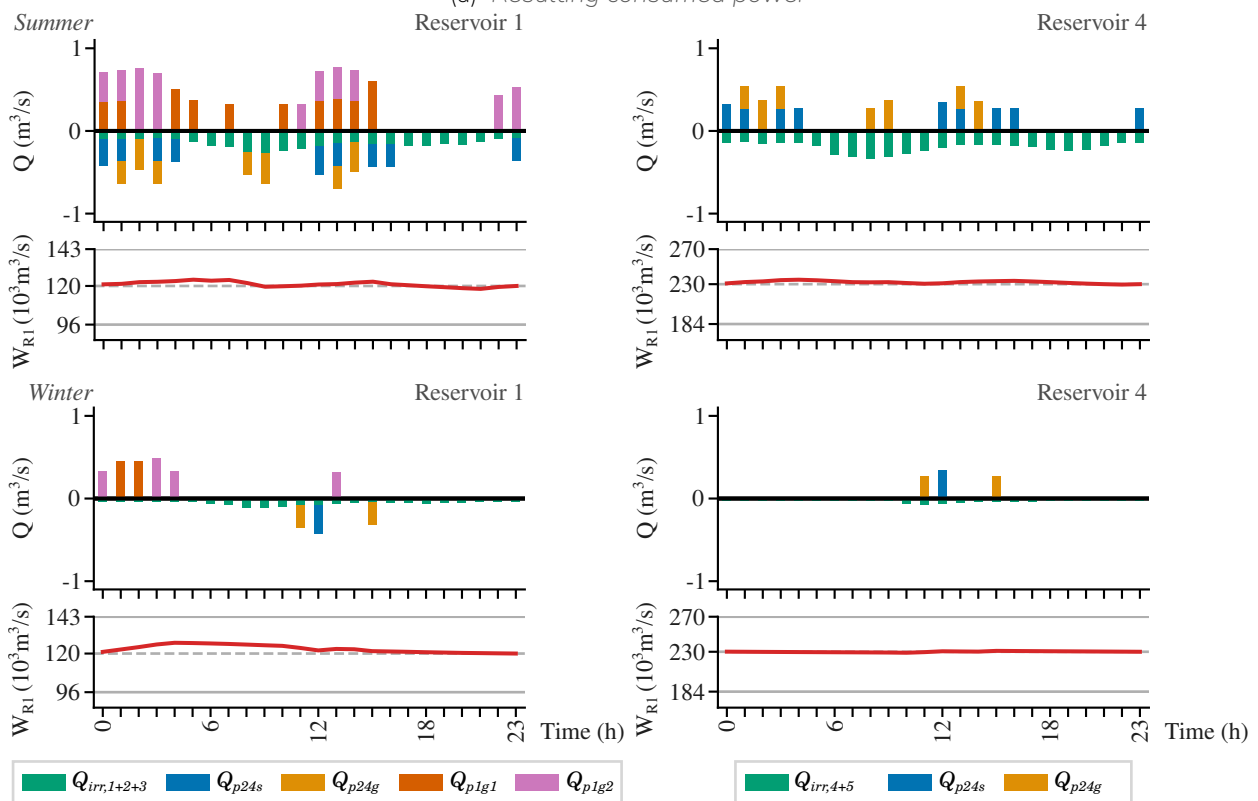


(b) Flows and volume of reservoirs R1 and R4

Figure 3.34 – CR Segrià-Sud lower results - Base case.

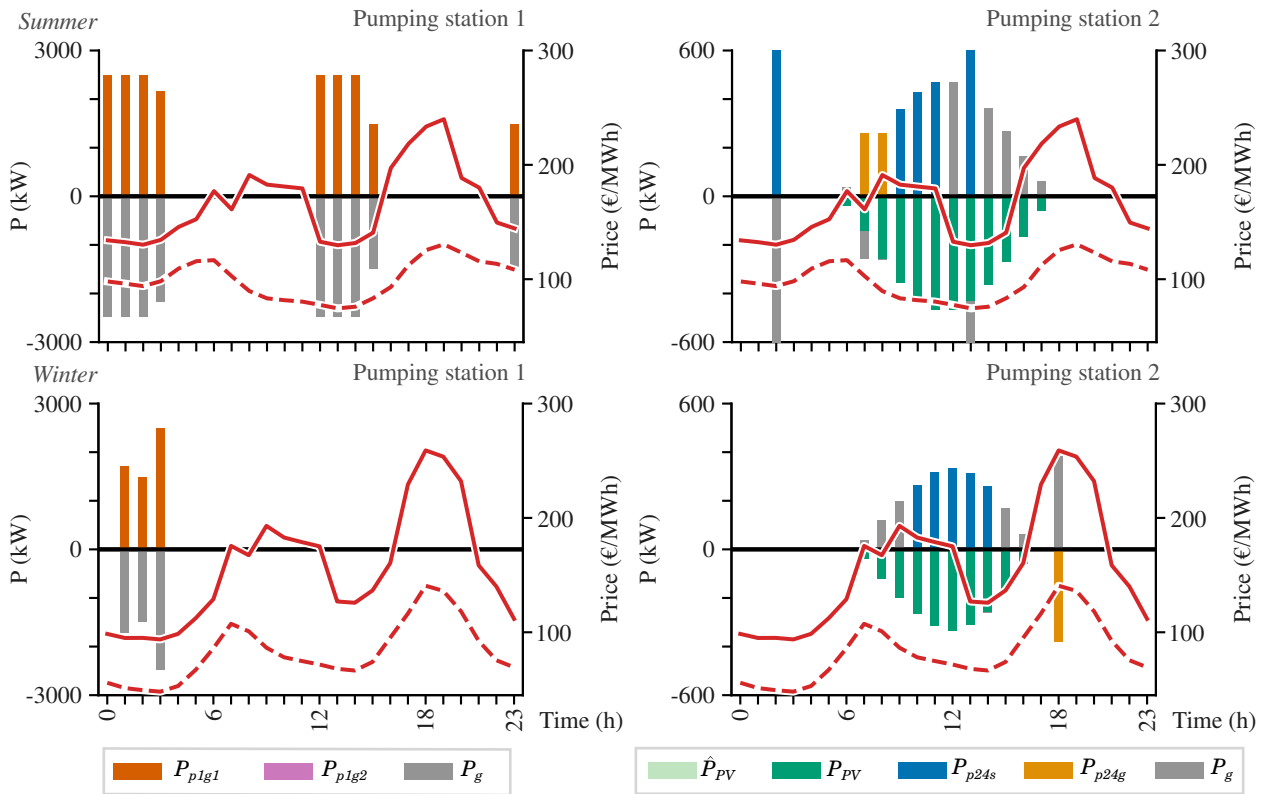


(a) Resulting consumed power

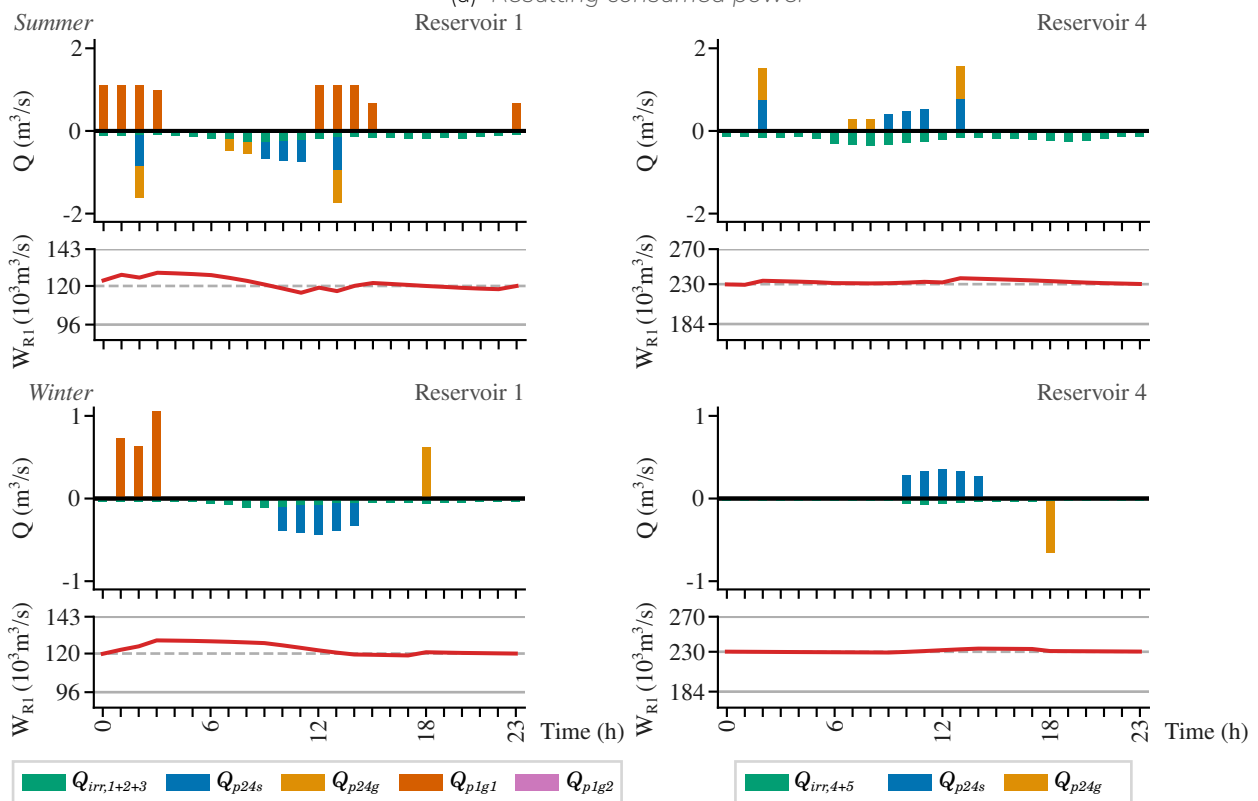


(b) Flows and volume of reservoirs R1 and R4

Figure 3.35 – CR Segrià-Sud lower results - grid connected case (Case 2).

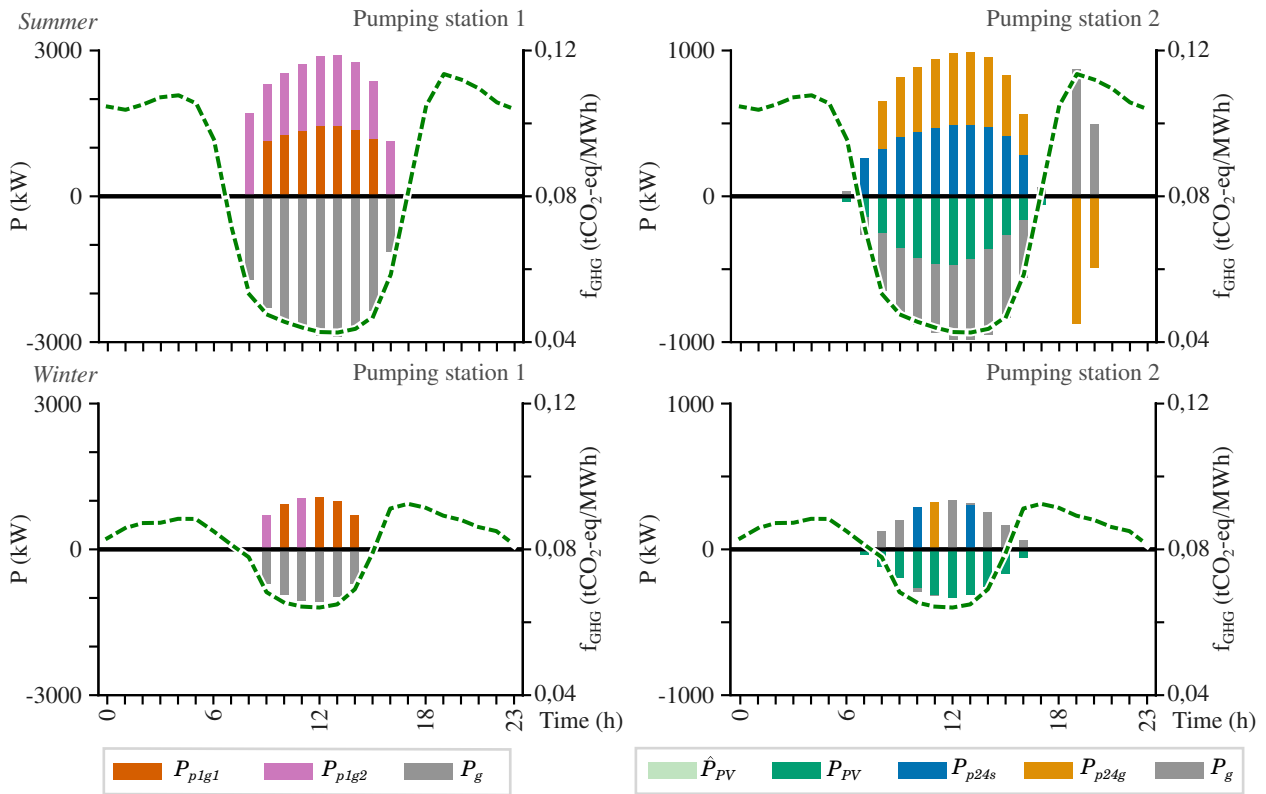


(a) Resulting consumed power

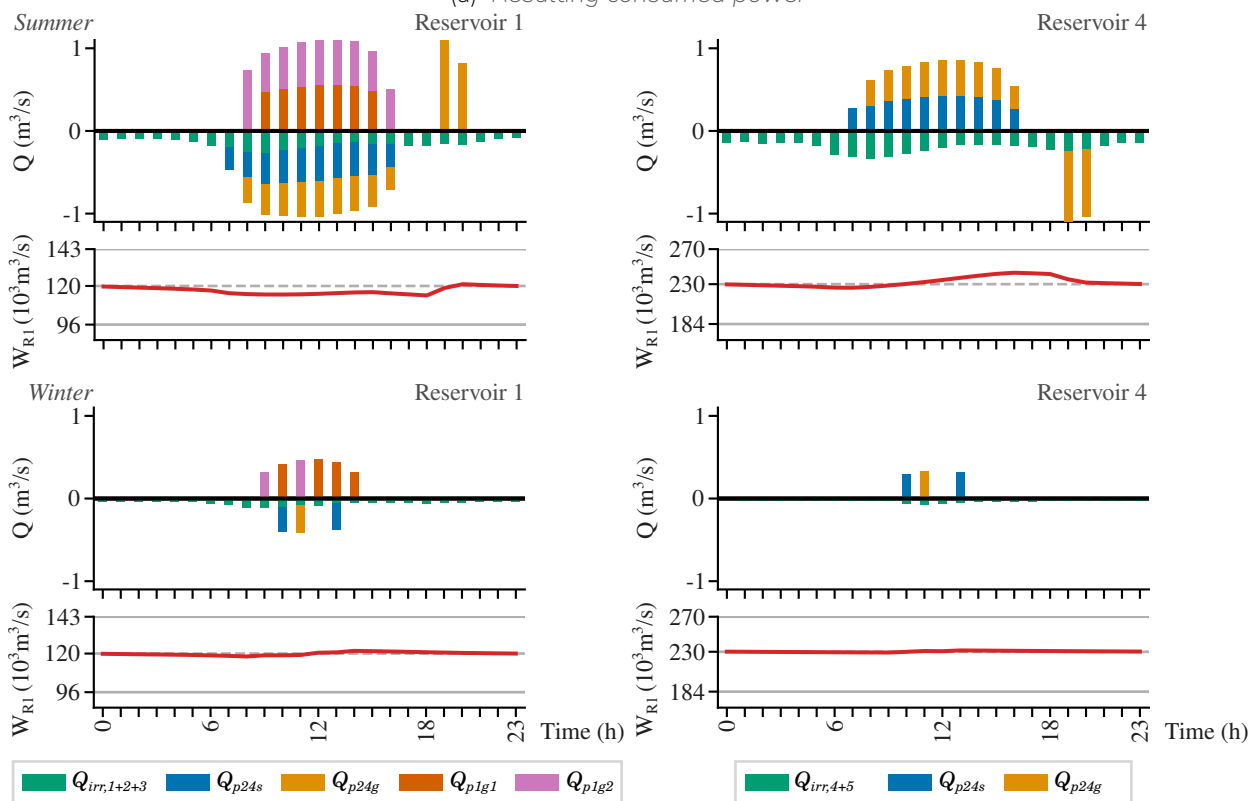


(b) Flows and volume of reservoirs R1 and R4

Figure 3.36 – CR Segrià-Sud lower results - PaT + grid connected case (Case 3).



(a) Resulting consumed power



(b) Flows and volume of reservoirs R1 and R4

Figure 3.37 – CR Segrià-Sud lower results - emissions case (Case 3-em).

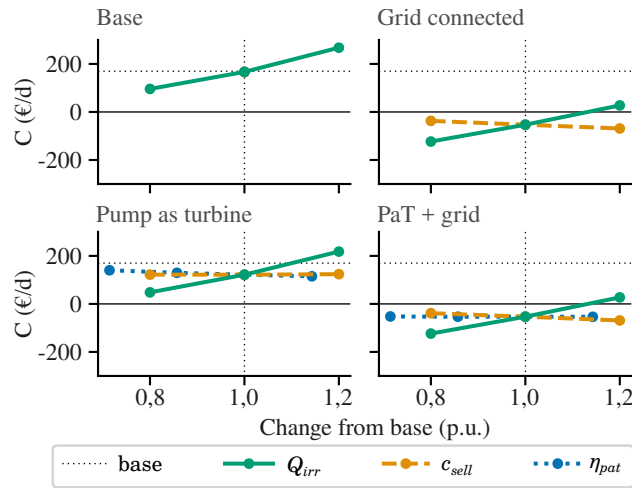


Figure 3.38 – Spiderplots resulting from the sensitivity analysis.

3.4.4 CEDER-CIEMAT

The study case of Centro de Desarrollo de Energías Renovables (CEDER)-Centro de Investigaciones Energéticas Medioambientales y Tecnológicas (CIEMAT) is modelled as follows in Figure 3.39. The center contains 3 small reservoirs of 2 000 m³, 1 500 m³ and 500 m³, a small 16 kW PV plant and a 40 kW turbine. There is a bank of pumps with a nominal power of 7,5 kW each, which can only operate at nominal power or be disconnected. Therefore, the *DiscretePumps* model used allows the activation of an integer number of pumps, ranging from 0 to the total number of installed pumps—in this case, 4 pumps. Initially, the pumps and turbines are connected to a common bus along with the PV plant and the grid, supplying the electrical loads of the center itself.

In order to model the system in a Pyomo environment, it is necessary to introduce several blocks. For example, the electrical loads block is used to model the center’s demand, and the hydraulic switch block is used to supply either the upper (R2) or middle (R1) reservoir. Note that a source block is used between reservoir 1 and reservoir 2 to model a pipe with a controllable valve without losses.

The *Discrete Pump* used in this case is modelled by adding to the *Pump* device the next constraint:

$$P_{e,i}(t) = P_{n,i} N_{on,i}(t) \quad (3.44)$$

Where $P_{n,i}$ the nominal power of the pump and is introduced as a parameter into the model. On the other hand, $N_{on,i}(t)$ is a integer variable that defines the number of working pumps, the variable have a minimum of 0 and a maximum of N_{pumps} that is the total number of installed pumps.

Various cases are carried out to evaluate the tool and the CEDER system. Each case considers different initial conditions and assumptions:

- Case 1: No battery nor PV sizing is considered.
- Case 2: Possibility of sizing a new battery and extra PV power.
- Case 3: Battery is already present and extra PV power can be sized.

The model is constructed using data provided by CEDER, such as electrical demand and solar irradiation measurements. Additionally, another source is used to obtain voluntary price for the small consumer (PVPC) data.

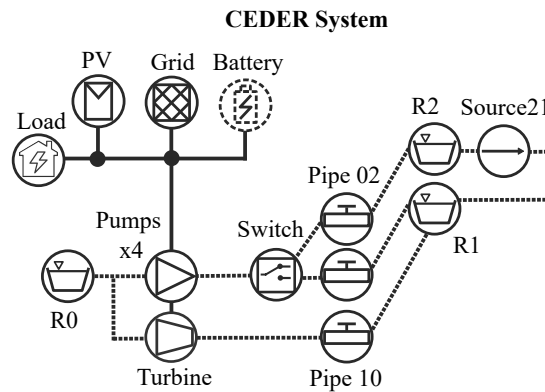


Figure 3.39 – CEDER case representation with Pyomo blocks.

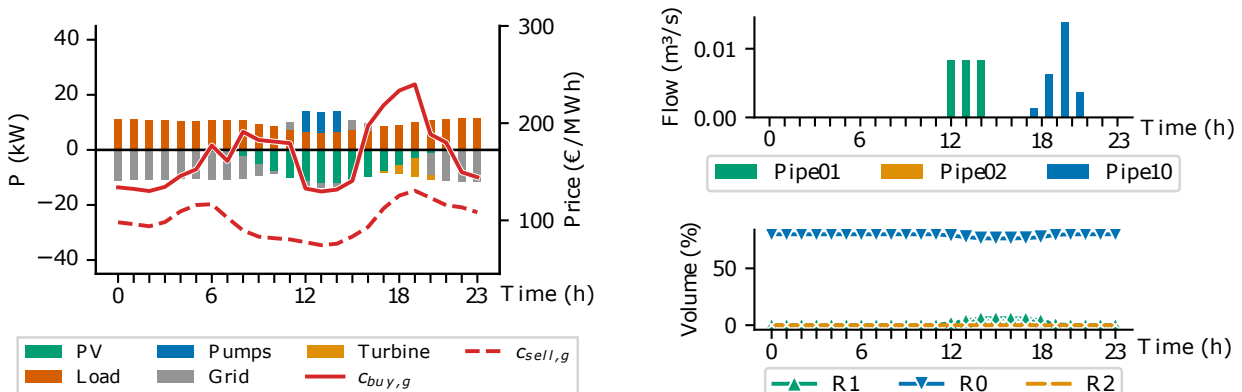
For each case, two simulations are performed: one considering typical summer data and another considering typical winter data. This approach allows the study of the tool's potential in each season with different irradiance levels, electrical demand, and electricity prices.

The initial conditions for a more accurate approach assume that reservoirs 1 and 2 are completely empty, while reservoir 0 is at maximum capacity. If a battery is considered, it is also assumed to be completely discharged. This approach ensures that no storage source has initial energy, whether electrical or gravitational.

Results

In each case, a plot is presented showing the balance of power consumed and generated, where power injected into the energy balance node is negative, while the remaining power is positive. Therefore, PV power will be shown as negative since it is generated and injected into the EB node. Additionally, a line plot represents the PVPC and the selling price per hour.

Case 1 : In summer, the system takes advantage of high solar irradiation during the day and turbines at night to supply the electrical demand. On the other hand, in winter, the model takes advantage of low energy prices at night to activate the pumps and store water, which will be used during high price peaks to meet the demand.



(a) Resulting consumed power.

(b) Reservoirs level.

Figure 3.40 – CEDER results - Case 1 in summer.

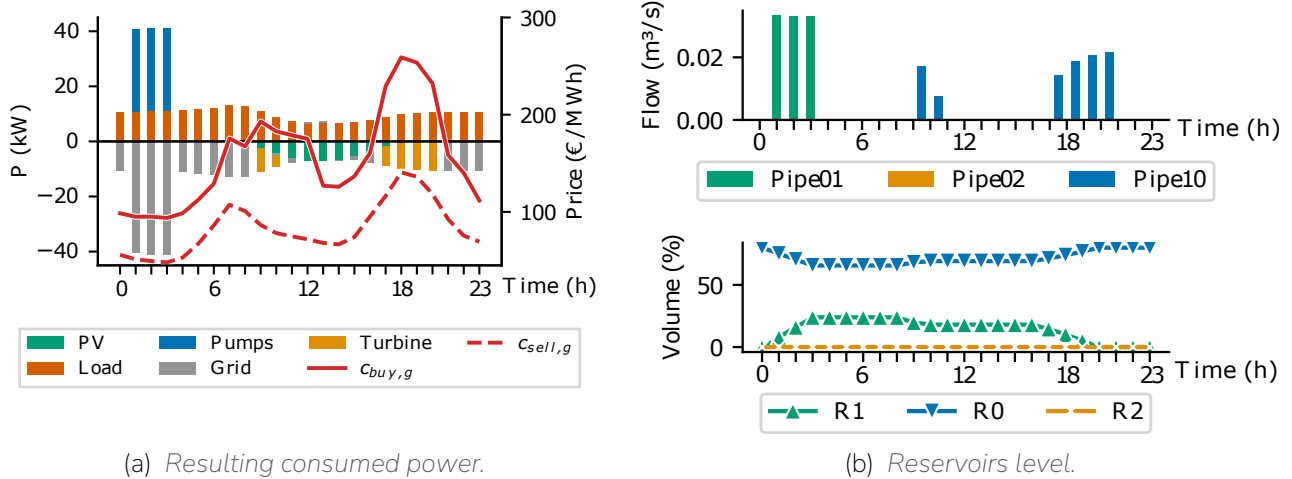


Figure 3.41 – CEDER results - Case 1 in winter.

Case 2 : The problem determines the maximum PV power capacity, up to 66 kW. In summer, the system utilizes high solar irradiation to store water in the upper reservoirs and sells the excess energy. At night, the stored water is turbined to supply the load demand. In winter, the system takes advantage of the high installed PV power to sell electricity to the grid during periods of high prices and to store water in the upper reservoirs. Then, during the night and peak price periods, the stored water is used for turbining to generate energy and supply the electrical loads. No battery is sized in this optimisation case.

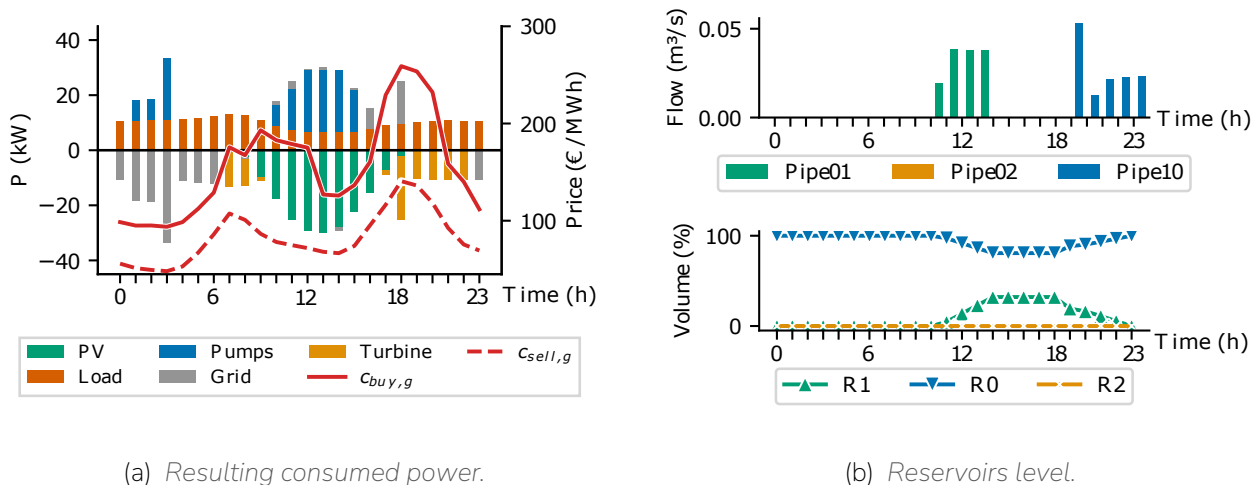
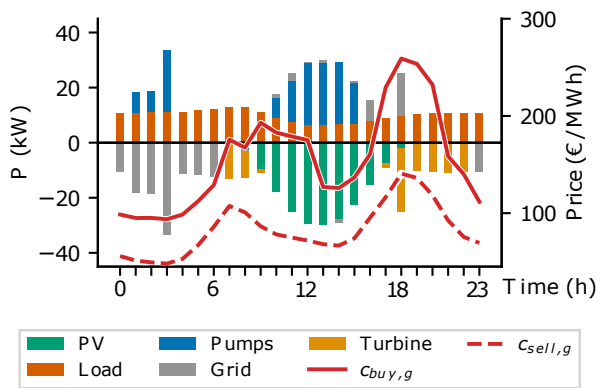


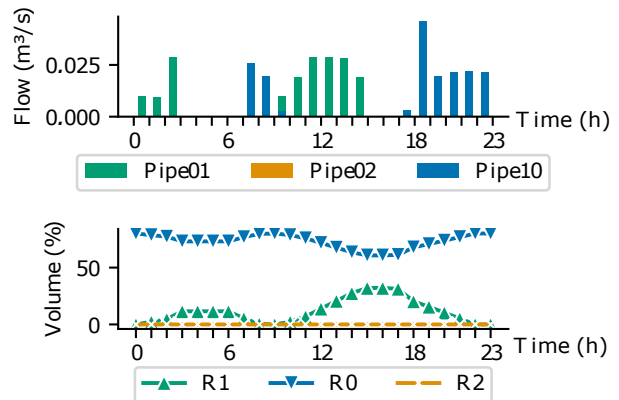
Figure 3.42 – CEDER results - Case 2 in summer.

Case 3 : In this case, the model considers an already installed battery. Since the battery's efficiency is higher than that of the water storage system, the optimisation prioritizes charging and discharging the battery over using the water system. Therefore, in summer, the surplus PV power is used to charge the battery, supply the loads at night, and sell electricity when prices are high. On the other hand, in winter, the system takes advantage of low electricity prices at night to charge the batteries and discharge them during high-price periods. Again, no additional battery capacity is sized.

Table 3.11 summarizes the operation and sizing costs per day after simulating each case under summer and winter conditions. It also displays the computation time in minutes on an 8th Gen Intel Core i5 @ 1,80 GHz laptop with 8,0 GB of RAM. From Table 3.11, it can be seen that Case 1 is the most expensive

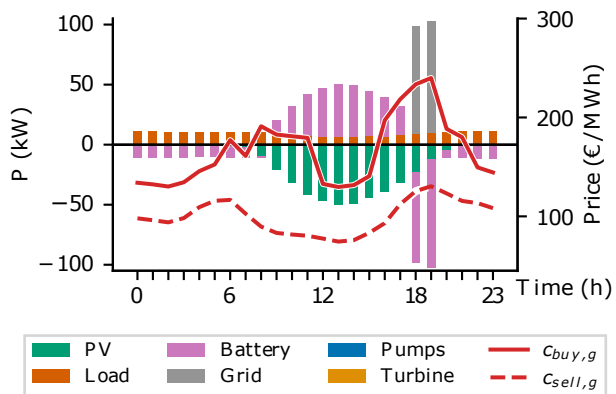


(a) Resulting consumed power.

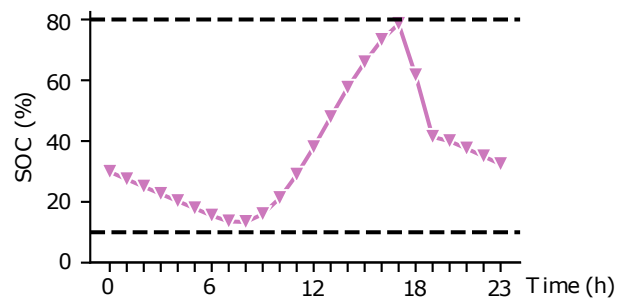


(b) Reservoirs level.

Figure 3.43 – CEDER results - Case 2 in winter.

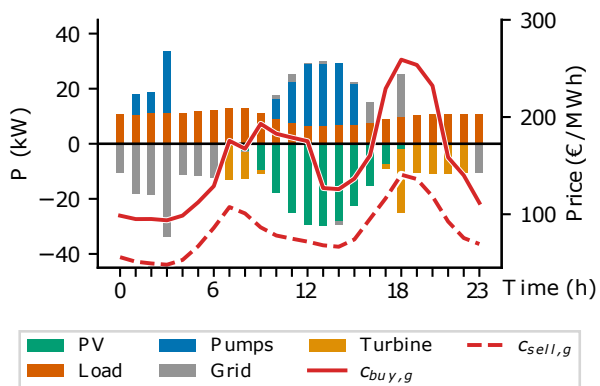


(a) Resulting consumed power.

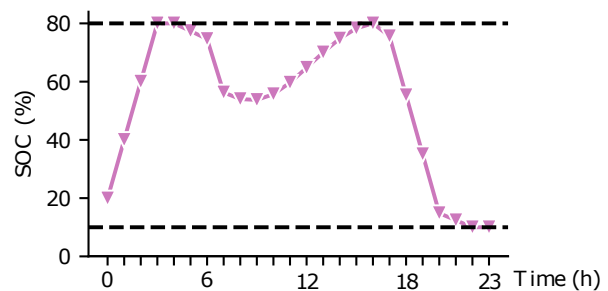


(b) State of charge of the battery.

Figure 3.44 – CEDER results - Case 3 in summer.



(a) Resulting consumed power.



(b) State of charge of the battery.

Figure 3.45 – CEDER results - Case 3 in winter.

solution, whereas remodelling to the Case 3 topology (installed battery) results in the most profitable option. In this case the problem was solved using the Bonmin solver.

Table 3.11 – Objectives values and execution time per case and season.

Case - season	Objective value [€/day]	Execution time [s]
Case 1 - Summer	21,84	1,31
Case 1 - Winter	26,58	6,15
Case 2 - Summer	-7,78	4,65
Case 2 - Winter	11,33	5,64
Case 3 - Summer	-21,83	2,44
Case 3 - Winter	-3,78	3,24

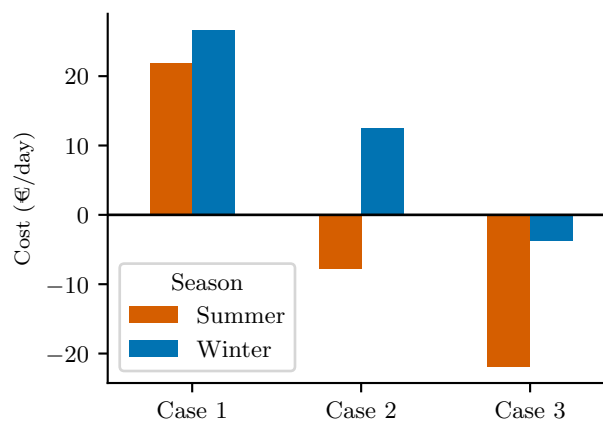


Figure 3.46 – CEDER costs results comparison.

3.5 Conclusions

The redesign of irrigation pumping facilities to convert them into grid-connected energy storage facilities has been developed within a mathematical optimisation framework. To facilitate analysis, the UPC team has developed an open-source tool that allows modelling an existing plant and sizing the new equipment needed to make irrigation communities to play an active role in the power systems.

Adjustments on the methodology and models to reduce the complexity of the MINLP problem allowed the analysis of the CR Segrià-Sud irrigation system, which is a complex system comprising several reservoirs and pumping stations. However, it still presents scalability issues that prevent a more detailed analysis of an irrigation system such as considering the facilities as a whole and increasing the number of evaluated hours.

In economic terms, the best strategy is to pump extra water using power from the PV plants and turbine it during higher sell price hours in winter. However, this is only effective in a sufficient price difference between solar hours and night hours scenario.

In emission terms, the optimal scheduling results in using the energy storage functionality in summer, which presents a large difference of emission factor between different times of the day.

The average round-trip efficiency of the facilities as an energy storage system resulted in 50,61 %. The performance of the system is conditioned by the efficiencies of the pumps and pumps as turbines as well as the pressure losses emerging from the hydraulic system.

The sensitivity analysis show very high influence of the irrigation demand over the scheduling of the system and a considerable influence of the selling price of electricity and efficiency of the pump as turbine. High irrigation demand prevents the system to operate as an energy storage system. High selling prices during solar hours and lower pump as turbine efficiencies make it more profitable to directly inject the photovoltaic power to the grid instead of storing the energy.

3.5.1 Future work

This section discusses gaps we identified during our research to work on future analysis.

Further reduce the complexity of the models and improve the computability of the problem is a critical objective to allow for more accurate and detailed analysis as well as larger and more complete systems.

We analysed the irrigation system study case for a long term daily energy storage scenario. A seasonal storage scenario would deliver insight on other operation approaches, however the limitations of the methodology this work has presented did not allow for such an analysis.

Analyse the efficiency of a pump as turbine and the effect on its maintenance costs and lifetime. There is not a consensus in the literature on this topic and requires further research.

Finally, apply the knowledge and methodology and implement and on-site demonstrator.

4 Energy storage sizing to prevent water hammer on PV pumping systems

Water distribution for irrigation on rural areas is typically managed through irrigation communities, whose facilities consist of reservoirs supplied by pumping stations. They require large amounts of energy to operate, up to some GWh annually. To cover such demand, they often set up solar photovoltaic pumping systems involving an off-grid photovoltaic plant coupled to a hydraulic pump through an inverter. These systems present little inertia, therefore when clouds shade the photovoltaic panels induce start-stop cycles causing fatigue, hydraulic shocks and severe mechanical loading on hydraulic assets. Our work proposes a methodology to size energy storage systems for photovoltaic pumping systems, such that their response against clouds shading on panels is improved. We propose a simple cost function based on capital and operation costs considering the effect of clouds, the optimal value of which can be analytically determined. Then, we apply it to a real study case in the facilities of Comunitat de Regants (CR) Segrià-Sud, located in Catalonia, north-east of Spain, and consisting of a 275 kWp photovoltaic plant and a 160 kW pump.

Also, we develop a methodology and analyse a grid connected case on the same facilities. This chapter follows the work developed at [79].

This chapter is structured as follows:

- i Section 4.1 introduces the problem and reviews the state of the art solutions.
- ii Section 4.2 describes the problem we are addressing and further establishes the objectives and assumptions.
- iii Section 4.3 defines the methodology for the off-grid case, which is applied in Section 4.4 on the real Comunitat de Regants Segrià-Sud scenario study case.
- iv Section 4.6 analyses the feasibility of an Aqueous-electrochemical recuperator (ECR) battery.
- v Section 4.5 develops the methodology and analyses the CR Segrià-Sud scenario considering the whole photovoltaic (PV) pumping facility is connected to the grid.
- vi Section 4.7 concludes the study and provides additional future research settled on the obtained results.

4.1 Introduction

Irrigation communities' pumping stations require large amounts of energy ranging from annual hundreds of MWh to tenths of GWh, for instance 12,5 GWh per year in [29] (Catalonia, Spain) and 80 GWh per year in [37] (Occitanie, France). The required energy is supplied either by the grid or diesel generators if the access of the system to the grid is limited. This is why many of them set up solar PV pumping systems to reduce their energy costs, consisting in feeding the hydraulic pumps directly from solar PV panels through a direct current (DC) to alternating current (AC) power converter. These systems are disconnected from the electrical grid and consequently only operate when the solar PV plant can provide the required power to the pump. Figure 4.1 illustrates the system from the study case of this document as an example, which involves a PV pumping system (highlighted) in parallel with 2 grid connected pumps that operate during night when the electricity prices are lower.

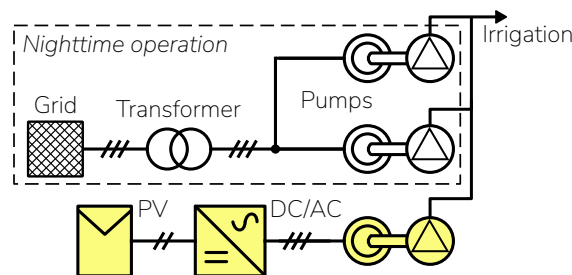


Figure 4.1 – Electrical scheme of a PV pumping system.

This practice may be found on many countries either to replenish reservoirs for gravity based irrigation as well as for drip or sprinkle pumped irrigation systems, for instance in the Mediterranean region or India [80, 81, 82]. Multiple reasons may exist for these systems to not be grid connected, being location a common one found in the literature, such as [83] in Sudan, but also legal or economic aspects. Nevertheless, off-grid PV pumping is an approach irrigation communities are currently taking. Table 4.1 collects the topmost of the PV pumping systems present in irrigation communities in the region of Catalonia, which are constantly being upgraded.

Table 4.1 – Irrigation communities' with PV pumping systems in Catalunya. P_{PV} is the total PV peak power and P_{pump} the total power of the pumps fed by the PV plants.

Irrigation community	P_{PV} (kWp)	P_{pump} (kW)	Last upgrade	Reference
Segrià Sud	798,0	475,0	2024	[27, 28]
Bassanova	350,5	N/D	2024	[15]
L'Albí	198,0	170,0	2023	[13]
Benissanet	513,0	330,0	2023	[16]
Les Planes i Aixalelles	217,8	110,0	2021	[19]
Garrigues Sud	601,9	584,8	2021	[35]
Fenollet	313,2	255,0	2020	[17]
Espluga Calba	52,6	30,0	2017	[20]

Academic research on PV pumping systems dates back to 1960's [84] and is predominantly focused on understanding the characteristics and behaviour of the system [85], sizing the PV plant and the pump [86, 87, 88] and optimising their control and energy management [89, 90].

4.1.1 Water hammer in PV pumping

A common setting involves an irradiance sensor installed among the PV panels, which triggers the system according to its readings, such as disconnecting the pump from the inverter in the event of sun irradiance G dropping below a certain threshold G_{th} (W/m^2) (Figure 4.2). Below that value, the PV plant is not capable of supplying enough power to meet the demand of the pump, causing it to stop.

This practice, although simple, has deleterious effects on the pumping system. On the one hand, start-stop cycles cause fatigue on the pumping system. On the other hand, when a pump is suddenly stopped during flow it causes a pulse of high pressure that propagates upstream at the sonic wave speed, known as *hydraulic shock* or *water hammer* [91, 92]. This effect may damage the pump and the containing pipes, as a result of large pressure variations, vibrations and cavitation, and induce water losses due to leaches, leading to extra costs of maintenance on repairs and an increase on pumping energy [92, Ch.6][93].

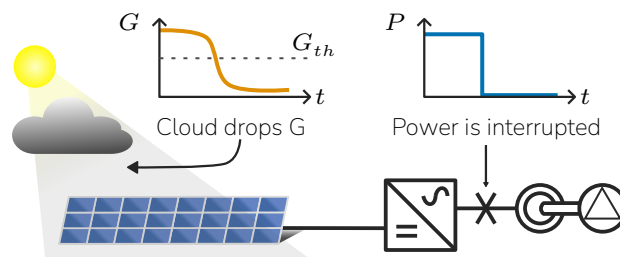


Figure 4.2 – Sketch representation of an irradiance drop event.

There are many proposals on reducing or eliminating the effect of the water hammer, substantially based on three major strategies: energy storage, control and infrastructure.

Energy storage

Increasing the moment of inertia of the pumping system results in a reduction of the maximum water hammer. Therefore, many authors propose attaching an energy storage system (ESS) capable of supplying the energy required to stop the pump smoothly, such as flywheels, batteries or ultracapacitors [94, 95], however their work focus on hydraulics and control. Authors in [96] successfully tested a battery and an ultracapacitor for this purpose on a small 14,4 W DC pumping system in West Bengal (India) and [97] compared the performances of operating a 2,44 kWp PV pumping system with and without a lithium-ion battery in Comunitat Valenciana (Spain). Their findings were positive on the inclusion of an ESS to prevent stops due to passing clouds.

Control scheme

An appropriate control scheme and tuning will produce a gradual shutdown of the pump. This is also observed with optimal control on valve actuation [98, 99]. Several maximum power point tracking (MPPT) PV control algorithms applied to DC pumps are reviewed in [100], including operation under partially shaded conditions. A real case study in Bejaia (Algeria) consisting on a domestic 990 W PV pumping system with a DC pump was analysed in [101], concluding the impact of shading the PV panels was difficult to model but introducing a proper MPPT control would mitigate its influence. The authors of the MASLOWATEN European project¹ propose to tune the converters in a PV pumping system appropriately such that clouds induce acceleration-deceleration cycles instead of start-stop cycles and tested it in the facilities of an irrigation community in Alicante (Spain) [102, 103]; the results showed that, with a proper

¹<https://maslowaten.eu>

tuning, the system could stand passing clouds of a few seconds. In turbines, appropriate gate and blade regulation manoeuvres would achieve the same results [104].

Hydraulic infrastructure

Selecting pipes' geometry and characteristics to increase the elasticity of the system help reduce the effective pressure wave velocity. Furthermore, the addition of air chambers, surge tanks and proper valving reduce the maximum pressure of such waves [92, Ch.10]. Some authors propose as well attaching a supplementary section of polymeric materials [94, 105, 106, 107].

4.1.2 Contributions

The main contribution of this work, as part of the Advanced Grid Interfaces for innovative Storage INtegration (AGISTIN) project, is the development of a sizing methodology of ESS to mitigate the negative water hammer effects derived from clouds shading over large PV pumping systems, which we found no previous work about. The methodology defines a cost function that considers capital and operation costs, including an statistical model of the clouds to consider their effect. The cost function can be solved analytically, requiring no iterative methods. We apply the methodology to a real study case using on-site data and analyse the feasibility and sensitivity of several ESS technologies, considering their environmental impact as well.

The objective of this chapter is to develop a methodology to size an ESS for large PV pumping systems, while analysing several technologies to determine their feasibility in such application. The aim of such ESS is to improve the response of these PV pumping systems when clouds shade the PV plant.

4.2 Problem description

Clouds shading over PV pumping systems derive in negative effects to the system such as water hammer. This work proposes the inclusion of an ESS to prevent water hammer by supplying the required energy to produce and sufficiently prolong a ramp of power when the pump stops. However, energy could also be supplied to maintain the pump running when the PV panels are shaded by a passing cloud, preventing the need to stop it. Therefore, the ESS is sized to accomplish two goals: (1) keep the pump running when a cloud shades the PV plant and (2) stop the pump smoothly, when required, following a ramp of power.

Figure 4.3 portrays the energy supplied by the ESS, represented by the blue highlighted area. When a *cloud event* initiates, the ESS commences to provide the lack of energy resulting from the cloud shading to avoid stopping the pump (① in Figure 4.3). If the cloud continues for long enough, the ESS supplies the required energy to smoothly stop the pump (② in Figure 4.3). This implies the ESS capacity is sized for the sum of the energy required for the ramp and that required for a certain assumed cloud:

$$E_{ESS} = E_{(1)} + E_{(2)}, \quad (4.1)$$

with $E_{(1)}$ (kWh) the energy required to save a certain *cloud event* and $E_{(2)}$ (kWh) that required to shift from running power P_{pump} (kW) to a complete stop $P = 0$ kW in the appropriate time Δt_{ramp} (s).

To establish the energy $E_{(1)}$ it is essential to evaluate the actual weather circumstances and behaviour on the real site. By gathering and analysing relevant on-site data we can develop a probability model which will be applied to comprehend the scale and behaviour of the clouds and, subsequently, to size the ESS accordingly to that particular situation.

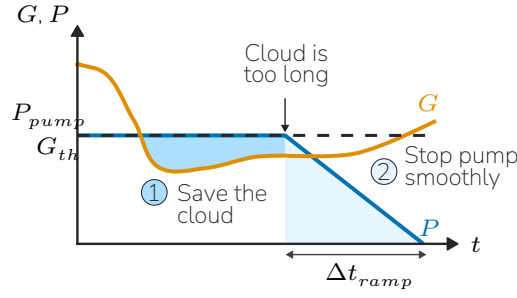


Figure 4.3 – Irradiance drop event with ESS.

The data required may be gathered by an irradiance sensor located in the PV system or its vicinities. This sensor measures the ambience irradiance and may be already installed to track and communicate the available power to the power converter.

A threshold value G_{th} (W/m^2) discerns in real time whether a cloud is shading the PV plant. A cloud is considered when the threshold value is reached and it stays until that value is not overcome (Figure 4.4), thus defining the duration of the cloud:

$$\Delta t_{cloud} = t_n - t_0, \quad (4.2)$$

where t_0 (s) is the observation before intersecting the threshold value for the first time and t_n (s) the observation after intersecting it for the second (and last) time. Consequently we use the measures that result in the worst case-scenario, i.e. the longest duration.

The maximum irradiance drop $\Delta G_{max,cloud}$ (W/m^2) is also considered in order to size the maximum power that the ESS is required to supply:

$$\Delta G_{max,cloud} = G_{th} - G_{min}. \quad (4.3)$$

The radiant exposure shaded by a cloud (J/m^2) is expressed as the area compressed between the threshold value of irradiance and the measured irradiance and corresponds to the blue highlighted area in Figure 4.4. Since the data are discrete, the area between two observations A_i (J/m^2) equals to that of a trapezoid

$$A_i = \frac{G_i - G_{th} + G_{i+1} - G_{th}}{2} \Delta t_i, \quad (4.4)$$

where Δt_i (s) is the time elapsed between observations G_i and G_{i+1} (W/m^2).

The terminal areas, this is the ones between the threshold value and G_0 or G_n , are assumed to intersect in the midpoint between both observations. Accordingly for A_0 , and analogously A_{n-1} :

$$A_0 = \frac{(G_1 - G_{th}) \Delta t_0}{2}, \quad (4.5)$$

$$A_{n-1} = \frac{(G_{n-1} - G_{th}) \Delta t_{n-1}}{2}. \quad (4.6)$$

The resulting radiant exposure shaded by a cloud A_{cloud} (J/m^2) is the summation of the areas of the trapezoids:

$$A_{cloud} = \sum_{i=0}^{n-1} A_i. \quad (4.7)$$

The energy shaded by a cloud E_{cloud} (kWh) is calculated with (4.8) and the maximum power drop $P_{max,cloud}$ (kW) with (4.9). These values are related to the specific PV system and refer to those required to achieve the same level of energy and power with an irradiance equal to G_{th} .

$$E_{cloud} = \frac{A_{cloud} P_{PV} \eta_{PV}}{1000 \cdot 3600}, \quad (4.8)$$

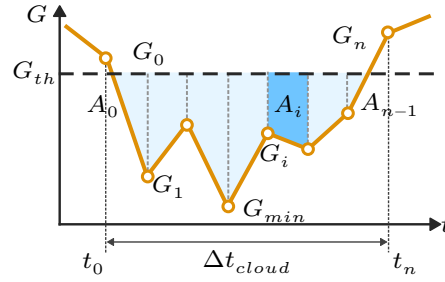


Figure 4.4 – Data key points that define a cloud.

$$P_{max,cloud} = \frac{G_{min,cloud}}{1000} P_{PV} \eta_{PV}, \quad (4.9)$$

where η_{PV} is the efficiency of the PV and inverter system and P_{PV} the peak power of the PV system (kWp).

Finally, it is crucial to disregard all instances of suspected cloud shading that are actually attributable to nighttime. These values are removed abiding by the following rule: if the date of the arrival of the cloud t_0 is different than that of its withdrawal t_n it is considered nighttime and the observation is removed.

4.3 Methodology (Off-grid)

This section defines the methodology we developed to size an ESS for the PV pumping system to improve its performance and prevent the undesirable effects from clouds. As defined in Section 4.2, the ESS requires to be sized on its power P_{ESS} and capacity E_{ESS} , which is split into $E_{(1)}$ and $E_{(2)}$ as defined in (4.1).

Power P_{ESS}

Since the maximum power to be provided will not surpass the pump's working power, the same is the power required by the energy storage system P_{ESS} :

$$P_{ESS} = P_{pump}. \quad (4.10)$$

The working power is determined by the operating point of the system and may not coincide with the nominal power of the pump.

Capacity $E_{(2)}$

We can find the energy required for the ramp to be provided when stopping the pump $E_{(2)}$ with the resulting triangle from Figure 4.3:

$$E_{(2)} = \frac{P_{pump} \Delta t_{ramp}}{2}. \quad (4.11)$$

The appropriate stopping time Δt_{ramp} (s) should be estimated, defined analytically, experimentally or given by the operators. Methods to obtain its value are out of the scope of this work.

Number of clouds N

Data analysed on Section 4.4.1 suggest the number of clouds per day N shading more than a certain energy E follows a law of power with negative exponent

$$N(E) = K E^\alpha, \quad (4.12)$$

with $K > 0$ and $\alpha < 0$. Applying properties of logarithms, it can also be expressed as a linear model:

$$\log(N(E)) = \log(K) + \alpha \log(E). \quad (4.13)$$

Therefore, we can fit a linear regression model using the method of least squares to estimate its parameters. For readability purposes, in this case, we apply a change of variables such that $y = \log(N(E))$, $\beta = \log(K)$ and $x = \log(E)$:

$$\alpha = \frac{\sum_{i=1}^{\mathcal{N}} (x_i - \bar{x})(y_i - \bar{y})}{\sum_{i=1}^{\mathcal{N}} (x_i - \bar{x})^2} \quad (4.14)$$

$$\beta = \bar{y} - \alpha \bar{x} \quad (4.15)$$

being \mathcal{N} the total number of data points representing the curve.

Total cost C

The total cost C (€) considers the capital and operating costs of the ESS itself and the costs associated to non-productive time, i.e. the pump stopping, during the lifetime of the ESS. We subdivided the total cost C into five conceptual parts, related to capital costs (4.17)-(4.18) and operation costs (4.19)-(4.20) of the ESS and operation costs of the facility (4.22). These subdivisions allow for a better subsequent understanding and analysis of the results:

$$C = C_{cap,E} + C_{cap,P} + C_{op,E} + C_{op,P} + C_{op,s}, \quad (4.16)$$

where $C_{cap,E}$ (€) is the total capacity capital costs of the ESS, $C_{cap,P}$ (€) the total power capital costs of the ESS, $C_{op,E}$ (€) the total variable operating costs of the ESS, $C_{op,P}$ (€) the total fix operating costs of the ESS and $C_{op,s}$ (€) the total stop operating costs of the PV pumping facility.

Capital costs

Capital costs include the expenses of purchasing the ESS. For such an equipment capital costs can be subdivided in energy capacity capital costs $C_{cap,E}$ (€) and power capital costs $C_{cap,P}$ (€). These costs are computed as the product of the unit price and its corresponding term:

$$C_{cap,E} = c_{cap,E,ESS} (E_{(1)} + E_{(2)}), \quad (4.17)$$

$$C_{cap,P} = c_{cap,P,ESS} P_{ESS}, \quad (4.18)$$

with $c_{cap,E,ESS}$ (€/kWh) the total cost per unit of energy of the ESS and $c_{cap,P,ESS}$ (€/kW) the total cost per unit of power of the ESS.

Operation costs

Operation costs include the maintenance expenses $C_{op,E}$ (€) and $C_{op,P}$ (€) of the ESS and the stopping costs, defined as the non-productive time that will have to be compensated with grid connected pumps $C_{op,s}$ (€). Variable operating costs consider the energy employed during both case (1), where the ESS can provide enough energy to save the cloud, and (2), where the pump is stopped (Figure 4.3). Otherwise, fixed operating costs relate to the installed power capacity:

$$C_{op,E} = c_{op,var,ESS} L_{ESS} E_{(1)} (\bar{N} - \hat{N}(E_{(1)} D_{ESS})) + c_{op,var,ESS} L_{ESS} (E_{(1)} + E_{(2)}) \hat{N}(E_{(1)} D_{ESS}), \quad (4.19)$$

where $c_{op,var,ESS}$ (€/kWh) is the variable operating costs of the ESS per utilised kWh, \bar{N} is the average number of stops per day without ESS, L_{ESS} (days) is the average lifetime of the ESS and D_{ESS} (p.u.) the depth of discharge of the ESS. Consider \hat{N} as the particular estimator of N from (4.12), which is discussed further in Section 4.4.1;

$$C_{op,P} = c_{op,fix,ESS} P_{ESS}, \quad (4.20)$$

where $c_{op,fix,ESS}$ (€/kW) is the fix operating costs of the ESS:

$$c_{op,fix,ESS} = \sum_{t=1}^T \frac{c_{op,fix,ESS,0}}{(1+i)^t}, \quad (4.21)$$

with $c_{op,fix,ESS,0}$ (€/kW·y) the fix operating costs per year of the ESS at the year of investment, T is the L_{ESS} expressed in years and i the real interest rate (p.u.);

$$C_{op,s} = c_{stop} L_{ESS} \hat{N}(E_{(1)} D_{ESS}), \quad (4.22)$$

where c_{stop} (€) is the cost per stop (4.23). In our study case cost per stop considers that the pumping system will have to operate grid connected during nighttime, however it should be adapted to the specific characteristics of each PV pumping facility. For instance, on a remote isolated area with no grid connection possibility other approaches would be considered such as just not pumping or utilising a diesel-driven pump. The former should contemplate losses due to lack of water for irrigation and the latter the price of fuel.

$$c_{stop} = 3600 \left(\frac{t_{stop}}{2} + t_{nw} + \frac{t_{start}}{2} \right) P_{pump} c_{grid} \quad (4.23)$$

Substitute the terms into (4.16) and cost C can be expressed as a function of the capacity $E_{(1)}$:

$$\begin{aligned} C(E_{(1)}) = & c_{cap,E,ESS} (E_{(1)} + E_{(2)}) + \\ & + c_{cap,P,ESS} P_{ESS} + \\ & + c_{op,var,ESS} L_{ESS} E_{(1)} (\bar{N} - \hat{N}(E_{(1)} D_{ESS})) + \\ & + c_{op,var,ESS} L_{ESS} (E_{(1)} + E_{(2)}) \hat{N}(E_{(1)} D_{ESS}) + \\ & + c_{op,fix,ESS} P_{ESS} + \\ & + c_{stop} L_{ESS} \hat{N}(E_{(1)} D_{ESS}), \end{aligned} \quad (4.24)$$

Capacity $E_{(1)}$

Finally, by deriving C

$$\begin{aligned} \frac{dC}{dE_{(1)}} = & c_{stop} L_{ESS} D_{ESS}^\alpha K \alpha E_{(1)}^{\alpha-1} + c_{op,var,ESS} L_{ESS} \bar{N} + \\ & + c_{op,var,ESS} L_{ESS} E_{(2)} D_{ESS}^\alpha K \alpha E_{(1)}^{\alpha-1} + \\ & + c_{cap,E,ESS}, \end{aligned} \quad (4.25)$$

we analytically obtain the expression for the capacity $E_{(1)}$ which minimises the cost (4.26):

$$\frac{dC}{dE_{(1)}} = 0 \Rightarrow E_{(1)} = \left(\frac{-c_{op,var,ESS} L_{ESS} \bar{N} - c_{cap,E,ESS}}{L_{ESS} D_{ESS}^\alpha K \alpha (c_{stop} + c_{op,var,ESS} E_{(2)})} \right)^{1/(\alpha-1)}. \quad (4.26)$$

4.4 Study case

In this section, we apply the methodology developed in the previous section to a real scenario located in the region of Lleida (Catalonia, Spain), north-eastern Iberian Peninsula, and utilising the facilities of the irrigation community *Comunitat de Regants Segrià-Sud*. The facilities are located at geographical coordinates N 41° 21' 40 E 0° 27' 31. The whole system comprises 5 reservoirs and 3 pumping stations. Figure 4.5 shows an ortophoto of such system. There are currently two working PV pumping systems and further one under construction, which corresponds to that of the study case. Such system is described in Table 4.2. Reservoirs on the study case's PV pumping system are 1 km apart and their difference of heights is 20 m. The irradiance sensor that provided the historic data is located on one of the PV plants. The PV plant utilises a North-South horizontal axis tracking system which increases the number of hours the system can pump per day, as demonstrated by [102].

Table 4.2 – Characteristics of the PV pumping system [28].

Concept		Value
Peak power	P_{PV}	275 kWp
Inverter's efficiency	η_{PV}	0,98
Irradiance threshold	G_{th}	400 W/m ²
Pump nominal power	$P_{pump,N}$	160 kW
Pump working power	P_{pump}	110 kW
Stopping time	t_{stop}	30 s
Startup time	t_{start}	30 s
Non-working time	t_{nw}	240 s
Cost of energy ²	c_{grid}	0,05 €/kWh
Real interest rate ³	i	4 %

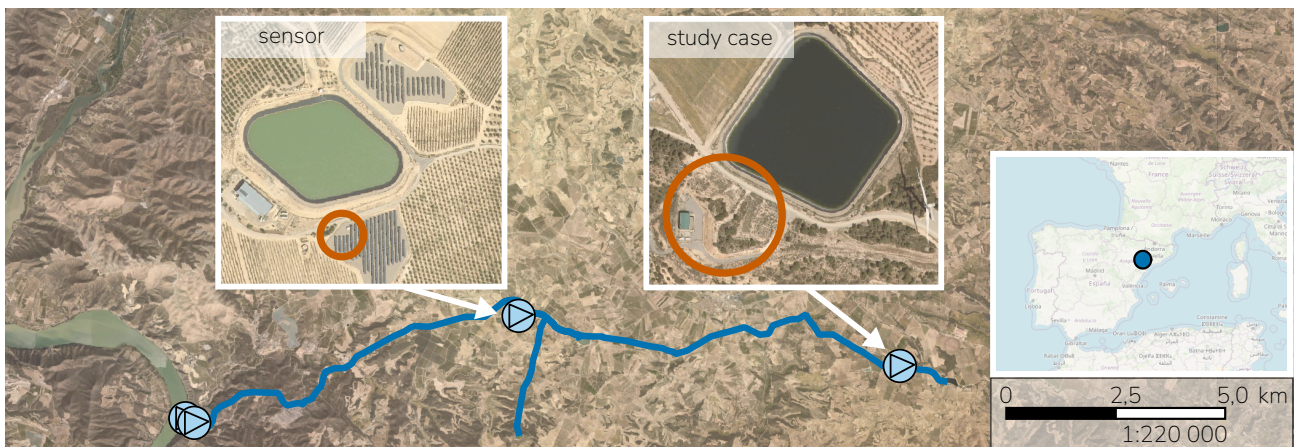


Figure 4.5 – Location of the irradiance sensor and study case on the CR Segrià-Sud facilities. Background maps obtained from Institut Cartogràfic i Geològic de Catalunya [31] and OpenStreetMap [32]. Figure elaborated in QGIS [110]

We compared several technologies on this analysis, comprising lead acid batteries (Lead), lithium-ion batteries (LIB), redox flow batteries (Flow), ultracapacitors (Uc) and flywheels (Fw). Since many different sources exist for ESS costs with huge ranges of values, we decided to assume the characteristics from [111], which are listed on Table 4.3.

²Based on data from OMIE [108]

³Based on data from Banco de España [109]

Table 4.3 – Capital and operation costs of the analysed energy storage systems [111]

Technology	$c_{cap,E}$ [€/kWh]	$c_{cap,P}$ [€/kW]	$c_{op,var}$ [€/MWh]	$c_{op,fix,0}$ [€/kW·y]	D [p.u.]	L [y]
Lead acid	299,20	116,45	0,44	4,34	1,00	3
Lithium-ion	272,00	209,10	0,44	8,50	0,80	10
Redox flow	410,55	116,45	0,44	5,01	1,00	15
Ultracapacitor	63 308,00	0,00	25,5	0,85	1,00	16
Flywheel	9 792,00	0,00	25,5	4,76	1,00	20

4.4.1 Clouds

Irradiance data comes from a solar irradiance sensor located besides one of the PV panels at the pumping station of the study case. This sensor feeds the control of the power converter. The dataset utilised was provided by the *Comunitat de Regants Segrià-Sud* and contains the sensor's gathered data of 347 days since 28 March 2020 until 27 July 2023 with a 20 to 30 s sample time in daily spreadsheet files. Figure 4.6 plots the data regarding power generation of the PV system and power consumption of the pump of a PV pumping system in the CR Segrià-Sud facilities. The plotted PV pumping system is characterised by a 523 kWp PV system, an irradiance threshold set at 400 W/m² and a pump with a nominal power of 315 kW.

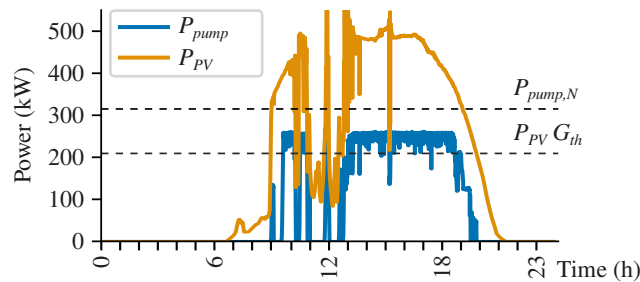


Figure 4.6 – Power generation and consumption of a PV pump system in the Segrià-Sud facilities, corresponding to 25th July 2022.

We observed a total amount of 4 753 cloud events. The longest cloud lasted $\Delta t_{cloud} = 269,50$ minutes and the largest shaded radiant exposure was $A_{cloud} = 1\,030,60$ Wh/m² (Table 4.4). With an average of 14 clouds per day (Table 4.5), we did not detect any monthly or annual pattern that would be relevant for the study case. The standard deviation (SD) for both the number of clouds and the time cloudy is considerable.

Table 4.4 – Statistical description of the properties of the observed clouds.

Concept	Mean (SD)	Min.	Median	Max.
Δt_{cloud} [min]	5,99 (15,5)	0,50	2,00	269,50
A_{cloud} [Wh/m ²]	14,59 (62,5)	0,01	1,24	1 030,60
G_{min} [W/m ²]	286,96 (86,3)	0,00	302,00	399,00

Figure 4.7 presents the rank distributions for the durations Δt_{cloud} and shaded radiant exposures A_{cloud} , defined in (4.2) and (4.7) respectively. Rank is defined as the complement of the cumulative distribution function and serves as a visualisation for analysing power law distributions with rare events such as black-out sizes in electrical systems [112]. A succinct analysis on them suggests that a power law behaviour is present for both the radiant exposure and duration, therefore short and faint clouds are considerably more usual than long and thick ones, as expected from the dry continental Mediterranean climate of the region, with annual total precipitations of 350-550 mm [113].

Table 4.5 – Statistical description of the clouds dataset.

Concept	Per day (SD)	Total in data
Number of clouds	14 (14)	4 753
Time cloudy	1 h 22 m (1 h 30 m)	19 d 22 h

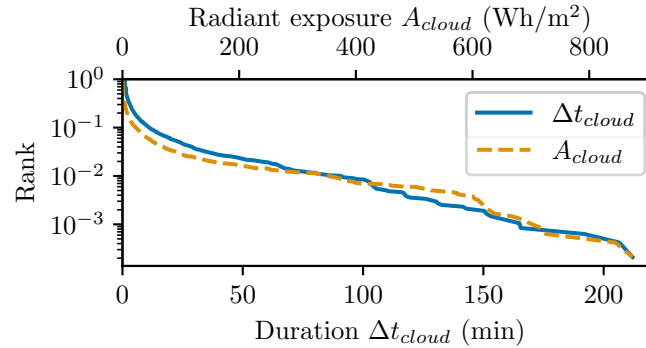


Figure 4.7 – Rank function plot of clouds' duration and shaded radiant exposure.

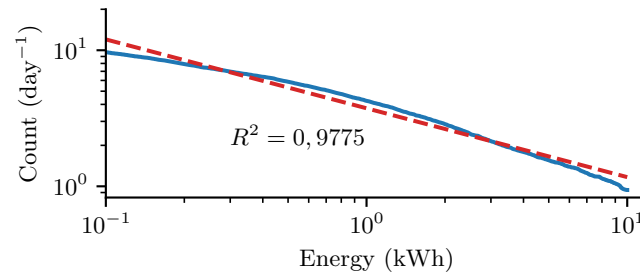
Although data contains clouds shading up to 277 kWh from the PV plant, those are rare events and more than 90 % of the cases are found under 10 kWh, which encourages to set the range of the study case to $E_{cloud} \in (0, 1, 10)$ kWh.

Applying the methodology from Section 4.2, this is (4.14) and (4.15), the model that fits the study case (Figure 4.8), with an $R^2 = 0,9775$, is

$$\hat{N}(E) = 3,746 E^{-0,51}, \quad (4.27)$$

with \hat{N} the number of estimated cloud events per day (day^{-1}), analogous to (4.12), and E the shaded energy (kWh), which will also correspond to the energy supplied by the ESS.

Alterations on the solar irradiance threshold G_{th} influence this model. In our study case coefficient K linearly grows with the threshold while exponent α lightly fluctuates around -0,47 and -0,51. The influence on the resulting ESS sizing is analysed on Section 4.4.4.


Figure 4.8 – Number of pump stopping events N shading a certain energy E , from data (—) and estimator \hat{N} (- - -)

4.4.2 Results

The following section analyses the results obtained from applying the developed methodology (Section 4.3) to the study case system (Table 4.2) for the technologies listed in Table 4.3.

We contemplate a base case as well. Base case considers no ESS either for stopping nor saving clouds and only serves as comparison for the cloud costs. It does not consider either the maintenance costs of the pumping system as a result of the effect of water hammer events, which is out of the scope of this

work. Its total cost C_{base} (€) is computed as the stopping operating expenses considering an average number of cloud events per day:

$$C_{base} = c_{stop} L_{base} \bar{N}. \quad (4.28)$$

To better compare the different ESS technologies, the total cost C is normalised by the lifetime L_{ESS} for each of them, obtaining the total cost per year in €/y. Table 4.6 summarises the resulting optimal size and costs for each ESS technology. As depicted in Figure 4.9, the results of the optimisation show a clear preference for redox flow batteries and flywheels for the application and study case of this work. Since the application requires ESS with capacities that do not exceed 10 kWh but has to be able to deliver $P_{pump} = 110$ kW (Table 4.2), the optimisation favours those technologies with lowest power related costs, but is not influenced that much by capacity related costs. However, low capacity costs allow for larger storage, leading to less impact of clouds on the performance of the system and thus lower stopping related operating costs. One should notice that additional maintenance and replacement costs should be accounted for the base case, however, as stated previously further research is yet to be conducted on how to adequately reckon them.

Table 4.6 – Sizing results

Technology	L [y]	$E_{(1)}$ [kWh]	$E_{(2)}$ [kWh]	P [kW]	\hat{N} [day ⁻¹]	Cost C [€]	C/L [€/y]
Base case	10	0	0	0	14	21 093,19	2 109,32
Lead acid	3	1,99	0,46	110,00	2,64	16 126,88	5 375,63
Lithium-ion	10	4,88	"	"	1,87	35 267,94	3 526,79
Redox flow	15	4,51	"	"	1,74	25 296,67	1 686,44
Ultracapacitor	16	0,17	"	"	9,18	64 184,49	4 011,53
Flywheel	20	0,60	"	"	4,85	34 390,07	1 719,50

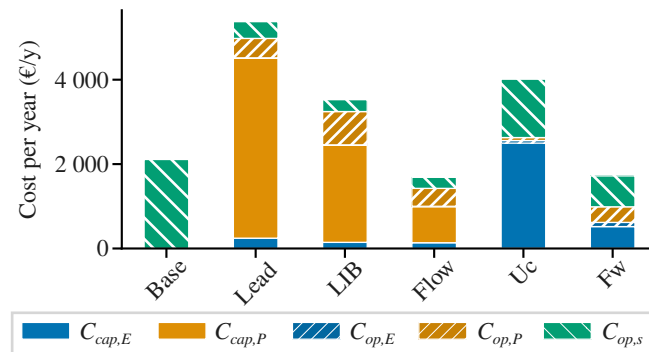


Figure 4.9 – Costs per year for different technologies and base case.

4.4.3 Feasibility and impact assessment

This section evaluates the feasibility of implementing the proposed solutions on the real site, considering its purpose and characteristics.

The specific objectives are to study the physical feasibility of the application of different energy storage systems. It will be analysed that the volume and mass required for the installation of each ESS fit within the facilities, the required power (P_{ESS}) is within the rated power, the response time is suitable for the operation, and the environmental impact and potential risks to health and environment of the ESS, taking into consideration where it will be located within the hydraulic installations and the fact that hydraulic installations are crucial to provide the water for the irrigation of large crop fields.

It is crucial to study the different spaces and weights that would be dedicated and required by the ESS. The possible range of specific energy e and energy density ρ for each ESS from [114] are used. Considering both the sized capacity E_{ESS} from Table 4.6, the possible range of mass m and volume v are found for each storage system. The results are presented in Table 4.7, which shows that vanadium redox flow batteries require a range of 166-497 kg and 151-311 l, significantly higher mass and volume compared to other technologies. In addition, flywheels and ultracapacitors present relatively low volume requirements compared to other systems (around 70 l), but significantly higher mass requirements (106 and 252 kg). Lead-acid and lithium-ion batteries have similar volume and mass characteristics (less than 50 l and 80 kg), and lithium-ion batteries is the ESS technology that would require less space and mass.

Table 4.7 – Properties of the ESS technologies [114]

Technology	e [Wh/kg]	ρ [Wh/l]	m [kg]	v [l]
Lead acid	30-50	50-80	49-82	31-49
Lithium-ion	75-200	200-500	27-71	11-27
Redox flow	10-30	16-33	166-497	151-311
Ultracapacitor	2,5-15	10-30	42-252	21-63
Flywheel	10-30	20-80	35-106	13-53

The ESS to be installed must be suited to deliver a specific amount of power, as calculated and presented previously in Table 4.6. Based on data from [115, 116], it is determined that since none of the evaluated ESS technologies have a rated power lower than the power of the pump (110 kW), all of them would be feasible in this regard.

The response time of the ESS to an event is also critical in this application. A delayed response could result in power loss to the pump, potentially inducing water hammer. The required time for the study case is of a few seconds, therefore all technologies have the ability to respond in time for this application, since their response time is in the order of milliseconds [117].

The facilities are neighbored by 8 875 hm² of cropland and take part in their irrigation tasks [22]. In consequence, it is crucial to recognise and understand the hazards that the different ESS technologies entail for both health and the environment.

There are different hazards regarding the use of each ESS. Lead acid and redox flow batteries may release hydrogen gases during normal operation, which can cause serious injury to humans [118]. Furthermore, lead acid batteries contain heavy metals that, in the event of damage or leakage [119], would release lead components into the soil, potentially contaminating water reservoirs or rivers, causing significant environmental damage. Likewise, lithium-ion battery cells may emit flammable gases such as hydrogen fluoride and hydrogen cyanide [118]. When exposed to water, air or high humidity, as is the case of the analysed application, they can undergo aggressive chemical reactions due to the corrosion of their components [118, 119], presenting a fire risk that could damage the equipments of the pumping station.

It is important to consider these factors and choose a suitable location for the ESS to avoid personal, material and environmental damage. When deploying electrochemical batteries, it is essential to consider the use of a highly ventilated space and other infrastructures to prevent environmental risks, such as properly isolating the battery from the soil.

The increase of the demand of electrochemical ESS might cause negative effects on the environment and social aspects of the countries involved in the chain of production [119]. These batteries are based on lithium, lead and vanadium, the three of which have relatively high abundance in the earth's crust and are not considered rare elements. However, their extraction induces environmental and social issues, specially in economically unstable countries with a lack of regulation in the mining activity. Nevertheless, both lead acid and lithium-ion batteries can be recycled, specially in case of lead acid batteries with a recycling efficiency up to 95 % [119].

Lifetime of the different ESS varies depending on the technology and its use. High lifetime expectancy is associated to a lower environmental impact, since the process of extraction and recycling is lower than for technologies with short lifetime. From Table 4.6 is seen that the lead acid batteries have a considerable lower lifetime (3 years) in comparison of the other technologies with a life time around from 10 to 20 years.

It has been observed that electrochemical ESS take up less space and weight (excluding flow batteries) than mechanical or electrical ESS. However, electrochemical ESS may present more risks related to the environment, equipment and people. In conclusion, it is important to consider these aspects when selecting an ESS system, as well as the cost of properly adapting the facilities for such.

4.4.4 Sensitivity analysis

This section examines the dependency of the cost per year of the considered technologies on interest rate i , cost of energy c_{grid} the irradiance threshold G_{th} . We analysed a variation of the interest rate between 2 % - 6 %, based on historical data from *Banco de España* [109], from 0,02 to 0,10 €/kWh for the cost of energy based on data from *OMIE* [108] and the irradiance threshold between 100 and 600 W/m².

The results for variations of interest rate and cost of energy displayed in Figure 4.10 suggest that, on the one side interest rate have little to no effect on the results, however on the other side cost of energy variations considerably impact the final costs, especially on those technologies with greater capacity costs (see the full results on Table 4.8).

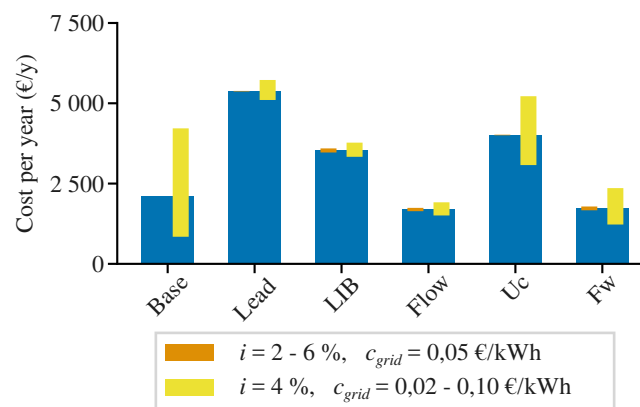


Figure 4.10 – Costs per year for different technologies and base case ($i = 4\%$ and $c_{grid} = 0,05\text{ €/kWh}$) and sensitivity for interest rate i and cost of energy c_{grid} .

When operating the system one may realise that the solar irradiance threshold G_{th} should either be increased due to malfunctioning of the system or could be lowered with little to no critical consequences. Increasing the peak power of the PV plant would as well allow to further decrease the threshold value. As detailed in Figure 4.11, sensitivity analysis on this parameter shows that for lower thresholds ESS technologies with lower power related costs benefit from not requiring as much capacity, while for higher thresholds capacity requirements are higher due to a greater number of considered clouds (see the full results on Table 4.9).

Figure 4.12 presents the evolution of the minimum total cost against $E_{(1)}$ value for each technology when varying the G_{th} value. The line (—) and filled point ● represent the cost value of the base case and its minimum. Circle marks ○ are the minimum cost for each threshold value.

Table 4.8 – PS3 sensitivity analysis results for cost of energy and real interest rate

Technology	c_{grid} [€/kWh]:	0,05	0,05	0,05	0,02	0,10
		i [%]:	4	2	6	4
Base case	$E_{(1)}$ [kWh]	0	0	0	0	0
	C/L [€/y]	2 109,32	2 109,32	2 109,32	843,73	4 218,64
Lead acid	$E_{(1)}$ [kWh]	1,99	1,99	1,99	1,08	3,15
	C/L [€/y]	5 375,63	5 384,46	5 367,23	5 102,64	5 725,26
Lithium-ion	$E_{(1)}$ [kWh]	4,88	4,88	4,88	2,66	7,73
	C/L [€/y]	3 526,79	3 594,76	3 467,55	3 333,33	3 774,58
Redox flow	$E_{(1)}$ [kWh]	4,51	4,51	4,51	2,46	7,14
	C/L [€/y]	1 686,44	1 743,10	1 639,89	1 506,67	1 916,69
Ultracapacitor	$E_{(1)}$ [kWh]	0,17	0,17	0,17	0,10	0,27
	C/L [€/y]	4 011,53	4 021,65	4 003,31	3 075,87	5 219,73
Flywheel	$E_{(1)}$ [kWh]	0,60	0,60	0,60	0,33	0,95
	C/L [€/y]	1 719,50	1 786,12	1 667,78	1 224,63	2 358,52

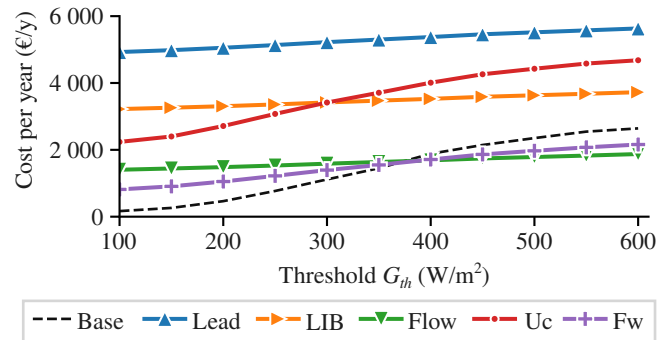
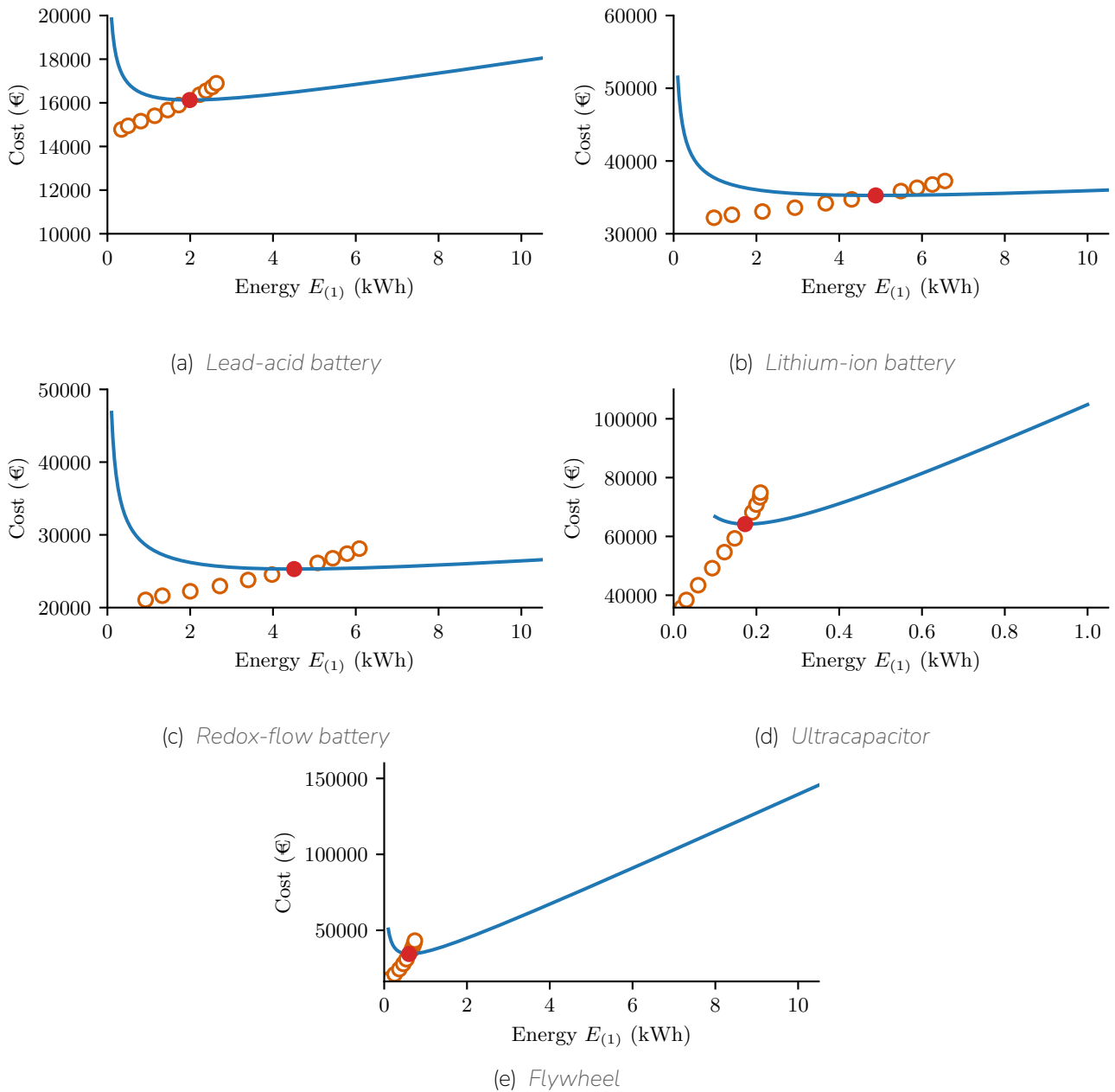

 Figure 4.11 – Sensitivity of the costs per year for different technologies and base case for irradiance threshold G_{th} ($i = 4\%$ and $c_{grid} = 0,05$ €/kWh).

Table 4.9 – PS3 sensitivity analysis results for irradiance threshold

Technology	K :	0,568	1,200	2,395	5,050	6,079
		α :	-0,29	-0,41	-0,49	-0,49
\bar{N} [day ⁻¹]:	G_{th} [W/m ²]:	1,1	3,1	7,4	15,6	17,5
		100	200	300	500	600
Base case	$E_{(1)}$ [kWh]	0	0	0	0	0
	C/L [€/y]	166,86	464,72	1 115,12	2 351,29	2 641,47
Lead acid	$E_{(1)}$ [kWh]	0,34	0,81	1,46	2,38	2,63
	C/L [€/y]	4 926,23	5 053,58	5 222,43	5 516,19	5 632,15
Lithium-ion	$E_{(1)}$ [kWh]	0,98	2,15	3,67	5,88	6,56
	C/L [€/y]	3 219,98	3 305,63	3 418,39	3 632,26	3 725,43
Redox flow	$E_{(1)}$ [kWh]	0,92	2,00	3,40	5,44	6,09
	C/L [€/y]	1 404,10	1 482,90	1 586,31	1 785,39	1 873,86
Ultracapacitor	$E_{(1)}$ [kWh]	0,02	0,06	0,12	0,12	0,21
	C/L [€/y]	2 237,34	2 712,75	3 415,61	4 426,36	4 680,46
Flywheel	$E_{(1)}$ [kWh]	0,10	0,25	0,46	0,70	0,74
	C/L [€/y]	816,02	1 052,21	1 394,19	1 970,74	2 159,32


 Figure 4.12 – Cost function and minimum value for different irradiance thresholds between 100 and 600 W/m².

4.5 Methodology (Grid connected)

Logic tells us that integrating the system to the grid could be the way to go in the future, a decision held back mainly due to contractual and legal matters. With this regard, we developed a methodology to analyse this arrangement as well. The system, as depicted in Figure 4.13, consists of a pump mainly fed by the PV system and also connected to the ESS and the electrical grid.

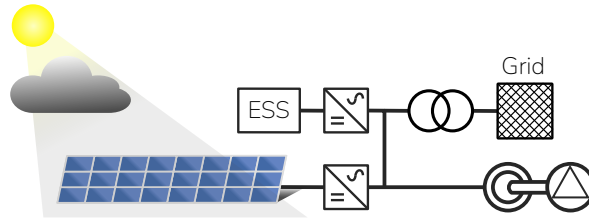


Figure 4.13 – Sketch representation of the grid connected PV pumping system.

Demanding uncontracted power from the grid might induce penalties due to excess power. In Spain this is currently legislated in [120], defining the penalty cost per day as

$$Penalty = \sum_{i=1}^{N_p} t_p 2 (P_{d,i} - P_{c,i}), \quad (4.29)$$

with t_p (€/kW) the excess power term, P_d (kW) the demanded power and N_p the number of time billing periods the contracted power P_c (kW) has been surpassed. Base case scenarios consider the values listed in Table 4.10. The contracted power was given by the irrigation community, the excess power term derives from the worst cases of billing information from several electrical companies and the choice of the number of billing periods is explained below.

Although there are a total of six time periods with different prices to consider during the year, each day is divided into three time periods, which may vary for each month. Time period $P6$ is the most economical and is perpetually located during nighttime. The usual strategy for irrigation communities is to contract high power and run the pumps fed from the grid on $P6$, then contract low power during other periods when the pumps will be stopped or running from PV systems. Consequently, we defined the cost of penalty c_{pen} (€/kW·day) considering 2 time periods per day where contracted power may be surpassed:

$$c_{pen} = 2 t_p 2. \quad (4.30)$$

Table 4.10 – Grid connected base case characteristics

Concept	Value
N_p	2
P_c	10,0 kW
t_p	0,11 €/kW

We have considered three possible strategies that may be followed when a cloud shades the PV system:

1. The PV system disconnects and the pump is not allowed to stop (Section 4.5.1)
2. The PV system disconnects and the pump is allowed to stop (Section 4.5.2)
3. The PV system does not disconnect and the pump is allowed to stop (Section 4.5.3)

4.5.1 PV disconnects, pump does not stop

This case considers that, in the event of a cloud, the converter will disconnect the PV from the system and the pump must keep running even if the ESS is depleted, i.e. the pump is not allowed to stop.

Figure 4.14 shows the two stages the system may be found on during a cloud. Stage 1 comprises the span during which the ESS delivers power to the pump, limited by its own sized power P_{ESS} and capacity E_{ESS} . Stage 2, which may not be met, covers the span from which the ESS depletes until the cloud is over, during which the pump demands power exclusively from the grid.

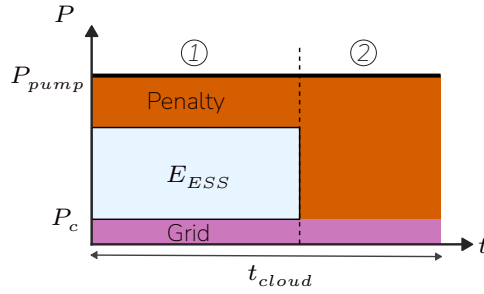


Figure 4.14 – Strategy 1.

The optimisation problem is defined by a non-linear programming (NLP) consisting in a cost function to minimise (4.31) subject to constraints (4.32)-(4.36). We expressed the problem in an averaged way, in the sense that we contemplate the average number of clouds \bar{N} with their average duration \bar{t}_{cloud} . Penalties must be considered just once per day, taking the highest value it achieves on each cloud, thus we consider only stage 1 on each cloud saved by the ESS ($\bar{N} - \hat{N}$ times) and stage 1 + stage 2 on each cloud that exceeds the capacity of the ESS (\hat{N} times). Energy consumed from the grid corresponds to that the ESS could not deliver.

$$\begin{aligned}
 \underset{E_{ESS}, P_{ESS}}{\text{minimise}} \quad C(E_{ESS}, P_{ESS}) &= c_{pen} L_{ESS} (P_{pump} - P_{ESS} - P_c) \left(1 - \frac{\hat{N}(E_{ESS} D_{ESS})}{\bar{N}}\right) + \\
 &+ c_{pen} L_{ESS} (P_{pump} - P_c) \left(\frac{\hat{N}(E_{ESS} D_{ESS})}{\bar{N}}\right) + \\
 &+ c_{grid} L_{ESS} \bar{N} (P_{pump} \bar{t}_{cloud} - E_{ESS} D_{ESS}) + \\
 &+ c_{op,var,ESS} L_{ESS} E_{ESS} \bar{N} + c_{cap,E,ESS} E_{ESS} + \\
 &+ c_{op,fix,ESS} P_{ESS} + c_{cap,P,ESS} P_{ESS}
 \end{aligned} \tag{4.31}$$

subject to

$$P_{pump} - P_{ESS} - P_c \geq 0 \tag{4.32}$$

$$\bar{N} - \hat{N}(E_{ESS} D_{ESS}) \geq 0 \tag{4.33}$$

$$P_{pump} \bar{t}_{cloud} - E_{ESS} D_{ESS} \geq 0 \tag{4.34}$$

$$P_{ESS} \geq 0 \tag{4.35}$$

$$E_{ESS} \geq 0 \tag{4.36}$$

Results

We used the Pyomo library [62] to write the NLP and COIN-OR interior point optimiser (IPOPT) [75] with a tolerance of $1e-4$ to solve it. Below we analyse the results obtained from applying the developed methodology to the study case system for the technologies listed in Table 4.3.

We subdivided the cost C (4.31) into six conceptual parts, related to capital costs (4.37)-(4.38) and operational costs (4.39)-(4.40) of the ESS, operational costs of the facility (4.41) and penalties (4.42). These subdivisions allow for a better understanding and analysis of the results:

$$C_{cap,E} = c_{cap,E,ESS} E_{ESS}, \quad (4.37)$$

$$C_{cap,P} = c_{cap,P,ESS} P_{ESS}, \quad (4.38)$$

$$C_{op,E} = c_{op,var,ESS} L_{ESS} E_{ESS} \bar{N}, \quad (4.39)$$

$$C_{op,P} = c_{op,fix,ESS} P_{ESS}, \quad (4.40)$$

$$C_g = c_{grid} L_{ESS} \bar{N} (P_{pump} \bar{t}_{cloud} - E_{ESS} D_{ESS}), \quad (4.41)$$

$$C_{pen} = c_{pen} L_{ESS} (P_{pump} - P_{ESS} - P_c) \left(1 - \frac{\hat{N}(E_{ESS} D_{ESS})}{\bar{N}}\right) + \quad (4.42)$$

$$+ c_{pen} L_{ESS} (P_{pump} - P_c) \left(\frac{\hat{N}(E_{ESS} D_{ESS})}{\bar{N}}\right),$$

where $C_{cap,E}$ (€) is the total capacity capital costs of the ESS, $C_{cap,P}$ (€) the total power capital costs of the ESS, $C_{op,E}$ (€) the total variable operational costs of the ESS, $C_{op,P}$ (€) the total fix operational costs of the ESS, C_g (€) the total cost of the energy acquired from the grid and C_p (€) the penalties for exceeding the contracted power P_c .

We contemplate a base case as well. Base case considers no ESS and serves as comparison for the ESS technologies costs. Its total cost C_{base} (€) is computed as

$$C_{base} = c_{grid} L_{base} \bar{N} P_{pump} \bar{t}_{cloud} + c_{pen} L_{base} (P_{pump} - P_c). \quad (4.43)$$

To better compare the different ESS technologies, the total cost C is normalised by the lifetime L_{ESS} for each of them, obtaining the total cost per year in €/y. Table 4.11 summarises the resulting optimal size and costs for each ESS technology. As depicted in Figure 4.15, the results of the optimisation show a clear preference for redox flow and lithium-ion batteries for the application and study case of this work. The addition of a penalty proportional to the excess power favours technologies with lower capacity costs, such that they can deliver the required energy during the clouds at a constant power (stage 1 from Figure 4.14) and avoid the penalties derived from stage 2.

Table 4.11 – Grid connected sizing results (Strategy 1)

Technology	L [y]	E [kWh]	P [kW]	\hat{N} [day ⁻¹]	Cost C [€]	C/L [€/y]
Base case	10	0	0	14,0	188 787,37	18 878,74
Lead acid	3	10,98	100,00	1,1	20 058,37	6 689,12
Lithium-ion	10	13,73	"	1,1	44 788,56	4 478,86
Redox flow	15	10,98	"	1,1	41 313,01	2 754,20
Ultracapacitor	16	0,69	"	4,5	171 389,30	10 711,83
Flywheel	20	3,28	"	2,0	133 708,21	6 685,41

The results for variations of interest rate, cost of energy and excess power term displayed in Figure 4.16 suggest that, on the one side interest rate have little to no effect on the results, cost of energy and excess power term variations have a considerable impact on the final costs, especially on those technologies with greater capacity costs (see the full results on Table 4.12).

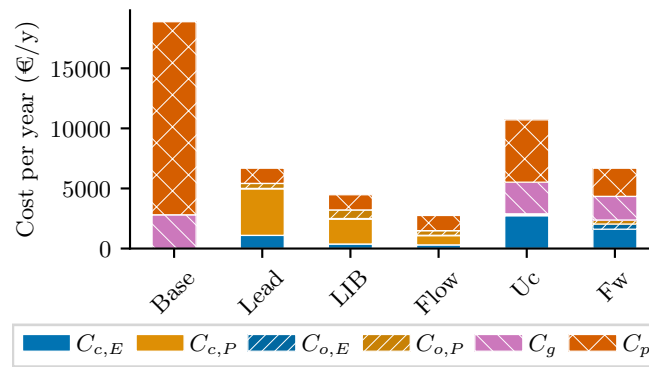


Figure 4.15 – Costs per year for different technologies and grid connected case 1.

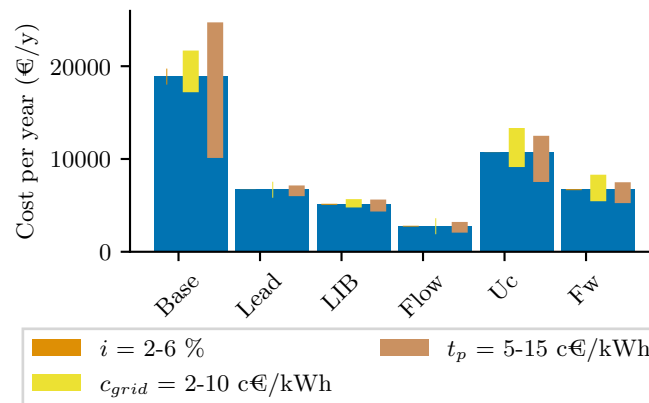

 Figure 4.16 – Costs per year for different technologies and base case ($i = 4\%$, $c_{grid} = 0,05$ €/kWh and $t_p = 0,11$ €/kWh) and sensitivity for interest rate i , cost of energy c_{grid} and penalty t_p .

Table 4.12 – PS3 sensitivity analysis results for cost of energy, real interest rate and excess power term

Technology	c_{grid} [€/kWh]:	0,05	0,05	0,05	0,05	0,02	0,10
	i [%]:	4	4	2	6	4	4
	t_p [€/kWh]:	0,05	0,15	0,11	0,11	0,11	0,11
Base case	E [kWh]	0	0	0	0	0	0
	C/L [€/y]	10 112,74	24 722,74	18 878,74	18 878,74	17 194,10	21 686,48
Lead acid	E [kWh]	10,98	10,98	10,98	10,98	10,98	10,98
	C/L [€/y]	5 995,09	7 1446,81	6 694,15	6 678,49	6 689,12	6 686,12
Lithium-ion	E [kWh]	10,98	10,98	10,98	10,98	10,98	10,98
	C/L [€/y]	4 337,99	5 628,53	5 174,10	5 058,45	4 475,39	5 673,86
Redox flow	$E_{(1)}$ [kWh]	10,98	10,98	10,98	10,98	10,98	10,98
	C/L [€/y]	2 063,17	3 214,89	2 805,71	2 711,87	2 754,20	2 754,20
Ultracapacitor	E [kWh]	0,41	0,85	0,69	0,69	0,67	0,72
	C/L [€/y]	7 522,94	12 499,42	10 721,03	10 704,36	9 131,83	13 338,82
Flywheel	E [kWh]	1,95	4,03	3,28	3,28	2,60	7,32
	C/L [€/y]	5 244,96	7 492,88	6 745,97	6 638,39	5 447,04	8 305,19



4.5.2 PV disconnects, pump can stop

This case considers that, in the event of a cloud, the converter will disconnect the PV from the system but the pump will be able to stop until the cloud has passed.

Figure 4.17 shows the two stages the system may be found on during a cloud. Stage 1 comprises the span during which the ESS delivers power to the pump, limited by its own sized power P_{ESS} and capacity E_{ESS} . Stage 2, which may not be met, covers the stopping of the pump.

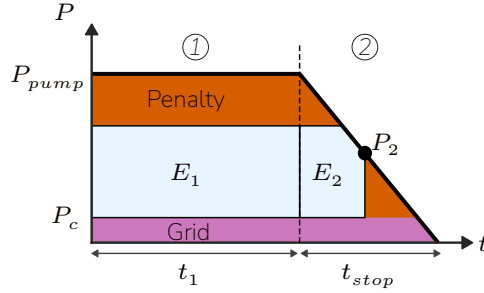


Figure 4.17 – Strategy 2.

The optimisation problem is defined by a NLP consisting in a cost function to minimise (4.44) subject to constraints (4.45)-(4.52). Penalties must be considered just once per day, taking the highest value it achieves on each cloud, thus we consider only stage 1 on each cloud saved by the ESS ($\bar{N} - \hat{N}$ times) and stage 1 + stage 2 on each cloud that exceeds the capacity of the ESS (\hat{N} times). Energy consumed from the grid corresponds to that the ESS could not deliver. To compute the penalty on stage 2 we require to know the value of the power P_2 (see Figure 4.17), which corresponds to the power that is left from the stopping ramp after utilising the whole capacity of the battery. Applying trivial trigonometry we can define such power as a function of the capacity $E_{2,ESS}$ (4.48). Also, the penalty which applies to stage 2 should be the maximum between two possible circumstances (4.45) and (4.46).

$$\begin{aligned}
 \underset{E_{ESS}, P_{ESS}}{\text{minimise}} \quad C(E_{ESS}, P_{ESS}) &= c_{pen} L_{ESS} (P_{pump} - P_{ESS} - P_c) \left(1 - \frac{\hat{N}(E_{1,ESS} D_{ESS})}{\bar{N}}\right) + \\
 &+ c_{pen} L_{ESS} P_{pen,2} \left(\frac{\hat{N}(E_{1,ESS} D_{ESS})}{\bar{N}}\right) + \\
 &+ c_{stop} L_{ESS} \hat{N}(E_{1,ESS} D_{ESS}) + \\
 &+ c_{grid} L_{ESS} \bar{N} E_{1,ESS} D_{ESS} \left(\frac{P_{pump}}{P_{ESS}} - 1\right) + \\
 &+ c_{grid} L_{ESS} \hat{N}(E_{1,ESS} D_{ESS}) \left(\frac{P_{pump} t_{stop}}{2} - E_{2,ESS} D_{ESS}\right) + \\
 &+ c_{op,var,ESS} L_{ESS} (E_{1,ESS} \bar{N} + E_{2,ESS} \hat{N}(E_{1,ESS} D_{ESS})) + \\
 &+ c_{cap,E,ESS} (E_{1,ESS} + E_{2,ESS}) + \\
 &+ c_{op,fix,ESS} P_{ESS} + c_{cap,P,ESS} P_{ESS},
 \end{aligned} \tag{4.44}$$

subject to

$$P_2 - P_c \leq P_{pen,2} \tag{4.45}$$

$$P_{pump} - P_{ESS} - P_c \leq P_{pen,2} \tag{4.46}$$

$$P_{pump} - P_{ESS} - P_c \geq 0 \quad (4.47)$$

$$P_2 = \sqrt{P_{pump}} \sqrt{P_{pump} - \frac{2 E_{2,ESS} D_{ESS}}{t_{stop}}} \quad (4.48)$$

$$P_{pen,2} \geq 0 \quad (4.49)$$

$$P_{ESS} > 0 \quad (4.50)$$

$$E_{1,ESS} \geq 0 \quad (4.51)$$

$$E_{2,ESS} \geq 0 \quad (4.52)$$

Results

We used the Pyomo library [62] to write the NLP and COIN-OR IPOPT [75] with a tolerance of 1e-4 to solve it. Below we analyse the results obtained from applying the developed methodology to the study case system for the technologies listed in Table 4.3.

We subdivided the cost C (4.44) into six conceptual parts, related to capital costs (4.53)-(4.54) and operational costs (4.55)-(4.56) of the ESS, operational costs of the facility (4.57)-(4.58) and penalties (4.59). These subdivisions allow for a better understanding and analysis of the results:

$$C_{cap,E} = c_{cap,E,ESS} (E_{1,ESS} + E_{2,ESS}), \quad (4.53)$$

$$C_{cap,P} = c_{cap,P,ESS} P_{ESS}, \quad (4.54)$$

$$C_{op,E} = c_{op,var,ESS} L_{ESS} (\overline{N} E_{1,ESS} + \hat{N}(E_{1,ESS} D_{ESS})), \quad (4.55)$$

$$C_{op,P} = c_{op,fix,ESS} P_{ESS}, \quad (4.56)$$

$$C_{op,s} = c_{stop} L_{ESS} \hat{N}(E_{1,ESS} D_{ESS}), \quad (4.57)$$

$$C_g = c_{grid} L_{ESS} E_{1,ESS} \overline{N} \left(\frac{P_{pump}}{P_{ESS}} - 1 \right) + \quad (4.58)$$

$$+ c_{grid} L_{ESS} \hat{N}(E_{1,ESS} D_{ESS}) \left(\frac{P_{pump} t_{stop}}{2} - E_{2,ESS} D_{ESS} \right),$$

$$C_p = c_{pen} L_{ESS} (P_{pump} - P_{ESS} - P_c) \left(1 - \frac{\hat{N}(E_{1,ESS} D_{ESS})}{\overline{N}} \right) + \quad (4.59)$$

$$+ c_{pen} L_{ESS} P_{pen,2} \left(\frac{\hat{N}(E_{1,ESS} D_{ESS})}{\overline{N}} \right),$$

where $C_{cap,E}$ (€) is the total capacity capital costs of the ESS, $C_{cap,P}$ (€) the total power capital costs of the ESS, $C_{op,E}$ (€) the total variable operational costs of the ESS, $C_{op,P}$ (€) the total fix operational costs of the ESS, $C_{op,s}$ (€) the total stop operational costs of the PV pumping facility, C_g (€) the total cost of the energy acquired from the grid and C_{pen} (€) the penalties for exceeding the contracted power P_c .

We contemplate a base case as well. Base case considers no ESS and serves as comparison for the ESS technologies costs. Its total cost C_{base} (€) is computed as

$$C_{base} = c_{stop} L_{base} \overline{N} + c_{grid} L_{base} \overline{N} \frac{P_{pump} t_{stop}}{2} + c_{pen} L_{base} (P_{pump} - P_c). \quad (4.60)$$

To better compare the different ESS technologies, the total cost C is normalised by the lifetime L_{ESS} for each of them, obtaining the total cost per year in €/y. Table 4.13 summarises the resulting optimal size and costs for each ESS technology. As depicted in Figure 4.18, the results of the optimisation show a clear preference for redox flow batteries, ultracapacitors and flywheels for the application and study case of this work. The results show the best strategy in such context is to size an ESS to strictly stop the pump on every cloud without incurring in any excess power penalties.

Table 4.13 – Grid connected sizing results (Strategy 2)

Technology	L [y]	E_1 [kWh]	E_2 [kWh]	P [kW]	\hat{N} [day ⁻¹]	Cost C [€]	C/L [€/y]
Base case	10	0	0	0	14,0	182 975,03	18 287,50
Lead acid	3	0,00	0,46	100,00	14,0	19 366,73	6 455,58
Lithium-ion	10	"	0,57	"	14,0	49 341,82	4 934,18
Redox flow	15	"	0,46	"	14,0	49 277,34	3 285,16
Ultracapacitor	16	"	0,45	"	14,0	64 522,13	4 032,63
Flywheel	20	"	0,45	"	14,0	54 570,14	2 728,51

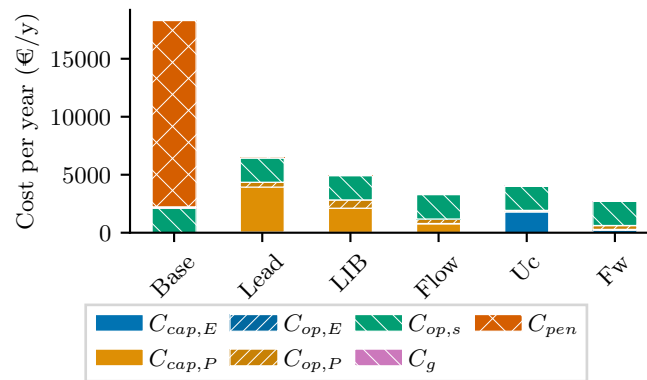
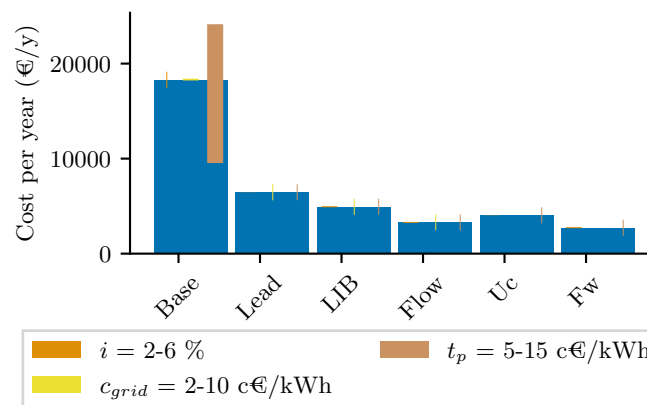


Figure 4.18 – Costs per year for different technologies and grid connected case 2.

The results for variations of interest rate, cost of energy and excess power term displayed in Figure 4.19 suggest that none of them have noticeable effects on the results.


 Figure 4.19 – Costs per year for different technologies and base case ($i = 4\%$, $c_{grid} = 0,05$ €/kWh and $t_p = 0,11$ €/kW) and sensitivity for interest rate i , cost of energy c_{grid} and penalty t_p .

Transient excess of power

In this scenario we could consider penalties only apply during stage 1, since stage 2 is a short lasting transient in comparison to the sampling rate of the registry, then $P_{pen,2} = 0$ kW.

The optimisation results reveal that the economically optimal solution should be not to size any ESS, since the operation costs of the excess power acquired from the grid do not surpass the capital costs an ESS would introduce. The cost per year would be $C/L = 2\,205,09$ €.

4.5.3 PV does not disconnect

This case considers that, in the event of a cloud, the converter will keep the PV connected to the system.

Figure 4.20 shows the two stages the system may be found on during a cloud. Stage 1 comprises the span during which the ESS delivers power to the pump, limited by its own sized power P_{ESS} and capacity E_{ESS} . Stage 2, which may not be met, covers the stopping of the pump.

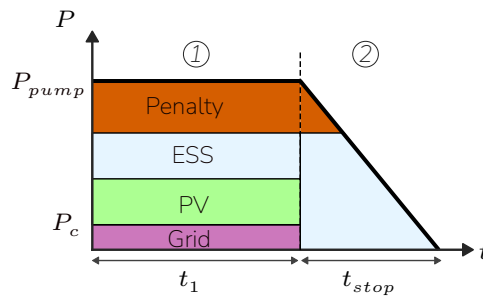


Figure 4.20 – Considered behaviour with grid and PV connected.

This scenario contemplates both the energy and power lost on the PV plant due to a cloud event. Statistically considering these two variables resulted in a complex optimisation problem, therefore, we used a data driven approach to analyse this scenario. The total of $N_{clouds} = 4\,753$ cloud data points during $N_{days} = 347$ days were evaluated for each ESS technology to find the most economically suitable sizing following the subsequent methodology. First, a range of $E_{ESS} \in (0,10)$ kWh in steps of 0,1 kWh, and $P_{ESS} \in (0,110)$ kW in steps of 1 kW, was defined as the possible sizing outcomes. In a combinatorial procedure, the final cost of each sizing was analysed, then the minimum was selected for each technology. The analysis methodology to find the final cost develops, for each cloud:

- The amount of power required from the grid is computed as the difference of the power shaded by the cloud P_{cloud} (4.9) and the power that the ESS will provide:

$$P_g = \max(P_{cloud} - P_{ESS}, 0) \quad (4.61)$$

- The power to be considered on the penalty computation (4.29) is the difference between the power required from the grid and the contracted power P_c . Penalties only apply for the considered time periods per day and not for each cloud, as defined in Section 4.5.

$$P_{pen} = \max(P_g - P_c, 0) \quad (4.62)$$

A penalty will only apply if the the energy shaded by the cloud E_{cloud} (4.8) is greater than the capacity of the ESS E_{ESS} , deducting the energy that will be saved to stop the pump in a ramp of power $E_{(2)}$ (4.11):

$$E_{cloud} > E_{ESS} - E_{(2)} \quad (4.63)$$

- The energy consumed from the grid results from the duration of the cloud Δt_{cloud} :

$$E_g = P_g \Delta t_{cloud} \quad (4.64)$$

- The energy used from the ESS is equivalent to that of the cloud:

$$E_{used,ESS} = \min(E_{missing}, E_{ESS}) \quad (4.65)$$

- Capital costs, for capacity $C_{cap,E}$ and power $C_{cap,P}$, are computed as:

$$C_{cap,E} = E_{ESS} c_{cap,E,ESS} \quad (4.66)$$

$$C_{cap,P} = P_{ESS} c_{cap,P,ESS} \quad (4.67)$$

- Operating costs, for energy $C_{op,E}$ and power $C_{op,P}$ usage, are computed as:

$$C_{op,E} = \frac{L_{ESS}}{N_{days}} \sum_{i \in N_{clouds}} E_{used,ESS,i} \quad (4.68)$$

$$C_{op,P} = c_{op,fix,ESS} P_{ESS}, \quad (4.69)$$

- Grid costs are computed from the energy used from the grid:

$$C_g = \frac{L_{ESS}}{N_{days}} \sum_{i \in N_{clouds}} E_{g,i} c_{grid} \quad (4.70)$$

- Operating costs of stopping the pump consider that non productive time should be compensated during nighttime with extra pumping operations, with $N_{clouds,ns}$ the number of clouds such that $E_{ESS} < E_{cloud}$ (*ns* standing for not sufficient) and considering c_{stop} defined in (4.23):

$$C_{op,s} = \frac{L_{ESS}}{N_{days}} \sum_{i \in N_{clouds,ns}} c_{stop} \quad (4.71)$$

- Finally, the total cost C is computed as the sum of the partial costs:

$$C = C_{cap,E} + C_{cap,P} + C_{op,E} + C_{op,P} + C_g + C_{pen} + C_{op,s} \quad (4.72)$$

To better compare the different ESS technologies, the total cost C is normalised by the lifetime L_{ESS} for each of them, obtaining the total cost per year in €/y. Table 4.14 summarises the resulting optimal size and costs for each ESS technology. As depicted in Figure 4.21, the results of the optimisation show a clear preference for redox flow batteries and flywheels for the application and study case of this work. It did not size a lead acid battery, which would be a more expensive solution than having no ESS.

The results for variations of interest rate, cost of energy and excess power term displayed in Figure 4.22 suggest that, all of the parameters have little influence on the results. It is remarkable the effect of the cost of energy on the lead acid batteries technology, caused by not being sized and depending on the grid instead. Since lithium-ion batteries are sized to allow some penalties, the cost of penalty have a significant influence on it as well as the cost of energy.

Table 4.14 – Grid connected sizing results (without PV disconnection)

Technology	L [y]	E [kWh]	P [kW]	Cost C [€]	C/L [€/y]
Base case	10	0	0	37 504,70	3 750,47
Lead acid	3	0,00	0,0	11 251,40	3 750,47
Lithium-ion	10	7,30	70,0	28 334,70	2 833,47
Redox flow	15	5,60	88,0	22 733,50	1 515,57
Ultracapacitor	16	0,10	104,0	45 213,80	2 825,86
Flywheel	20	1,30	97,0	36 795,80	1 839,79

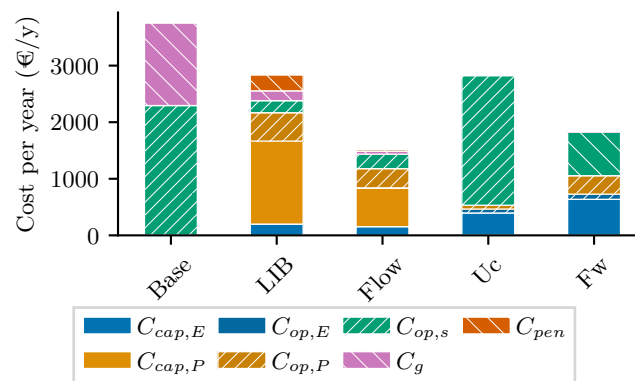
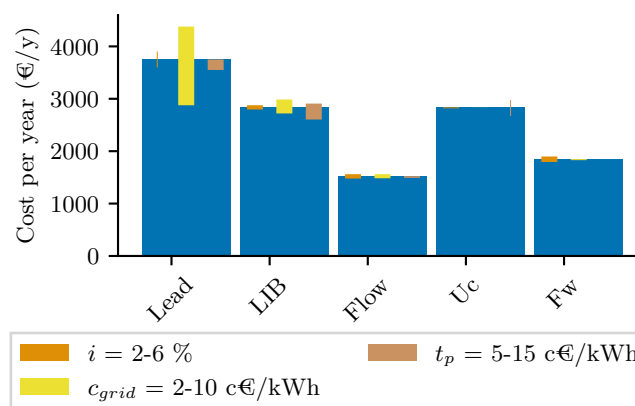


Figure 4.21 – Costs per year for different technologies and grid connected with PV.


 Figure 4.22 – Costs per year for different technologies and base case ($i = 4\%$, $c_{grid} = 0,05$ €/kWh and $t_p = 0,11$ €/kW) and sensitivity for interest rate i , cost of energy c_{grid} and penalty t_p .

4.6 Aqueous ECR battery

Although other storage technologies with higher readiness level may be suitable, as part of the AGISTIN⁴ project this chapter considers setting up an aqueous ECR. These low-energy storage batteries, currently in pre-commercial state (TRL-5), are supposed to supply high-power charge/discharge cycles with no significant degradation for 1 million cycles. Allegedly, in terms of energy stored and supplied power, this technology would fall in the mid ground of a LIB and an ultracapacitor. However, the aforementioned is to be tested and proven in the project on a demonstrator.

Little to no actual information is available about aqueous ECR batteries but a white paper from the developer company [121], alleging the following characteristics:

- Based in a solution of unspecified inorganic chemicals dissolved in pure water.
- Specific energy up to 10,69 Wh/kg (tenths to hundreds of Wh per battery).
- Specific power up to 5 kW/kg.
- Projected life of more than 1 million cycles.
- Deteriorates faster when charged, so it is advised to keep it discharged as much as possible and no overcharging it.
- Suited for high power and high cyclability applications.

4.6.1 Results

Applying the methodology from 4.3 we can obtain the capital costs at which an Aqueous ECR could be considered. Assuming a result of $E_{(1)} \leq 0,10$ kWh, which is out of the analysed domain, implies that the sized ESS is not profitable, we can find the maximum capital cost to meet such condition. By solving (4.26) for $c_{cap,E,ESS}$

$$c_{cap,E,ESS} = -L_{ESS} (c_{stop} + c_{op,var,ESS} E_{(2)}) D_{ESS}^{\alpha} K \alpha E_{(1)}^{(\alpha-1)} - c_{op,var,ESS} L_{ESS} \bar{N}, \quad (4.73)$$

with $E_{(1)} = 0,10$ kWh we find expression for the maximum capital prices for an Aqueous ECR battery on this application. Table 4.15 compiles the results for different costs of energy. For a range of $E_{(1)}$ see Figure 4.23.

Table 4.15 – Maximum capital cost for $E_{(1)} \leq 0,1$ kWh for different cost of energy values

Cost of energy (€/kWh)	CAPEX (€/kWmin)
0,10	40,19
0,05	20,10
0,02	8,04

4.6.2 Results (Grid connected)

Applying the methodology from 4.5 to a range of the ESS capital costs we can obtain those at which an Aqueous ECR could be considered. Table 4.16 summarises the results obtained for all of the considered strategies.

⁴<https://www.agistin.eu/>

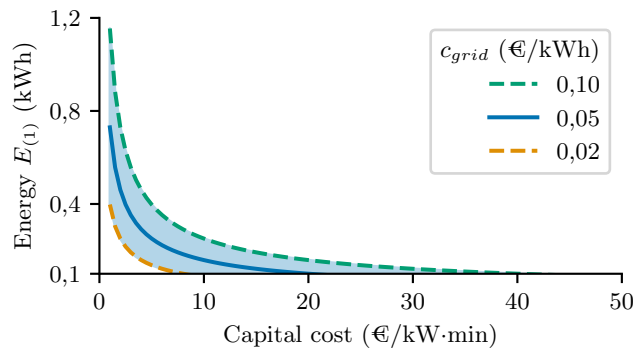


Figure 4.23 – Optimal sizing $E_{(1)}$ for the Geyser Aqueous ECR energy storage system for a range of capital cost and sensitivity for cost of energy c_{grid} .

Table 4.16 – Maximum capital cost for different excess power term (grid connected cases)

Excess power term (€/kW)	Strategy 1 CAPEX (€/kWmin)	Strategy 2 CAPEX (€/kWmin)
0,05	11,00	12,00
0,11	24,00	26,00
0,15	33,00	36,00

4.7 Conclusion

The application analysed in this work requires medium capacity (few kWh) but high power (hundreds of kW) energy storage. Our findings show that flywheels and redox flow batteries obtain the lower costs, benefiting from moderate storage capacity costs but low power related costs, as stated in the NREL literature. Ultracapacitor and lithium-ion prove to be solid technologies but are penalised by capacity capital costs and power capital costs respectively. Finally, lead acid batteries manifest low lifetime and high economic and environmental costs for such an application. However, such economic decisions are subject to the specific location and market conditions and should be analysed accordingly.

It should be emphasized that the costs used in the study case are extrapolated from data provided by NREL, which originates from analysing higher capacity systems and could not be representative for this study case. This might be particularly relevant for the redox flow and lithium-ion batteries, as the results of the sizing methodology are allocated in the low-kWh range, forcing an important extrapolation of the cost range for them, typically in the 10-100 kWh range. This consideration challenges the optimal results obtained, as high-power, low-kWh redox flow and lithium-ion batteries might show a higher cost than the ones used for the analysis.

Sensitivity analysis revealed that fluctuations of the cost of energy have a significant impact on the output of the optimisation, since low energy prices reduce the economical suitability for an ESS. This is especially relevant for energy storage technologies with higher capacity costs such as ultracapacitors and flywheels.

Modifying the threshold value of irradiance that discerns clouds from having or not an effect on the system also considerably influences the final decision. Higher thresholds imply a greater number of considered clouds and energy to deliver, therefore storage capacity requirements are higher which benefits technologies with lower capacity costs.

Flow batteries appear to be the most suitable option in terms of space requirements and installation mass, while still offering adequate response performance for the intended application. However, when considering environmental impact and lifetime, flywheel storage demonstrates advantages.

4.7.1 Future work

This section discusses gaps we identified during our research to work on future analysis.

Maintenance costs

Start-stop cycles and consequent induced water hammer damage the infrastructure, which translates into increased maintenance and replacement costs. These costs are not reckoned in this study since we were not in possession of neither their financial worth nor any method of evaluation. Future analysis should be carried out in order to determine their value and account for them in further research on this topic.

Control and management of the energy storage system

Although, as mentioned in Section 4.1 other authors have worked in the implementation of a control strategy on the ESS and designing an energy management system (EMS), we did not find any that considered large reservoir-based PV pumping systems. Such systems carry their own challenges related to high power usage and large extensions of the PV systems.

On-site implementation

Implementing the ESS on the real site, after an energy management system is designed, will provide further insight on the behaviour and performance of the whole system that otherwise is not possible to appreciate.

5 Potential grid services

This chapter summarises all potential grid services that irrigation communities can offer to the electrical grid. It takes into account the potential services provided by both short term and long term installations. The short term perspective considers an energy storage system (ESS) with low capacity and fast response times, such as flow or aqueous batteries. On the other hand, the long term approach involves a high-capacity ESS with relatively slower response times, such as pumped-storage hydropower (PSH).

This chapter examines the potential services described in the literature and their practical application within the framework of European and Spanish grid codes and legislative standards.

5.1 Legislative context

Under the guidance of the Agency for Cooperation of Energy Regulators (ACER), the European Network of Transmission System Operators for Electricity (ENTSO-E) created the regulation known as grid codes. The grid connection or network connection is one of the main covered by the aforementioned codes. The codes establish the requirements of generation elements connected to the grid, ensuring safe and effective power system operation. However, there are some emerging technologies that are not considered in this codes, such as the storage devices.

At the moment the latest amendments to the European electricity grid connection network codes considers sites including mixed technologies. For example in Figure 5.1 corresponds to one of the slides shared by ACER where the different possibilities of aggregating units in terms of power park modules (PPMs) are considered. It is seen that if generation, storage and loads are considered, each of the category must be considered like three different PPMs with one connection point (CP). The approach facilitates the coordination of the same technologies, but results harmful for hybrid combination as it prevents several synergies from being captured, and forces grid connection to be larger than actually needed [122].

In the specific case of the regulation in Spain the hybrid installations are considered in *Real Decreto* 1183/2020. The legislation allows for the hybridization of electrical installations, as long as the installation includes a primary renewable energy generation source or incorporates an energy storage system.

Furthermore, in *Real Decreto* 944/2019, Article 58 states that the incorporation of new generation and storage capacity into the grid must be facilitated, removing any obstacles that hinder access for new market participants and electricity from renewable energy sources. Therefore, despite a defined legislative gap in grid codes for storage systems or hybrid installations, there is a clear willingness in both the European Union and Spain to standardize and promote these types of installations.

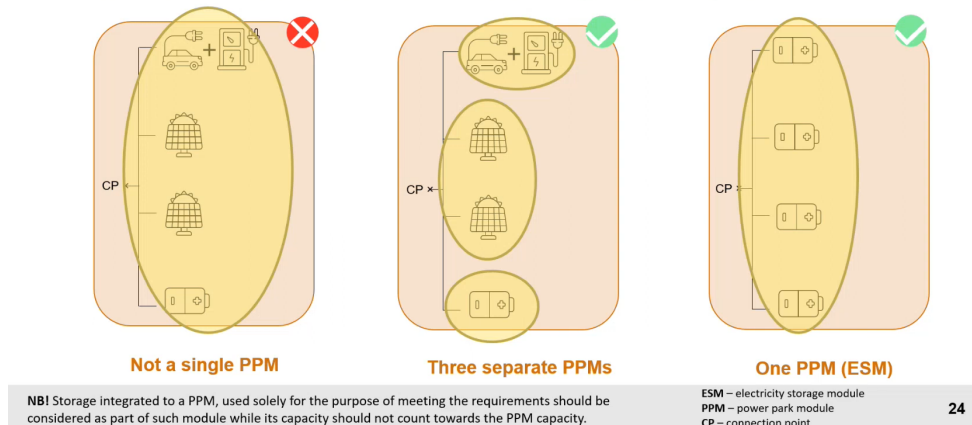
New recital to tackle units of different classes behind a single connection point


Figure 5.1 – ACER’s proposal on Requirements for generation in mixed-technology sites [123]

5.2 Applications in power system operation

This section presents the potential grid and ancillary services that can be offered to the power system, following a technical approach and as recommended by the literature.

5.2.1 Long term storage

For long term storage, pumped-storage hydropower (PSH) is considered the primary solution. PSH is a large-scale energy storage system whose operating principle is based on managing gravitational potential energy. Due to its characteristics, energy losses during inactivity are very low, making this technology ideal for long term energy storage.

This technology is particularly well-suited for the integration of renewable power generation [124], especially when there is a surplus of energy from sources such as photovoltaic or wind power. For instance, [125] analyses the potential of PSH for wind power applications.

Furthermore, PSH systems are widely recognized for their ability to provide essential grid services, such as time shifting, peak shaving, and load levelling [124]. Time shifting is achieved by storing energy during periods of low electricity prices and discharging it during peak demand, requiring power ratings in the range of 1 to 100 MW [124]. Peak shaving involves using stored energy during off-peak hours to compensate for power generation shortfalls during peak demand periods. Load levelling, on the other hand, balances large fluctuations in energy demand. A demonstration of peak shaving and load levelling is presented in [126], where an optimisation model is applied to a PSH system in two isolated power grids in the Canary Islands, Spain.

Transmission and distribution stabilization is another important grid service that PSH can provide. It supports the synchronous operation of components on a transmission or distribution line, regulating power quality and reducing congestion [124].

In [127], the potential of using optimisation models for PSH to design and operate systems for grid stabilization in offshore low-head applications is explored. Potential applications of this technology include frequency balancing operations such as frequency containment reserve (FCR), automatic frequency

restoration reserve (aFRR), and manual frequency restoration reserve (mFRR), which correspond to primary, secondary, and tertiary regulation, respectively, as defined in the Spanish legislative framework. Note that these terms are further defined in Section 5.2.4. However, [127] focuses on the provision of FCR services due to the decreasing use of mFRR and aFRR in Europe. Despite this, Spain does not provide any revenue for FCR services, while mFRR and aFRR are monetized. Figure 5.2 shows the different types of regulations mentioned, along with their corresponding power and time responsibilities.

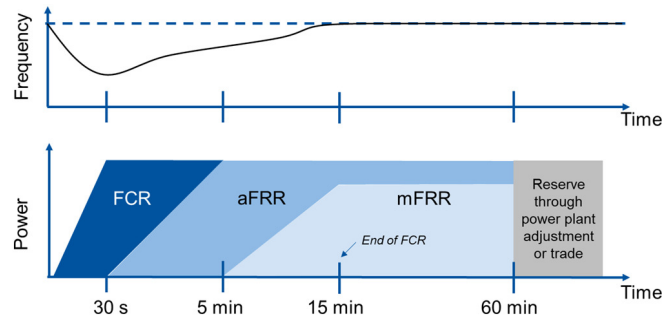


Figure 5.2 – Division of frequency regulation, frequency curve example (top) and power type responsibilities (bottom)[128]

However, PSH systems may face challenges during rapid transitions between pumping and generating modes, leading to increased switching times [129]. Nevertheless, [130] demonstrates the feasibility of fast switching operations by implementing control strategies using a Full Size Frequency Converter (FSFC) for a synchronous motor-generator. Furthermore, [131] investigates the potential of a Double Fed Induction Machine (DFIM) as a variable-speed hydro-generating solution, particularly under fault conditions and during start-up and braking scenarios, highlighting the dynamic capabilities of this configuration. In [117], it is demonstrated how storage systems with high energy capacity, such as PSH, can significantly contribute to network expansion. Additionally, [117] also highlights how PSH can be a promising solution for renewable energy (RE) backup. Finally, for large PSH systems (30 - 500 MW), there is potential for providing seasonal storage due to the low energy losses over extended periods [124].

5.2.2 Short term storage

Short term storage refers to technologies capable of providing service with a relatively short response time (order of milliseconds) and low energy capacity, compared to long term storage. Therefore, given the definition the technologies that might be suitable are flow batteries, flywheels and aqueous batteries. Since currently there is no information on aqueous batteries, the study focuses solely on the potential application of flywheels and flow batteries.

The vanadium redox flow battery is one of the most mature flow battery systems [124]. The response time of the flow battery might not be fully established due to their relatively early stage of commercialization and ongoing technological advancements that continue to evolve system design and performance characteristics. However, some authors documented that this technology might be suitable to provide ancillary services to the grid [124, 132, 133]. For example, a quick response time of 1 ms [124], or that due to the fast electrochemical kinetics if the electrodes are kept full of electrolytes and pumps in standby promptly take over, the response time is in order to milliseconds [132]. Moreover, [133] concluded experimentally that kW-class vanadium flow batteries are capable of discharging quickly enough to provide fast services in 50–60 Hz electrical grids, if they are properly controlled by the power conditioning system. Furthermore, this technology is capable of being fully discharged without damaging the system, and it exhibits very low self-discharge [125].

Flow batteries can be used in a wide range of applications, including improving power quality for stationary applications and Uninterruptible Power Supplies (UPS) devices [124].

In [124], it is mentioned that flow batteries have been shown to provide several services to the grid, including renewable energy (RE) and emergency backup for batteries ranging from 100 kW to 40 MW, ramping load changes to meet electricity demand with batteries at the MW level, black start recovery with batteries up to 40 MW, and voltage and network fluctuation control with the technology operating at the MW level.

According to the same study [124], flow batteries show promise for several additional applications, including damping grid oscillations and frequency regulation with batteries of less than 1 MW, thanks to the quick response time of the technology. In high-power applications (up to 20 MW), flow batteries could be promising for renewable energy integration. They also hold promise for low voltage ride-through, which is essential for RE generation systems, as they are capable of voltage control during periods of voltage dips in the grid. Finally, due to their relatively high capacity, flow batteries may also be promising for peak shaving, time shifting, and load levelling, similar to the aforementioned PSH technology.

On the other hand, flywheels are classified as mechanical storage system and composed by five primary components: a fly wheel, a group of bearings, a reversible electric motor and generator and a vacuum chamber [124]. Exist two types of flywheel, low speed and high speed. Low speed use steel as the flywheel and rotates below $6 \cdot 10^3$ rpm, while high speed uses advanced composite materials such as carbon fiber which can rotate up to $\sim 10^5$ rpm [124]. Low speed are typically used in short term applications of low or medium power applications, while high speed are expanding to uses in high power systems, such as power quality and ride through capability [124]. However, due to their characteristics high speed flywheels are commonly more expensive than low speed.

Some of the advantages of the technology are a high cycle efficiency (up to ~ 95 % at rated power), relatively high power density, no depth-of-discharge effects and easy maintenance [124]. However, when being in stand by can be noted high self discharge, up to ~ 20 % of the stored capacity in one hour [124].

5.2.3 Comparison and requirements of long and short term storage

In this section, the services that long term and short term storage systems can offer to the grid will be compared based on the literature. Furthermore, Table 5.1 presents the rated power, response time, and discharge time required for each technology to provide the corresponding grid service. Each service is catalogued between two categories depending on their maturity. Experienced express that the technology has been proven with positive results, whereas promising refers that the technology in paper could offer the given service but has not been proven.

The grid services examined are briefly explained below.

- Damping oscillations refers to the ability of any device to eliminate the phenomenon of angle stability of power systems under small perturbations.
- Frequency regulation is the capacity to change the frequency deviations from the standard frequency of the grid.
- Ride-through capability consists in the injection of usable power for a limited time during a power loss.
- Fast meteorological events can produce certain power fluctuations to the grid due to the RES, some energy storage can compensate this power fluctuations contributing to the RES integration.

- Due to the nature of the RE their availability depends on the meteorological events or the time of the day, therefore is needed a back up as energy storage in order to achieve the demand when RE can not.
- Emergency back-up is the service used in order to power specific areas or devices when the regular energy source is not available.
- Ramping and load follow refers to the ability of an energy storage system to avoid suddenly power loss.
- Peak shaving consists on the consumption of energy when is generated a surplus.
- Time shifting consists into the capability of an energy storage to displace the demand from a certain moment to another one.
- Load levelling refers to the mitigation of power demand variability during a period of time
- Black start is the ability of an energy source to restore the grid during a black out event.
- Low voltage ride though consists in the capability of a energy source to stay connected to the grid during a low voltage event in a short period of time.
- Some energy storage assists on the development of the network avoiding distribution network expansions when demand rises.
- Voltage regulation and control avoid or mitigate the dynamics in the voltage during changes of active and reactive power.
- Grid fluctuations consist on the mitigation of grid fluctuations that could damage the sensible electronics.
- Standing reserve is used to provide energy whenever the demand is bigger than the expected or programmed.

From Table 5.1, it can be concluded that short term energy storage is optimal for applications requiring rapid response times, such as ride-through capability, renewable energy buffering, black start support, voltage regulation and control, and the mitigation of grid fluctuations and oscillations. Specifically, fly-wheels have proven to be effective for RES, although their potential for voltage regulation and control has yet to be demonstrated. In contrast, long term energy storage is more suitable for applications involving extended discharge durations and slower response times, including peak shaving, time shifting, load levelling, and maintaining supply–demand balance over prolonged periods. Additionally, long term storage can support network expansion in regions with limited generation capacity but expected growth in electricity demand.

5.2.4 Services with revenue in Spain

As mentioned earlier, some of the grid services outlined in the previous section are not included in European or Spanish grid codes or legislation, meaning there is no revenue for offering them to the grid, for example FCR that is mandatory but not remunerated. However, there are others that are considered by current Spanish legislation and are eligible for revenue.

The Spanish and European legislative frameworks recognize Balancing Service Providers (BSPs), which are market participants with generation, demand, or storage units that have a minimum capacity of 1 MW. These BSPs earn revenue for the services they provide to the grid. The services included are secondary, tertiary regulation and replacement reserve (RR).

Table 5.1 – Comparison and requirements.

Service	Short	Long	Rated power	Response time	Discharge time	Ref
	Flow Fw					
Damping oscillations	★		≤ 1 MW	ms	ms to s	[124]
Frequency regulation	★	●	Up to 100 MW	ms to m	s to 60 m	[124, 127]
Ride-through capability	●		100 kW to 10 MW	Up to 1 s	m to h	[124]
RES integration	★ ●		Up to 20 MW	Up to 1 s	m to h	[124, 117]
RE back-up	●	★	100 kW to 40 MW			[117]
Emergency back-up	● ●		Up to 1 MW	ms to m	24 h	[124, 117]
Ramping and load follow	●		MW level	Up to 1 s	m to few h	[124]
Peak shaving	★	●	100 kW to 100 MW	Few m	≤ 10 h	[124, 117]
Time shifting	★	●	1 to 100 MW	Few m	3 to 10 h	[124, 117]
Load levelling	★	●	MW level	Few m	≤ 10 h	[124, 117]
Black start	●		Up to 40 MW	Few m	s to h	[124]
Seasonal storage		★	Large scale (30 to 500 MW)	m	Up to weeks	[124, 117]
Low voltage ride-through	★		Lower than 10 MW	ms	m	[124]
Network expansion		●				[117]
Voltage regulation and control	● ★		Up to few MW	ms	Up to m	[124]
Grid fluctuations	●		Up to MW level	ms	Up to m	[124]
Standing reserve		★	1 to 100 MW	≤ 10 m	1 to 5 h	[124, 117]

Legend: ● - Experienced, ★ - Promising. Flow - Vanadium flow battery. Fw - Flywheel

Secondary regulation

Secondary regulation (aFRR) is a discretionary service aimed at maintaining the balance between generation and demand by automatically correcting deviations in grid frequency. The response time for this service ranges from 20 seconds to 15 minutes.

Each day, the system operator publishes the reserve requirements for secondary regulation for each period of the corresponding program for the next day. The generation units eligible for the service submit their offers for the secondary regulation band. Once the service is assigned, it continues to cover the system's needs according to a minimal cost rule [134].

The service is compensated through two market mechanisms: availability (regulation band) and utilization (the energy provided).

Currently, this service is managed at a local level by the Spanish TSO. However, it is expected to be integrated and standardized with the European aFRR product and will be managed through the implementation of the European platform PICASSO.

Tertiary regulation

Tertiary regulation (mFRR) is a balancing service that activates active power reserves with the aim of maintaining network frequency and balance. The service is triggered manually, with a maximum activation time of 15 minutes, and it can be activated for at least 30 minutes.

The energy provided by tertiary regulation is paid at the marginal price, following an allocation process that takes place 15 minutes before the scheduled period. Similar to secondary regulation, this process is currently managed at the local level by the TSO, but it is expected to be transferred to the European level through the implementation of the MARI platform [134].

Additionally, the P.O. 7.3 "Regulación terciaria" mentions the potential of pumping stations to provide this service [135].

Replacement reserve

The activation of the Replacement Reserve (RR) is a balancing service that activates active power reserves with the goal of resolving deviations between generation and demand that may be identified after the day-ahead market. It aims to restore or maintain the energy levels required for frequency recovery. Activation can be either manual or automatic (using secondary and tertiary regulation energies), depending on the need to prepare for imbalances or frequency deviations. The service must be activated within a maximum time of 30 minutes and is managed through the European platform LIBRA [134].

Service providers submit their RR offers to the local TSO, which, after a validation process, sends the offers to the European TSO. The European TSO then uses the LIBRA platform to optimise and determine activations at the local level, as well as the international energy exchanges [134].

6 Real-time operation & control for innovative irrigation canal-based energy storage systems

The proper operation of the irrigation facilities depends on the effective management of water resources. In the framework of this project, this involves to ensure that the necessary volumes of water for irrigation are available while providing grid services. Optimising the control of irrigation systems, particularly those involving reservoirs and pumps, presents a complex mathematical challenge. In addition to this challenge, incorporating uncertainties in water demand, availability, and meteorological and grid conditions represents a further complex aspect of the task.

This chapter presents a mathematical description of the problem under consideration, including the classical elements of the irrigation system and the elements determined by the long-term optimisation tool described in 3. Furthermore, uncertainty sources are identified. The chapter then introduces the methodology employed in developing the plant controller capable of ensuring optimal operation, even in conditions that deviate from the expected operating scenario. Finally, the developed algorithm is tested in a simulation environment. The results are then presented and discussed.

Specifically, this chapter is structured as follows:

- i Section 6.1 provides an overview of the current state of the art in the field, introducing the topic and reviewing the available solutions.
- ii Section 6.2 outlines the controller's objectives and reviews the major challenges facing the irrigation system operation. It then introduces the mathematical formulation of the problem.
- iii Section 6.3 describes the methodology on which the optimal controller is based and develops the formulation for determining the proposed algorithm.
- iv Section 6.4 provides an analysis of the performance of the control algorithm developed on different case studies.
- v Section 6.5 concludes the chapter with the conclusions drawn. It also provides a description of the next steps to be taken in the project.

6.1 Introduction

The irrigation system under consideration in this project is currently comprised of a series of reservoirs connected by pipes, with water flow facilitated by pumps organised in pumping stations. These reservoirs facilitate the storage and distribution of water to the fields. The plant operators then use heuristic rules to determine the demand for a certain amount of electrical power from the grid to maintain sufficient water in the upper reservoirs from the lower reservoirs.

The primary objective of this operational model is to reduce electricity costs. To this end, energy demand is scheduled to occur during periods of the day when, as stipulated in the contract, the price per kWh is lower, typically at night. In addition, off-grid photovoltaic panels are being installed to supply an isolated pump, so that when sufficient power is available, the pump associated with the PV installation will pump water.

Within the framework of this project, the intention is to exploit the potential performance of the reservoirs as a store of electrical energy in the form of water. This will require the installation of new assets that allow for the bi-directional flow of water and the extraction of energy from water flows to be returned to the power grid. The introduction of new assets within the system will enable new functionalities, thereby increasing the complexity of plant operation. This will overrule the heuristic rules that operators have developed over the years.

This new, larger and more complicated system will require more sophisticated control schemes to optimally balance water distribution, energy consumption, and grid support. Traditional rule-based or reactive control methods may no longer be sufficient as they lack the flexibility to anticipate future fluctuations in water availability, electricity prices and crop irrigation requirements. Instead, advanced optimisation-based approaches are needed to ensure real-time adaptability and long-term efficiency.

The optimisation tool, which is explained in detail in Chapter 3, provides as output, in addition to the dimensioning of the plant elements, an optimal operating strategy for a specific scenario. However, from a control perspective, solving an offline optimisation problem (with all data known or estimated) and implementing its output as a set-point for a physical system is a feedforward approach. This approach can be considered adequate in cases where the plant model is perfectly known, both in terms of topology and parameters, and where the forecast of disturbances is estimated with high accuracy.

In systems where uncertainty is a significant concern, such as the system under consideration in this project, however, achieving optimal control is complicated due to several interdependent factors:

- Uncertainty in water demand: water requirements depend on soil conditions and external environmental conditions, creating variability in irrigation needs.
- Accurate weather forecast: rainfall and evaporation rates are inherently unpredictable and have a significant impact on the availability of water in reservoirs. In addition, the production of photovoltaic energy is also dependent on climatic conditions.
- Integration with the power grid: water storage in reservoirs serves as an energy reserve to support the electricity grid. However, the times when the grid is subject to disturbances are completely unpredictable.

Given the stochastic nature of the system, robust and stochastic control techniques can help mitigate the effects of uncertainty by incorporating probabilistic models of rainfall, evaporation, and agricultural water demand. However, these methods can sometimes result in excessively conservative policies that may under-utilise available resources.

In contrast, feedback optimisation structures offer a powerful framework for enhancing control robustness and adaptability. Unlike open-loop strategies that rely solely on forecasts and precomputed schedules, feedback-based methods continuously incorporate real-time measurements into the optimisation process. Such measurements can include reservoir levels, weather data and power grid signals, allowing the system to respond rapidly to unexpected disturbances.

Embedding optimisation within a feedback loop enables the controller to adjust decisions as new information becomes available, thereby reducing the impact of modelling errors and forecast inaccuracies. Feedback optimisation provides a natural way to handle constraint violations and system nonlinearities,

ensuring safe and efficient operation even under highly variable conditions. When coupled with predictive strategies like Model Predictive Control (MPC), feedback optimisation enables anticipatory yet reactive decision-making, balancing long-term planning with short-term response - an essential feature of modern, multi-objective irrigation systems.

MPC techniques provide an effective framework by explicitly considering future system dynamics within a receding horizon optimisation problem. MPC continuously updates its decisions based on new measurements and forecasts, optimising the operation of pumps and reservoirs. By leveraging predictive models and constraints, MPC can schedule water transfers and pumping operations in a way that minimises energy costs, prevents shortages, and strategically aligns water storage with periods of excess renewable energy generation. However, it should be noted that this methodology still relies on an accurate model of the existing plant to be optimised.

In recent years, there has been a growing interest in the fact that many numerical optimisation algorithms, specially first order iterative algorithms, can be interpreted as dynamical systems. According to this interpretation, it is possible to construct an extended dynamical system consisting of plant dynamics and the dynamics of an algorithm for solving an optimisation problem. Therefore, this system will autonomously drive the plant to an optimal operating point. In the context of this notion, a technique known as Online Feedback Optimisation (OFO) has been introduced in the literature.

The key idea of OFO is to implement optimisation algorithms as feedback controllers, which are connected with a physical plant to form a closed loop. Therefore, OFO-based controllers employs real-time measurements to adapt control actions as and when required. Moreover, OFO strategies demand minimal model information, making it particularly beneficial in situations where accurate models are challenging to acquire. The time evolution of the plant state converging to the solution of an optimisation problem follows the following structure:

- The set of real-time measurements are collected in the central controller.
- The controller updates the control actions by solving an iteration of the optimisation problem.
- The new control actions are dispatched to the system by updating the set-points of the controllable devices.
- After a waiting period during which the fastest transients disappear and the system measurements are taken again. Then, the process is repeated as the system converges to the solution of the optimisation problem.

It is important to note that within the OFO framework, the plant is considered a constraint enforcer routine, i.e. given an input, the physical system will produce an output that satisfies the input-output relationship. As a consequence, there is no need to evaluate the (possibly nonlinear) functions describing the system's behaviour, thereby reducing the computational cost. This feature provides OFO-based control structures with a high degree of scalability, making it an attractive option for large-scale and complex systems. Furthermore, feedback the measurement set, instead of being model dependent, inherently includes the effect of exogenous disturbances and the corresponding control actions are updated without the need to forecast them.

Given these advantages, the application of OFO-based controller in combination with the developed classical optimisation tools on this irrigation system is a promising approach to achieving an optimal trade-off between water availability, economic efficiency, and grid integration.

6.2 Problem definition

Consider a non-linear dynamic system which is herein referred to as the plant. The behaviour of the system under consideration is determined by the following equations:

$$\begin{aligned}\frac{d}{dt}\zeta &= \mathbf{f}(\zeta, \mathbf{u}), \\ \mathbf{y} &= \mathbf{g}(\zeta) + \mathbf{d},\end{aligned}\tag{6.1}$$

where $\zeta \in \mathfrak{R}^n$ denotes the column vector comprising the n states of the system, $\mathbf{u} \in \mathfrak{R}^p$ and $\mathbf{y} \in \mathfrak{R}^q$ are respectively the control actions and the measurable outputs of the plant. The vector field $\mathbf{f}(\cdot)$ and the map $\mathbf{g}(\cdot)$ describe the dynamic evolution of the plant and the output measurement process, respectively. In addition, in this plant, a set of disturbances is considered to be present which are represented by the column vector $\mathbf{d} \in \mathfrak{R}^w$. Note that these disturbances are considered to affect the system in an additive manner.

One of the primary assumptions regarding this plant is that, given a constant input \mathbf{u} and a constant disturbance \mathbf{d} , the plant exhibits asymptotically stable behaviour. This implies that transients dissipate rapidly, leading to a fast convergence of the operating point towards a stationary state. Furthermore, it is assumed that a unique steady-state is reached for a given input: $\zeta_{ss} = \mathbf{h}_s(\mathbf{u})$, which implies the following:

$$\mathbf{0} = \mathbf{f}(\zeta_{ss}, \mathbf{u}) = \mathbf{f}(\mathbf{h}_s(\mathbf{u}), \mathbf{u}).\tag{6.2}$$

It can be concluded that a direct consequence of this is the existence of a stationary mapping between disturbance-free measurements and control actions, as follows:

$$\mathbf{y}_s = \mathbf{h}(\mathbf{u}) := \mathbf{g}(\mathbf{h}_s(\mathbf{u})),\tag{6.3}$$

Here, it is necessary to consider that $\mathbf{h}(\cdot)$ is continuously differentiable in \mathbf{u} .

In the system previously described, consider the problem of determining the values of the set-points, which are bounded by a feasible set, in order to minimise a given cost function while satisfying certain constraints on the set of output signals. This can be mathematically expressed as follows:

$$\begin{aligned}\underset{\mathbf{u}}{\text{minimise}} \quad & \phi(\mathbf{y}, \mathbf{u}) \\ \text{subject to} \quad & \mathbf{h}(\mathbf{u}) + \mathbf{d} - \mathbf{y} = \mathbf{0} \\ & \mathbf{y} \in \mathcal{Y} \\ & \mathbf{u} \in \mathcal{U},\end{aligned}\tag{6.4}$$

where $\phi(\cdot)$ denotes a scalar function that encompasses the objective to be minimised. The objective in question may be dependent either on the inputs \mathbf{u} or the outputs \mathbf{y} , or indeed on both types of variable. \mathcal{Y} and \mathcal{U} are used to denote, respectively, the sets of admissible steady-state values of the measured variables and the control actions. Finally, $\mathbf{h}(\cdot)$ is the steady-state input-output (probably non-linear) map of the dynamic plant, and \mathbf{d} denotes the disturbance vector.

The fundamental problem is therefore to steer the operating point of the plant to a state that satisfies all constraints while minimising the cost function value.

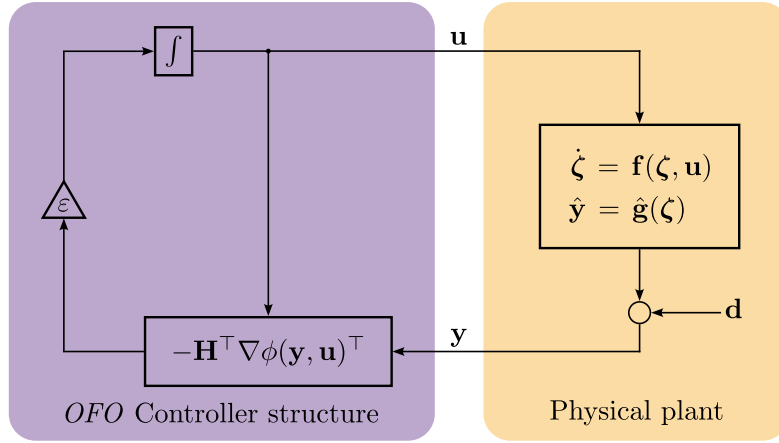


Figure 6.1 – Online Feedback optimisation structure based on gradient flow.

6.3 Methodology

This section outlines the procedure for obtaining the feedback control law that solves problem (6.4), described in the previous section.

The objective of the algorithm is to drive the operating point of the plant to a point that minimises the function $\phi(\mathbf{y}, \mathbf{u})$ which is a function of the plant output \mathbf{y} and input \mathbf{u} . Considering that both the mathematical model of the stationary mapping and the disturbances are known, then the cost function can be reduced as follows:

$$\hat{\phi}(\mathbf{u}) := \phi(\mathbf{h}(\mathbf{u}) + \mathbf{d}, \mathbf{u}). \quad (6.5)$$

For a moment, assume that the minimisation problem 6.4 is unconstrained. In this case, the optimum can be reached by means of a simple gradient flow algorithm [136]:

$$\begin{aligned} \frac{d}{dt} \mathbf{u} &= -\nabla_{\mathbf{u}} \hat{\phi}(\mathbf{u}) \\ &= -\nabla_{\mathbf{u}} \mathbf{h}(\mathbf{u})^T \nabla \phi(\mathbf{h}(\mathbf{u}) + \mathbf{d}, \mathbf{u})^T, \end{aligned} \quad (6.6)$$

where $\nabla_{\mathbf{u}} \mathbf{h}(\mathbf{u})$ is a consequence of the chain rule applied to $\phi(\mathbf{h}(\mathbf{u}) + \mathbf{d}, \mathbf{u})$. Note that $\nabla_{\mathbf{u}} \mathbf{h}(\mathbf{u})$ is the *Jacobian* matrix of the function $\mathbf{h}(\cdot)$ at \mathbf{u} . This matrix will be referred to as \mathbf{H} from here on in. This matrix provides an indication of the sensitivity of the outputs to the inputs.

Problem (6.6) can be solved in a closed loop without the need for additional information until an equilibrium point (ζ^*, \mathbf{u}^*) is reached. This stationary point of the plant satisfies $\nabla \phi(\mathbf{h}(\mathbf{u}) + \mathbf{d}, \mathbf{u})^T = \mathbf{0}$, thus, it is a critical point of the cost function $\phi(\cdot)$.

An alternative proposition is to recognise in (6.6) that the expression $\mathbf{h}(\mathbf{u}) + \mathbf{d}$ corresponds to the set of measurements of the plant, i.e. \mathbf{y} . In this case, the algorithm (6.6) is rewritten in an open loop form, as follows:

$$\frac{d}{dt} \mathbf{u} = -\nabla_{\mathbf{u}} \mathbf{h}(\mathbf{u})^T \nabla \phi(\mathbf{y}, \mathbf{u})^T. \quad (6.7)$$

The new algorithm (6.7) requires knowledge of the set of measurements \mathbf{y} , but avoids the need to compute the plant model $\mathbf{h}(\cdot)$ and thus avoids the need to know explicitly the disturbances \mathbf{d} . The primary benefit of this approach is that it facilitates the construction of a closed-loop system, wherein the plant (6.1) is governed by algorithm (6.7) as the controller. The controller is referred to as Online Feedback Optimisation [137, 138]. The interconnection of these two systems is illustrated in Figure 6.1.

The integral control nature of (6.7) guarantees the convergence to a steady-state optimal point [139]. In order to avoid large excursions in control actions, a gain (ϵ) with a small positive value is added to the controller. Therefore, the whole interconnected system is expressed as follows:

$$\begin{aligned}\frac{d}{dt}\zeta &= \mathbf{f}(\zeta, \mathbf{u}) \\ \mathbf{y} &= \mathbf{g}(\zeta) + \mathbf{d} \\ \frac{d}{dt}\mathbf{u} &= -\epsilon \mathbf{H}^T \nabla \phi(\mathbf{y}, \mathbf{u})^T.\end{aligned}\tag{6.8}$$

Due to its feedback nature, the OFO approach is robust to model inaccuracy and disturbance effects. Therefore, there is no need for a forecast of disturbance behaviour or comprehensive knowledge of the plant; only an estimation of sensitivity is required.

Now that the unconstrained OFO operation has been reviewed, let's return to the original problem and consider the constraints on the control actions and outputs of the plant. A variety of strategies can be employed to incorporate the constraints in the construction of the OFO-based control algorithm:

1. Gradient methods with penalty terms
2. Gradient methods with barrier functions
3. Projected gradient flows [140, 141]
4. Primal-Dual saddle points [142, 143]

The first two methods have the disadvantage of modifying the objective function, so they can only converge to a value close to the optimum. Furthermore, it should be noted that the use of penalty-based methods does not ensure that the solution will satisfy the constraints.

Primal-Dual saddle point methods have demonstrated excellent performance in converging to an optimal solution for convex-definite problems. Generally, these algorithms consist of a gradient descent in the primal problem and a gradient ascent in the dual problem. Controllers based on these algorithms have even been tested experimentally [142, 144]. However, if the objective function or constraints are non-convex, convergence to a saddle point cannot be guaranteed. This requires the addition of regularisation terms to both the primal and dual problems. While this ensures convergence of the flow, the saddle points of the new problem will no longer correspond to those of the original problem.

Finally, projected gradient flows enforce inequality constraints by utilising projection mechanisms. Classical projected gradient descent is based on the Euclidean minimum norm, which is used to project the result of each iteration onto the feasible region. In the interior of the feasible set, therefore, trajectories follow the gradient direction, whereas at the boundary they follow the steepest feasible direction. It should be noted that these methods are discontinuous systems by definition and therefore require non-smooth analysis techniques.

For the purposes of this study, it was decided that an algorithm of the projected gradient flow type would be best suited to facilitating the integration of the problem's inequality constraint. Specifically, the algorithm presented in [141] has been adopted, which functions by projecting the gradient iteration on a linearisation of the feasible set at the current point.

The k -th iteration of the integral feedback controller, formulated in discrete time, can be expressed as follows:

$$\mathbf{u}[k + 1] = \mathbf{u}[k] + \epsilon \sigma(\mathbf{u}[k], \mathbf{y}[k]),\tag{6.9}$$

where $\epsilon > 0$ is a small fixed step-size, and $\sigma(\mathbf{u}, \mathbf{y})$ is defined as:

$$\begin{aligned} \sigma(\mathbf{u}, \mathbf{y}) &:= \arg \min_{\mathbf{w}} \|\mathbf{w} + \mathbf{G}^{-1} \mathbf{H}^{-1} \nabla \phi(\mathbf{y}[k], \mathbf{u}[k])\|_{\mathbf{G}}^2 \\ &\text{subject to } \mathbf{A}(\mathbf{u}[k] + \epsilon \mathbf{w}) \leq \mathbf{b} \\ &\quad \mathbf{C}(\mathbf{y}[k] + \epsilon \mathbf{H} \mathbf{w}) \leq \mathbf{d}, \end{aligned} \quad (6.10)$$

where \mathbf{G} is a continuous metric on the feasible set.

The expression (6.10) determines the resulting vector from projecting the control action that reduces the objective function onto the linearisation of the feasible search region. Note that the constraints are evaluated at the point to which the system is expected to evolve in the linearised space, rather than at the current point.

The remaining issue to be addressed in the implementation of the algorithm concerns the determination of the plant sensitivity matrix \mathbf{H} . It is important to note that this matrix is not constant unless the plant can be characterised by a linear time-invariant (LTI) system, however, in realistic environments, the Jacobian matrix is state or time dependent. A salient feature of controllers that are based on OFO techniques is that, due to the feedback structure, they exhibit a high degree of robustness against inaccuracies in the values of the sensitivity matrix [145]. However, improved estimation of the values of this matrix lead to enhanced convergence of the system to the desired operating point. Therefore, it is highly desirable to have a good estimate of the input-output sensitivity.

In cases where a model of the plant is available, the most direct approach is to evaluate the derivative at the desired operating point, thereby obtaining the sensitivity matrix analytically. A more direct approach, or online procedure, would be to perturb each of the control actions sequentially and determine their effect on the outputs. This would be equivalent to applying the finite difference method to the Jacobian matrix. In systems where such methods are not applicable, it is sufficient to determine a matrix with 0, 1 and -1, depending on whether the input has a zero effect on the output, whether it is directly proportional or inversely proportional. Each of these methods provides a value of the sensitivity at an operating point. It is therefore desirable that this matrix be updated online by comparing the expected variation with that obtained at each step.

6.3.1 Development of OFO-based controller for pump-based irrigation plants

The first step in the OFO-based controller formulation is to identify the control variables and the measured variables. In pump-based irrigation systems, we consider that the control actions can be:

1. Electrical power supplied to the pump p_e , for pumping directly connected to the main grid.
2. Electrical power supplied to the pump p_e and mechanical speed of the motor n at those stations equipped with frequency regulating assets.

In both cases, the electrical power shall remain in steady state within established operating limits:

$$\underline{p}_e \leq p_e \leq \bar{p}_e, \quad (6.11)$$

where \underline{u} denotes the minimum value that u can reach, whereas \bar{u} is used to identify its maximum value.

Where applicable, the rotational speed of the pump must also be forced to remain within the limits of steady state operation:

$$\underline{n} \leq n \leq \bar{n}. \quad (6.12)$$

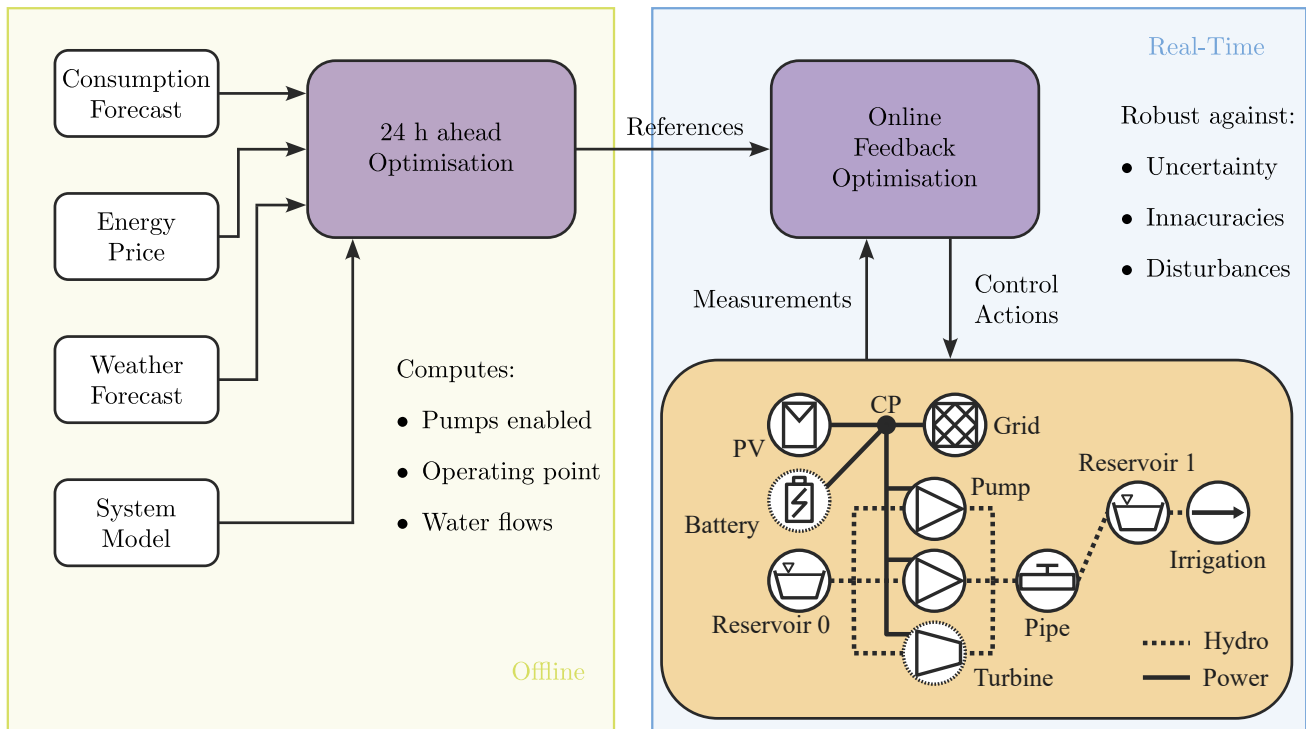


Figure 6.2 – Relationship between offline and online optimisation tools.

The constraints defined in equations (6.11) and (6.12) are of the box-constraint type and can be formulated linearly in a compact form as follows:

$$\mathbf{A}\mathbf{u} \leq \mathbf{b}, \quad (6.13)$$

where the column vector \mathbf{u} groups the control actions. The matrix \mathbf{A} contains only 1 and -1 for the signs of the inequalities, and the column vector \mathbf{b} contains the previously defined upper and lower limits of operation.

The disturbances that are considered unknown in this problem are the flows demanded for irrigation.

With regard to the system's outputs, it is essential to closely monitor the level of the reservoirs, z , (or the volume of water contained W), and the state of charge of the batteries SOC . It may also be advisable to consider measures of water flows. All these variables, along with their respective minimum and maximum limits, represent a set of box constraints that can be expressed as a linear inequality constraint, in the same way as equation (6.13).

It is important to note that in this problem the objective is not exactly to reach an optimal operating point, but to determine an optimal water use planning. For that reason, the OFO-based controller is considered to interact with the long term offline optimiser presented in Section 3.3 through the objective function. Figure 6.2 details the interconnection between these two tools.

Specifically, the system is considered to follow the optimal strategy coming from the offline optimiser. However, this optimisation depends on a weather forecast and a water demand forecast, which may be inaccurate. Therefore, the objective of the OFO-based controller will be to keep system operation as close as possible to the optimal strategy, while correcting any deviations caused by conditions that differ from those predicted during offline optimisation.

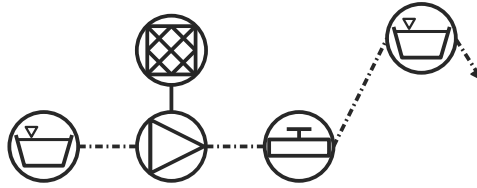


Figure 6.3 – Model of the simplest test case.

6.4 Performance assessment

This section presents the results of the application of the control algorithm developed using the methodology described above on a case study. The objective of the present studies is to analyse the functionalities of the proposed controller.

6.4.1 Study case

To date, only one case study has been analysed. This irrigation plant model is a simple system that allows for straightforward evaluation of the controller's performance.

The system consists of two reservoirs, one positioned at a higher level than the other, connected by a pipe. It is assumed that the irrigation system takes water from a river, so the volume of the modelled lower reservoir is much larger than the upper reservoir. The pumping station, which is connected to the main grid, is located adjacent to the lower reservoir. A schematic of the system is shown graphically in Figure 6.3 and Table 6.1 lists the main system parameters.

Table 6.1 – Parameters of the simple test case.

Parameter	Value
Maximum volume of the downstream reservoir	10^6 m^3
Minimum volume of the downstream reservoir	0 m^3
Maximum height of downstream reservoir	1 m
Minimum height of downstream reservoir	0 m
Maximum volume of the upstream reservoir	600 m^3
Minimum volume of the upstream reservoir	400 m^3
Maximum height of upstream reservoir	80 m
Minimum height of upstream reservoir	60 m
Linear pressure loss coefficient of the pipe	$0.05 \frac{\text{s}^2}{\text{m}^5}$
Pump coefficient A	120 m
Pump coefficient B	$0,002 \frac{\text{s}^2}{\text{m}^5}$
Pump efficiency	72 %
Pump maximum power	16 kW

The initial volume of the downstream reservoir is 10^5 m^3 , while the upstream reservoir 2 has a volume of 500 m^3 at the beginning of the simulation. Finally, it is considered that the pump is inactive. The irrigation water consumption profile has been randomly generated.

The offline optimisation tool, which determines the optimal consumption profile of the pump, is considered to update its references every hour. The OFO-based controller updates the control actions every minute, in this first study only the power consumed by the pump.

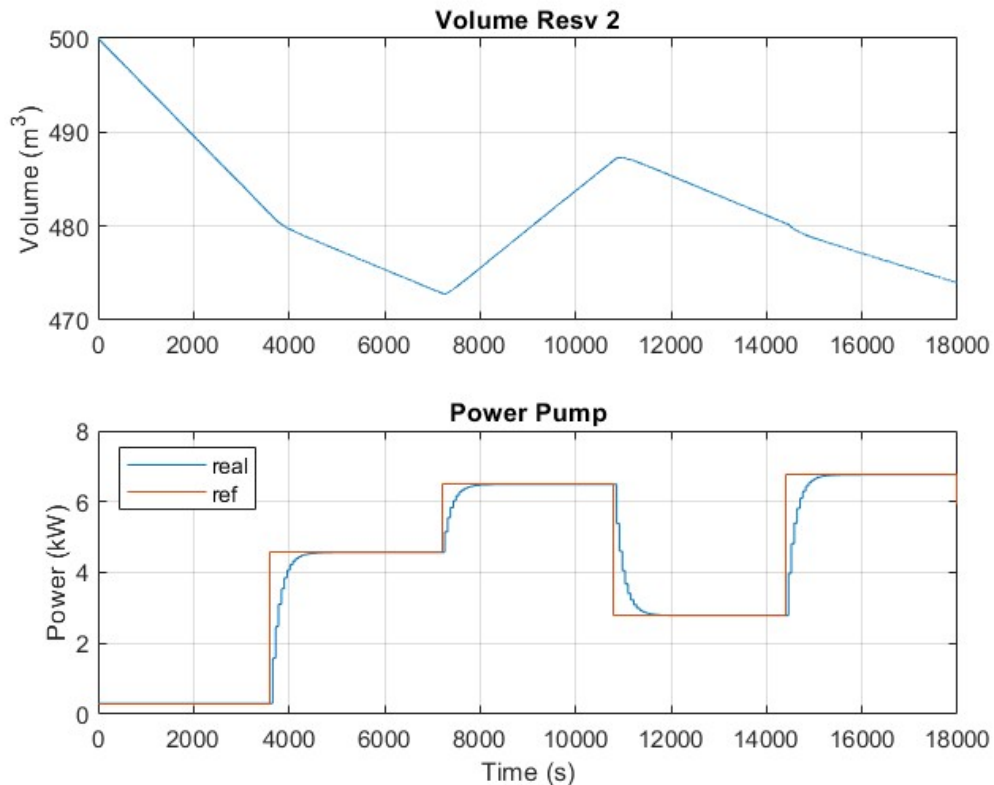


Figure 6.4 – Testing of the plant with a good estimation of water consumption for irrigation.

6.4.2 Preliminary results

Two test runs have been simulated on the described plant. In both cases an operating time of 5 hours was simulated.

In the first test, a power consumption profile for the pump was created to guarantee the water level in the upper reservoir remained within the specified limits during the duration of the simulation. Therefore, the primary function of the OFO-based controller is to regulate the electrical power supplied to the pump, ensuring that the offline designed profile is tracked.

The results of this test are plot in Figure 6.4. The upper graph depicts the behaviour of the water volume in the upstream reservoir. A decrease in water volume indicates higher water consumption than the water pumped, and vice versa. It should be noted that at no time does the water volume approach the 400 m^3 lower limit.

The graph below shows the electrical power delivered to the pump. The orange curve shows the power profile dictated by the offline optimisation tool, while the blue curve shows the electrical power determined by the OFO-based controller. Please note that, following the transient phase, the steady-state power consumption is precisely as stipulated by the offline optimisation tool.

The second test was characterised by an error in predicting the demand for irrigation water, in particular, the actual amount of irrigation is twice the estimated amount. As a consequence, the power consumption profile for the pump was the same than the previous case.

The results of this test are plot in Figure 6.5. Again, the upper graph depicts the behaviour of the water volume in the upstream reservoir. In this test, the drop in water level is much more abrupt because the

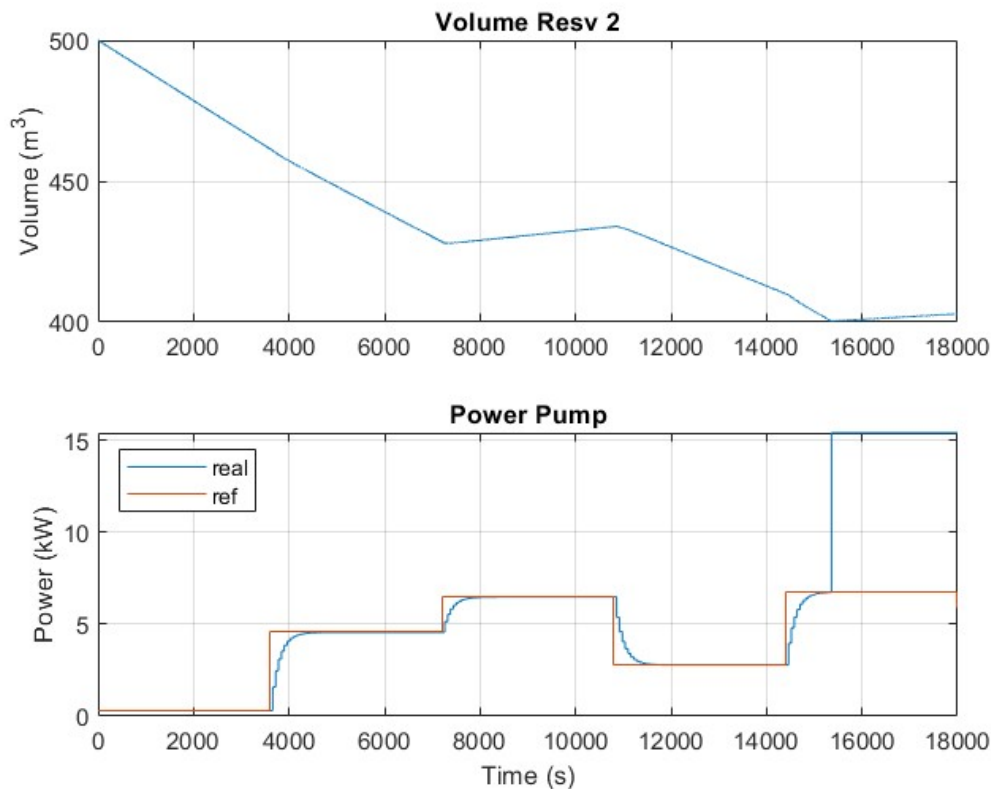


Figure 6.5 – Testing of the plant with a wrong estimation of water consumption for irrigation.

amount of water consumed for irrigation is much higher. Even at the instant $t = 15000$ seconds, the water level in the reservoir reaches the lower limit.

The consequence of this can be seen in the electrical power demand of the pump, shown in the lower graph of the figure. Most of the time, the pump's power consumption follows the profile provided by the offline optimisation tool. However, when the water level in the upstream reservoir reaches the lower boundary, the power demand increases to increase the pumped water flow and maintain the reservoir level.

6.5 Conclusions

This section details the development of the algorithm for real-time plant control. The desired controller's characteristics have been outlined, and the rationale behind utilising a controller based on the OFO methodology has been substantiated. The text then goes on to argue for the fulfilment of the necessary assumptions to develop this technique, before finally justifying the type of algorithm on which the controller is based.

In addition to dealing with the uncertainty and inaccuracies of the underlying mathematical model, the use of an OFO-based methodology allows us to take advantage of the volume of available information used to feed the long-term optimisation tool.

Preliminary results obtained from the implementation of the OFO-based controller on a simple case have been satisfactory. Our studies has demonstrated the efficacy of integrating offline optimisation with an online controller, with both components complementing each other to enhance performance and address the limitations of the other. However, further modifications and tests are required.

6.5.1 Future work

The preliminary test results have been satisfactory. Further testing is required to fully verify the performance of this controller.

One of the objectives on which work is already underway is the reformulation of the OFO-based controller objective, with a view to improving the anticipation of irrigation deviations. However, it is interesting to observe how well the effort to meet the constraints is working.

Verification of the controller on a more complex system is an indispensable requirement. Despite the demonstrator plants comprising only two reservoirs, the objective is to operate and manage multiple reservoir systems, in which the behaviour of the output variables is strongly related.

Following the completion of the simulation environment tests, the experimental validation of the controller must be carried out in the project's demonstrator plants.

7 Fundamental AGI topologies and control strategies

Grid services can be provided by implementing various control schemes in the converter that connects the irrigation microgrid to the main electrical grid. The control scheme of this primary converter must be coordinated with the control systems of other power electronic equipment within the microgrid, each of which may have its own programmed logic. The choice of control strategy will depend on factors such as the number of converters present in the microgrid and the specific functionalities required.

This chapter presents various configurations for providing grid services, including a comparison between AC and DC microgrid approaches, with a detailed analysis of the advantages and disadvantages of each. Four microgrid configurations are examined, focusing on integrating converter-based components and their implications. The chapter also explores several control architectures for the primary converter and discusses their impact on system performance. Finally, both linear and non-linear models are introduced to support further analysis of the microgrid's interaction with the primary grid. This includes power flow calculations, developing a linear state-space model, and validating the linear model using MATLAB-Simulink.

Specifically, this chapter is structured as follows:

- i Section 7.1 provides an overview of the elements introduced in this chapter and gives a general view of the limitations and possible configurations.
- ii Section 7.2 compares two possible approaches for the presented microgrid and decides the leading technology.
- iii Section 7.3 presents the state-of-the-art control architectures which could be implemented in the main converter and explores a newly proposed control architecture to enhance the converter functionalities.
- iv Section 7.4 discusses the possible AGI configurations and gives insight into the pros and cons between these possible configurations.
- v Section 7.5 presents the models that can be used to assess the studies needed to achieve a proper interconnection between the microgrid and the primary grid.
- vi Section 7.7 suggests future work based on the work presented during this chapter.

7.1 Introduction

The irrigation system under consideration comprises several water reservoirs, including several pumping systems. These pumping systems run with electricity, the energy of which is taken from the electrical grid. The high consumption of these systems makes it worth considering installing a photovoltaic (PV) plant

nearby to feed the pumping installation. This even makes more sense if it is possible to run the pumping facilities without depending on the connection to the primary grid, i.e., running in isolation mode. The straightforward improvement of this configuration is to include storage to further increase the number of operation hours that the facility could run without depending on the energy supplied by the grid. This is especially interesting considering that some of these facilities might be located in remote areas where the stability and robustness of the electrical grid are not always ensured.

The installation of this PV plant and its possible storage system must be appropriately integrated with the rest of the existing system, mainly the pumping system connected to the primary grid. In most applications, the PV plant is connected to the grid using two power converters. One converter converts the nature of the produced electrical energy from the PV system from DC to AC. The second converter (DC/DC) adjusts the DC voltage where the PV plant is connected to optimise the amount of energy that can be extracted from the PV plant. A similar configuration, based on two power converters, can be followed to interconnect the battery system with the rest of the elements. These configurations will be further explained in Section 7.2.

This new converter-based structure has to be appropriately integrated with the pumping installation. In general, this existing facility also includes a power converter-based topology that regulates the angular velocity of the pumps. This is, in general, composed of two converters that decouple the grid's frequency from the frequency at which the pumps rotate. One converter converts the current from AC to DC, and the other converts the current back to AC while regulating the AC frequency.

Converter-based systems, the PV plant, and the pumping system could be integrated into AC or DC. This is one of the main selections needed while considering incorporating these systems and will be covered in Section 7.2. As a result of the discussions included in this chapter, the selected technology on which the microgrid will be based is DC.

Different possibilities arise for the microgrid configuration once the main microgrid technology is selected. This will depend on the number of elements considered, PV and battery storage, and the inclusion of a dedicated DC/DC converter for the PV system. Thus, 2^2 possible configurations exist. The pros and cons of these configurations are intensely discussed in Section 7.4.

In all possible configurations explored, there is a key element in the interconnection between the microgrid and the grid. This is the power converter interconnecting both facilities. Depending on the control architecture applied in this converter, different functionalities can be programmed, enhancing the operation and grid services that the irrigation system can provide to the grid. The other control architectures are discussed in Section 7.3. Apart from the state-of-the-art control architectures, a recently presented one has also been explored as it is spotted that this new configuration can enhance the facility's operation.

Studying the connection between the microgrid and the primary grid requires considering different aspects. Between them, three are highlighted in this Chapter.

The first one is the steady-state response of the system. This can be studied by solving the power flow of the system. In this case, as the system is composed of AC and DC components, the classic power flow solving approach can not be used, as these are mainly designed only for AC systems. Thus, Section 7.5 reviews methods to solve an AC/DC power flow and presents the equations that need to be considered to solve the AC/DC power flow.

The second one is small-signal stability. This is especially useful for studying the system's stability for different operation points and spotting possible interactions between converter-based resources. It is also convenient for control tuning. These studies are done with linear models. In general, the linear models are expressed in state-space form. Section 7.5 includes the state-space system of the microgrid and the connection to the primary grid.

The third one is transient stability. These studies are used to understand the system's stability when significant transients occur. This includes AC and DC faults, big generation or load changes, and possible

disconnections from the primary grid. The non-linear behaviour of these phenomena does not permit the study of these transients with the previously defined linear models. Therefore, the use of non-linear models is mandatory. Thus, Section 7.5 includes an initial non-linear model to evaluate these transients.

7.2 Comparing AC and DC microgrid approaches

The irrigation system uses pumps that manage the water from the different reservoirs. These pumps, in general, are based on power electronic equipment to properly manage the pump shaft's angular velocity (rotational speed). This is achieved by controlling the angular velocity at which the electric motor that drives the pump rotates. The control of this angular velocity is essential for different aspects. The main one is to match the water flow and pressure to the specified objective and real-time demand. Also, some pumps have specific angular velocities that must be met depending on the water flow. Thus, it is essential to meet these standards to avoid damaging the pump and extend its useful life. The control of the motor speed is done through a converter, which is usually called a Variable Frequency Drive (VFD). The main functionality of this converter is to adjust the frequency of the AC feeding the motor and the voltage at the point of connection. Adjusting these two parameters allows the motor to change its velocity to meet the previously defined standards. The scheme followed to achieve this usually involves two stages. In the first stage, a converter converts the AC power to DC. Secondly, another converter converts the DC back to AC with the appropriate voltage and frequency. This last converter regulates the voltage and frequency that the motor driving the pump sees at its point of connection. So, this previous converter is essential. However, the first stage could be suppressed if the second converter is directly connected to a DC grid, as will be discussed afterward.

As previously introduced, including PV systems in the irrigation scheme seems a valuable system enhancement. Power converters also drive these PV systems. In this case, a similar scheme to the pump configuration is followed. In this case, following a two-stage process is necessary to optimally connect a PV system with another AC system. In this case, one converter is a DC/DC converter, whereas the other is an AC/DC converter. The inclusion of this two-stage process is necessary to adjust the DC voltage that the PV systems see. The amount of power that can be extracted from a PV depends on the DC voltage that the photovoltaic panels see. Therefore, to extract the maximum power, the DC voltage is adjusted to meet the optimal one (see Figure 7.1). The algorithm to meet the optimal DC voltage is known as Maximum Power Point Tracking (MPPT). This algorithm is implemented in the DC/DC converter, whereas the other converter (AC/DC) controls the amount of active and reactive power injected into the AC grid.

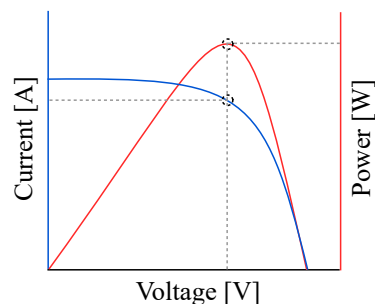


Figure 7.1 – Maximum Power Point Tracking.

Based on the previously discussed configurations, the usual way to connect these systems is based on AC. This generally does not create a grid, as both converters are directly connected to the primary grid. The main advantage of this configuration is its simplicity, as the state-of-the-art technology and available converter schemes for pumps and PV are connected in this way. This translates to a cheaper initial cost. However, this configuration has one main limitation. The system can not operate in isolation mode, i.e., it needs a stable AC grid to run. If the grid is unavailable, the system can not operate as all the connections

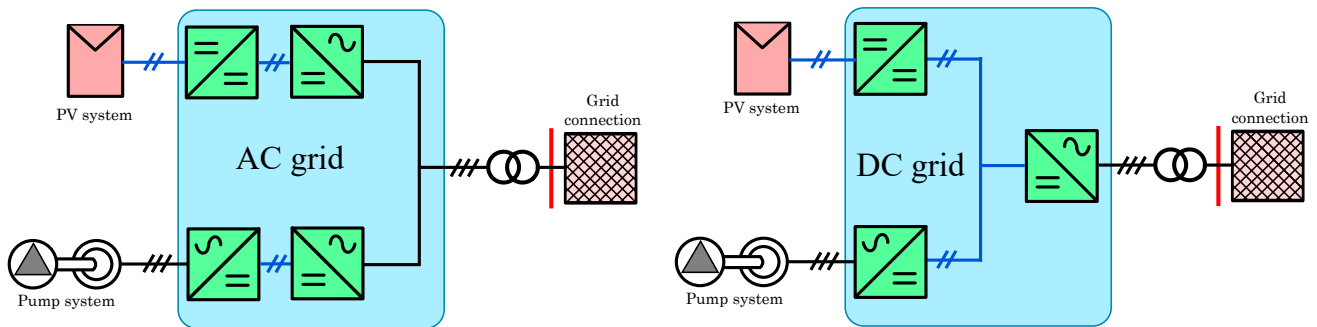


Figure 7.2 – AC vs DC interconnections.

pass through the primary grid. This also has implications on the flow of energy, and it is not possible to directly control which energy is delivered to the grid and which is fed to the pumping system. Based on these facts, it is interesting to consider connecting these two systems with DC. The difference between these two schemes is shown in Figure 7.2.

The DC configuration maintains the two essential converters for the pumping and PV systems while interconnecting them using a DC microgrid. It includes an additional converter to interconnect this system to the principal AC grid. This configuration's main advantage is the possibility of operating in islanded mode. The pumping system can be fed directly from the PV system without bypassing the electrical energy through the principal grid. Even if the grid is down, the system could still operate. The main disadvantage is its higher initial cost and its complexity. However, its higher price can eventually compensate for more hours of operation in islanded mode, i.e., without buying energy from the principal grid, and the possibility of offering grid services from the converter connecting this system to the principal grid. This configuration makes it easier to provide grid services from the main converter. It is suitable for operating in islanded mode and is considered a valid option for this application.

7.3 Control architectures for the converter connected to the primary grid

On the DC grid interconnection strategy, there are at least three converters. The first one, the DC/DC converter of the PV system, performs the MPPT algorithm; the second one is the AC/DC converter of the pumping system, which regulates the frequency of the pumping shaft and its voltage. The control to be applied at the third converter must still be defined. This section's main subject is an initial discussion on which possible control architectures can be applied to this converter.

The literature contains control strategies and architectures to fulfil different requirements. Some of the most common state-of-the-art control architectures and functionalities are highlighted here. Specifically, three controllers are presented: PQ control, DC voltage control, and AC grid-forming control.

PQ control, or AC grid-following control, relies on a Phase-Locked Loop (PLL) to synchronize with the grid voltage. This element reads the grid's voltage and takes out the angle so the converter's internal angle reference rotates at the same angle as the grid. It operates in the synchronous $dq0$ reference frame and regulates the output current to independently control the active (P) and reactive (Q) power delivered to the grid. This control strategy is typically used in systems where the strong grid provides a stable voltage reference. Thus, it depends on the presence of an external AC voltage source to function correctly. The same happens on the DC side; it relies on a stable DC grid voltage to be connected, as this controller cannot form the DC side voltage.

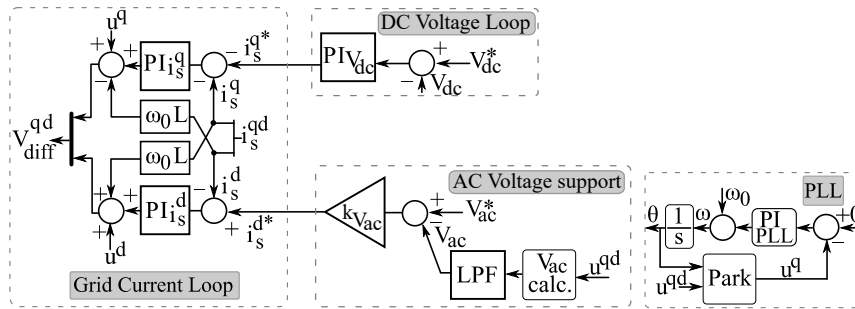


Figure 7.3 – Example of a DC voltage control architecture.

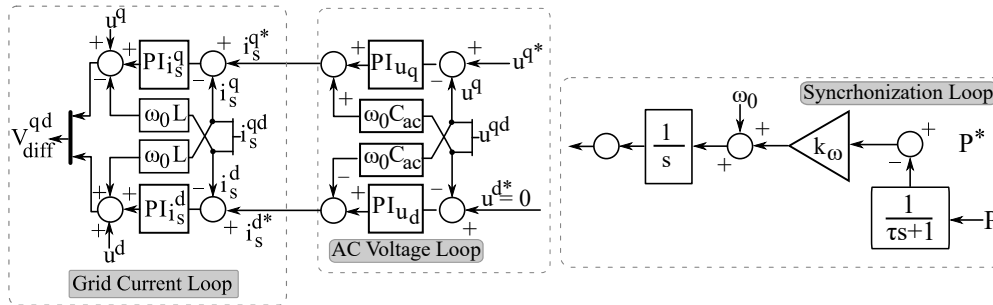


Figure 7.4 – Example of an AC grid-forming control architecture with droop control.

An alternative, that does not require a stable DC voltage to be connected with, is the DC voltage control scheme (see Figure 7.3), as this controller is used to regulate the voltage of the DC link by adjusting the active power exchange on the AC side of the converter. This control scheme is usually implemented in $dq0$ and requires a PLL to synchronize with the AC grid voltage. Thus, it also depends on the presence of an external AC voltage source to function correctly. An alternative control architecture that does not require an external AC voltage source is AC grid-forming control.

AC grid-forming control, often implemented through virtual synchronous machine models, droop control, or power-angle regulation, replaces the PLL with an internal voltage and frequency reference (see Figure ?? for example). This allows the converter to regulate both voltage amplitude and frequency, making it suitable for operation in islanded systems, weak grids, or black-start conditions. Grid-forming control enables the VSC to act as the system's voltage source. It can emulate inertia and damping, facilitating load sharing and system stability in inverter-dominated networks. It is essential to note that a stable DC voltage is required on the DC side, as this control strategy can form the AC voltage but not the DC. Different control architectures have been proposed in the literature [146, 147] to overcome this limitation, one of which is presented next.

7.3.1 Dual-Port control

The previously discussed control architectures cannot provide grid-forming functionalities to both AC and DC sides. In the literature, several proposed control architectures [146, 147] exist that can provide this service on both sides. One proposed in [147] is the one depicted in Figure 7.5. The general scheme is very similar to a traditional AC grid-forming control, which includes an AC voltage vector control with a cascaded grid current control. The main difference comes in the synchronization loop, where a different scheme is used instead of a classical PLL. This scheme uses the DC voltage to synchronize the converter with the grid angle.

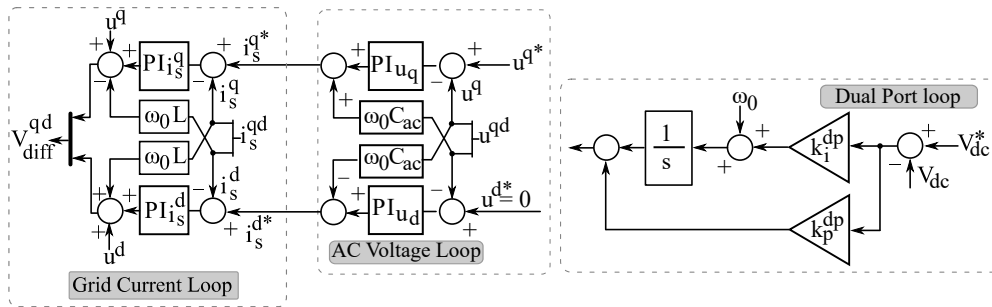


Figure 7.5 – Dual-Port control architecture.

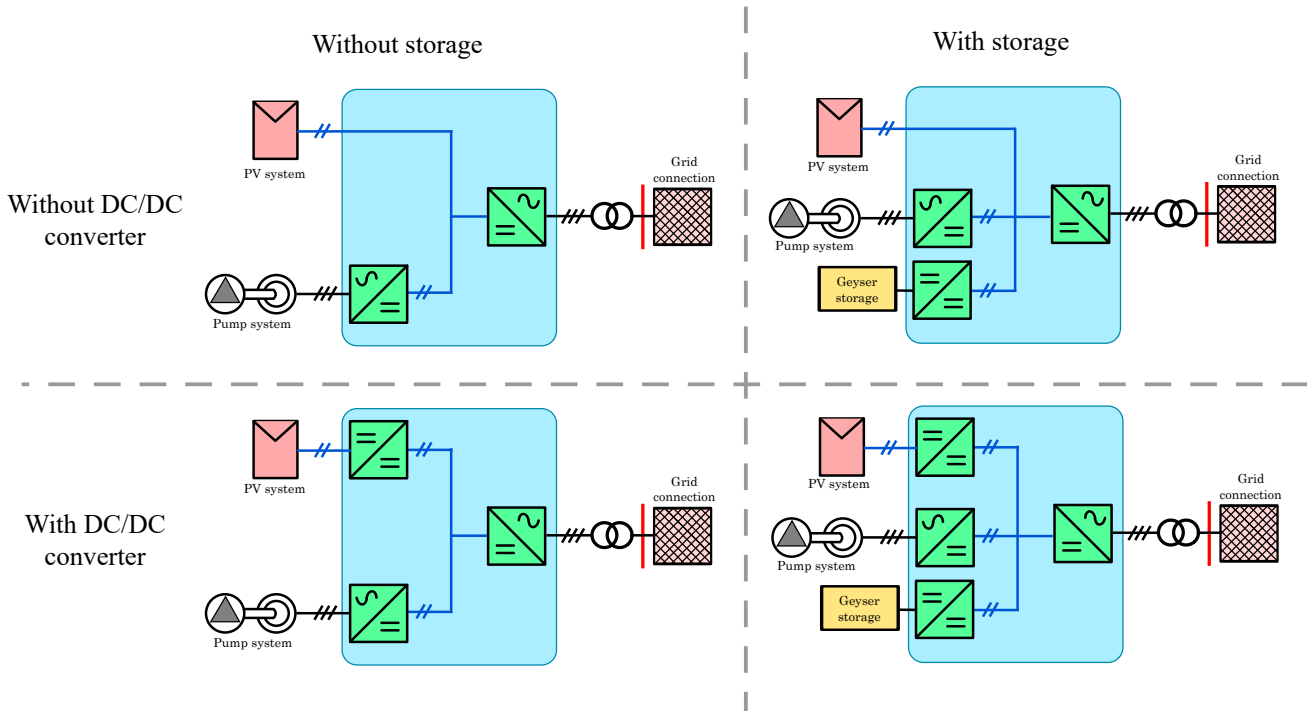


Figure 7.6 – Schemes of the analysed AGI configurations.

7.4 Discussion on possible AGI configurations

Four different configurations can be analysed based on previous discussions on the elements to be included in the system. This depends on whether to install storage and if the PV system consists of a DC/DC converter or is directly connected to the DC grid. Figure 7.6 represents these four configurations. These configurations are next analysed based on which control architecture is included in the converter interconnecting the system with the grid.

Considering the configuration without the DC/DC converter complicates the option of operating the PV system following an MPPT. Depending on the control scheme configured in the main converter, some limited MPPT can be provided. It is limited in the sense that the DC voltage level on the DC grid cannot vary up and down without limits, as other converters are connected to this DC grid, such as the pump station converter. Moreover, very low or high levels on the DC side can cause under- and over-modulation problems on the converter. The converter schemes that could provide limited MPPT are the DC voltage and Dual-Port control. The main limitation of the DC voltage control is that it can offer only limited grid service, i.e., only the ones requiring reactive power. The other control scheme, AC grid-forming, can not provide MPPT as it can not regulate the DC voltage. However, it will be possible to offer grid services.

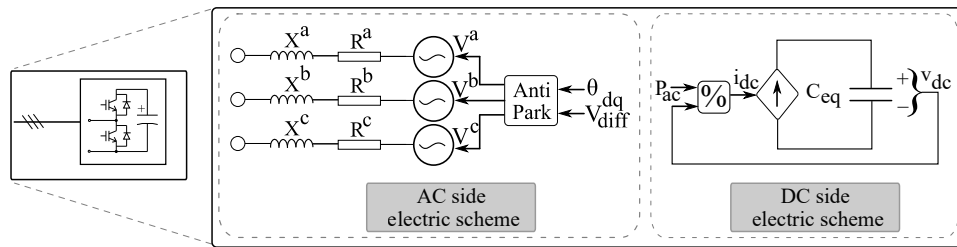


Figure 7.7 – VSC electric scheme model.

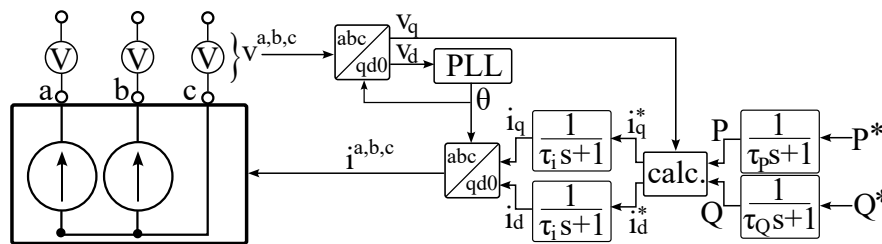


Figure 7.8 – Controlled current source model.

Including a DC/DC converter with the PV systems ensures the possibility of including MPPT. In this case, if the central controller is equipped with DC voltage control, similarly to the previous case, the grid services to provide are limited.

A possibility is to include some battery storage. This can help to smooth transients and enhance the operation in stand-alone mode.

When considering the different controls to apply to the main converter, a general, important consideration is to study how the perturbations propagate between the AC and DC systems.

7.5 Models to study the connection to the primary grid

Different models have been implemented to properly study the connection to the primary grid, emulating the DC grid configuration. The main converter is modelled as a two-level VSC converter. The electric model includes the AC electrical side with its transformer/RL-filter, and the control inputs are applied via a controlled voltage source. The DC side is modelled as a controlled current source, ensuring the power balance between the AC and DC sides and including a capacitor. The model scheme used is depicted in Figure 7.7.

The pumping system has been modelled with a two-level VSC converter and a controlled current source. The pumping system is connected to the DC side via a converter with the same scheme as the one used for the main converter (Figure 7.7). The controlled current source is modelled as in Figure 7.8.

Finally, the storage has been modelled as a constant capacitor, and the PV system has been modelled as a current source.

These elements are modelled in different ways. Three different types of models are included. These are described next.

7.5.1 Steady-state Model

The steady-state model is used to calculate the power flow scenario. It can calculate steady-state performance indices, such as voltage droop between lines, power distribution inside the DC grid, etc. Moreover, it will be helpful to calculate the linear model's linearization point and properly initialize the MATLAB-Simulink model.

To solve the power flow in this case, it has to be considered that the algorithm used has to account for AC and DC grids. Generally, two different methods exist, categorized into sequential and unified approaches. Sequential methods involve solving AC and DC equations step-by-step, as seen in [148, 149, 150]. Unified methods simultaneously solve the AC and DC systems, as demonstrated in reference [151]. One advantage of the sequential method is its compatibility with existing AC-based power flow software, allowing for the integration of DC systems without requiring extensive program modifications, unlike the unified approach, which necessitates changing the entire implementation to solve both AC and DC systems simultaneously.

An alternative approach, suitable for small-sized systems, is to include all non-linear equations conforming to the power flow scenario and solve them with a non-linear solver. This is badly scaled if the system needs to be increased, but it has the advantage that it can be fully configured. Considering that the system in this case is small, this approach is used to solve the power flow.

To compute the steady-state solution of the system, we solve a non-linear constrained optimisation problem. The problem is formulated as:

$$\begin{aligned} & \underset{\mathbf{x}}{\text{minimise}} \quad \mathbf{f}(\mathbf{x}) \\ & \text{subject to} \quad \mathbf{g}(\mathbf{x}) = \mathbf{0}. \end{aligned} \tag{7.1}$$

Where:

- $\mathbf{x} \in \mathbb{R}^n$ is the vector of system variables, initialized with \mathbf{x}_0 , which includes voltages magnitudes, voltage angles and powers.
- $f(\mathbf{x})$ is an auxiliary objective function used to regularize or select among multiple feasible solutions. The implementation may return zero or a minor norm-based penalty.
- $\mathbf{g}(\mathbf{x}) = \mathbf{0}$ represents the nonlinear equality constraints imposed by the power flow equations and converter steady-state conditions.

There are no other constraints imposed besides $\mathbf{g}(\mathbf{x}) = \mathbf{0}$.

- No linear inequality constraints ($\mathbf{Ax} \leq \mathbf{b}$),
- No linear equality constraints ($\mathbf{A}_{\text{eq}}\mathbf{x} = \mathbf{b}_{\text{eq}}$),
- No explicit upper or lower bounds on variables ($\mathbf{l}_b = -\infty$, $\mathbf{u}_b = +\infty$).

The problem is solved using MATLAB's `fmincon` function with the interior-point algorithm:

$$\mathbf{x}^* = \text{fmincon}(f, \mathbf{x}_0, \mathbf{A}, \mathbf{b}, \mathbf{A}_{\text{eq}}, \mathbf{b}_{\text{eq}}, \mathbf{l}_b, \mathbf{u}_b, \mathbf{g}, \text{options}).$$

The solution \mathbf{x}^* contains the steady-state operating point of the system.

7.5.2 Linear Model

Small-signal studies involve analysing the system around its operating point via a linear model. Generally, the models used are non-linear; these models need to be linearized around the operation point, which can be calculated based on the steady-state analysis, i.e., solving the AC/DC power-flow previously formulated.

Small-signal studies provide valuable insights into the system's dynamic stability and control performance. However, building these linear models is challenging, and some mistakes can be made during the process. Therefore, verifying the models by comparing the results obtained in the linear model with the non-linear one is essential.

The steps followed with the linear model consider the following:

1. Computation of the system's operation point via an AC/DC power flow.
2. Linearization point calculation.
3. Construction of all the linear models included in the AC/DC system.
4. Integrate all the linear models.
5. Linear model validation.
6. Linear model analysis.

The computation of the complete linear model of the system can be divided into sub-linear models. Once all the sub-linear models are computed, they can be interconnected using linear algebra. One sub-linear model is connected to another if the output of this sub-linear model is the input of another one, and vice versa. Next, the most critical sub-linear models are included.

rl-circuit

The state-space model for an AC *rl*-circuit connecting an AC node x to an AC node y can be represented as:

- State vector: $\Delta x(t) = [\Delta i_{xy}^q, \Delta i_{xy}^d]^T$
- Input vector: $\Delta u(t) = [\Delta v_x^q, \Delta v_x^d, \Delta v_y^q, \Delta v_y^d]^T$
- Output vector: $\Delta y(t) = [\Delta i_{xy}^q, \Delta i_{xy}^d]^T$

$$A = \begin{bmatrix} -\frac{R}{L} & -\omega_0 \\ \omega_0 & -\frac{R}{L} \end{bmatrix}; B = \begin{bmatrix} \frac{1}{L} & 0 & -\frac{1}{L} & 0 \\ 0 & \frac{1}{L} & 0 & -\frac{1}{L} \end{bmatrix}; C = [J_{2 \times 2}]; D = [0_{2 \times 4}], \quad (7.2)$$

where $v_x^{q,d}$ and $v_y^{q,d}$ are the qd voltages at the AC nodes x and y , respectively; $i_{xy}^{q,d}$ is the current flowing from node x to node y and R and L are the π -section line resistance and inductance, respectively. This model can represent the converter's AC side electrical scheme and a Thévenin equivalent model.

qd-angle Rotation

All the blocks linked to the AC system are represented in the converter local *qd*-frame, which is given by its angle reference estimated by its PLL. To properly interconnect these subsystems, it is necessary to transform the inputs of the different blocks from the global frame (AC grid) to the local frame (converter local *qd*-frame). This is done with a rotation matrix (7.4), which takes into account the PLL deviation (Δe_θ) while it is estimating the grid frequency (ω_g).

$$\begin{bmatrix} \Delta x_l^q \\ \Delta x_l^d \end{bmatrix} = T_{g-l} \begin{bmatrix} \Delta x_g^q \\ \Delta x_g^d \\ \Delta e_\theta \end{bmatrix}, \quad (7.3)$$

$$T_{g-l} = \begin{bmatrix} \cos(e_{\theta_0}) & -\sin(e_{\theta_0}) & -\sin(e_{\theta_0})x_{0_g}^q - \cos(e_{\theta_0})x_{0_g}^d \\ \sin(e_{\theta_0}) & \cos(e_{\theta_0}) & \cos(e_{\theta_0})x_{0_g}^q - \sin(e_{\theta_0})x_{0_g}^d \end{bmatrix}, \quad (7.4)$$

$$\Delta e_\theta = (\Delta \omega_{PLL}(s) - \Delta \omega_g), \quad (7.5)$$

where T_{g-l} is the transformation matrix, Δx_l^q and Δx_l^d are the state transformed variables in the local frame, Δx_g^q and Δx_g^d are the state variables in the global frame, e_{θ_0} is the angle difference in the steady-state operation point between the global and the local frame and $x_{0_g}^q$ and $x_{0_g}^d$ are the variables to be transformed at the operation point expressed in the global frame. The outputs have to be transformed from the local frame to the global frame using (7.7), as:

$$\begin{bmatrix} \Delta x_g^q \\ \Delta x_g^d \end{bmatrix} = T_{l-g} \begin{bmatrix} \Delta x_l^q \\ \Delta x_l^d \\ \Delta e_\theta \end{bmatrix}, \quad (7.6)$$

$$T_{l-g} = \begin{bmatrix} \cos(e_{\theta_0}) & \sin(e_{\theta_0}) & -\sin(e_{\theta_0})x_{0_l}^q + \cos(e_{\theta_0})x_{0_l}^d \\ -\sin(e_{\theta_0}) & \cos(e_{\theta_0}) & -\cos(e_{\theta_0})x_{0_l}^q - \sin(e_{\theta_0})x_{0_l}^d \end{bmatrix}, \quad (7.7)$$

where $x_{0_l}^q$ and $x_{0_l}^d$ are the variables to be transformed and expressed in the local frame at the steady-state linearization point.

Phase-Locked Loop

The PLL controller representation in state-space form is included next.

- State vector: $\Delta x(t) = [\Delta x_{pll}]$
- Input vector: $\Delta u(t) = [\Delta v_{g,c}^d]$
- Output vector: $\Delta y(t) = [\Delta \omega_{IPC}]$

$$A = [0]; B = [1]; C = [-k_i^{PLL}]; D = [-k_p^{PLL}], \quad (7.8)$$

where $v_{g,c}^d$ is the *d* component of the grid voltage seen by the converter, ω_{IPC} is the PLL's estimated frequency. The proportional and integral PLL parameters are k_p^{PLL} and k_i^{PLL} . Note that all variables used in this block refer to the converter angle ($v_{g,c}^d$).

Converter angle difference

From the obtained ω_c frequency and the reference frequency ω_{grid} , the angle difference used to apply the reference change between global and local variables can be represented in state-space form as:

- State vector: $\Delta x(t) = [\Delta\theta_e]$
- Input vector: $\Delta u(t) = [\Delta\omega_c, \Delta\omega_{grid}]^T$
- Output vector: $\Delta y(t) = [\Delta\theta_e]$

$$A = [0]; B = [1 \quad -1]; C = [1]; D = [0_{1 \times 2}], \quad (7.9)$$

where $\Delta\omega_c$ is the frequency estimated by the PLL, $\Delta\omega_{grid}$ is the AC grid reference frequency, and θ_e is the difference angle between the grid reference and the converter.

Grid current control

The state-space representation of this controller can be represented as:

- State vector: $\Delta x(t) = [\Delta x_q, \Delta x_d]^T$
- Input vector: $\Delta u(t) = [\Delta i_s^{q*}, \Delta i_s^{d*}, \Delta i_s^{q,c}, \Delta i_s^{d,c}]^T$
- Output vector: $\Delta y(t) = [\Delta v_{diff}^{q,c}, \Delta v_{diff}^{d,c}]^T$

$$A = [0_{2 \times 2}]; B = \begin{bmatrix} 1 & 0 & -1 & 0 & 0 & 0 \\ 0 & 1 & 0 & -1 & 0 & 0 \end{bmatrix};$$

$$C = \begin{bmatrix} k_{i-i_s} & 0 \\ 0 & k_{i-i_s} \end{bmatrix}; D = \begin{bmatrix} k_{p-i_s} & 0 & -k_{p-i_s} & \omega_0 L_{eq} & 1 & 0 \\ 0 & k_{p-i_s} & -\omega_0 L_{eq} & -k_{p-i_s} & 0 & 1 \end{bmatrix} \quad (7.10)$$

where $i_s^{q,d*}$ are the current references, $i_s^{q,d,c}$ are the *diff* circuit currents expressed in the converter local frame and, $v_{diff}^{q,d,c}$ are the voltages applied at the AC circuit in the converter local frame. The proportional and integral control parameters are k_{p-i_s} and k_{i-i_s} , ω_0 is the nominal grid frequency, and L_{eq} is the equivalent inductance of the AC circuit.

7.6 Initial Results

The previously discussed controls and models have been implemented in the case study shown in Figure 7.9. The main converter control selected for these initial results is the dual-port control depicted in Figure 7.5. The PV system is modelled as a current source where the injected current depends on the DC voltage. The Geyser storage is modelled as a supercap that includes an average DC/DC converter model controlling the supercap's voltage level. The pump system is modelled as a voltage source converter imposing a voltage and frequency and a controlled load as depicted in Figure 7.8.

The PV system power is 275 kW, the pump system power is 160 kW, and the Geyser storage is considered to give 100 kW for 1 minute. Thus, the supercap is dimensioned to 18,75 F. The main converter power is 320 kVA, and it is connected at 400 V. The connection to the main grid is done via a transformer

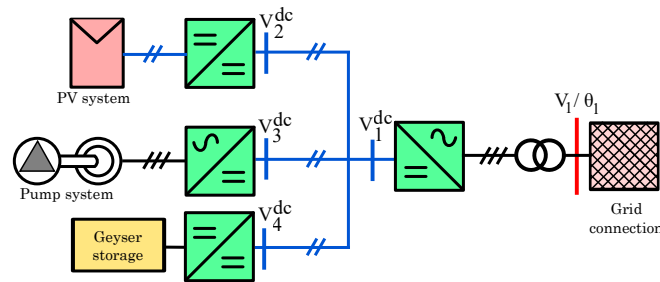


Figure 7.9 – Initial case study scheme.

Table 7.1 – Main converter parameters.

Parameter	Symbol	Value	Units
Resistance filter	R	0,01	pu
Impedance filter	X	0,1	pu
DC side condenser	C	1e-3	F
Current control proportional gain	k_p^c	0,16	V/A
Current control integral gain	k_i^c	5	V/A
Voltage control integral gain	k_i^v	2	A/V
Voltage control proportional gain	k_p^v	3	A/V
Synchronization integral gain	k_i^{dp}	0,1	rad/(V·s)
Synchronization proportional gain	k_p^{dp}	1	rad/V

that elevates the voltage from 400 V to 25 kV. The grid's SCR is considered to be 2. Thus, emulating a relatively weak grid. The DC voltage level of the DC grid is 800 V. The main converter's parameters are given in Table 7.1

7.6.1 Power flow solution

The case study presented considers the following scenario. The PV system injects full power to the DC grid, i.e., is injecting 275 kW, and the pump system is working at full power, i.e., absorbing 160 kW from the DC grid. The power flow is solved considering the main converter injects 0 var to the AC grid. The solution to the power flow is solved as explained in Section 7.5.1 and the results are given in Table 7.2. From the solution of the power flow, it can be seen that the scenario considered is well defined, as all voltages are set at a reasonable level. Moreover, it can be concluded that the algorithm to solve the power flow is well designed. The solution is reached in 3 iterations.

Table 7.2 – Power flow solution.

Parameter	Value	Units
V_1	401,96	V
θ_1	6,42	degree
P_{VSC}	112,63	kW
Q_{VSC}	0	kvar
V_1^{dc}	800	V
V_2^{dc}	799,79	V
V_3^{dc}	800,34	V
V_4^{dc}	800	V

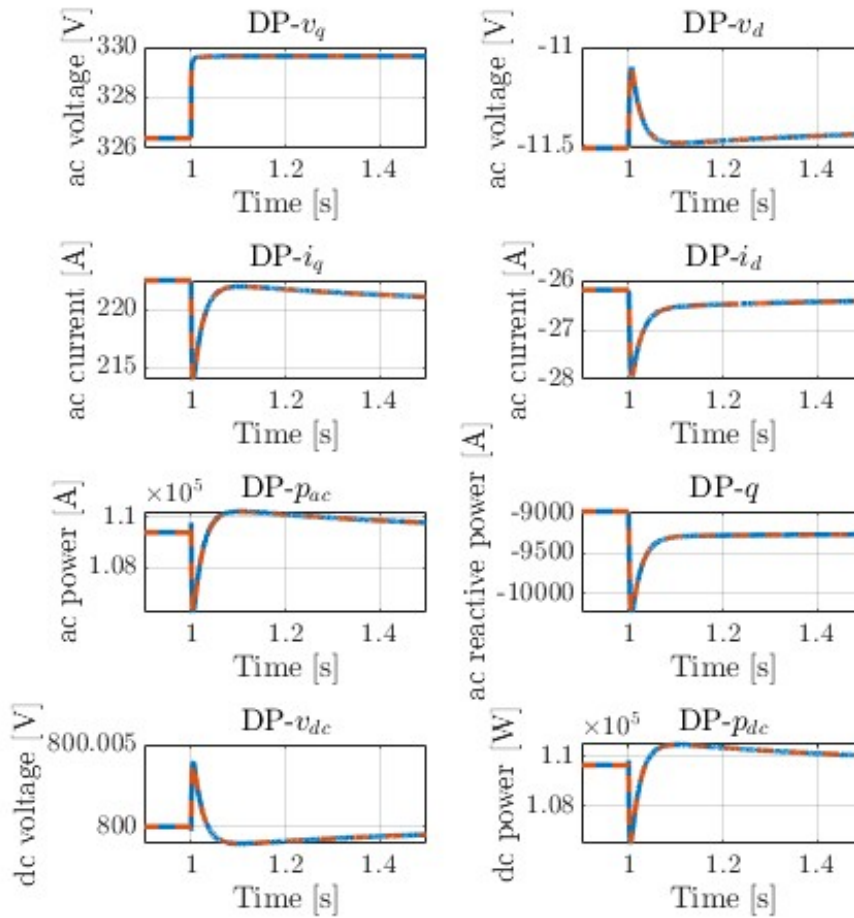


Figure 7.10 – Linear and non-linear models comparison.

7.6.2 Small-Signal analysis

The linear model of the case study is computed. The linear model will give important information about the system stability and control performance. Firstly, to ensure the linear model's validity, the linear model is compared with the non-linear model when a small perturbation is made. In this case, a 1% voltage change in the connection to the main grid is simulated. The comparison is shown in Figure 7.10.

Next, the system's eigenvalues are computed. These are shown in Tab. 7.3. All eigenvalues have a negative real part; therefore, the system is stable. Moreover, all the eigenvalues have a damping higher than 5 %, which indicates that, in general, the system dynamics will respond appropriately.

7.6.3 PV step change

The system is checked when a sudden step change in the generated power in the PV system occurs. This can emulate a loss of generations due to an unexpected cloud that covers the PV panels. The generated power is changed from full (275 kW) to 0 kW.

The main converter terminals' active and reactive powers magnitudes are shown in Figure 7.11. The converter can adjust the new operation point by adjusting the amount of active and reactive power delivered to the grid. As shown, at the initial point, the converter injects approximately 100 kW, while after the disturbance, it absorbs around 200 kW.

Table 7.3 – System's eigenvalues.

Mode	Real	Imaginary	Frequency	Damping
1	-0,46869	0,00000	0,00000	1,00000
2	-0,83100	0,32278	0,05137	0,93215
3	-0,83100	-0,32278	0,05137	0,93215
4	-31,41382	0,00000	0,00000	1,00000
5	-31,42476	0,00000	0,00000	1,00000
6	-134,31950	0,00000	0,00000	1,00000
7	-354,46777	61,57802	9,80045	0,98524
8	-354,46777	-61,57802	9,80045	0,98524
9	-59530,25556	113,97892	18,14031	1,00000
10	-59530,25556	-113,97892	18,14031	1,00000
11	-99844,61077	0,00000	0,00000	1,00000
12	-100000,00000	0,00000	0,00000	1,00000
13	-100000,00000	0,00000	0,00000	1,00000
14	-382254,59558	0,00000	0,00000	1,00000
15	-2618246,03318	0,00000	0,00000	1,00000
16	-8286806,34355	315,00067	50,13391	1,00000
17	-8286806,34355	-315,00067	50,13391	1,00000

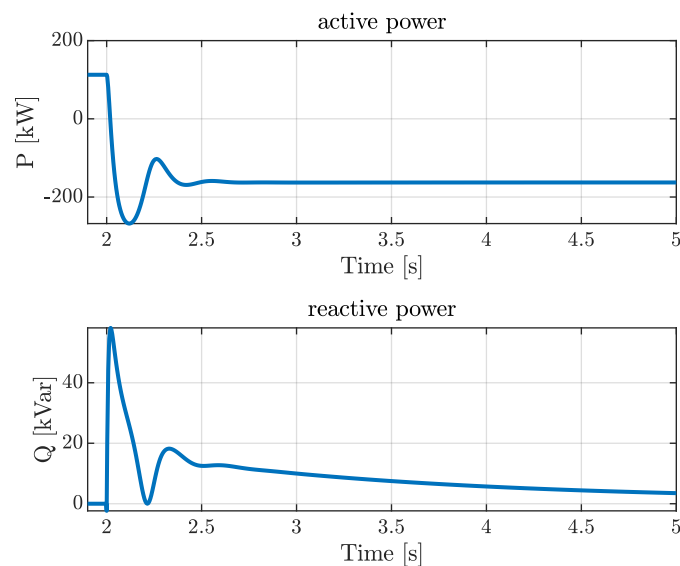


Figure 7.11 – Main converter active and reactive power.

The change in the active power direction is done without affecting the DC voltage grid's stability, as shown in Figure 7.12. The DC voltage can be kept at 800 V. Moreover, the synchronization with the AC grid is also kept stable as shown by the angle difference between the converter and the grid in Figure 7.12.

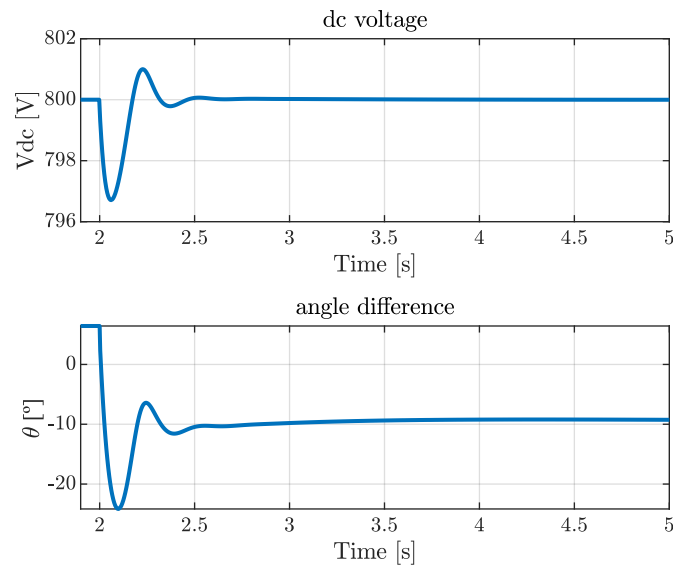


Figure 7.12 – Main converter dc voltage and angle.

7.6.4 Grid angle step change

A general simulation in different tests for grid-forming capabilities is an angle step change on the grid's voltage [152]. This test is performed in Figure 7.14 and Figure 7.13.

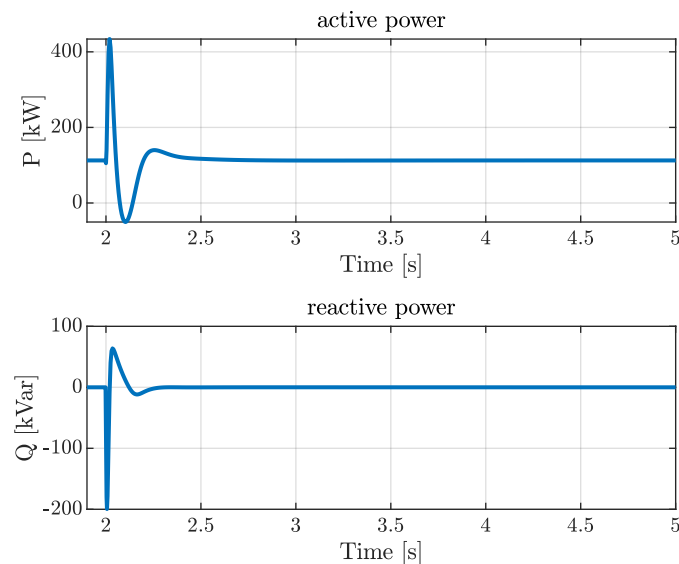


Figure 7.13 – Main converter active and reactive power.

As shown in Figure 7.14, the angle difference between the grid and the converter is changed to -30° . The converter can continue its operation while properly controlling the DC bus voltage. As seen in Figure 7.13, the angle change produces a transitory deviation on the active and reactive power injected by the converter. Still, after this transient, the converter can control these two magnitudes properly.

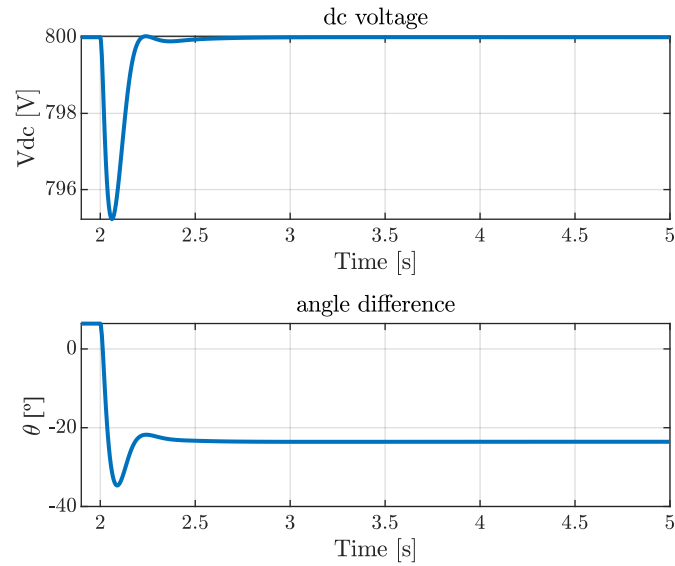


Figure 7.14 – Main converter voltage and current magnitudes.

7.7 Future work

The initial case study showcases that the tested control algorithm properly integrates the DC system with the AC grid. However, other tests might be done to increase further the potential benefits of using the dual-port approach. Especially relevant tests are enumerated next,

1. AC faults.
2. DC faults.
3. Black-start capability.
4. Operation in islanded mode.

Moreover, the initial case study considers only limited elements on the AC side. To properly ensure the viability of implementing these controllers, the integration of the DC system should consider an expanded AC grid. This should include the nearby elements next to these installations, including nearby PV and wind plants, and local consumption. These tests should be evaluated to determine if incorporating this facility into the existing grid might trigger new interactions and how these possible interactions might spread over the DC and AC systems.

Bibliography

- [1] Subsecretaría de agricultura, pesca y alimentación. Encuesta sobre superficies y rendimientos de cultivos. año 2023. Technical report, Ministerio de Agricultura, Pesca y Alimentación, 2023.
- [2] Pesca i Alimentació Departament d'Agricultura, Ramaderia. Mapa de cultius dun-sigpac. <https://agricultura.gencat.cat/ca/ambits/desenvolupament-rural/sigpac/mapa-cultius/>, 2025.
- [3] Ignasi Grau Roca. Text refós del Pla de regadius de Catalunya 2008-2020 (Clau E1-VR-07943.A), 02 2012. Available online: https://agricultura.gencat.cat/ca/ambits/desenvolupament-rural/infraestructures-agraries/dar_regadius/dar_pla_regadius_2008_2020 (accessed on 11/10/2024).
- [4] Real Decreto 329/2002, de 5 de abril, por el que se aprueba el Plan Nacional de Regadíos. Boletín Oficial del Estado, 101, de 27 de abril de 2002, April 2002. Available online: <https://www.boe.es/buscar/doc.php?id=BOE-A-2002-8129>.
- [5] Instituto Nacional de Estadística. Encuesta sobre el uso del agua en el sector agrario. serie 2000-2018. <https://www.ine.es/dynt3/inebase/index.htm?path=/t26/p067/p03/serie>, 2018.
- [6] Andrés del Campo. Transversalidad del agua en otras políticas y sectores: Innovación y avances tecnológicos en materia de regadíos, October 2019.
- [7] RTVE. Cafè d'idees 08/01/2025 Òscar ordeig, josé antonio ponseti i judit marín. Emitted 08 jan 2025, retrieved from <https://www.rtve.es/play/videos/cafe-didees/oscar-ordeig-jose-antonio-ponseti-judit-martin/16398282/>, minute 28:50, January 2025.
- [8] Departament d'Agricultura, Ramaderia, Pesca i Alimentació. Xarxes de regadius de Catalunya, 3 2019.
- [9] Agència Catalana de l'Aigua. Registre de seguretat de preses i embassaments de Catalunya, 2024.
- [10] Confederación Hidrográfica del Ebro. Geodatos, 2024.
- [11] Generalitat de Catalunya. Regadius de Catalunya, 2014. Archived at <https://web.archive.org/web/20141019032941/http://www.regadius.cat/actuacions/regadius/> (Wayback Machine).
- [12] Infraestructures de la Generalitat de Catalunya, SAU. Projecte constructiu de nova captació al Regadiu de la Comunitat General de Regants d'Aigües del Riu Montsant, des del Regadiu del Garrigues Sud (Clau: ER-24322), September 2024.

- [13] Carlos Estarán. Projecte de suport fotovoltaic del bombament i obres annexes a la Comunitat de Regants de l'Albi per al reg de recolzament de l'oliver a l'Albi, Pobla de Cèrvoles, Cervià de les Garrigues, el Vilosell i les Borges Blanques (les Garrigues). PC-2023-007., 05 2023. Available online: <https://contractaciopublica.cat/ca/detall-publicacio/058503c0-57a8-4029-833e-ba91c1458cc4/300130905> (accessed on 11/11/2024).
- [14] Carlos Estarán. Projecte d'arranjament de la làmina d'impermeabilització d'un embassament agrícola de regulació i ampliació del suport fotovoltaic del bombeig a la Comunitat de Regants d'Aubarrells toma C-072-0, al TM d'Almenar. (Clau: PC-2023-002). Estarán Enginyeria i Consultoria., 10 2022. Available online: <https://contractaciopublica.cat/ca/detall-publicacio/e0e382ca-7d13-4ae4-b736-895bc7704b25/200166575> (accessed on 11/11/2024).
- [15] Gustau Carrillo. Projecte de modernització del sistema de regadiu de la Comunitat de Regants de la Bassanova - Fase V (TM Almenar). (Clau: PC-2023-006), 11 2023. Available online: <https://contractaciopublica.cat/ca/detall-publicacio/3fe42741-01a2-469e-a095-75d375e05a12/300237907> (accessed on 11/11/2024).
- [16] Josep M. Liébana and Xavier Luján. Instal·lació de planta solar aïllada (513 kWp), a l'estació de bombament de la Comunitat de Regants de Benissanet (Ribera d'Ebre), 07 2023. Available online: <https://contractaciopublica.cat/ca/detall-publicacio/207bdf00-486a-465f-b764-b7a708e394bb/300140892> (accessed on 11/11/2024).
- [17] Carlos Estarán. Projecte de instal·lació fotovoltaica de 313,20 kWp d'autoconsum per una potencia nominal de 270 kW per al bombeig del reg a pressió forçat i obres annexes a la Comunitat de Regants de la partida Fenollet C-77,7 i C-78,4, als termes municipals d'Almenar i Alguaire (Lleida). (Clau: PC-2020-003), 08 2020. Available online: <https://contractaciopublica.cat/ca/detall-publicacio/fed60e50-675d-9766-af9c-0e46a3102a57/84400987> (accessed on 11/11/2024).
- [18] Esteve Niubó and Irene Torra. Projecte del regadiu Garrigues Sud. Etapa IV. TTMM Ulldemolins (Priorat) i Pobla de Cèrvoles (Garrigues) Clau: ER – 11208, January 2015.
- [19] Gabriel Garriga. Projecte constructiu d'una planta fotovoltaica per al bombament de la Comunitat de Regants de Les Planes i Aixal·les (Clau: ER-20214). Garriga Enginyeria, S.L.P., 03 2021. Available online: <https://agricultura.gencat.cat/ca/detalls/Article/Projecte-constructiu-planes> (accessed on 21/12/2023).
- [20] Xavier Guixà and Joan Latorre. Projecte constructiu d'impulsió mitjançant bombament solar, des de la bassa de regulació del sector 8 de SSG, a la bassa de regulació del reg de l'Espluga Calba i Maldà. Clau: VI-16281., 07 2017.
- [21] Joan Creixans and Iolanda Huguet. Projecte de regulació del Segrià Sud. Xarxa de regulació i distribució. Fase 3B (Clau: ER-00942.3B), 07 2017. Available online: <https://infraestructures.gencat.cat/licitacions/download.php?NDQ1MzQ%3D> (accessed on 31/12/2023).
- [22] Germán Mateo Cerdá. Projecte constructiu de l'ampliació del regadiu del Segrià Sud, zones M5 i M5I als TTMM de Flix, Llardecans, Maials i Torrebesses (Ribera d'Ebre i Segrià). (Clau: ER-00942.10), November 2022.
- [23] Manel Lladós. Projecte d'ampliació del regadiu de la comunitat de regants de Vingalis a la Serra del Rovelló (Clau: AG-2019-1168), December 2019.
- [24] Projecte constructiu del regadiu de la Terra Alta. Bombament, impulsió i bassa de regulació 4 (Clau: ER-06908-1), 2011.



- [25] Sergi Costa Dilmé, Carla Cinto Campmany, Pau Garcia Motilla, and Eduardo Prieto Araujo. Potential available energy storage capacity of irrigation reservoirs in Catalunya. V1. <https://doi.org/10.34810/data2189>, 2025.
- [26] O. Schmidt, A. Hawkes, A. Gambhir, and I. Staffell. The future cost of electrical energy storage based on experience rates. *Nature Energy*, 2(8), July 2017.
- [27] Xavier Farreny, Josep M. Liébana, Xavier Luján, and Òscar Trindade. Planta solar de 523 kWp a l'estació de bombament EB2 del regadiu del Segrià Sud (T.M. Seròs - Segrià), 10 2018.
- [28] Miguel Ángel Bofill. Instal·lació de autoconsumo fotovoltaico Segrià Sud 236 kW (274,584 kWp), 04 2022.
- [29] Josep M. Liébana, Xavier Luján, and Òscar Trindade. Instal·lació de planta solar aïllada (527,5 kWp), a l'estació de bombament EB2 del regadiu del Segrià Sud (T.M. Seròs - Segrià), 07 2021. Available online: <https://gencat.cat/agricultura/informacio-publica/pc-2022-002/projecte.pdf> (accessed on 21/12/2023).
- [30] Departament d'Agricultura, Ramaderia, Pesca i Alimentació. Ordre d'estudi - informe previ. projecte constructiu de l'ampliació del regadiu del segrià sud, zones m5 i m5i als tmm de flix, llardecans, maials i torrebesses (ribera d'ebre i segrià). techreport, Generalitat de Catalunya, July 2020.
- [31] Institut Cartogràfic i Geològic de Catalunya. WMS d'Ortofoto Territorial. Institut Cartogràfic i Geològic de Catalunya, July 2024.
- [32] OpenStreetMap contributors. Planet dump retrieved from <https://planet.osm.org>. <https://www.openstreetmap.org>, 2023.
- [33] Departament d'Acció Climàtica, Alimentació i Agenda Rural. Visita a la nova planta fotovoltaica per al bombament de la Comunitat de Regants de les Planes i Aixal·lles. Agenda del Govern, 03 2023. Available online: <https://govern.cat/salaprensa/agenda-govern/438193/visita-a-nova-planta-fotovoltaica-al-bombament-comunitat-regants-planes-aixal·lles> (accessed on 28/12/2023).
- [34] Antonio Gironès. Estat de dimensions i característiques de l'obra executada del projecte modificat 1 i complementari 1 i 2 de millora del reg de Les Planes i Aixal·lles. T.M. Flix i Ascó. (Claus: ER-01962-M1-OE, ER-01962-C1-OE, ER-01962-C2-OE). CIG Enginyeria., 2005.
- [35] Josep M. Liébana, Xavier Luján, and Òscar Trindade. Instal·lació planta solar aïllada (601,88 kWp) a l'estació de bombament EB1 del regadiu del Garrigues Sud. TM Flix (Ribera d'Ebre) (Clau: PC-2021-005), 09 2021. Available online: https://contrataciondelestado.es/wps/poc?uri=deepLink%3Adetalle_licitacion&idEvl=mPlp5jA05QJrhB1EHQFSKA%3D%3D (accessed on 21/12/2023).
- [36] Josep M. Liébana, Xavier Luján, and Òscar Trindade. Instal·lació planta solar aïllada (462,24 kWp) a l'estació de bombament EB2 del regadiu del Garrigues Sud. (T.M. Bovera - Garrigues), May 2021.
- [37] G. Belaud, L. Mateos, R. Aliod, M.-C. Buisson, E. Faci, S. Gendre, G. Ghinassi, R. Gonzales Perea, C. Lejars, F. Maruejols, and N. Zapata. Irrigation and energy: Issues and challenges. *Irrigation and Drainage*, 69(S1):177–185, April 2019.
- [38] Federico Milano, Florian Dörfler, Gabriela Hug, David J. Hill, and Gregor Verbič. Foundations and challenges of low-inertia systems (invited paper). In *2018 Power Systems Computation Conference (PSCC)*, pages 1–25, 2018.
- [39] Raj Kumar Pan, Kimmo Kaski, and Santo Fortunato. World citation and collaboration networks: uncovering the role of geography in science. *Scientific Reports*, 2(1), November 2012.



- [40] S.P. Adhau, R.M. Moharil, and P.G. Adhau. Mini-hydro power generation on existing irrigation projects: Case study of indian sites. *Renewable and Sustainable Energy Reviews*, 16(7):4785–4795, September 2012.
- [41] Alessandro Morabito and Patrick Hendrick. Pump as turbine applied to micro energy storage and smart water grids: A case study. *Applied Energy*, 241:567–579, May 2019.
- [42] Navid Mousavi, Ganesh Kothapalli, Daryoush Habibi, Choton K. Das, and Ali Baniyasi. A novel photovoltaic-pumped hydro storage microgrid applicable to rural areas. *Applied Energy*, 262:114284, March 2020.
- [43] Navid Mousavi, Ganesh Kothapalli, Daryoush Habibi, Mehdi Khiadani, and Choton K. Das. An improved mathematical model for a pumped hydro storage system considering electrical, mechanical, and hydraulic losses. *Applied Energy*, 247:228–236, August 2019.
- [44] Nicholas Gilmore, Thomas Britz, Erik Maartensson, Carlo Orbegoso-Jordan, Sebastian Schroder, and Martino Malerba. Continental-scale assessment of micro-pumped hydro energy storage using agricultural reservoirs. *Applied Energy*, 349:121715, November 2023.
- [45] Sergi Costa-Dilmé, J. Carlos Olives-Camps, Paula Muñoz-Peña, Pau García-Motilla, Oriol Gomis-Bellmunt, and Eduardo Prieto-Araujo. Redesign of large-scale irrigation systems for flexible energy storage. In *2024 IEEE PES Innovative Smart Grid Technologies Europe (ISGT EUROPE)*, pages 1–5. IEEE, October 2024.
- [46] Li Wang, Dong-Jing Lee, Jian-Hong Liu, Zan-Zia Chen, Zone-Yuan Kuo, Jin-Shi Hsu, Cheng-Mei Chen, Shen-Syi Chiu, Ming-Hua Tsai, Wei-Taw Lin, and Yun-Chung Lee. Economic analysis of installing micro hydro power plants in chia-nan irrigation association of taiwan using water of irrigation canals. In *2008 IEEE Power and Energy Society General Meeting - Conversion and Delivery of Electrical Energy in the 21st Century*, pages 1–5. IEEE, July 2008.
- [47] Li Wang, Dong-Jing Lee, Jian-Hong Liu, Zan-Zia Chen, Zone-Yuan Kuo, Huei-Yuan Jang, Jiunn-Ji You, Jin-Tsang Tsai, Ming-Hua Tsai, Wey-Tau Lin, and Yeun-Jong Lee. Installation and practical operation of the first micro hydro power system in taiwan using irrigation water in an agriculture canal. In *2008 IEEE Power and Energy Society General Meeting - Conversion and Delivery of Electrical Energy in the 21st Century*, pages 1–6. IEEE, July 2008.
- [48] Ilaria Butera and Roberto Balestra. Estimation of the hydropower potential of irrigation networks. *Renewable and Sustainable Energy Reviews*, 48:140–151, August 2015.
- [49] François Prevost and G Guichard. Réalisation et exploitation d'une microcentrale: modalités d'un partenariat durable entre l'asco des irrigants de la crau et la société du canal de provence. In *ICID Conference, Special Session 'Irrigation and Energy', Montpellier, France, 2015*.
- [50] Demetrio Antonio Zema, Angelo Nicotra, Vincenzo Tamburino, and Santo Marcello Zimbone. A simple method to evaluate the technical and economic feasibility of micro hydro power plants in existing irrigation systems. *Renewable Energy*, 85:498–506, January 2016.
- [51] Tommaso Brazzini, Edgar Lorenzo-Saez, Vicent Sales Martínez, Esther López Pérez, Mar V. Ortega-Reig, and Guillermo Palau-Salvador. Is small-scale hydropower energy recovery a viable alternative for climate change mitigation and adaptation? the case of the traditional irrigation system in valencia (spain). *Energy Reports*, 12:736–749, December 2024.
- [52] Miguel Crespo Chacón, Juan Antonio Rodríguez Díaz, Jorge García Morillo, and Aonghus McNabola. Hydropower energy recovery in irrigation networks: Validation of a methodology for flow prediction and pump as turbine selection. *Renewable Energy*, 147:1728–1738, March 2020.



- [53] Miguel Crespo Chacón, Juan Antonio Rodríguez Díaz, Jorge García Morillo, and Aonghus McNabola. Estimating regional potential for micro-hydropower energy recovery in irrigation networks on a large geographical scale. *Renewable Energy*, 155:396–406, August 2020.
- [54] Santoshkumar M. Hunachal, G. Arunkumar, Sushil Sirsat, P. R. Shankar, Rajat Shirgaonkar, and Bhushan Khandzode. Irrigation water as a renewable energy source in pico hydropower generation. In *2020 International Conference on Renewable Energy Integration into Smart Grids: A Multidisciplinary Approach to Technology Modelling and Simulation (ICREISG)*, pages 27–31. IEEE, February 2020.
- [55] A. Merida García, J. Gallagher, M. Crespo Chacón, and A. Mc Nabola. The environmental and economic benefits of a hybrid hydropower energy recovery and solar energy system (pat-pv), under varying energy demands in the agricultural sector. *Journal of Cleaner Production*, 303:127078, June 2021.
- [56] Angel V. Mercedes Garcia, Francisco Javier Sánchez-Romero, P. Amparo López-Jiménez, and Modesto Pérez-Sánchez. A new optimization approach for the use of hybrid renewable systems in the search of the zero net energy consumption in water irrigation systems. *Renewable Energy*, 195:853–871, August 2022.
- [57] William E. Hart, Jean-Paul Watson, and David L. Woodruff. Pyomo: modeling and solving mathematical programs in python. *Mathematical Programming Computation*, 3(3):219–260, August 2011.
- [58] Zev Friedman, Jack Ingalls, John D. Siirola, and Jean-Paul Watson. Block-oriented modeling of superstructure optimization problems. *Computers & Chemical Engineering*, 57:10–23, October 2013.
- [59] Jorge Nocedal and Stephen J. Wright. *Numerical optimization*, pages 1–664. Springer Series in Operations Research and Financial Engineering. Springer Nature, 2006.
- [60] Sergi Costa-Dilmé, J. Carlos Olives-Camps, Paula Muñoz-Peña, Pau García-Motilla, Oriol Gomis-Bellmunt, and Eduardo Prieto-Araujo. Multi-physics operation and sizing optimisation in pyomo: Application to large irrigation systems. In *2024 Open Source Modelling and Simulation of Energy Systems (OSMSES)*, pages 1–6. IEEE, September 2024.
- [61] Dariush Fooladivanda and Joshua A. Taylor. Energy-optimal pump scheduling and water flow. *IEEE Transactions on Control of Network Systems*, 5(3):1016–1026, September 2018.
- [62] Michael L. Bynum, Gabriel A. Hackebeil, William E. Hart, Carl D. Laird, Bethany L. Nicholson, John D. Siirola, Jean-Paul Watson, and David L. Woodruff. *Pyomo—optimization modeling in python*, volume 67. Springer Science & Business Media, third edition, 2021.
- [63] The MathWorks Inc. Statistics and machine learning toolbox, 2023.
- [64] Pauli Virtanen, Ralf Gommers, Travis E. Oliphant, Matt Haberland, Tyler Reddy, David Cournapeau, Evgeni Burovski, Pearu Peterson, Warren Weckesser, Jonathan Bright, Stéfan J. van der Walt, Matthew Brett, Joshua Wilson, K. Jarrod Millman, Nikolay Mayorov, Andrew R.J. Nelson, Eric Jones, Robert Kern, Eric Larson, C J Carey, İlhan Polat, Yu Feng, Eric W. Moore, Jake VanderPlas, Denis Laxalde, Josef Perktold, Robert Cimrman, Ian Henriksen, E. A. Quintero, Charles R. Harris, Anne M. Archibald, Antônio H. Ribeiro, Fabian Pedregosa, Paul van Mulbregt, and SciPy 1.0 Contributors. SciPy 1.0: Fundamental Algorithms for Scientific Computing in Python. *Nature Methods*, 17:261–272, 2020.
- [65] Ahmed S. Zamzam, Emiliano Dall’Anese, Changhong Zhao, Josh A. Taylor, and Nicholas D. Sidiropoulos. Optimal water–power flow-problem: Formulation and distributed optimal solution. *IEEE Transactions on Control of Network Systems*, 6(1):37–47, March 2019.



- [66] Juan I. Pérez, José R. Wilhelmi, and Luis Maroto. Adjustable speed operation of a hydropower plant associated to an irrigation reservoir. *Energy Conversion and Management*, 49(11):2973–2978, November 2008.
- [67] H. Ramos and A. Borga. Pumps as turbines: an unconventional solution to energy production. *Urban Water*, 1(3):261–263, September 1999.
- [68] Maxime Binama, Wen-Tao Su, Xiao-Bin Li, Feng-Chen Li, Xian-Zhu Wei, and Shi An. Investigation on pump as turbine (pat) technical aspects for micro hydropower schemes: A state-of-the-art review. *Renewable and Sustainable Energy Reviews*, 79:148–179, November 2017.
- [69] Omprakash K. Gupta and A. Ravindran. Branch and bound experiments in convex nonlinear integer programming. *Management Science*, 31(12):1533–1546, 1985.
- [70] Pierre Bonami, Lorenz T. Biegler, Andrew R. Conn, Gérard Cornuéjols, Ignacio E. Grossmann, Carl D. Laird, Jon Lee, Andrea Lodi, François Margot, Nicolas Sawaya, and Andreas Wächter. An algorithmic framework for convex mixed integer nonlinear programs. *Discrete Optimization*, 5(2):186–204, 2008. In Memory of George B. Dantzig.
- [71] Roger Fletcher and Sven Leyffer. Solving mixed integer nonlinear programs by outer approximation. *Mathematical Programming*, 66:327–349, August 1994.
- [72] I. Quesada and I.E. Grossmann. An LP/NLP based branch and bound algorithm for convex MINLP optimization problems. *Computers & Chemical Engineering*, 16(10):937–947, 1992. An International Journal of Computer Applications in Chemical Engineering.
- [73] Kumar Abhishek, Sven Leyffer, and Jeff Linderoth. FilMINT: An Outer Approximation-Based Solver for Convex Mixed-Integer Nonlinear Programs. *INFORMS Journal on Computing*, 22(4):555–567, 2010.
- [74] Francisco Díaz-González, Andreas Sumper, and Oriol Gomis-Bellmunt. *Energy Storage in Power Systems*. Wiley, March 2016.
- [75] R. Lougee-Heimer. The common optimization interface for operations research: Promoting open-source software in the operations research community. *IBM Journal of Research and Development*, 47(1):57–66, January 2003.
- [76] Sergi Costa-Dilmé, J. Carlos Olives-Camps, Pau García-Motilla, Carla Cinto Campmany, Oriol Gomis-Bellmunt, and Eduardo Prieto-Araujo. Redesign of large-scale irrigation systems for flexible energy storage. unpublished, 2025.
- [77] REE. Reedata, 2025. <https://www.ree.es/es/datos/aldia>.
- [78] Ted G. Eschenbach. Spiderplots versus tornado diagrams for sensitivity analysis. *Interfaces*, 22(6):40–46, December 1992.
- [79] Sergi Costa-Dilmé, Pau García-Motilla, Oriol Gomis-Bellmunt, and Eduardo Prieto-Araujo. Energy storage sizing for clouds shading over solar photovoltaic pumping systems. unpublished, 2025.
- [80] Giuseppe Todde, Lelia Murgia, Paola Antonia Deligios, Rita Hogan, Isaac Carrelo, Madalena Moreira, Antonio Pazzona, Luigi Ledda, and Luis Narvarte. Energy and environmental performances of hybrid photovoltaic irrigation systems in Mediterranean intensive and super-intensive olive orchards. *Science of The Total Environment*, 651:2514–2523, February 2019.
- [81] Ramazan Senol. An analysis of solar energy and irrigation systems in turkey. *Energy Policy*, 47:478–486, August 2012.
- [82] P.C. Pande, A.K. Singh, S. Ansari, S.K. Vyas, and B.K. Dave. Design development and testing of a solar PV pump based drip system for orchards. *Renewable Energy*, 28(3):385–396, March 2003.



- [83] Ali A. Hamza and Azmi Z. Taha. Performance of submersible pv solar pumping systems under conditions in the sudan. *Renewable Energy*, 6(5–6):491–495, July 1995.
- [84] Olga V. Shepovalova, Alexander T. Belenov, and Sergei V. Chirkov. Review of photovoltaic water pumping system research. *Energy Reports*, 6:306–324, November 2020.
- [85] Olga V. Shepovalova and Alexander T. Belenov. Investigation of dc motors mechanical characteristics with powered by comparable capacity pv array. *Energy Procedia*, 119:990–994, July 2017.
- [86] Z.Abidin Firatoglu and Bulent Yesilata. New approaches on the optimization of directly coupled pv pumping systems. *Solar Energy*, 77(1):81–93, 2004.
- [87] Daniele Fiaschi, Roberto Graniglia, and Giampaolo Manfrida. Improving the effectiveness of solar pumping systems by using modular centrifugal pumps with variable rotational speed. *Solar Energy*, 79(3):234–244, September 2005.
- [88] R.H. Almeida, J.R. Ledesma, I.B. Carrêlo, L. Narvarte, G. Ferrara, and L. Antipodi. A new pump selection method for large-power pv irrigation systems at a variable frequency. *Energy Conversion and Management*, 174:874–885, October 2018.
- [89] Hicham Karmouni, Mohamed Chouiekh, Saad Motahhir, Hassan Qjidaa, Mohamed Ouazzani Jamil, and Mhamed Sayyouri. Optimization and implementation of a photovoltaic pumping system using the sine–cosine algorithm. *Engineering Applications of Artificial Intelligence*, 114:105104, September 2022.
- [90] Wissem Nemouchi, Youssef Amrane, Hichem Nemouchi, and Najib Lakhdar Boucetta. Energy management for optimal design of pv/wind/diesel system for water pumping irrigation in semi-arid climate. *Energy Conversion and Management*, 304:118216, March 2024.
- [91] Victor L Streeter, E Benjamin Wylie, and Keith W Bedford. *Fluid mechanics*. Mc Graw Hill Education, Dec 1997.
- [92] E Benjamin Wylie and Victor Lyle Streeter. *Fluid transients*. Mc Graw Hill Inc., 1978.
- [93] Andrew F. Colombo and Bryan W. Karney. Energy and costs of leaky pipes: Toward comprehensive picture. *Journal of Water Resources Planning and Management*, 128(6):441–450, November 2002.
- [94] Jalil Emadi and Abbas Solemani. Maximum water hammer sensitivity analysis. *World Acad. Sci. Eng. Technol*, 73:416–419, 2011.
- [95] Josh A. Taylor, Richard Perryman, Aimy Bazylak, and Bryan Karney. Safely landing water networks during power outages with energy storage. In *2018 56th Annual Allerton Conference on Communication, Control, and Computing (Allerton)*, pages 346–350. IEEE, October 2018.
- [96] Madhumita Das and Ratan Mandal. A comparative performance analysis of direct, with battery, supercapacitor, and battery-supercapacitor enabled photovoltaic water pumping systems using centrifugal pump. *Solar Energy*, 171:302–309, September 2018.
- [97] S. Orts-Grau, P. Gonzalez-Altozano, Francisco J. Gimeno-Sales, I. Balbastre-Peralta, C. I. Martinez Marquez, M. Gasque, and S. Segui-Chilet. Photovoltaic water pumping: Comparison between direct and lithium battery solutions. *IEEE Access*, 9:101147–101163, 2021.
- [98] Tehuan Chen, Zhigang Ren, Chao Xu, and Ryan Loxton. Optimal boundary control for water hammer suppression in fluid transmission pipelines. *Computers & Mathematics with Applications*, 69(4):275–290, February 2015.

- [99] J. K. Roy, P. K. Roy, and P. Basak. Water hammer protection in water supply system: A new approach with practical implementation. In *2011 International Conference on Communication and Industrial Application*, pages 1–6. IEEE, December 2011.
- [100] Packiam Periasamy, N.K. Jain, and I.P. Singh. A review on development of photovoltaic water pumping system. *Renewable and Sustainable Energy Reviews*, 43:918–925, March 2015.
- [101] A. Mohammedi, N. Mezzai, D. Rekioua, and T. Rekioua. Impact of shadow on the performances of a domestic photovoltaic pumping system incorporating an mppt control: A case study in bejaia, north algeria. *Energy Conversion and Management*, 84:20–29, August 2014.
- [102] L. Narvarte, J. Fernández-Ramos, F. Martínez-Moreno, L.M. Carrasco, R.H. Almeida, and I.B. Carrêlo. Solutions for adapting photovoltaics to large power irrigation systems for agriculture. *Sustainable Energy Technologies and Assessments*, 29:119–130, October 2018.
- [103] Universidad Politécnica de Madrid. MASLOWATEN. Especificaciones Técnicas para Sistemas de Riego Fotovoltaico, 2018. Available online: <https://maslowaten.eu> (accessed on 30/01/2024).
- [104] Anton Bergant, Jernej Mazij, and Uroš Karadžić. Design of water hammer control strategies in hydropower plants. *Applied Engineering Letters: Journal of Engineering and Applied Sciences*, 3(1):27–33, 2018.
- [105] G. Remenieras. Dispositif simple pour réduire la célérité des ondes Élastiques dans les conduites en charge. *La Houille Blanche*, 38(sup1):172–196, January 1952.
- [106] Jinzhe Gong, Mark L. Stephens, Martin F. Lambert, Aaron C. Zecchin, and Angus R. Simpson. Pressure surge suppression using a metallic-plastic-metallic pipe configuration. *Journal of Hydraulic Engineering*, 144(6), June 2018.
- [107] Michał Kubrak. Water hammer mitigation by internal rubber hose. *Archives of Civil Engineering*, pages 275–288, March 2024.
- [108] OMIE: Operador del Mercado Ibérico de Energía - Polo Español. OMIEData Resultados del Mercado. www.omie.es/es, 2024.
- [109] Banco de España. Series: Statistical Bulletin. <https://www.bde.es/wbe/en/publicaciones/informacion-estadistica/boletin-estadistico/>, 2024.
- [110] QGIS Development Team. *QGIS Geographic Information System*. QGIS Association,
- [111] Chad Augustine and Nathan Blair. *Storage Futures Study: Storage Technology Modeling Input Data Report*. NREL, May 2021.
- [112] Benjamin A. Carreras, Eder Batista Tchawou Tchuisseu, José M. Reynolds-Barredo, Damià Gomila, and Pere Colet. Effects of demand control on the complex dynamics of electric power system blackouts. *Chaos: An Interdisciplinary Journal of Nonlinear Science*, 30(11), November 2020.
- [113] Javier Martín Vide. *El Clima i el relleu. Geografia General dels Països Catalans*. Enciclopèdia Catalana, Barcelona, 1992.
- [114] Haisheng Chen, Thang Ngoc Cong, Wei Yang, Chunqing Tan, Yongliang Li, and Yulong Ding. Progress in electrical energy storage system: A critical review. *Progress in Natural Science*, 19(3):291–312, March 2009.
- [115] Behnam Zakeri and Sanna Syri. Electrical energy storage systems: A comparative life cycle cost analysis. *Renewable and Sustainable Energy Reviews*, 42:569–596, February 2015.
- [116] Md Mustafizur Rahman, Abayomi Olufemi Oni, Eskinder Gemechu, and Amit Kumar. Assessment of energy storage technologies: A review. *Energy Conversion and Management*, 223:113295, November 2020.



- [117] Choton K. Das, Octavian Bass, Ganesh Kothapalli, Thair S. Mahmoud, and Daryoush Habibi. Overview of energy storage systems in distribution networks: Placement, sizing, operation, and power quality. *Renewable and Sustainable Energy Reviews*, 91:1205–1230, August 2018.
- [118] Ernest Moa and Yun Go. Large-scale energy storage system: safety and risk assessment. *Sustainable Energy Research*, 10, 09 2023.
- [119] A.R. Dehghani-Sanij, E. Tharumalingam, M.B. Dusseault, and R. Fraser. Study of energy storage systems and environmental challenges of batteries. *Renewable and Sustainable Energy Reviews*, 104:192–208, April 2019.
- [120] Circular 1/2025, de 28 de enero, de la Comisión Nacional de los Mercados y la Competencia, por la que se modifica la Circular 3/2020, de 15 de enero, por la que se establece la metodología para el cálculo de los peajes de transporte y distribución de electricidad. BOE-A-2025-2044, January 2025.
- [121] Geyser Batteries Oy. Geyser battery: Introduction to a power-dense battery for heavy-duty applications, 2021. [White paper]. Available online: <https://www.geyserbatteries.com/technology> (accessed on 29/01/2024).
- [122] AGISTIN Project Consortium. D2.1: Energy Storage Integration Requirements, Incentives and Constraints: EU-wide Analyses. Technical Report D2.1, Horizon Europe Program, European Commission, December 2023. Grant Agreement Number: 101096197, Lead Participant: EPRI, Submitted: 25/12/2023.
- [123] EU ACER. ACER webinar on amendments to the European electricity grid connection network codes. Online, July 2023. Available onlien: https://www.youtube.com/watch?v=ptrP4qSX10&ab_channel=EUACER.
- [124] Xing Luo, Jihong Wang, Mark Dooner, and Jonathan Clarke. Overview of current development in electrical energy storage technologies and the application potential in power system operation. *Applied Energy*, 137:511–536, 2015.
- [125] Francisco Díaz-González, Andreas Sumper, Oriol Gomis-Bellmunt, and Roberto Villafáfila-Robles. A review of energy storage technologies for wind power applications. *Renewable and Sustainable Energy Reviews*, 16(4):2154–2171, 2012.
- [126] Enrique Lobato, Lukas Sigrist, and Luis Rouco. Use of energy storage systems for peak shaving in the spanish canary islands. In *2013 IEEE Power & Energy Society General Meeting*, pages 1–5, 2013.
- [127] E.B. Prasasti, M. Aouad, M. Joseph, M. Zangeneh, and K. Terheiden. Optimization of pumped hydro energy storage design and operation for offshore low-head application and grid stabilization. *Renewable and Sustainable Energy Reviews*, 191:114122, 2024.
- [128] Jan Figgenger, Benedikt Tepe, Fabian Rücker, Ilka Schoeneberger, Christopher Hecht, Andreas Jossen, and Dirk Uwe Sauer. The influence of frequency containment reserve flexibilization on the economics of electric vehicle fleet operation. *Journal of Energy Storage*, 53:105138, 2022.
- [129] Krishnakumar R. Vasudevan, Vigna K. Ramachandaramurthy, Gomathi Venugopal, J.B. Ekanayake, and S.K. Tiong. Variable speed pumped hydro storage: A review of converters, controls and energy management strategies. *Renewable and Sustainable Energy Reviews*, 135:110156, 2021.
- [130] C Nicolet, O Braun, N Ruchonnet, J. Hell, A Béguin, and F Avellan. Simulation of pump-turbine prototype fast mode transition for grid stability support. *Journal of Physics: Conference Series*, 813(1):012040, mar 2017.

- [131] Anto Joseph, Raghu Selvaraj, Thanga Raj Chelliah, and S. V. Appa Sarma. Starting and braking of a large variable speed hydrogenerating unit subjected to converter and sensor faults. *IEEE Transactions on Industry Applications*, 54(4):3372–3382, July 2018.
- [132] Eduardo Sánchez-Díez, Edgar Ventosa, Massimo Guarnieri, Andrea Trovò, Cristina Flox, Rebeca Marcilla, Francesca Soavi, Petr Mazur, Estibaliz Aranzabe, and Raquel Ferret. Redox flow batteries: Status and perspective towards sustainable stationary energy storage. *Journal of Power Sources*, 481:228804, 2021.
- [133] Andrea Trovò, Vito Di Noto, Joseph Epoupa Mengou, Chiara Gamabaro, and Massimo Guarnieri. Fast response of kw-class vanadium redox flow batteries. *IEEE Transactions on Sustainable Energy*, 12(4):2413–2422, 2021.
- [134] Red Eléctrica de España. Guía descriptiva: Ser proveedor de servicios de balance, January 2024. Accessed: 2025-01-29.
- [135] Comisión Nacional de los Mercados y la Competencia. Resolución de 3 de octubre de 2024, de la Comisión Nacional de los Mercados y la Competencia, por la que se modifican los procedimientos de operación eléctricos 14.1 y 14.4 para la adaptación de la liquidación al ISP cuarto-horario. *Boletín Oficial del Estado*, 248:131410–131478, October 2024. Reference: BOE-A-2024-20995, Accessed: 2025-01-29.
- [136] David G. Luenberger and Yinyu Ye. *Linear and Nonlinear Programming*. Springer Publishing Company, Incorporated, 2015.
- [137] Adrian Hauswirth, Alessandro Zanardi, Saverio Bolognani, Florian Dörfler, and Gabriela Hug. Online optimization in closed loop on the power flow manifold. In *2017 IEEE Manchester PowerTech*, pages 1–6, 2017.
- [138] Miguel Picallo, Dominic Liao-McPherson, Saverio Bolognani, and Florian Dörfler. Cross-layer design for real-time grid operation: Estimation, optimization and power flow. *Electric Power Systems Research*, 212:108378, 2022.
- [139] Marcello Colombino, Emiliano Dall’Anese, and Andrey Bernstein. Online optimization as a feedback controller: Stability and tracking. *IEEE Transactions on Control of Network Systems*, 7(1):422–432, 2020.
- [140] Adrian Hauswirth, Saverio Bolognani, Gabriela Hug, and Florian Dörfler. Projected gradient descent on riemannian manifolds with applications to online power system optimization. In *2016 54th Annual Allerton Conference on Communication, Control, and Computing (Allerton)*, pages 225–232, 2016.
- [141] V. Häberle, A. Hauswirth, L. Ortmann, S. Bolognani, and F. Dörfler. Non-convex feedback optimization with input and output constraints. *IEEE Control Systems Letters*, 5(1):343–348, 2020.
- [142] Lukas Ortmann, Adrian Hauswirth, Ivo Caduff, Florian Dörfler, and Saverio Bolognani. Experimental validation of feedback optimization in power distribution grids. *Electric Power Systems Research*, 189:106782, 2020.
- [143] J. C. Olives-Camps, A. Rodríguez del Nozal, J. M. Mauricio, and J. M. Maza-Ortega. A model-less control algorithm of dc microgrids based on feedback optimization. *International Journal of Electrical Power & Energy Systems*, 141:108087, 2022.
- [144] E.A. Rodríguez-Gonzalez, J.C. Olives-Camps, F.P. García-Lopez, A. Rodríguez Del Nozal, J.M. Mauricio, and J.M. Maza-Ortega. Experimental validation of a real-time distributed model-less control for dc microgrids. In *2022 International Conference on Smart Energy Systems and Technologies (SEST)*, pages 1–6, 2022.



- [145] Marcello Colombino, John W. Simpson-Porco, and Andrey Bernstein. Towards robustness guarantees for feedback-based optimization. In *2019 IEEE 58th Conference on Decision and Control (CDC)*, pages 6207–6214, 2019.
- [146] Jaume Girona-Badia, Vinícius Albernaz Lacerda, Daniel Westerman Spier, Eduardo Prieto-Araujo, and Oriol Gomis-Bellmunt. Resource-aware grid-forming synchronization control: Design, analysis and validation. *IEEE Transactions on Energy Conversion*, pages 1–12, 2024.
- [147] Irina Subotić and Dominic Groß. Universal dual-port grid-forming control: Bridging the gap between grid-forming and grid-following control. *IEEE Transactions on Power Systems*, 39(6):6861–6875, 2024.
- [148] M.E. El-Hawary and S.T. Ibrahim. A new approach to AC-DC load flow analysis. *Electric Power Systems Research*, 33(3):193–200, 1995.
- [149] Ugur Arifoglu. The power flow algorithm for balanced and unbalanced bipolar multiterminal ACDC systems. *Electric Power Systems Research*, 64(3):239–246, 2003.
- [150] Jef Beerten, Stijn Cole, and Ronnie Belmans. A sequential AC/DC power flow algorithm for networks containing multi-terminal VSC HVDC systems. In *IEEE PES General Meeting*, pages 1–7, 2010.
- [151] M. M. El-marsafawy and R. M. Mathur. A new, fast technique for load-flow solution of integrated multi-terminal DC/AC systems. *IEEE Transactions on Power Apparatus and Systems*, PAS-99(1):246–255, 1980.
- [152] Fnn guideline: Grid forming behaviour of hvdc systems and dc-connected ppms. Technical guideline, Forum Netztechnik/Netzbetrieb (FNN), VDE, 2023.